Natural and Synthetic GHSR1a Agonists as Neuroprotective Agents in Models of Parkinson's disease

Rees, Daniel J.

Natural and Synthetic GHSR1a Agonists as Neuroprotective Agents in Models of Parkinson's disease

Daniel James Rees

Submitted in fulfilment of the requirements for the Degree of Doctor of Philosophy

Swansea University

2017

Abstract

Parkinson's disease (PD) is the second most prevalent neurodegenerative disorder in humans. It is characterised by the progressive loss of the A9 (Girk2+) subpopulation of dopamine (DA) neurones in the Substantia Nigra Pars Compacta (SNpc) resulting in resting tremor, bradykinesia and rigidity. The majority of PD cases are idiopathic. However, environmental toxins that inhibit the mitochondrial electron transport chain cause PD-like symptoms and recent studies of rare familial PD implicate metabolic dysfunction as a possible cause of DA nerve cell loss. We propose that the homeostatic hormone, acyl-ghrelin, may prevent DA neurone loss by preserving nerve cell metabolism during bioenergetics stress. In the in-vivo MPTP-toxin model of PD acyl-ghrelin prevents SNpc DA neurone loss in an acyl-ghrelin receptor (GHSR)-dependent manner (Andrews et al.2009). Here, using the eGFP-GHSR reporter mouse we demonstrate co-localised expression of the GHSR with TH+ and Girk2+ SNpc neurones. This suggests that acyl-ghrelin may exert a direct protective effect on A9 DA neurones via GHSR+ signalling. We show that acyl-ghrelin attenuated the 6-OHDA-induced SN lesion in unilateral lesioned rats. Moreover, this neuroprotection is consistent with the preservation of motor function. Using a mouse-midbrain-derived neuronal cell line (SN4741), immune-positive for TH+/ Girk2+/GHSR+, we assess the neuroprotective potential of acyl-ghrelin and GHSR1a agonist, JMV2894, in an in-vitro rotenone-based PD model. Furthermore, we show acyl-ghrelin as a modulator of intra-cellular AMPK and ACC phosphorylation and investigate the protective effects on mitochondrial health and morphology using automated images analysis and TEM. Acyl-ghrelin activated cellular pathways associated with protecting against energetic stress and promoting healthy aging. These data suggest that Acyl-Ghrelin may be a potential new therapeutic target for PD.

Declaration and Statements

DECLARATION

This work has not previously been accepted in substance for any degree and is not being concurrently submitted in candidature for any degree.

Signed ..... (candidate)

Date .....

STATEMENT 1

This thesis is the result of my own investigations, except where otherwise stated.

Other sources are acknowledged by footnotes giving explicit references. A bibliography is appended.

Signed ..... (candidate)

Date .....

STATEMENT 2

I hereby give consent for my thesis, if accepted, to be available for photocopying and for inter-library loan, and for the title and summary to be made available to outside organisations.

Signed ..... (candidate)

Date .....

Table of Contents

List of Figures

Chapter 4

List of Tables

Acknowledgements

To Jeff Davies for his great guidance throughout my PhD studies, I would like to give my utmost gratitude. The knowledge and skills he has imparted upon me have been essential in carrying out this research and are tools I will continue to carry into my career.

An expression of deepest gratitude to Marc Clement for the inspirational direction and advice shown as I have worked through my PhD. The vital wisdom, knowledge and opportunities he has afforded me have been pivotal to this research and further successes. As I continue my career, I know it would not be possible without his input, something I will always appreciate and be extremely thankful for.

Special thanks to Jayne Daniels for her crucial help and unwavering support. Were it not for the assistance she has given me, this research would not be possible and I am deeply appreciative of everything she has done for me.

Special thanks to Dan Murphy for his steadfast friendship and willingness to help with anything. The support he has shown has been of great benefit and comfort to me and the many caffeine-fuelled late nights are appreciated.

A heartfelt thank you to Gareth Davies and Siân Roderick for their ongoing support and assistance in my studies and in all other areas.

To my parents, my family and all my friends a great depth of gratitude for every ounce of support and word of encouragement. Words cannot express my appreciation for the imperative support you have shown me during my studies. Thank you all so much.

I dedicate this to my late brother, Steffan. His courage and strength will always be an inspiration and motivation. We miss you.

1.0. Chapter 1: Introduction

1.1. Parkinson's Disease

Parkinson's Disease (PD) is the second most prevalent neurodegenerative disorder worldwide, following Alzheimer's disease. PD patients experience debilitating progressive motor and cognitive decline. PD itself is not a direct cause of mortality, however, it results in life-threatening complications such as pneumonia or severe swallowing difficulties (Bertram & Tanzi, 2005). In the later stages of PD, patients require full-time care. PD is usually diagnosed in the mid to late stages of life (over ~60 years) although there is exception in rare cases of early onset PD (Van Den Eeden et al., 2003). Prevalence of PD is likely to parallel the increase in average age of the population. According to research carried out by Parkinson's UK: 1 in every 500 person has Parkinson's (roughly 127,000 in the UK) and by 2020 the number of people with Parkinson's in the UK is set to rise by 28% (Parkinson's UK). This predicted increase in PD prevalence establishes PD as a major disease with unmet clinical need that will pose increasing pressure on healthcare sectors.

PD is characterised by the progressive degradation of dopaminergic neurones (catecholamine sub-group A9) that project to the dorsal striatum from the substantia nigra (SN) pars compacta (pc) region of the midbrain (Bjorklund & Dunnett, 2007). The pathway between the SN and striatum is part of the basal ganglia motor loop. Striatal function in this pathway is to regulate controlled movement (Stocco, Lebiere, & Anderson, 2010). The progressive death of SNpc dopamine (DA) neurones results in decreased release of the neurotransmitter, DA, in the striatum and decreased DA turnover rate. Disruption of the nigrostriatal pathway results in motor control dysfunction. PD patients also suffer non-motor symptoms i.e. cognitive decline, loss of appetite, smell, weight, and reduced gastric motility/emptying (Faulkner, 2014). Typically, PD sufferers remain mostly asymptomatic prior to the death of ~60-70% of SN DA cells (Schapira, 2007). The severity and time of onset of symptoms in PD varies between individuals, however end-stage PD results in a vegetative state (Van Den Eeden, et al., 2003).

The neuropathology of PD is not restricted to SN A9 DA cells (Bjorklund & Dunnett, 2007). Cellular dysfunction and abnormalities have been found in various other DA and non-DA cell groups (Dauer & Przedborski, 2003). Besides progressive cell death, another key hallmark of PD is the accumulation of intracellular proteinaceous inclusions (which are partly composed of α-synuclein) named Lewy Bodies (LBs) that deter normal cellular function (Bove, Prou, Perier, & Przedborski, 2005). Alpha-

synuclein is a 140-amino acid long protein coded for by the gene SNCA. Since alpha-synuclein does not possess a defined structure in aqueous, it is called a “natively unfolded protein”. However, this protein can form alpha-helical structures upon interaction with the negatively charged lipids of the phospholipid cell membrane. Beta-sheet-rich structures may also form under these conditions with prolonged incubation times. Alpha-synuclein is composed of 3 main domains. The first is a 60-residue long apolipoprotein inclusive of lipid-binding motifs which are thought to form amphiphilic helices that form alpha helical structures upon binding to the cell membrane. Secondly, a central hydrophobic region spanning residues 61 to 95. This region has been termed non-Aβ component (NAC) which is thought to contribute to formation of beta-sheets. The third distinct domain is a negatively charged carboxyl terminus that is prone to an unstructured form. Alternative splicing results in at least 2 shorter alpha-synuclein variants of the SNCA gene transcript. However, the exact roles in normal physiology and detrimental pathological roles are yet to be fully elucidated. In addition, there are at least two shorter alternatively spliced variants of the SNCA gene transcript that have not been well characterized (Maroteaux, Campanelli, & Scheller, 1988; Maroteaux & Scheller, 1991; Ueda et al., 1993).

As the death of dopaminergic neurons (TH^+) due to apoptosis, mitochondrial dysfunction, and/or oxidative stress are well-established causes of PD and underlie its characteristic symptoms (Albarran-Zeckler, Sun, & Smith, 2011; Fedorow et al., 2005; German & Manaye, 1993) this project will focus on examining the A8, A9 & A10 DA neurones of the SN. The DA neurones in this region project towards many other regions including striatum, globus pallidus, and subthalamic nucleus of the basal ganglia, playing an integral role in regulating motor function in the central nervous system (CNS) (Bjorklund & Dunnett, 2007).

The cause of PD is unknown. However currently identified PD-associated genes (see table 1) are thought to account for ~5% of cases (Pirkevi, Lesage, Brice, & Basak, 2009). Identification and study of PD-associated genes is a means of (1) increasing risk prediction and (2) delineating possible defects in cellular pathways that may contribute to non-familial PD pathology. Many genetic targets have been uncovered with potential PD pathology-associated effects (see table 1. for some PD-associated genes).

Mutations found in PD-genes appear to either: (1) alter pathways affecting mitochondrial function (Valente et al., 2004), (2) lead to protein accumulations (i.e. alpha-synuclein and protein tangle deposits) (Olanow & Brundin, 2013) or (3) promote

a dysfunctional clearance of damaged/unnecessary protein inclusions and cellular organelles (e.g. dysfunctional mitochondria) in autophagy/mitophagy (Kanki et al., 2009). Mitochondrial function and clearance of damaged organelles is essential to maintain cellular integrity. Therefore, such genetic mutations may contribute to pathogenic pathways that effect mitochondrial activity, increase oxidative stress and impair proteasome function resulting in neuronal death (Bayliss & Andrews, 2013). Collectively, it is evident that mitochondrial bioenergetics, function and metabolism is a key area of interest in uncovering pathways in PD pathology (Hardy, 2010).

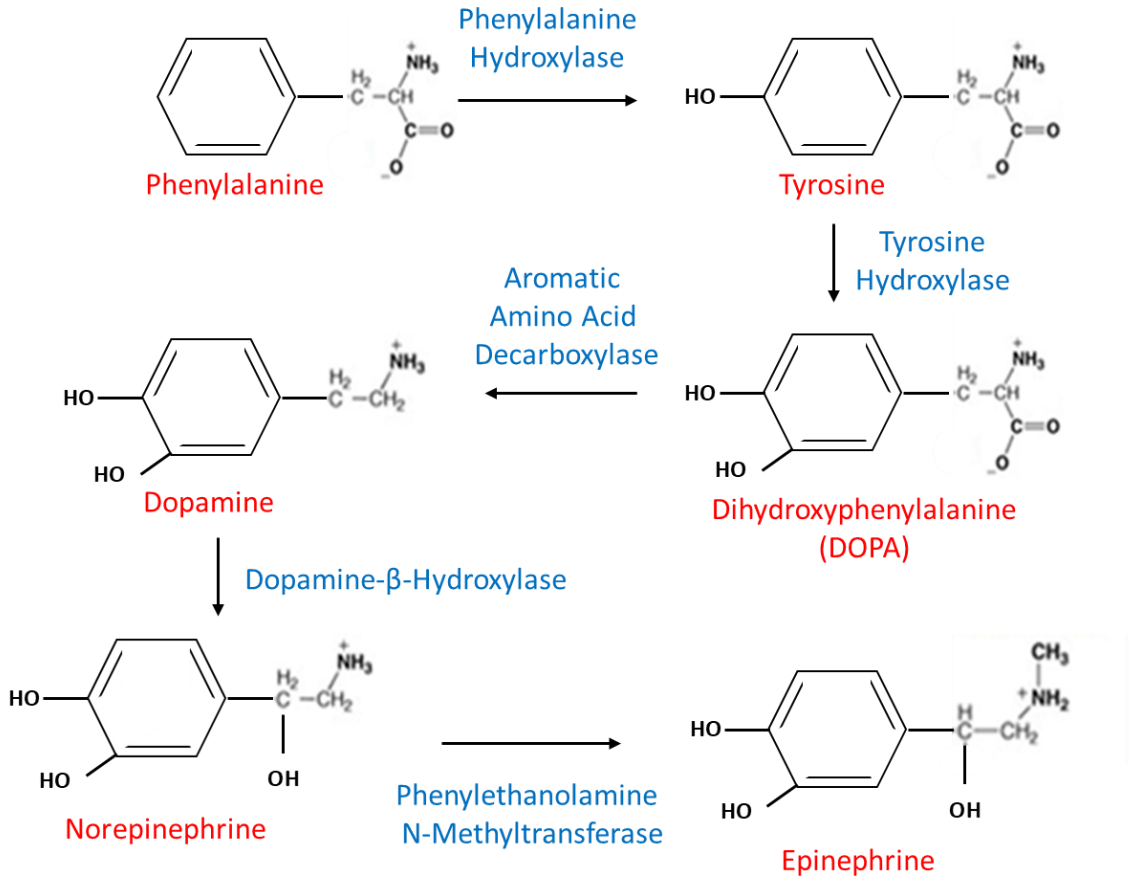

Figure 1: Catecholamine Biosynthesis Pathway.

This illustration shows the catecholaminergic biosynthesis pathway. Names of the catecholamine products are shown in red; names of the enzymes involved in the enzymatic conversions between products are shown in blue

1.2. Current PD Therapy

Current therapies aim to replenish lost DA. Levodopa (L-DOPA) is a molecular precursor for DA and is currently the most common and effective drug given to PD sufferers (see figure 2 for L-DOPA mode of action). This treatment is often supplemented with other drugs to increase L-DOPA efficacy. (See table 2 for more details on PD drugs and their side-effects). L-DOPA treatment is not effective in ~50% of patients and the majority of patients develop debilitating side effects termed L-DOPA induced dyskinesia's (LIDS) after prolonged use. However, there are no therapeutics in use to attenuate the dopaminergic cell death which lies at the heart of PD.

In light of this, current research showed that the orexigenic stomach hormone, ghrelin exerts neuroprotection in a mouse model of PD (Andrews, 2011). Further studies show that these effects are at least partially mediated via an un-coupling protein 2 (UCP-2) dependent pathway following ghrelin receptor agonization (Andrews, 2011); (Andrews et al., 2009).These findings have fuelled intense interest in understanding the molecular mechanisms underpinning ghrelin receptor involvement in neuroprotection. The utilization of ghrelin and other ghrelin receptor agonists as novel neurodegenerative disease therapeutics may hold the key to attenuating the progressive dopaminergic cell death displayed in PD.

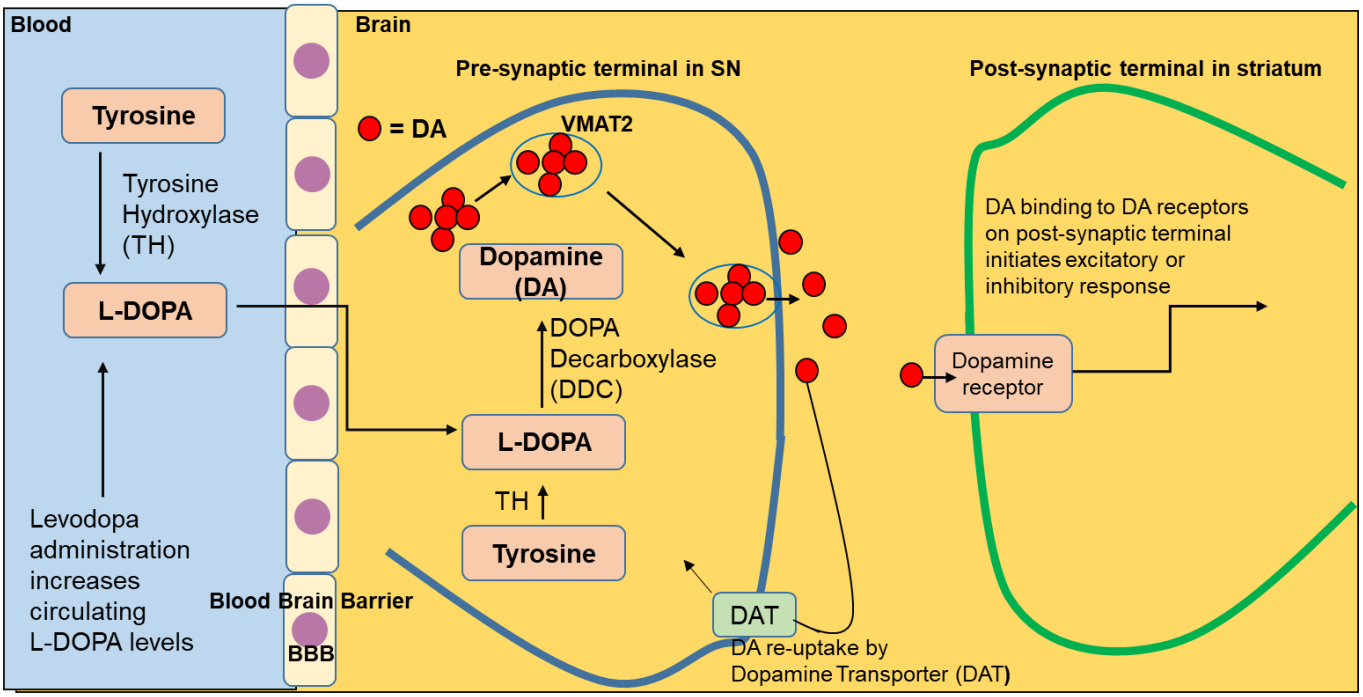

Figure 2: Current PD Treatment.

The most common current PD treatment, which is orally administrated dopamine-replacement therapy using dopamine precursor molecule dihydroxyphenylalanine (L-DOPA). L-DOPA is the immediate precursor molecule to dopamine (DA) (see figure 1). Unlike dopamine, L-DOPA can transverse the blood brain barrier and is utilised in the catecholamine biosynthesis pathway at the terminals of nigrostriatal dopaminergic nerones. Decarboxylation of L-DOPA by DOPA Decarboxylase (DDC) produces DA. DA is stored in synaptic vesicles before its release into the synaptic cleft (space between vesicles). This acts to replenish decreased midbrain DA levels and normalise motor function associated with DA depletion (Jenner & Rose, 1974). This treatment strategy is only effective in ~50% of patients, and the treatment itself has a short time of efficacy (~5 years) before increased doses are required. Short-term side effects include nausea and vomiting. In addition, Levodopa-induced dyskensias (uncontrollable, involuntary movements) arise following prolonged use (~5-10 years) of L-DOPA based treatments, resulting in progressive debilitating side-effects over time (Udd et al., 2017). Vesicular Monoamine Transporter 2 (VMAT2) is an integral membrane protein which transports monoamine neurotransmitters such as dopamine within synaptic terminals. (See table 2 for an overview of other PD drugs and side effects)

Table 1: Overview of PD-Associated Genes and Roles in Pathology

Gene	Gene locus	Mutation	Inheritance: Autosomal-Dominant (AD) or Autosomal-Recessive (AR)	Clinical features in PD	Gene mutations contribution to PD pathology	Lewy bodies
α-synuclein (SNCA)	4q21	Park 1 / 4	AD	Typical PD but sometimes have dementia presentation. Onset/age 40s	SNCA encodes for alpha synuclein protein. A large component of degradable protein deposits. Leads to protein accumulation & LBs	Yes
Parkin	6q25	Park 2	AR	Presents itself very slowly and progressively at an early age of onset (early onset-PD) with sleep benefit.Onset/age 20s	Gene encodes a component of ubiquitin ligase associated with z region of the ligase proteasome system – playing a role in recycling of unneeded cellular components.	No
PINK1	1p35	Park 6	AR	Usually very slow progressive early onset disease usually with sleep benefit. Onset/ age 30s	One case with LBs.	?
DJ-1	1p36	Park 7	AR	Onset/age 30s	Little data-similar to Parkin. DJ-1 is thought to protect cell from oxidative stress.	?
Leucine rich repeat kinase 2 (LRRK2)	12p	Park 8	AD	Typical PD	Encodes for protein in cytoplasmic protein 'Dardarin'. This protein also associates itself with mitochondrial membranes. Mutations associated with macro-autophagy dysfunction. Usually LBs, sometime protein tangles. Rare cases of no protein accumulation.	Yes/No

1.3. Ghrelin

Ghrelin was discovered in 1999 by Kojima et al following the earlier discovery of a growth hormone secreting receptor, the growth hormone secretagogue receptor (GHS-R) (Smith et al., 1999). Ghrelin is a circulating 28-amino acid acylated hormone discovered by reverse pharmacology as the endogenous ligand for the GHS-R (Kojima et al., 1999). Since its discovery, research has highlighted the complexity of ghrelin's roles in a multiplicity of biological functions mediating endo/para and autocrine actions on a variety of tissues. Ghrelin is predominantly produced in the stomach and is regulated by feeding. Circulating levels of ghrelin are increased under calorie restriction and decrease following feeding (Andrews, 2011).

Table 2: Overview of Current PD Drug Treatment and Side Effects

PD Therapy	Action in PD Patient	Side effects
Levodopa	Orally administered drug (often co-administered with benserazide or carbidopa to ensure efficient dose if L-dopa crosses blood-brain barrier). As an input to the catecholamine biosynthesis pathway, L-dopa is converted to dopamine, increasing dopamine concentration in the brain, thus alleviating motor dysfunction. Usually administered after the efficacy of catechol-O-methyl transferase (COMT) and monoamine oxidase (MAO-B) inhibitors are decreased.	Short term use can lead to nausea and vomiting as body adjusts to the drug. Long term use of levodopa results in uncontrolled/involuntary movement termed dyskinesia. As DA neurone death progresses, the drug's effect decreases and dosage must be increased incrementally.
COMT inhibitors	Orally administered. Act primarily on the intestine to reduce breakdown of levodopa in the periphery and enhance its penetration into the central nervous system. Dose of levodopa can be decreased if used in conjunction with COMT inhibitors.	May increase side effects caused by levodopa (dyskinesia). Other reported side effects include abdominal pain, diarrhoea and discoloured urine. (https://www.parkinsons.org.uk/information-and-support/comt-inhibitors)
MAO-B inhibitors	Orally administered. MAO-A and MAO-B metabolise synaptic DA by auto-oxidation. MAO inhibitors increase synaptic DA half-life and degree of DA re-uptake by pre-synaptic terminals by reducing synaptic DA breakdown.	When taken with levodopa, side effects such as dyskinesia, hallucinations or vivid dreaming may sometimes occur or worsen. When taken without levodopa, most common side effects include: headache, aching joints, flu-like symptoms and depression. Not to be taken with some anti-depressants as some drug-drug interactions result in increased blood pressure (https://www.parkinsons.org.uk/information-and-support/mao-b-inhibitors)
Dopamine receptor agonists	Orally administered. Drug is absorbed and crosses blood-brain barrier in order to activate dopamine receptors (D1, D2 & D3 receptors). Drug dose must be increased incrementally according to drug efficacy.	Common side effects include: Nausea and vomiting, headache, constipation, drowsiness and sudden onset of sleepiness. Dizziness or fainting due to low blood pressure. Pathological gambling and punting Delusions or hallucinations and confusion. Existing dyskinesia becoming more troubling initially (https://www.parkinsons.org.uk/information-and-support/dopamine-agonists

Ghrelin is produced in ghrelinergic cells of the gastrointestinal tract and is the product of proteolytic cleavage and posttranslational modification/acylation of inactive preproghrelin (Andrews, 2011; Kojima, et al., 1999; Korbonits et al., 2002). Ghrelin is produced by X/A cells in the stomach at times of negative energy balance where it is post-transcriptionally modified to Acyl-Ghrelin by enzymatic activity of ghrelin-o-acyltransferase (GOAT) which catalysed the addition of an acyl side chain to the nascent ghrelin peptide at serine 3 (Kojima, Hamamoto, & Sato, 2016; Kojima, et al., 1999). In humans this inactive peptide is coded by a single copy gene located of the short (p) arm of chromosome 3, GHRL (Gahete et al., 2014), which is detailed in (Figure 3). Transcription of GHRL produces a 117-amino acid nascent product containing an N-terminus signal peptide (23-amino acids) and pro-ghrelin peptide (94-amino acids). Transcribed mRNA sequence is ribosomally translated on the rough endoplasmic reticulum (RER) surface. Signal peptides are identified by signal recognition particles (SRPs) associated with the RER. Translation of nascent peptide is then momentarily retarded until SRP docks at the ER membrane-bound SRP receptor. Co-translational translocation then resumes, and the peptide is fed through RER translocon (sec61 translocation complex, in eukaryotes) into the ER lumen. Preproghrelin signal peptide is then cleaved in the ER lumen, producing proghrelin. Here proghrelin is post-translationally modified by an integral membrane protein, ghrelin o-acyl transferase (GOAT) (Gutierrez et al., 2008). Un-acylated ghrelin (UAG) is also a product of the GHRL gene. This ghrelin isoform accounts for ~90% of circulating ghrelin - however its physiological role and receptor is yet to be elucidated (Andrews, 2011; Delhanty, van der Eerden, & van Leeuwen, 2014; Gahete, et al., 2014).

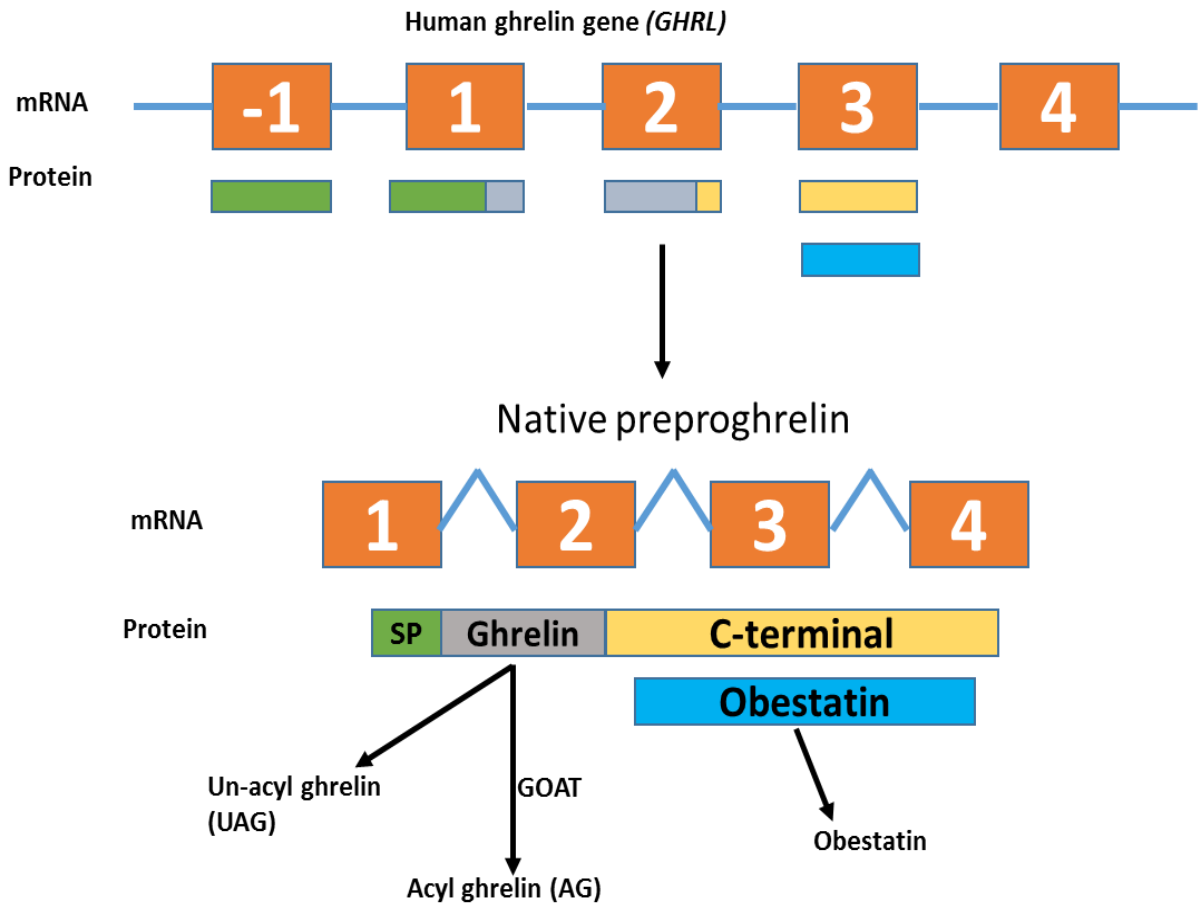

Figure 3: Overview of Human Ghrelin Gene Structure and Variants

This is an overview of the human ghrelin (GHRL) gene structure and gene-derived variants (UAG, AG and Obestatin), transcripts and putative peptides. Signal peptide (SP) is shown in green, ghrelin in grey, obestatin in blue and C-peptides in yellow. This figure was modified from (Gahete, et al., 2014).

1.4. Ghrelin O-Acyl Transferase (GOAT)

The human GOAT gene, MBOAT4, is located on chromosome 8p12 (Gutierrez, et al., 2008). GOAT is expressed in a variety of human tissues including pancreas, skeletal muscle, heart, intestine, bone and predominantly in the stomach - specifically the ghrelin-containing oxyntic cells of the gastric mucosa (Bayliss & Andrews, 2013). Here there is extensive expression of GOAT mRNA and protein (Gahete, et al., 2014; Muller et al., 2011).

Within the vertebrate subphylum the amino acid sequence of GOAT is highly conserved, much like ghrelin (~90% in the case of GOAT). This high homology is substantiated in rat and mouse GOATs ability to catalyse the acylation of human ghrelin. Also, a strong homology exists between rat and human ghrelin as their peptide sequences only differ by 2 amino acids (Date et al., 2000).

The enzyme product of *MBOAT4* utilizes fatty acids as acyl-CoA donors to catalyse the addition of octanoic acid to the N-terminal ser3 residue of pro-ghrelin. Once acylated, ghrelin is often referred to as acyl-ghrelin (AG) (Kojima, et al., 1999). Acylation of Ser3 is essential for the activation of the GHS-R type 1a (GHS-R1a). The 5 N-terminus ghrelin amino acids [Glycine]-[Serine]-[acyl-Serine]-[phenylalanine]-[Leucine] are the minimal requirement for GHS-R1a activation (Date, et al., 2000).

1.5. Growth Hormone Secretagogue Receptor (GHS-R)

GHS-R1a receptors are primarily expressed in β-cells of pancreatic islets, distinct areas of the hypothalamus (known to play roles in body weight and food intake), pituitary somatotrophs, hippocampus, the ventral tegmental area (VTA), the dorsal raphe nucleus, all three components of the dorsal vagal complex and the substantia nigra (SN) (Albarran-Zeckler, et al., 2011) (Zigman, Jones, Lee, Saper, & Elmquist, 2006)

In humans, as well as in rats and mice, there are two identified GHS-R receptor sub-types (GHS-R1a and GHS-R1b), both of which are products of alternative splicing of a single-copy gene located on chromosome 3q26.31. The *GHSR* gene was first cloned from human pituitary glands and hypothalamus in 1996 (Howard et al., 1996). The sequence is highly conserved throughout many vertebrate species including humans, chimpanzees, mice and rats, swine and cows (H. J. Wang et al., 2004). GHS-R1a mRNA includes exon 1 and 2 of the *GHSR* gene, encoding a 366 amino acid long 7 transmembrane (TM) G-protein coupled receptor (GPCR). GHS-R1b

mRNA is produced by the retention of intron 1 separating exon 1 and 2. This mRNA product produces a 289-amino acid long 5TM GPCR isoform (Gahete, et al., 2014). Interestingly, codons 1-265 are identical in both isoforms. However, sequence variation between subtype 1a and 1b exists at a 24-amino acid sequence at the C-terminus. In GHS-R1b, the 24 amino acids following 265Leu are encoded by the intron of GHS-R1a (Camina, 2006; H. J. Wang, et al., 2004)

On-going research is yet to elucidate the function of the C-terminal truncated GHS-R1b and whether *GHS-R*1b encodes a functional protein or not. (Gahete, et al., 2014; Gnanapavan et al., 2002). The GHS-R1b gene is expressed in various tissues, so it is possible that GHS-R1b's function is yet to be elucidated. Moreover, some studies show that GHSR1b acts as a dominant negative mutant of the ghrelin receptor(Leung et al., 2007). When over-expressed in HEK-293 cells it decreases the constitutive activity of GHS-R1a. Indicating that GHS-R1b may act as an endogenous modulator for GHS-R1a constitutive activity (Chu et al., 2007; Yin, Li, & Zhang, 2014).

1.6. Hypothalamic and Extra-Hypothalamic Functions of Ghrelin

The role of AG, which is secreted from the stomach into the circulation, is a hot topic in endocrine and neuro-molecular studies (Bayliss & Andrews, 2013; H. J. Wang, et al., 2004). The ghrelin-GHS-R1a axis modulates and influences an array of complex biological functions relating to energy homeostasis, including adiposity and gastrointestinal mobility (Bayliss & Andrews, 2013; Engel & Jerlhag, 2014). Binding of AG to hypothalamic and pituitary gland GHS-R1a stimulates food intake and growth hormone release, respectively, in order to regulate energy homeostasis and body weight (Andrews, 2011). GHS-R1a is responsible for the signal transduction of natural 'active' AG and various synthetic growth hormone secretagogues (GHSs) (Andrews, 2011; Gahete, et al., 2014; Moulin et al., 2007). The G-proteins, Gi/o, are associated with GHS-R1a. Once a ligand has bound to the receptor the heterotrimeric G proteins (Gα, β, and γ subunits) dissociate, leaving a free Gα subunit and a βγ complex (Niswender et al., 2008). Hypothalamic expression of GHS-R1a is important in the ghrelin-GHS-R1a axis in metabolic homeostasis as it stimulates the orexigenic neuropeptide-Y and agouti gene-related protein NPY/AgRP neurones to induce feeding (Cowley et al., 2003). Ghrelin activation of GHS-R1a mediates an increase in [$Ca2^{+}$] and downstream signalling pathways: (1) mitogen-activated protein kinase (Waseem, Duxbury, Ashley, & Robinson, 2014); (2) Phosphoinositide 3-kinase / Protein kinase 3 (PI3K/Akt) (Waseem, et al., 2014; Yin, et al., 2014); (3) nitric oxide

synthase (Slomiany & Slomiany, 2014); (4) AMP Activated Protein Kinase (AMPK) cascades (Andersson et al., 2004) and (5) mechanistic target of rapamycin (mTOR) signalling in a multiplicity of cellular systems (Pazos, Casanueva, & Camina, 2008; Yin, et al., 2014).

Recently, the role of ghrelin in extra-hypothalamic brain regions has generated significant research interest. This is substantiated by the growth in evidence for ghrelin's role(s) in neuronal function and association with learning and memory (Carlini et al., 2010; Diano et al., 2006), reward and motivation (Menzies, Skibicka, Leng, & Dickson, 2013) and neuroprotection (Andrews, et al., 2009). Further studies are necessary to elucidate the potential neuroprotective properties of ghrelin and its therapeutic implications in PD.

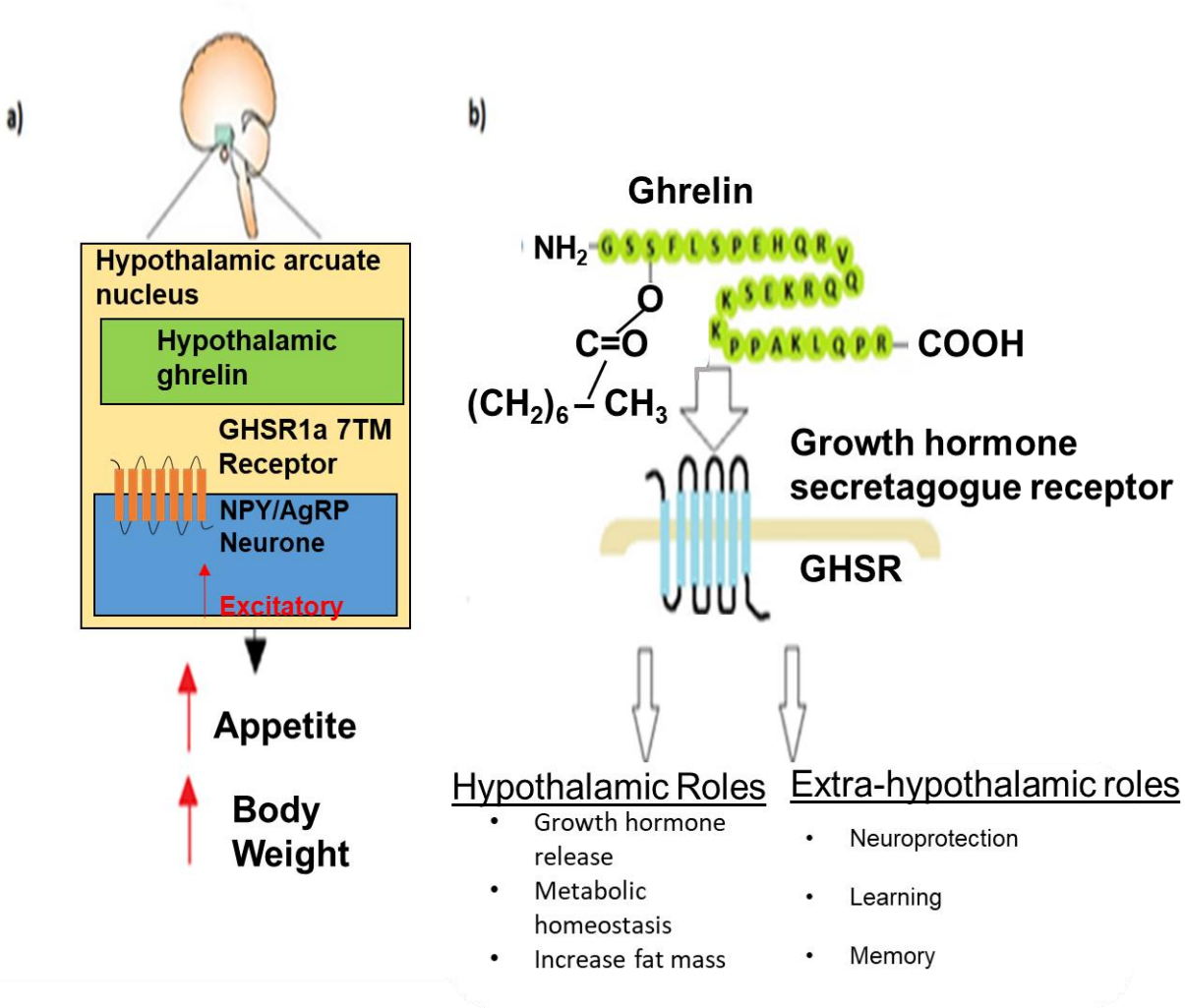

Figure 4: Hypothalamic and Extra-Hypothalamic Roles of Ghrelin.

(a) This is a schematic of ghrelin's appetite regulating effects via activation of neuropeptide-Y (NPY) neurons in the hypothalamic arcuate nucleus. Ghrelin and other GHS-R agonists bind to GHS-R1a on orexigenic NPY neurons and increase appetite and fat mass. NPY neurons are also sensitive to both leptin and insulin. (b) This diagram shows the sequence of 28 amino acids of ghrelin (in their abbreviated form) and lists ghrelin's hypothalamic and extra-hypothalamic roles.

1.7. PD Toxin Models

Little is known about the initial cause and progression of PD (Bove, et al., 2005). However, over the last 20 years information regarding PD pathophysiology has been brought to light thanks to many clinical trials, autopsy investigations and *in-vitro* / *in-vivo* pre-clinical models of PD (Dauer & Przedborski, 2003). Nonetheless there are significant limitations to our understanding of PD at cellular and molecular levels.

Consequently, due to the reproducibility of cell specific cytotoxicity, *in-vitro* and *in-vivo* neurotoxin-based PD models are well-established tools for investigating the underpinning molecular mechanisms of cell death in PD.

Common neurotoxins used to model neurone loss in PD are (1-methyl-4-phenyl-1, 2, 3, 6-tetrahydropyridine (MPTP), 6-hydroxydopamine, paraquat and rotenone (Dauer & Przedborski, 2003). Due to reproducibility and reliability in previous experiments (Beynon et al., 2013), we have chosen to use rotenone in order to simulate DA cell death *in-vitro*. See figure 5 for detail on rotenone's mode of action.

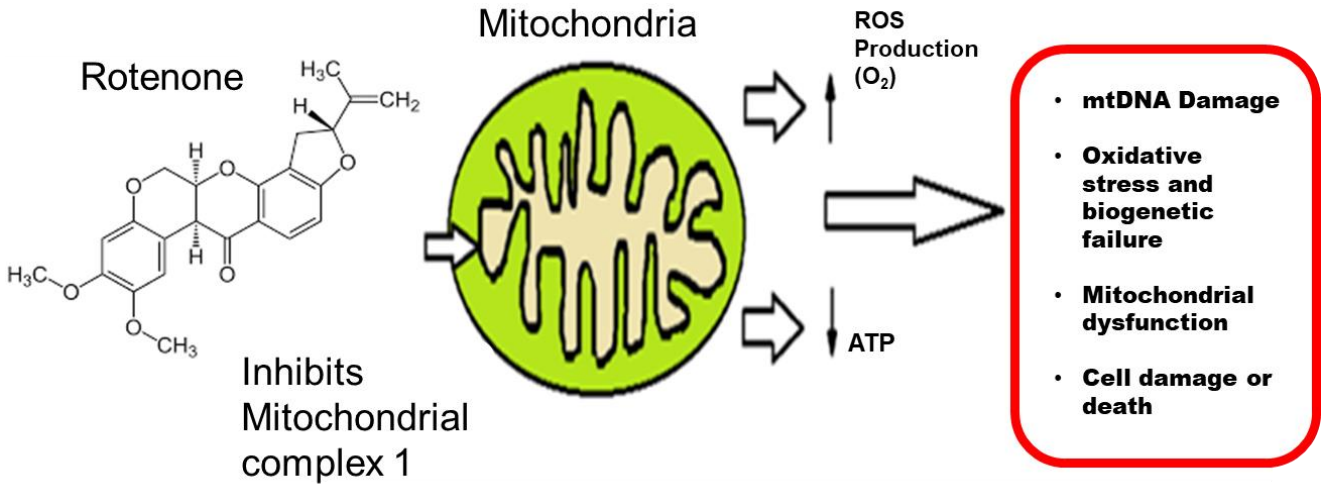

Figure 5: Complex 1 Inhibitor Rotenone as a Neurotoxin.

The lipophilic nature of Rotenone allows ease of access into tissue, organelle and cellular membranes. Rotenone is utilized in *in-vivo* mouse models of PD. Rotenone is an inhibitor of the electron transport system's complex 1 (NADH Dehydrogenase). Inhibition of electron transfer from NADH ubiquinone in complex 1 of the electron complex system causes a build-up of electrons in mitochondrial inter-membrane space. This results in the reduction of molecular oxygen and subsequent formation of radical species (i.e. 0_2 → 0_2-). Reactive oxygen species may damage DNA and other mitochondrial components (Mehta & Li, 2009).

In-vivo rat studies investigating rotenone neurotoxicity show that midbrain neurones are particularly sensitive to rotenone-induced cell toxicity (Choi, Palmiter, & Xia, 2011). Exposure to Rotenone has been proven to cause highly selective nigrostriatal dopaminergic lesions in animals (Sherer, Kim, Betarbet, & Greenamyre, 2003). Rats challenged with rotenone displayed a significant increase in the gene expression of cytoplasmic pro-inflammatory cytokine allograft inflammatory factor 1 (AIF-1) and the pro-apoptotic caspase-3, as well as a decrease in midbrain TH levels. Suggesting that rotenone-neurotoxicity is mediated via microglial activation and apoptosis (Swarnkar et al., 2013). Moreover, previous findings from our group show that this mitochondrial toxin exerts a dose-dependent increase in cell death on midbrain derived cell line (SN4741) *in-vitro*.

Literature has already described acyl-ghrelin (AG) as a potential neuroprotection agent in 1-methyl-4-phenyl-1,2,5,6 tetrahydropyridine (MPTP) models of PD. Studies have suggested that ghrelin induces an enhancement of uncoupling protein 2 (UCP-2) dependent mitochondrial respiration and proliferation. This results in a bioenergetic status which makes DAergic neurons more resistant to cellular stress, suggesting that UCP-2 has a key role in AG-induced neuroprotection in MPTP models (Andrews, et al., 2009). (Bayliss, Lemus, Stark, et al., 2016) found that AG mediates the neuroprotective capability of calorie restriction by attenuating the effects induced by MPTP, such as loss of TH neurons, TH neuronal volume and dopamine content in the striatum. It is also found that AMPK in SN dopamine neurons is a molecular target for the neuroprotective effects of AG (Bayliss, Lemus, Stark, et al., 2016). It is concluded that acyl ghrelin, and its target AMPK, can produce the neuroprotective effects of calorie restriction without the need for severe dietary control. This implicates AG-AMPK signalling as having therapeutic applications in the treatment of PD (Bayliss, Lemus, Stark, et al., 2016).

The AG-mediated neuroprotection is paralleled with MPTP *in-vitro* MPTP models of PD. Published work shows that MPTP-induced neurotoxicity via anti-oxidation in MES23.5 cells is attenuated by AG. This study by (L. Liu et al., 2010) shows that these MTPT-induced effects are abolished in cells treated with AG (L. Liu, et al., 2010). MPTP has also been proven to cause upregulation and aggregation of α-synuclein, a major constituent in Lewy bodies (Bezard, Yue, Kirik, & Spillantini, 2013). Despite these findings, MPTP does have its limitations. It is well known that MPTP induces multi-systemic lesions, despite being presented as specific to DAergic neuron it has been shown to attack all three types of catecholaminergic cell as well as the brain stem, spinal cord and the enteric nervous system (Bezard, et al., 2013). These

limitations highlight the need for the testing of AG in other PD models. One such model is the very well-established 6-hydroxydopamine (6-OHDA) model, which also has the added benefit of assessing sensorimotor function (Simola, Morelli, & Carta, 2007). The effectiveness of AG as a neuroprotector in the 6-OHDA model is not widely studied in the literature and any such testing is novel and innovative in nature. This would contribute knowledge to wider field of PD study.

1.8. Proposed Neuroprotective Mechanism of Ghrelin

Studies to date have delineated the stomach hormone ghrelin as a promoter of DA neurone survival via reduced microglial (M. Moon et al., 2009) and caspase activation and improved mitochondrial function (Andrews, et al., 2009). Mitochondrial dysfunction results in decrease ATP synthesis, increased reactive oxygen species (ROS) production that can result in damage to other cellular components (lipids, proteins etc.), ultimately leading to neuronal dysfunction and death. Mitochondrial dysfunction is a prominent feature in PD (Winklhofer & Haass, 2010) and therefore enhancing or restoring mitochondrial function may represent a potential therapeutic option. See figure 6 for schematic and brief description of ghrelin's proposed neuroprotective mechanism- modified from (Andrews, 2011).

In order for a neuroprotective therapeutic to be of use to a patient it must be able to cross the blood brain barrier (BBB). Endogenous UAG and AG readily passes through the BBB (Banks, 2012), raising the possibility of UAG acylation at region specific sites in the brain. Recent studies using exogenous small-molecule ghrelin receptor agonists have shown that non-peptide agonists also pass this barrier- possibly offering a new approach to treat CNS diseases (Atcha et al., 2009).

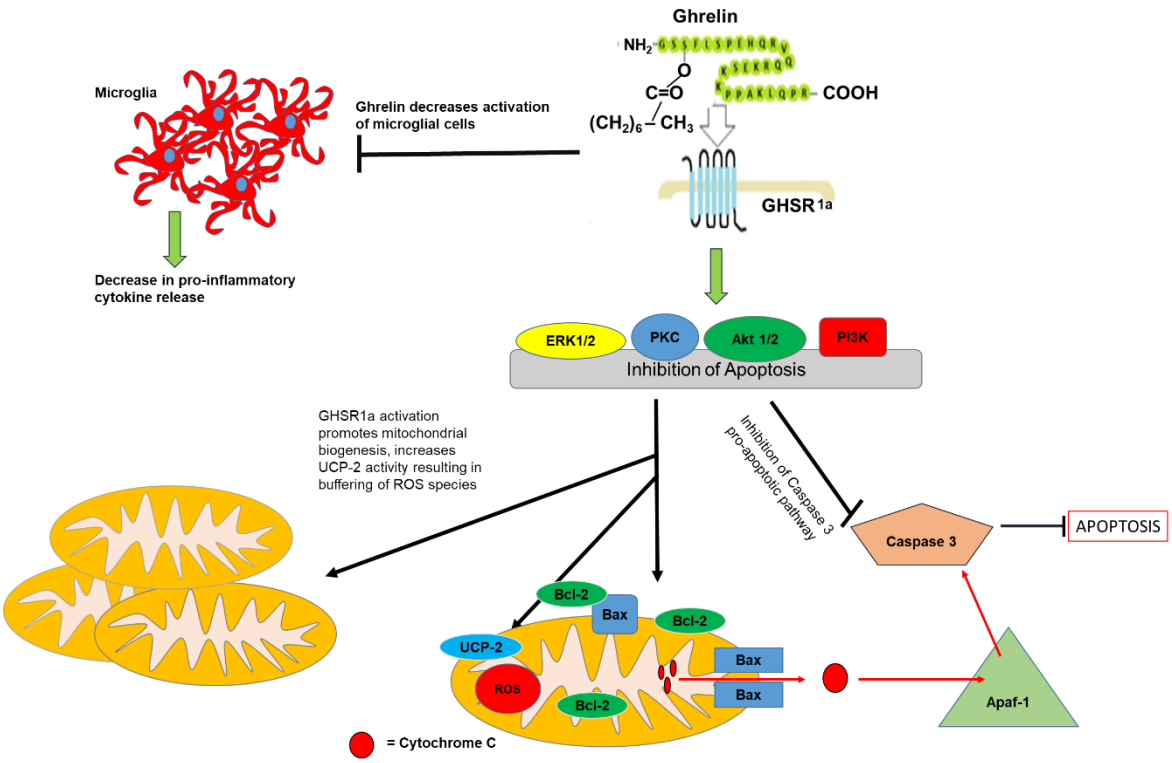

Figure 6: Ghrelin's Proposed Neuroprotective Mechanisms.

Whilst both AG and UAG demonstrate DA cell protection in-vitro by upregulating ERK1/2, AKt1/2, PI3K and PKC, the proposed neuroprotective mechanisms for UAG remains unknown (Andrews, et al., 2009). However, it is well documented both in-vivo and in-vitro that AG mediates its neuroprotective actions in a UCP2 dependant manner via GHSR1a. Binding of receptor agonists, AG, results in the activation of kinase signalling pathways (Albarran-Zeckler, et al., 2011; Andrews, et al., 2009). Evidence from MPTP PD models suggests that AG attenuates neurodegeneration by synergistically restricting DA cell loss; regulating intracellular apoptotic modulators Bcl-2 and Bax; inhibition of microglial activation and reduction of their pro-inflammatory markers Tumour Necrosis Factor α (TNF-α), interleukin-6 (IL-6) and interleukin-1β (IL-1β) and upregulation of mitochondrial UCP-2 which buffers reactive oxygen species (ROS) (Andrews, et al., 2009). Excessive ROS production may initiate apoptosis via apoptosis regulating proteins, such as Bcl-2 family of proteins. The many roles of these proteins include the regulation of the osmotic potential of the mitochondrial membrane. One such protein is Bax. Upon activation Bax oligomerizes in the outer mitochondrial membrane. This Bax oligomerisation leads to depolarization of the mitochondrial membrane potential and release of cytochrome C, the final enzyme of the electron transport chain, from the inter-membrane space- which can occur as a result of excessive ROS production. This is achieved by the formation of membrane spanning pores in the mitochondrial outer membrane or by interaction with

the mitochondria's pore-forming proteins which allow cytochrome C, which is usually associated with the inner membrane of the mitochondria, to flow out. Upon release, cytochrome C, it binds to cytosolic Apoptosis protease activating factor-1 (Apaf-1), thus driving formation of the apoptosome and apoptosis via caspase pathways (Elmore, 2007). Activation of GHSR1a is thought to inhibit this pro-apoptotic pathway by reducing ROS production in a UCP-2 dependant manner (Andrews, et al., 2009). This figure is a modified version of ghrelin's neuroprotective mechanisms from (Andrews, 2011).

Evidence suggests that ghrelin is neuroprotective in several pre-clinical models. However, key questions remain to be answered. For example, 1) does AG exert neuroprotective effects on SNpc neurones by direct binding to cell surface receptors? 2) does AG mediated neuroprotection require other molecular triggers (e.g. Growth Hormone, Insulin-like Growth Factor-I) to mediate its effects? 3) Is GHS-R expressed on particular DA cell phenotypes within the SN? E.g. the A9 subset which express the G-protein-activated inwardly rectifying potassium 2 (Girk2) channel or the A10 subset that express calbindin – these markers are used to distinguish between the DA neurones of the SN and VTA , respectively (Bjorklund & Dunnett, 2007).

1.9. Hypothesis

Published studies suggest that AG-based therapies may prevent or slow the progression of PD. I will test the hypothesis that AG and novel synthetic GHS-R agonists provide direct protection to DA neurones in toxin-based models of PD.

1.10. Aims/objectives:

We will;

1) Characterize GHS-R expression in dopaminergic nerve cells of the SNpc

2) Determine whether AG and a novel GHS-R agonist directly protect DA neurones in *in-vitro* toxin PD model using SN4741 mouse cell line.

3) Determine whether elevated AG, either directly (infusion) or indirectly (restricted feeding), protects SNpc DA neurones and motor function in the rat unilateral 6-OHDA MFB-lesion model of PD.

4) Characterise cellular signalling pathways underlying AG-mediated neuroprotection.

5) Develop a computer protocol for high-throughput analysis of cellular organelle form and function.

2.0. Chapter 2: Characterization of Rodent Midbrain and SN4741 Midbrain Derived Cell Line.

2.1. Introduction

Growing literature supports the neuroprotective effects of acyl-ghrelin (AG) *in vivo* disease models, however the exact mechanism of action observed remains elusive (Andrews, 2011). Both AG and unacylated-ghrelin (UAG) levels are increased during hunger and peaks prior to meal initiation (Bayliss, Lemus, Santos, et al., 2016) but AG is termed the 'active' form of ghrelin as it stimulates the release of growth hormone from the pituitary gland when bound to its endogenous receptor, the Growth Hormone Secretagogue Receptor Type-1a (GHSR1a) (Kojima, et al., 1999). The enzymes modulating the acylation status of ghrelin (GOAT in the endoplasmic reticulum and Acyl-Protein-Thioesterase-1 (APT-1) in plasma) play a pivotal role in determining the ratio of circulating AG to UAG (Satou, Nishi, Yoh, Hattori, & Sugimoto, 2010). If acyl-ghrelin binding to GHSR1a is the initiator of sub-cellular events leading to the neuroprotection observed in models of PD (Bayliss, Lemus, Santos, et al., 2016), then the AG-GHSR1a axis and its acylation/de-acylation enzymes represent putative therapeutic targets to explore within the mammal midbrain, more specifically the SNpc. As defining the localization of GOAT and APT-1 in mammal midbrain neurons may enhance our understanding of ghrelin's acylation and de-acylation dynamics in an area of the brain strongly associated with PD pathology.

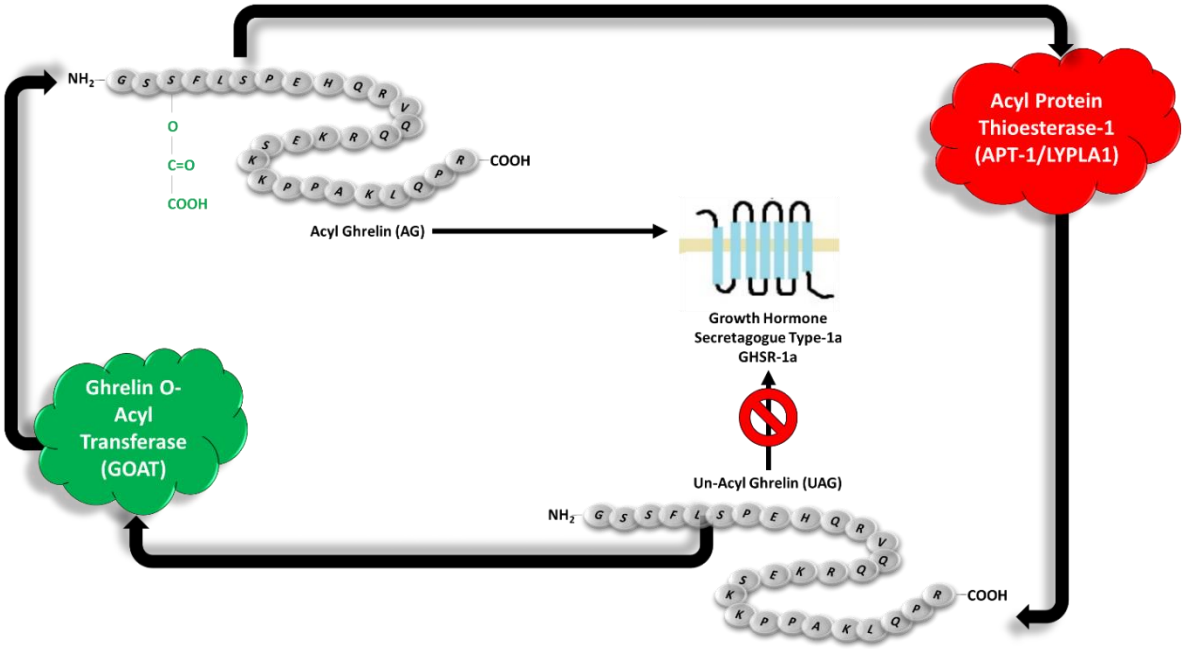

Figure 7: Acylation and De-Acylation Enzymes GOAT and APT-1

Acylation and De-Acylation Enzymes GOAT and APT-1. Schematic of ghrelin acylation and de-acylation cycle. An acyl side-chain [O-CO-$(CH_2)_6CH_3$] is attached enzymatically to the third amino acid of the ghrelin peptide (Serine) to form AG, a ligand for GHSR1a. The acyl side-chain of AG may be enzymatically cleaved via APT-1/LYPLA1, forming UAG, a ghrelin peptide incapable of agonising GHSR1a.

This chapter will investigate the expression of key ghrelin axis proteins, GOAT and APT-1 in the rat midbrain. To further the characterisation of ghrelin axis proteins we will also investigate the expression of GHSR1a on TH^+ and $Girk2^+$ neurones of the mouse SNpc. We will also characterize a mouse midbrain-derived neuronal cell line, SN4741, to validate whether these cells are an appropriate choice of cells to develop an *in vitro* PD model. We aim to utilise this *in vitro* PD model to test for direct neuroprotective effects of AG and other GHSR1a agonists against neurotoxin-mediated cell loss.

2.1.1. Girk2 and Calbindin as Markers of Midbrain Dopaminergic Sub-Types

Published work shows a strong expression of the G protein-gated inwardly rectifying potassium channel 2 (GIRK2) (a member of an ion channel family involved in the regulation of neuronal activity (Kobayashi & Ikeda, 2006; Reyes et al., 2012) in the dorsal and ventral TH^+ neurones of the SNpc and VTA of rodent midbrain (Eulitz, Pruss, Derst, & Veh, 2007; Fu et al., 2012). This expression is also observed in the majority of human TH^+ neurones in the SNpc and VTA (Reyes, et al., 2012). Many previous studies use GIRK2 expression to distinguish between the dorsal and ventral tier of SNpc TH^+ neurones (Thompson, Barraud, Andersson, Kirik, & Bjorklund, 2005). However, other studies find no significant difference in GIRK2 expression in both ventral and dorsal tier of human DA neurones (Reyes, et al., 2012). Another DA neurone subtype predominating in the midbrain is the A10 subtype. Classically the calcium binding protein, calbindin, is used to classify A10 subtype of DA neurones which predominate in the VTA (J. H. Rogers, 1992) (Damier, Hirsch, Agid, & Graybiel, 1999a; Liang, Sinton, & German, 1996; McRitchie, Hardman, & Halliday, 1996) versus the A9 subtype predominating the SNpc of rodent and humans (Schein, Hunter, & Roffler-Tarlov, 1998).

Some literature proposes (Luscher & Slesinger, 2010; Rajesh & Kelly, 2007) that the $Girk2^+$ A9 subtype of DA neurones of the SNpc may possess a higher vulnerability to degeneration and are therefore preferentially lost in PD. This hypothesis was suggested as a result of early SNpc neurone degeneration observed in Weaver mice containing a Girk2 mutation. However, an accepted explanation of this observation has yet to be provided. Furthermore, a previous small study of familial and sporadic PD cases showed no mutation in the pore forming H5 region of Girk2 (Rajesh & Kelly, 2007).

Whether the presence of Girk2 protein contributes to the susceptibility of SNpc DA neurone degeneration in PD or not; TH^+ neurones in the SNpc show higher Girk2 immunoreactivity and mRNA levels in comparison to VTA (Chung et al., 2005; Fu, et al., 2012). Therefore, characterizing the SN4741 cell line for Girk2 and TH expression is fundamental in verifying, at least to some extent, the SN4741 cells as an appropriate cell line to model the neurodegeneration (cell loss) observed in the SNpc in PD. To assess the direct effects of AG or AG-mimetics in an *in-vitro* setting the endogenous ghrelin receptor should be expressed on the SN4741 cell line. The expression of GHSR1a on the TH^+ (and $Girk2^+$) neurones of the rodent SNpc and the

SN4741 cells would present some transferability between *in vitro* and in/*ex-vivo* studies.

2.1.2. Immunochemistry Identifying the Ghrelin receptor

Using fluorescence immunohistochemistry, we have tested whether GHSR1a is co-localized with Girk2 and TH immunoreactivity in the mouse SNpc. GHSR1a is a G-Protein Coupled Receptor. GPCRs possess an extracellular N-terminus which varies in length depending on which sub-type/family the GPCR belongs to (Family A, B, C or Frizzled). The extracellular termini are followed by 7-Transmembrane Domains (7-TMD) found embedded in the cell membrane lipid bilayer. 7-TMDs transverse back and forth through the lipid bilayer, exposing fractions of its structure extracellularly. The 7^{th} GPCR TMD is bound to an intracellular portion of the receptor, the C-terminus. Conformational change to the 7TM portion, upon ligand binding, results in the activation of the intracellular C-terminus and associated G-Proteins (K. Rogers, 2017).

Raising antibodies against GPCRs is challenging and GPCRs-specific antibodies can be difficult to acquire, especially for sub-types of receptors (e.g. as in the case of human adrenergic receptor sub-types) (Hamdani & van der Velden, 2009; Pradidarcheep et al., 2009).

The challenges of raising antibodies to GPCRs are in obtaining a suitable antigen/epitope. GPCRs are often expressed at low levels in cells; the largest portion of the GPCR which might present a viable option for epitope structure is embedded in the lipid bilayer, and once the protein of interest is purified their 3D structures are unstable. Subsequently, antibodies generated may be specific for antigens of partially misfolded or altered structures. An accumulation of such challenges means that selection of GPCR antibody should not be taken lightly, particularly when the research of interest is receptor sub-type specific (Hutchings, Koglin, & Marshall, 2010).

To address this challenge, whole eGFP-GHSR reporter mice brains were used to determine GHSR expression (a kind gift from Dr Zane Andrews, Monash University, Australia). Whole brains were processed for immunohistochemistry to investigate the expression and co-localization of the eGFP-tagged ghrelin receptor with dopaminergic (TH^+) and A9 sub-type ($Girk2^+$) neurones in the mouse SNpc. A specific antibody raised against eGFP was used to localize GHSR in the mouse SNpc.

Characterization of GHSR expression in SN4741 cells was carried out using an antibody directly against an extracellular portion (2^{nd} loop, amino acid residues 197-

207 of the rat GHSR (Alomone Labs). Two transcript variants of GHSR are expressed: GHSR1a and GHSR-1b. GHSR1a excises an intron and encodes a functional protein, the receptor for the acyl-ghrelin ligand in turn a pathway for growth hormone release is defined. GHSR-1b retains the intron and thus does not bind to acyl-ghrelin. By decreasing the cell surface expression of GHSR1a, GHSR-1b also acts as a repressor for GHSR1a activity. GHSR-1b contains 298 amino acids corresponding to the first 5 TMDs encoded by exon 1 of the GHSR gene, therefore the antibody is not specific to either GHSR1a or -1b and so will bind to both receptors (Yin, et al., 2014). Therefore, it must be considered that any immunoreactivity observed is due to the presence of GHSR1a and/or GHSR-1b. To define the expression of AGs endogenous receptor, GHSR1a, in the SN4741 cells we will also collect protein and perform a Western blot using a GHSR1a-specific antibody. To study and characterise the SN4741 cell line, cells were grown under standard growth conditions (see methods) prior to fixation for immunocytochemistry or cell lysis for RNA/protein extraction for subsequent polymerase chain reaction (PCR)/Western blotting.

2.2. Aims

As little is known about ghrelin-axis protein expression in the mid-brain, in this chapter we will characterise;

- The expression of ghrelin axis acylation and de-acylation proteins, GOAT and APT-1, in the adult Sprague Dawley rat midbrain;
- The immunoreactivity of TH in the Sprague Dawley rat SNpc.
- The expression of GHSR in TH^+ and $Girk2^+$ positive mouse SNpc neurones; and
- The protein expression of the GHSR, GOAT, APT-1, TH, Girk2 & Calbindin immunoreactivity in the SN4741 mouse midbrain derived cell line.

2.3. Methods and Materials

2.3.1. Nickel 3, 3'-diaminobenzidine (DAB) Immunohistochemistry

2.3.1.1. Nickel (3, 3'-diaminobenzidine) DAB

DAB (3,3'-diaminobenzidine) is oxidized in the presence of peroxidase and hydrogen peroxide resulting in the deposition of an alcohol-insoluble precipitate at the site of enzymatic activity. DAB (3, 3'-diaminobenzidine) is commonly used in immunohistochemistry as the reaction product is insoluble, stable and not light sensitive so stained samples may be preserved for extended periods of time without losing sensitivity and quality of prepared tissue samples. DAB reaction is also applicable for Western blot visualisation.

2.3.1.2. Preparation of Nickel DAB (3, 3'-diaminobenzidine) Reaction Reagents

The nickel DAB solution was prepared by the mixing of 2 preliminary solutions using specific DAB designated equipment for health & safety purposes. Solution 1 was prepared in 100ml of 0.2M sodium acetate by dissolving 5g nickel sulphate, 400mg glucose and 80mg ammonium chloride. A second solution was prepared by dissolving 50mg DAB (3, 3'-diaminobenzidine) DAB in 100. Both solutions were then mixed together and aliquoted into 15ml centrifuge tubes and wrapped in foil to protect from light before storage in the freezer -20^{o}C.

Glucose oxidase (5mg/ml) is necessary for the nickel DAB reaction. This was prepared by dissolving 40mg of glucose oxidase in 8ml H_2O. 5mg/ml glucose oxidase solution was then pipetted into 500ul aliquots for storage at -20^{o}C.

2.3.1.3. Histology: Tissue Preparation for Nickel DAB Immunohistochemistry

The animal procedures described, including those involving genetically modified animals, were conducted in accordance with the UK Animals (Scientific Procedures) Act, 1986 (Dr T Wells' Project Licence: 30/2979) and the ARRIVE Guidelines, and were specifically approved by ethical review at Cardiff University. Rat age: 3 months Rat weight range: 212-250g. After rotational testing on day 35 rats were anaesthetised with sodium pentabarbitone (Euthetal), nose-anus length measured, and subjected to throracotomy. After withdrawal of a terminal blood sample by cardiac puncture, rats were killed by transcardial perfusion of 1.5% paraformaldehyde. After perfusion,

brains were excised, and post-fixed in 1.5% PFA overnight at 4°C. Sprague Dawley rat brains were mounted onto the Freezing microtome (*Microm HM 450)* (-30°C) with *JUNG-tissue fixing medium*® for coronal sectioning (30µm thick). Sectioned tissue was collected 1:6 in a labelled 12-well plate and immersed in PBS+0.2% Sodium Azide *(Sigma Aldrich).* The tissue sections were then stored at 4°C prior to immunohistochemical preparation.

2.3.1.4. Protocol for DAB Immunohistochemistry

All incubations and wash step from here on were carried out in CELLSTAR® 12-well plate [665180] (greiner bio-one, UK) at room temperature and with gentle agitation unless stated otherwise. Free-floating tissue sections were removed from storage conditions washed thoroughly (2 x 10 mins) in PBS (Sigma Aldrich) with gentle rocking/agitation at room temperature. PBS washes were removed prior to permeabilization of tissue sections using 0.03% Triton-x100 in PBS (0.03% PBS-T) for 10mins. Following permeabilization tissue sections are immersed in 1.5% H_2O_2 in PBS for 20 mins in order to remove endogenous peroxidase activity before being washed for another 2 x 10 mins in PBS and 1 x 10 mins in 0.03% PBS-T. Tissue sections were then blocked using 5% Normal Goat serum (5% NGS) (*Sigma Aldrich*) in 0.1% PBS-T for 60 min at room temperature to block non-specific binding sites. Excess block was then removed prior to application of a primary antibody diluted in 2% NGS in PBS-T and incubation at 4°C, overnight (approx. 16-24hrs). Primary antibody stained sections were then washed another 2 x 10 mins in PBS and 1 x 10 mins in 0.03% PBS-T before a 70 minute incubation with biotinylated secondary antibody raised in goat with gentle agitation at room temperature whilst being protected from light. All steps from here onwards are carried out with minimum exposure to light as the sample is now light sensitive until the final oxidation reaction occurs and DAB precipitate has formed. Again, the sections were washed 2 x 10 mins in PBS and 1 x 10 mins in 0.03% PBS-T prior to incubation with VECTASTAIN®Elite® ABC Kit [PK-6100] (Vector laboratories, UK) ABC solution (a mix of 0.4% reagent solution A and 0.4% reagent solution B in 0.1% PBS-T). The VECTSTAIN®Elite® uses preformed Avidin and Biotinylated enzyme complexes to give a reproducible staining method which relies on the form and amount of active enzyme molecules within the reagents. ABC solutions A (Avidin DH solution) & B (biotinylated enzyme) were pre-mixed in 0.1% PBS-T for 30mins, making-up the ABC solution prior to its addition to sample tissues for 90mins. ABC solution was then removed and the tissue sections were washed 2 x 10mins in PBS before a final wash 10 minute wash in 0.1M

sodium acetate pH 6.0. Excess sodium acetate solution was then removed prior to initiating the DAB reaction by mixing 1ml Nickel DAB solution with 60ul of glucose oxidase solution (5mg/ml) in the presence of tissue sections. This reaction was performed in the following way:

1ml of Nickel DAB solution was pipetted into a well of a corner of a weighing boat and 60ul of glucose oxidase was pipetted adjacently but were not mixed. A fine-tipped painting bush was used to transfer tissue sections into the 1ml of DAB solution immediately prior to the mixing with glucose oxidase. The plate was then swirled (3-4 times) to ensure solutions were thoroughly mixed prior to gentle rocking/agitation for nickel DAB staining to develop.

Once sufficient Nickle DAB staining had developed, a paint brush was used carefully to transfer tissue sections from the DAB-glucose oxidase reaction solution into to PBS and washed twice for 10 mins in PBS. This reaction was also performed in a 12-well plate. This method was preferred as tissue section were easier to retrieve from the well of a 12-well plate rather than a weighing boat. This reduced the extent of mechanical sheering of precious sample tissue once sufficient stain had developed.

2.3.1.5. DAB immunohistochemistry: Tyrosine hydroxylase (TH)

Tissue Sections were incubated with the primary antibody, rabbit anti-TH [ab6211] (1:500, Abcam®, UK). Following this incubation, excess 1◦ antibody was removed and tissues were washed thoroughly and incubated in complementary 2◦ antibody, Biotinylated Goat Anti-Rabbit IgG Antibody (Vector Laboratories [BA-1000).

2.3.1.6. DAB immunohistochemistry: LYPLA1, or acyl-protein thioesterase 1 (APT-1)

Tissue Sections were incubated with the primary antibody, rabbit anti-Lysophospholipase-1 [ab91606] (1:1000, Abcam®, UK). Following this incubation, excess 1◦ antibody was removed and tissues were washed thoroughly and incubated in complementary 2◦ antibody, Biotinylated Goat Anti-Rabbit IgG Antibody [BA-1000] (1:500, Vector Laboratories).

2.3.1.7. DAB Immunohistochemistry: Ghrelin-O-Acyl-Transferase (GOAT)

Tissue Sections were incubated with the primary antibody, rabbit anti-GOAT [H-032-12] (1:2000, Phoenix Pharmaceuticals.Inc). Following this incubation, excess 1◦ antibody was removed and tissues were washed thoroughly and incubated in complementary 2◦ antibody, Biotinylated Goat Anti-Rabbit IgG Antibody [BA-1000] (1:500, Vector Laboratories).

Table 3: Table of primary and secondary antibodies used in Nickel DAB Immunohistochemistry

Target	Primary antibody	Primary antibody concentration in PBS-T (0.1%)	Secondary antibody	Secondary antibody concentration in PBS-T (0.1%)
Tyrosine Hydroxylase	rabbit anti-TH [ab6211] (Abcam®, UK)	1:500	Biotinylated Goat Anti-Rabbit IgG Antibody [BA-1000] (1:500, Vector Laboratories).	1:500
LYPLA1 Or APT-1	Rabbit anti-Lysophospholipase-1 [ab91606] (1:1000, Abcam®, UK).	1:1000	Biotinylated Goat Anti-Rabbit IgG Antibody [BA-1000] (1:500, Vector Laboratories).	1:500
GOAT	Rabbit anti-GOAT [H-032-12] (1:1000, Phoenix Pharmaceuticals.Inc).	1:2000	Biotinylated Goat Anti-Rabbit IgG Antibody [BA-1000] (1:500, Vector Laboratories).	1:500

2.3.1.8. Sample Dehydration, Delipidation and Slide Preparation

Following 2 x PBS washes tissue sections were suspended in TBS (*Sigma Aldrich*) filled petri dish. The tissue sections were mounted onto SuperFrost®Plus slides [25 x 75 x 1.0mm] (*VWR International LTD*) and allowed to dry overnight. Once dry, tissue samples underwent dehydration by submerging the slides in increasing concentrations of ethanol (70%, 90%, 100%, and 100 %) for 3 minutes each. Samples were then de-lipified by submerging slides in Histo-Clear [HS-200] (national diagnostics) twice for 3 minutes. Slides were removed from Histo-Clear and 50ul of Entellan® [107960] (MerckMillipore) was pipetted evenly over the slide prior to carefully lowering a MENZEL-GLÄSER 24 x 60mm glass coverslip (Thermo Scientific, Germany) to complete slide preparation. Sample slides were then left to dry prior to inspection via light microscopy.

2.3.1.9. Light Microscope Imaging

Examination and imaging of tissue sections was carried out on Nikon ELIPSE 50i light microscope.

2.3.2. Immunofluorescence

In order to identify key targets of interest, immunofluorescence (IF) was utilized to characterize cells in mouse SN brain sections and midbrain-derived cell line (SN4741) using immunohistochemistry (IHC) and immunocytochemistry (ICC) techniques, respectfully.

Primary antibodies were applied to all sections/cells, followed by addition of fluorescent-secondary antibodies. Primary antibody was omitted from negative controls.

2.3.2.1. Histology: Tissue Preparation for Immunohistochemistry

GHSR-GFP mouse brains were bisected: one hemisphere was selected and mounted onto the Freezing microtome (*Microm HM 450)* (-30◦C) with *JUNG-tissue fixing medium*® for coronal sectioning (30µm thick). Sectioned tissue was collected 1:6 in a labelled 96-well plate and immersed in PBS+0.2% Sodium Azide *(Sigma Aldrich).* The tissue sections were then stored at 4ºC prior to immunohistochemical preparation.

2.3.2.2. General Fluorescence Immunohistochemistry Protocol

Free-floating tissue sections were washed thoroughly (3x) in PBS *(Sigma Aldrich)* (5 min) with gentle rocking/agitation before permeabilization with 1ml of methanol *(Fisher Scientific)* at -20◦C (2min). Before staining tissue sections were then washed thoroughly (3x) in PBS and blocked using 5% Normal Goat serum (5% NGS) (*Sigma Aldrich*) for 2º antibodies raised in goat, or 5% Normal Donkey Serum (5% NDS) *(Sigma Aldrich)* and 0.1% Triton X-100 in PBS (0.1% PBS-T) for 60 min at room temperature to block non-specific binding sites. Excess block was then removed prior to application of primary antibodies and subsequent secondary antibodies, both diluted in 0.1% PBS-T. Primary antibody incubations were carried out overnight (approx.16-24 hours) at 4ºC. Subsequent secondary antibody incubations were carried out for 60 minutes at room temperature and protected from light. Dilutions of primary and secondary antibodies were prepared in 0.1% PBS-T prior to incubation with tissue sections.

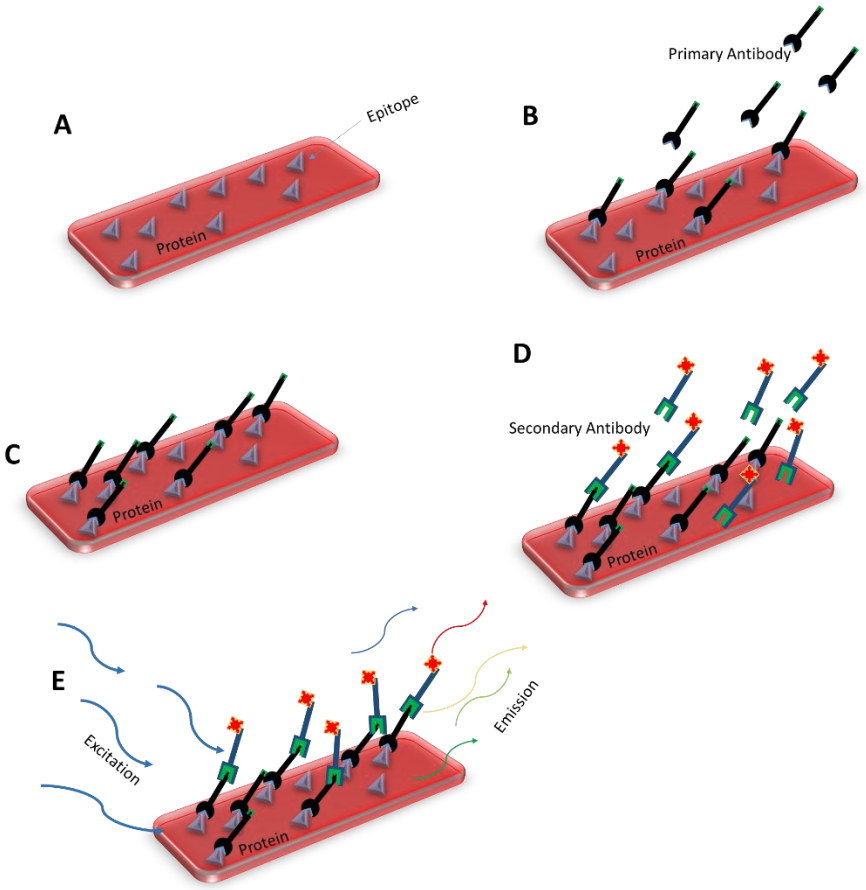

Figure 8: Illustration of Immunofluorescence Protocols.

(A) Primary antibody binds specifically to epitope of target protein on prepared samples. (B) Excess Primary antibodies are washed away leaving only specifically bound antibodies on target sites. (C) Samples are incubated with excess fluorescent-secondary antibody complimentary to primary antibody. Samples is then washed again to remove excess secondary antibodies leaving primary-secondary complex conjugated to target proteins. (D) Fluorescent probes are excited and give emissions at specific wavelengths of light.

2.3.2.3. Fluorescence Immunohistochemistry: Tyrosine Hydroxylase (TH)

Tissue sections were incubated with the primary antibody, TH [ab6211] (1:500, *Abcam*®). Following this incubation, excess 1◦ antibody was removed and tissues were washed thoroughly washed again in PBS (3x 5min) and incubated in complementary 2◦ Goat anti-rabbit AlexaFluo®568 [A11041] (1:500, Invitrogen molecular probes, Oregon, USA), for fluorescent staining.

2.3.2.4. Fluorescence Immunohistochemistry: GHSR-eGFP

Tissue sections were incubated with the primary antibody, Chicken anti-GFP [ab13970] (1:1000, Abcam®). Following this incubation, excess 1◦ antibody was removed and tissues were washed thoroughly and incubated in complementary 2◦ antibody, Goat anti-chicken AlexaFluo®488 [A-11039] (1:500, Invitrogen molecular probes, Oregon, USA) for fluorescent staining.

2.3.2.5. Fluorescence Immunohistochemistry: Girk2

Tissue sections were incubated with the primary antibody, Rabbit anti-Girk2 [APC-006] (1:200, Alomone Labs, Isreal). Following this incubation, excess 1◦ antibody was removed and tissues were washed thoroughly and incubated in complementary 2◦ antibody, Goat anti-rabbit AlexaFlour®488 [A-11034] (1:500, Invitrogen molecular probes, Oregon, USA), for fluorescent staining.

2.3.2.6. Fluorescence Immunohistochemistry: Calbindin

Tissue Sections were incubated with the primary antibody, Rabbit anti-Calbindin [ab108404] (1:50, Abcam®, UK). Following this incubation, excess 1◦ antibody was removed and tissues were washed thoroughly and incubated in complementary 2◦ antibody, Goat anti-rabbit AlexaFluo®568 [A11041] (1:500, Invitrogen molecular probes, Oregon, USA), for fluorescent staining.

2.3.2.7. Fluorescence Immunohistochemistry: TH & GHSR-eGFP co-localization

Tissue sections were incubated with the first primary antibody, TH [ab6211] (1:500, Abcam®). Following this incubation, excess 1◦ antibody was removed and tissues

were washed thoroughly and incubated in complementary 2◦ antibody, 2◦ Goat anti-rabbit AlexaFluo®568 [A11041] (1:500, Invitrogen molecular probes, Oregon, USA). Removal of excess 2° antibody was followed by another (x3) PBS wash (5min) and a 24hr incubated in the second 1◦ antibody, Chicken anti-GFP [AB13970] (1:1000, Abcam®). Following the removal of excess primary antibody, the tissues were thoroughly washed again in PBS (3x 5min) before the application of the final 2◦ antibody, Goat anti-chicken AlexaFluo®488 [A-11039] (1:500, Invitrogen), and incubated for fluorescent staining.

2.3.2.8. Fluorescence Immunohistochemistry: Girk2 & GHSR-eGFP + Girk2

Tissue sections were incubated with the first primary antibody, Rabbit anti-Girk2 [APC-006] (1:200, Alomone Labs, Isreal). Following this incubation, excess 1◦ antibody was removed and tissues were washed thoroughly and incubated in complementary 2◦ antibody, Goat anti-rabbit AlexaFluo®568 [A11041] (1:500, Invitrogen molecular probes, Oregon, USA). Removal of excess 2° antibody was followed by another (x3) PBS wash (5min) and 24hr incubation in the second 1◦ antibody, Chicken anti-GFP [AB13970] (1:1000 Abcam®). Following the removal of excess secondary antibody the tissues were thoroughly washed again in PBS (3x 5min) before the application of the final 2◦ antibody, Goat anti-chicken AlexaFluo®488 [A-11039] (1:500, Invitrogen), and incubated for fluorescent staining.

2.3.2.9. Slide Preparation and Analysis

Finally, excess final secondary antibody was removed and the tissue sections were thoroughly washed (x3) PBS (5mins) before being suspended in TBS (*Sigma Aldrich, Gillingham, UK*) filled petri dish. The tissue sections were mounted onto SuperFrost®Plus slides [25 x 75 x 1.0mm] (*VWR International LTD*) and allowed to dry. 50µl of prolong gold (Life Technologies) anti-fade mounting media was applied to the slides before a MENZEL-GLÄSER coverslip was placed upon it - ensuring that no air bubbles formed over the tissue sections - and allowed to dry. Examination and imaging of tissue sections was carried out on Fluorescent microscope *ZEISS Imager.M1* system with AX10cam HRM.

Table 4: Table of primary and secondary antibodies applied in fluorescence Immunohistochemistry

Target	Primary antibody	Primary antibody concentration in PBS-T (0.1%)	Secondary antibody	Secondary antibody concentration in PBS-T (0.1%)
GHSR-eGFP	Chicken anti-GFP [AB13970] (Abcam®, UK)	1:1000	Goat anti-chicken AlexaFluo®488 [A-11039] (Invitrogen molecular probes, Oregon, USA),	1:500
Tyrosine Hydroxylase	rabbit anti-TH [ab6211] (Abcam®, UK)	1:500	Goat anti-rabbit AlexaFluo®568 [A11041] (Invitrogen molecular probes, Oregon, USA),	1:500
Calbindin	Rabbit anti Calbindin ab108404 (Abcam®, UK)	1:50	Goat anti-rabbit AlexaFluo®568 [A11041] (Invitrogen molecular probes, Oregon, USA)	1:500
Girk2 (Anti-Kir3.2 antibody)	Rabbit anti-Girk2 [APC-006] (Alomone Labs, Isreal)	1:200	Goat anti-rabbit AlexaFlour®488 [A-11034] & AlexaFluo®568 [A11041] (Invitrogen molecular probes, Oregon, USA)	1:500

2.3.3. Fluorescence Immunocytochemistry (ICC)

2.3.3.1. SN4741 Cells Sample Preparation for ICC

SN4741 cells were seeded at 3000/well into a 96-well plate Corning® Costar® 3596 flat-bottom cell culture plate (CLS3596 SIGMA), and incubated for 24hrs (37◦C, 5% CO2) to allow SN4741 cells to adhere. Cells were then washed once with 200ul PBS and fixed with 100ul 4% paraformaldehyde (PFA) (15mins). 4% PFA was then removed and the SN4741 cells were washed (3x) in 100ul PBS. Following the removal of the final PBS wash, cells are ready to be used or can be stored at 4ºc prior to beginning ICC protocol.

2.3.3.2. Protocol for ICC

PBS submerging the cells was removed and cells were blocked at room temperature using 5% Normal Donkey Serum (5% NDS) (Sigma Aldrich, St Louise, USA) for 60 min. Excess block was removed and 1◦ antibody was applied to cells for 24 hours at 4◦C. Excess 1◦ antibody was removed and cells were washed (x3) in PBS (5min). 2◦ antibody was then applied and left to incubate in the dark for 60min. Removal of excess antibody was then followed by another (x3) PBS wash (5min). Cells were stored in the final PBS wash at 4ºC prior to fluorescence imaging of samples. See table 2 for a details on primary and secondary antibodies utilized.

2.3.3.3. Fluorescence Microscope Imaging of Samples

Immuno-reactive SN4741 samples were examined using Olympus IX51 inverted fluorescence microscope powered by PRIOR Lumen 200 and In Cell Analyser 2000 HCA system (GE Healthcare).

Table 5: Table of Primary and Secondary Antibodies used in Immunocytochemistry.

Target	Primary antibody	Primary antibody concentration in PBS-T (0.1%)	Secondary antibody	Secondary antibody concentration in PBS-T (0.1%)
Tyrosine Hydroxylase	Rabbit anti-Tyrosine Hydroxylase [ab6211] (1:1000, Abcam®).	1:1000	Donkey anti-rabbit AlexaFluo®488 [A11041] (Invitrogen molecular probes, Oregon, USA)	1:500
GHS-R (Anti-Ghrelin Receptor (extracellular))	Rabbit anti-GHS-R [AGR-031] (Alomone Labs, Isreal)	1:1000	Donkey anti-rabbit AlexaFluo®488 [A11041] (Invitrogen molecular probes, Oregon, USA)	1:500
Girk2 (Anti-Kir3.2 antibody)	Rabbit anti-Girk2 [APC-006] (Alomone Labs, Isreal)	1:200	Donkey anti-rabbit AlexaFluo®488 [A11041] (Invitrogen molecular probes, Oregon, USA)	1:500
Calbindin	Rabbit anti-Calbindin [ab108404] (Abcam®, UK)	1:50	Donkey anti-rabbit AlexaFluo®488 [A11041] (Invitrogen molecular probes, Oregon, USA)	1:500

2.3.4. Western Blot

2.3.4.1. Protein Extraction and Estimation from SN4741 Cells

50,000 SN4741 cells were seeded into 6 well Greiner CELLSTAR® culture plates (M8562, SIGMA) and incubated in routine SN4741 cell culture media at 37ºC, 5% CO2 until cells were 80% confluent (~48hrs). Cell culture media was then removed and the cells were washed 2x in cold PBS. PBS wash was then removed and 125ul lysis buffer (50ml lysis buffer was prepared containing: 2.5ml 50mM Tris HCl, pH 7.5; 1.5ml 150mM NaCl; 0.5ml/1% of IGEPAL [I8896, SIGMA]; 0.5% sodium deoxycholate (DOC); 0.1% SDS; 45.5ml dH_2O) containing 1% protease inhibitor cocktail was pipetted into the wells. Using a syringe plunger, the cells were scraped from the well surface. Contents of the well were then transferred to a 0.6ml micro-centrifuge tube on ice. Another 125ul of lysis buffer was added to the same well and the process was repeated. Contents were mechanically homogenized by passing through a 25G needle 10 times. Homogenate was left on ice for 15 mins prior to centrifugation at 14,000 RPM to remove the cellular debris from protein. Following centrifugation 20ul and ~200ul of protein containing supernatant was collected carefully as to not disturb the pelleted cellular debris. To prepare protein samples for gel electrophoresis ~200ul supernatant was mixed 1:1 with Laemmli Lysis-Buffer [DTT, 400mM; Glycerol, 20%; SDS, 4%; TRIS, 0.125M] (38733, SIGMA) and briefly vortexed. Protein samples were left to denature at room temperature for 1hr before being stored at -20ºC and being thawed out prior to use.

Table 6: General Ratio of Lysis Buffer to Size of Cell Culture Vessel.

Plate	Volume of Lysis Buffer (µl)
35mm	250
60mm	500
100mm	1000

Estimation of protein sample concentrations were carried out using the absorption-based Pierce™ BCA Protein Assay Kit (23227, Thermo Scientific). A standard curve of known protein concentrations (0.0, 0.1, 0.2, 0.4, 0.6, 0.8 & 1.0 ug/ul) was generated using Albumin Standard (23209, Thermo Scientific). Blanked sample concentrations were calculated by extrapolation against the BSA standard curve.

2.3.4.2. General Western Blot Protocol

Preparing SDS-PAGE Gel: Glass gel molding plates were washed with tap and distilled water prior to a final 70% ethanol before use. Molding plates were then placed into a gel casting frame and clamped shut using a spacer to ensure liquid-tight seal. Seal was ensured by filling the area between molding plates with d.H_2O and visual checking for leakage. 10ml (per gel) of the required acrylamide running gel was then prepared to the required percentage of acrylamide (see *table 7*) and pipetted into a sealed glass mold.

Table 7: Acrylamide Gel Preparation Reagents

Reagent	**7.5%**	**10%**	**12%**	**15%**
Water	5 ml	4.2 ml	3.5 ml	2.5 ml
4x Tris and SDS	2.5 ml	2.5 ml	2.5 ml	2.5 ml
30% acrylamide	2.5 ml	3.3 ml	4 ml	5 ml
APS	1 small spatula	1 small spatula	1 small spatula	1 small spatula
TEMED	10 µl	10 µl	10 µl	10 µl

Polymerizing reagents, APS and TEMED, were added immediately prior to casting. Following the transfer of running gel into a glass casting mold, water-saturated butanol was gently pipetted on top of the gel to ensure a smooth, even gel edge. Running gel was then left to set for approximately 30 mins. Water-saturated butanol was poured away and the gel edge was rinsed 4 times with d.H2O. A stacking gel (3ml) was then prepared (see table 8) and poured on top of the running gel before a well-comb was inserted.

Table 8: Stacking Gel Reagents

Water	1.75 ml
4x Tris and SDS	0.75 ml
30% acrylamide	0.5 ml
APS	Half Spatula
TEMED	3 µl

After approximately 20 mins the comb was removed and excess un-polymerized acrylamide was washed away with $d.H_2O$. Casting plates were then removed from casting frame and inserted into the Mini-PROTEAN® Tetra System (Bio-Rad) electrode assembly clamping frame. Two gels were used per frame. In the absence of a second gel, a buffer dam was used. Once the clamping frame was placed into the Mini Tank the central reservoir was then filled with running buffer. A protein marker (5ul) and samples were then added to casted wells according to maximum volume or protein concentration before PowerPac Basic (Bio-Rad) was attached to the electrode assemble and run at 200 (Volts) V for 40 mins or until protein bands have sufficiently resolved.

Semi-dry membrane transfer: a piece of Polyvinylidene difluoride PVDF membrane (1620177, Biorad.) was washed in methanol for 30 secs, then water for 2 mins before incubation in transfer buffer (5 mins). At the same time the SDS-PAGE gel was released from its clamping frame and casting mold and placed into transfer buffer (5 mins). Both were placed on rocker for gentle agitation (30 RPM). At this time 2 pieces of Criterion™ size Extra Thick Blot (filter) Paper (1703967, Bio-Rad) were submerged in transfer buffer. A piece of filter was placed onto an opened cassette from the Trans-Blot® Turbo™ Transfer system (Bio-Rad) and rolled out to eliminate air bubbles. PVDF membrane followed by SDS-PAGE gel was then placed on top of the filter paper. The second piece of filter paper was then placed onto the transfer stack and rolled again (See figure 2 for transfer stack illustration). The cathode plate-containing lid of the transfer cassette was then placed onto the transfer stack and locked closed by engaging the latched with a clock-wise turn of the lids dial. The transfer cassette was then re-introduced into the main unit of the transfer system and transfer was initiated for 75 mins at 15V.

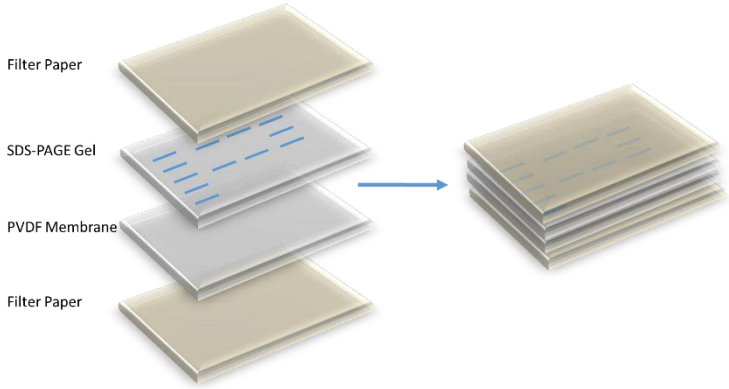

Figure 9: Stack preparation for SDS-PAGE gel to PVDF membrane protein transfer.

All components are soaked in transfer buffer and placed into transfer cassette as seen above (figure 9). Filter paper, PVDF membrane, SDS-PAGE gel and finally filter paper. The stack is rolled out a final time to remove any air bubble before transfer cassette lid is close and locked into place.

Visualization of proteins on PVDF membrane: Following protein transfer into the PVDF, SDS-PAGE gel and filter papers are removed and PVDF membrane is placed in Penceau red stain. PVDF membranes are placed into Penceau red and shaken until protein bands are visible on the blotting paper. Penceau stain was then recycled and water was added to the blot membrane which was subsequently labeled with pencil and cut into band regions of interest using scissors. Blotting paper was then washed in TBS-Tween20 with mild agitation for approximately 5 mins to remove pink/red colour from blotting paper.

Membrane blocking: 5% non-fat milk (NFM) blocking buffer solution was prepared in TBS-Tween20 by dissolving 1.25g of NFM powder in 25ml of TBS-Tween20. PVDF membrane was placed in a plastic dish and incubated in blocking buffer on a shaker for 1hr at room temperature or overnight at 4^{o}C.

Primary and secondary antibody incubation: Blocking buffer was removed and blots were incubated with 1.5ml primary antibody (see *table 7* for antibody dilutions) between 2 plastic sheets sealed with CaiTronic (heat mechanism). Plastic bags were checked for leaks before being placed in a TBS-Tween20 filled vessel for 1-2hr

incubation at room temperature or overnight at 4^{o}C. Following incubation, the sealed bag was opened and primary antibody was collected for re-use (3 times). Blotting membrane was then washed 5x in TBS-Tween20 - 5 mins for each wash. PVDF membranes were then incubated with secondary antibody diluted in blocking buffer (1:2500) between CaiTronic-sealed plastic sheets. Plastic bags containing blots and secondary antibody were placed in a TBS-Tween20 containing vessel and incubated at room temperature for 1-2hr on a rocker. Following incubation, secondary antibody was discarded and the blot was washes again 5 times for 5 mins in TBS-Tween20 with mild agitation.

Blot Development and Visualisation- Enhanced Chemi-luminescence (ECL): ECL solution was prepared by the 1:1 mixing of the 2 reagents (Peroxide Solution and Luminol Solution) from the Amersham^{TM} ECL Select^{TM} Western Blotting Detection Reagent (RPN2235, GE Healthcare) and protected from direct light. Blots were incubated face-down in ECL solution for 1 minute on a flat plastic case before being positioned face-up for visualisation on the ChemiDoc XRS (Bio-Rad) tray using Quantity One Basic Software. Following visualisation and acquisition of pictures at a range of exposure times, the images were transformed using 'AutoDisplay' Quantity One software feature and saved. Blots were stored at 4^{o}C in TBS-Tween20 should they need to be stripped and re-probed for another protein target.

Stripping and re-probing: Blots destined for stripping and re-probing was removed from 4^{o}C and placed in TBS-Tween20 for 10 mins at room temperature. To strip, blots were then sealed (CaiTronic) between 2 plastic sheets with 1.5ml Restore^{TM} PLUS Western Blot Stripping Buffer (46430, Thermo Scientific). Once sealed, bags were placed in a TBS-Tween20 containing vessel and incubated at room temperature for 15-20 mins on a rocker. Following this incubation the stripping buffer discarded and the blots were washed twice in fresh water for 1 minute and once inTBS-Tween20 for 5 mins on a shaker. To re-probe, steps '*Membrane Blocking'* through '*Blot Development and Visualisation- Enhanced Chemi-luminescence (ECL)'* were repeated with adjustments to primary and secondary antibodies.

Table 9: Table of Primary and Secondary Antibodies used in Western blot

Target	Primary Antibody	Dilution	Secondary Antibody	Dilution
GHSR1a 41kDa	Goat anti GHSR1a (F-16) Sc-10359, Santa Cruz	1:200 In 5% NFM	Anti-goat IgG-HRP linked in 5% NFM	1:2500 In 5% NFM
LYPLA1 25kDa	Ab91606, Abcam	1:5000 In 5% NFM	Anti-Rabbit IgG, HRP-linked Antibody (7074S, Cell Signaling Technology) in 5% NFM	1:2500 In 5% NFM
MBOAT4 50kDa	Rabbit anti-MBOAT4	1:500 In 5% NFM	Anti-Rabbit IgG, HRP-linked Antibody (7074S, Cell Signaling Technology) in 5% NFM	1:2500 In 5% NFM

2.3.5. Endpoint / Semi-Quantitative PCR

2.3.5.1. General Endpoint/Semi-Quantitative PCR Protocol

End-point/ semi-quantitative PCR was carried out to investigate GHS-R1a, LYPLA1 and MBOAT4 (encodes for ghrelin acylation enzyme, GOAT) mRNA expression in SN4741 cell line.

RNA extraction: 50,000 SN4741 cells were seeded into 12 well-plate (150628, NUNC™) and incubated overnight at 37ºC, 5% CO_2,Total RNA was isolated from SN4741 cell line using NORGEN Biotek corp. RNA/Protein Purification Kit (NORGEN, Canada (Cat#23500) with on-column DNA digestion by the deoxyribonuclease according to the manufacturer's instructions. Purity and concentration of RNA extracts are subject to Nanodrop® ND 8000 8-sample spectrophotometer (Thermo Scientific) readings. RNA was stored at -80°C for future cDNA synthesis. *cDNA Synthesis*: Four micrograms of the total RNA were reverse transcribed using superscript III RT (Life Technologies) in a total reaction volume of 20µl. 0.5µl of the resulting cDNA was used for endpoint PCR. PCR amplifications were performed with primers listed in the table below and Promega (USA) GoTaq® Green Master Mix [cat. #M7111]; following manufacturer's instructions. DNA sample were then stored at -20ºC. PCR reaction was performed in Bio-Rad T100 Thermal cycler PCR System (BioRad, Herefordshire, UK) PCR was performed with the primers and ladder in table 10.

Preparation of agarose electrophoresis gel: using UltraPure™ agarose (16500-100, Thermo Scientific) electrophoresis gels were prepared at desired concentration for DNA resolution. See table 11 for agarose ratio to resolution range for 50ml gel. Desired weight of agarose is mixed with 50ml 1x Tris/Acetic Acid/EDTA (TAE buffer) (prepared from 50x TAE #1610743EDU, Bio-Rad) and swirled to evenly distribute in a glass conical flask. TAE-agarose mixture was then microwaved for 1.5 mins until all agarose powder had dissolved. Molten agarose gel solution was then cooled to approximately 60ºC before 5ul (1:10,000 dilution) of SYBR®Safe DNA gel stain (S33102, Invitrogen) was added and swirled through the liquid. Stoppers and well combs were then put into place prior to pouring the molten agarose gel into a cast laying in a Life Technologies Horizon 58 PCR electrophoresis tank (41060039, Labrepco). Air bubbles were swiftly removed using a pipette before the gel was cooled and set.

Table 10: Table of Forward (Sense) and Reverse (Anti-Sense) Primer Sequences used in PCR.

Target	Forward primer sequence 5'→3'	Reverse primer sequence 5'→3'	Predicted Amplicon size (bp)
mGHSR1a (Europhins)	CTCCGATCTGCTCATCTTCC	CCACAGCAAGCATCTTCACTG	539
mBOAT4 1 (kirchner) (Europhins)	ACCCGGGCCAGGTACCT	ACCCATGGCAGCAAAAGC	63
LYPLA1 (Europhins)	GCAGCAGAAACCGTAAAAGC	GGCACTGGACGGAAATA	235 or 133
Ladder [*Bioline*® Hyper Ladder IV]	N.A	N.A	1000, 900, 800, 700, 600, 500, 400, 300, 200, 100 bp marker

PCR agarose gel electrophoresis: combs and stoppers were removed from solidified gel before being submerged in 1x TAE buffer. 10ul DNA base-pair (bp) standard ladder (NO467G or NO468G, New England Bio-labs) and 5ul of cDNA samples were pipetted into wells. A lid containing electrodes was placed on the electrophoresis tank and power supply (BioRad) was set at 100V for 30 mins. Following electrophoresis gels were visualized under UV using the Chemidoc XR (1708265, BioRad) and analysed using Quantity One software. DNA bound to SYBR®Safe DNA stain appears bright white under UV light.

Table 11: Ratio of Agarose Percentage to Agarose Electrophoresis Gel Resolution Range

Agarose Concentration	Resolution Range	Weight of Agarose for 50ml gel
0.8%	500bp-12kb	0.4g
1.0%	400bp-10kb	0.5g
1.5%	200bp-4kb	0.75g
2.0%	100bp-2kb	1.00g
4.0%	10bp-400bp	2.00g

2.3.6. General SN4741 Mouse Midbrain Derived Neuronal Cell Line Cell Culture

SN4741 are an immortalized mouse midbrain derived cell line (Son et al., 1999) from Fred Gage's lab in the 1990's

2.3.6.1. SN4741 Cell Revival

SN4741 cell were revived from liquid nitrogen storage. Cell name, date and passage were noted. Frozen cryovials were thawed by swirling 37ºC water bath until only a small amount of ice remains. Using a P1000, content of the thawed cryovial were placed into a T75 cell culture flask containing 18ml of pre-warmed SN4741 cell culture medium (High-glucose (4.5g/L) DMEM supplemented with 10% filtered FBS, 1% PenStrep, 1% (100x) L-glutamine and 3% glucose (20% solution in d.d.H_2O). The flask was then gently swirled to ensure even distribution of SN4741 cells. T75 flask containing cells was incubated at 37ºC, 5%CO_2 overnight (approx.16hrs). This allows the SN4741 (which are an adherent) cell line to settle to the floor of the culture vessel and become attached. The following day SN4741 cell culture media was removed, cells were washed 1x in 10ml PBS before 18ml fresh media was transferred into the flask. Cells were routinely passaged or cryo-frozen for a future date once they became 80-90% confluent. Confluency refers to the approximate percentage of the cell culture vessel which is covered in cells. i.e. The floor of a 100% confluent flask has a complete monolayer covering of cells. Whereas a 0% confluent cell culture vessel or flask has no cells. Sterile technique was maintained throughout this procedure and other cell culture practice to ensure sterility where possible.

2.3.6.2. Seeding SN4741 Cells in Preparation for Experiment

In order to seed cells for an experiment, cell culture media was removed and the SN4741s were washed 1x with 10ml PBS. PBS was removed and 4ml 1xTrypsin/EDTA is pipetted into the culture flask before placing the T75 into a cell culture incubator at 37ºC, 5%CO_2 for 5 mins. After 5 minutes T75 flasks were removed and inspected under a light microscope to ensure cell detachment. If cells were not fully detached a gentle tap was given to dislodge the remaining loosely-adhered SN4741s. Using a 10ml pipette cell/Trypsin/EDTA solution was taken up and expelled 5-10 time to produce a single-cell suspension prior to neutralization of Trypsin/EDTA with 6ml of SN4741 cell culture medium. Contents of the flask were then pipetted up and down another 5-10ml for thorough mixing. A 20ul solution of 1:1 cell suspension and trypan blue was subsequently prepared to quantify percentage (%) cell viability.

Cell viability was determined and the number of cells required for an experiment were seeded into experimental vessel of choice depending on downstream application. Prepared cells were returned to standard culture conditions (cell culture incubator at 37^{o}C, 5%CO_2 for 5 mins).

2.3.6.3. Sub-Culturing SN4741 Cells from 80-90% Confluent T75 Flask

- Add 0.5ml of SN4741 cell suspension to 19.5ml cell culture medium→80-90% confluent in 4 days.
- Add 1ml of SN4741 cell suspension to 19ml cell culture medium→ 80-90% Confluent in 3 days
- Add 2ml of SN4741 cell suspension to 18ml cell culture medium→ 80-90% Confluent in 2days
- Add 3ml of SN4741 cell suspension to 17ml cell culture medium→80-90% Confluent in approx. 24hrs.

Every 2-3 days cell culture media was removed and cells were washed (PBS) before replenishment of culture vessel with fresh medium. Label all flasks and experimental plates.

Preparation of SN4741 cell stocks

Table 12: Cryopreservation Medium Reagents

Cryopreservation Medium			
Reagents	**FBS**	**DMSO**	**SFM (serum free medium)**
Volume	12.5ml	5ml	32.5ml
Ratio	2.5	1	6.5

SN4741 cell culture medium was removed from an 80-90% confluent culture flask and cells were washed 1x in 10 ml PBS before addition of Trypsin/EDTA (4ml) and a 5 minute incubation in general cell culture conditions. Once cells had detached a 10ml pipette was used to create a single cell suspension (almost no clumps of cells) and the cell suspension was placed in a 50ml tube. The cell suspension was then centrifuged at 300 xg for 5min at room temperature to form a cell pellet. Supernatant/Medium was carefully removed as not to disturb the pelleted cells. Cell

pellet was re-suspended in 1-2 ml of cryopreservation medium. Quickly, re-suspension was transferred into a cryovial labelled with cell type, date, passage and name and placed into a Nalgene™ (bottom contains Isopropanol) container and transfer to -80ºC freezer. After 24hrs the cryovial was transferred into liquid nitrogen. Note was made of the deposit.

2.4. Results

2.4.1. Immunohistochemistry: Tyrosine Hydroxylase

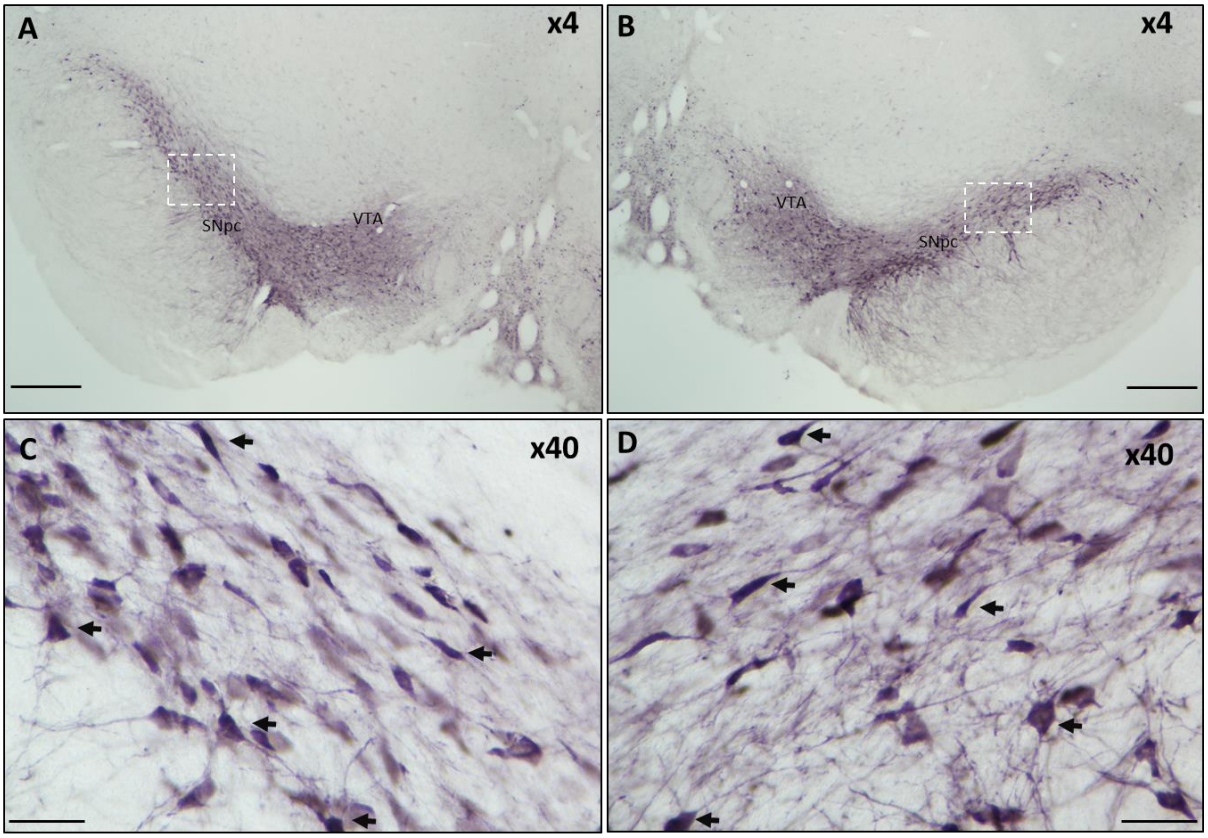

Figure 10:Tyrosine Hydroxylase (TH) is Expressed on Adult Rat Midbrain SNpc and VTA Neurones

Images of right (A) and left (B) hemisphere at x4 magnification demonstrates TH immunoreactivity in the SNpc. White dashed boxed areas in (A) and (B) highlight the SNpc regions which are displayed as x40 magnification in (C) and (D). (C) and (D) represent left and right hemisphere SNpc, respectively. Black arrows highlight TH^{+}ve SNpc neurones Scale bar; 500 µm (in A & B), 50 µm (in C & D). VTA, ventral tegmental area; SNpc, substantia nigra pars compacta.

2.4.2. DAB Immunohistochemistry: Acyl-Protein Thioesterase 1 (APT-1)

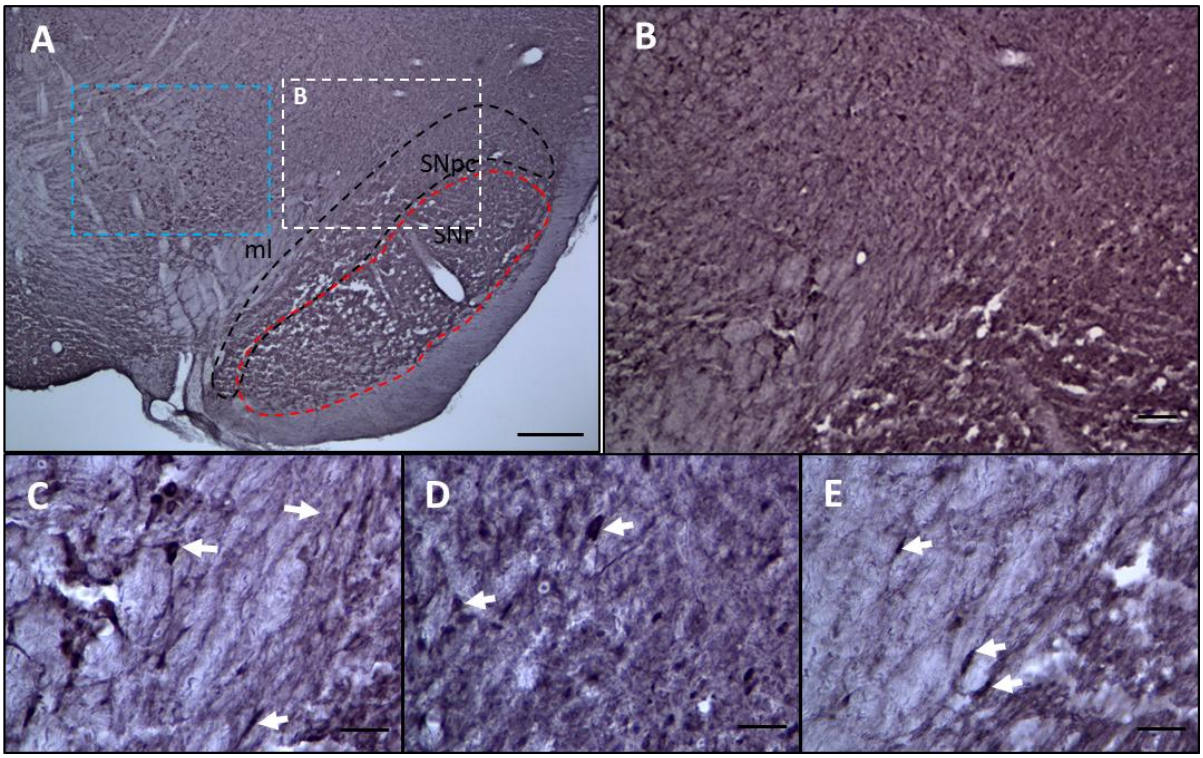

Figure 11: APT-1 is expressed on adult rat midbrain SNpc.

Adult male Sprague Dawley rats express APT-1 immunoreactivity on mid-brain SNpc & red nucleus neurones.. Image (A) demonstrates APT-1 immunoreactivity in rat midbrain regions including the SNpc at x4 magnification. Dashed blue box (in A) outlines region containing APT-1 $^{+}$ve neurones in the red nucleus. White dashed boxed region (in A) shows the area of x10 magnification image of SNpc-SNr cross section (B). C, D & E show x40 magnification images of APT-1^{+}ve neuones in the SNpc. Dashed black and red lines outline SNpc and SNr, respectively in x4 magnification image (A). White arrows seen in x40 images of SNpc (C, D and E) mark examples of APT-1 $^{+}$ve SNpc neurones. Scale bar; 500 µm (in A), 100 µm (in B), 50 µm (in C, D & E). SNpc, substantia nigra pars compacta; SNr, Substantia Nigra pars reticulata; ml, medial lemniscus.

2.4.3. DAB Immunohistochemistry: Ghrelin-O-Acyl-Transferase (GOAT)

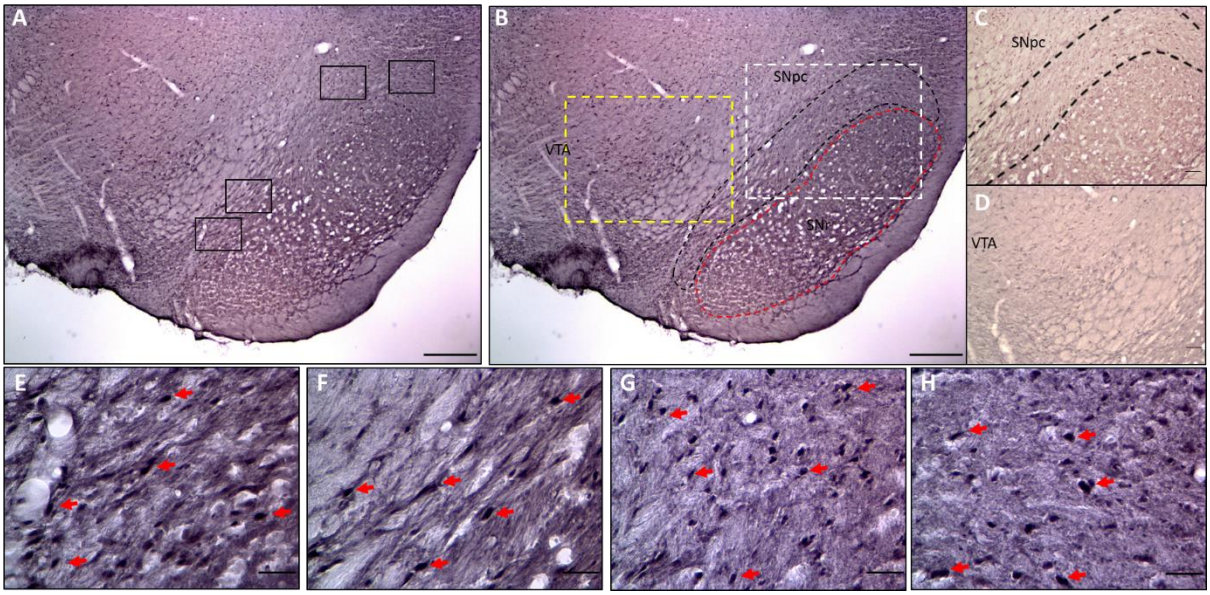

Figure 12:Ghrelin-O-Acyl-Transferase (GOAT) is expressed on adult rat midbrain SNpc and VTA neurons.

Adult male Sprague Dawley rats express GOAT immunoreactivity on mid-brain SNpc & VTA neurones. Image (A) demonstrates GOAT immunoreactivity in rat SNpc & VTA at x4 magnification. Solid black line boxed regions (in A) along the SNpc denote areas of x40 magnification images (E, F, G & H). Dashed Black and red lines outline SNpc and SNr, respectively in x4 magnification image (B). Whereas the dashed white and dashed yellow boxes (in B) highlight the location of x10 magnification images of SNpc (C) and VTA (D). Red arrows seen in x40 images of SNpc (E, F, G and H) mark examples of GOAT +ve SNpc neurones. Scale bar; 500 µm (in A & B), 100 µm (in C & D), 50 µm (in E, F, G & H). VTA, ventral tegmental area; SNpc, substantia nigra pars compacta; SNr, Substantia Nigra pars reticulata.

2.4.4. Fluorescence Immunohistochemistry: Tyrosine Hydroxylase + GHSR-eGFP Co-localization

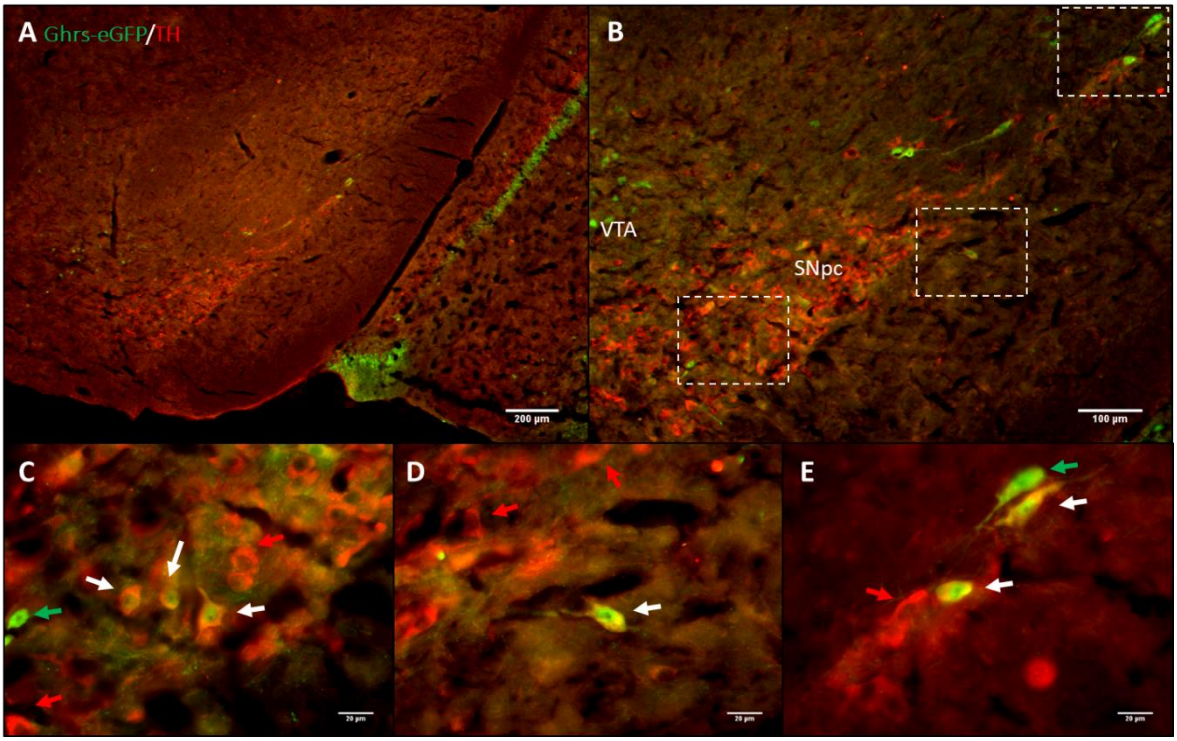

Figure 13: Ghrelin Receptor is Expressed on TH+ Cells in Adult Mouse Midbrain.

Adult male GHSR-eGFP mice co-express eGFP (green) and TH (red) in mid-brain SNpc neurones. (A) x4 and (B) x10 magnification images demonstrate TH^+/GHSR-$eGFP^+$ co-localization in the SNpc. Boxed medial and lateral SNpc regions shown at 40x magnification in (C), (D) and (E), confirm TH^+/GHSR-$eGFP^+$ co-localization (white arrow heads). Green arrows and red arrows indicate $eGFP^+$ and TH^+ cells, respectively. Scale bar; 200 µm (in A), 100 µm (in B) and 20 µm (in C, D & E). VTA, ventral tegmental area; SNpc, substantia nigra pars compacta.

2.4.5. Fluorescence Immunohistochemistry: Girk2

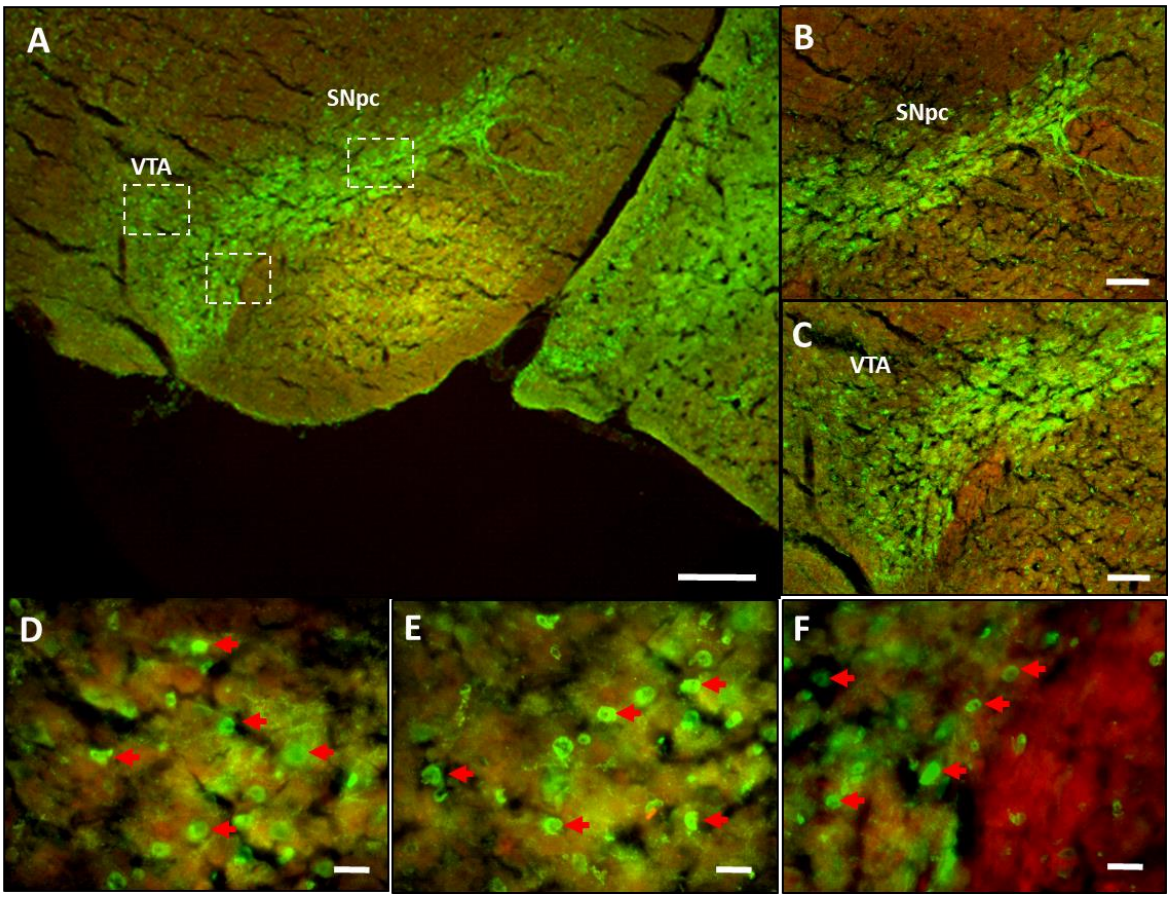

Figure 14: Girk2 is Expressed in Neurones of Adult Mouse Midbrain VTA & SNpc.

Girk2^{+} cells (Red arrows in D, E & F) are found extensively in mouse midbrain SNpc & VTA (B & C respectively). 4x magnification image demonstrates Girk2^{+} cells in VTA and lateral SNpc (A). (B) & (C) represent 10x magnification images of SNpc and VTA, respectively. Boxed VTA and lateral SNpc regions shown at 40x magnification in (D, E and F). Scale bar; 200 µm (in A), 100 µm (in B) and 20 µm (in D - F). VTA, ventral tegmental area; SNpc, substantia nigra pars compacta.

2.4.6. Fluorescence Immunohistochemistry: Calbindin

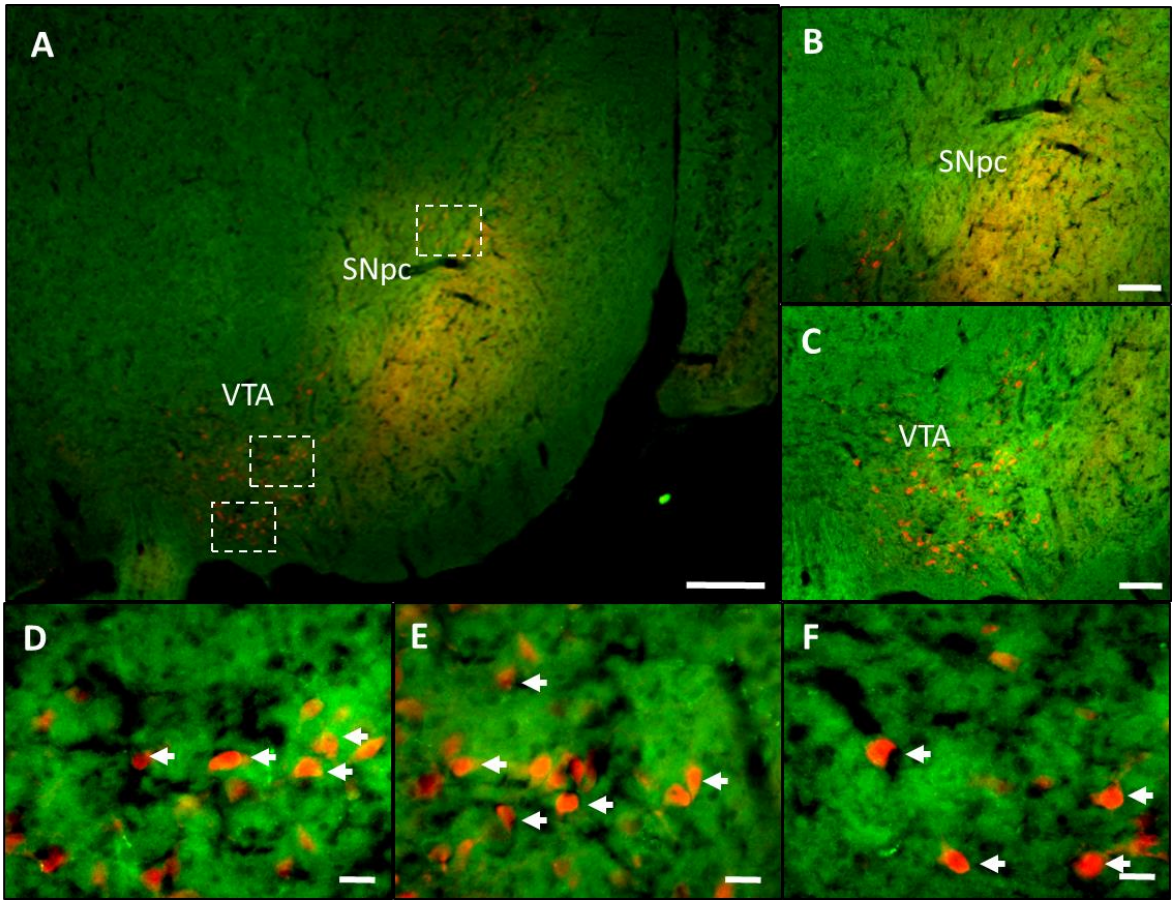

Figure 15: Calbindin is Expressed In Neurones of Adult Mouse Midbrain VTA & SNpc.

Calbindin^{+} cells (White arrows in D, E & F) are found extensively in mouse midbrain VTA. Calbindin^{+} immunoreactivity is also seen in the lateral SNpc (B & F). (A) 4x magnification image demonstrates Calbindin^{+} cells in VTA and lateral SNpc. (B) & (D) represent 10x magnification images of SNpc and VTA, respectively. Boxed VTA and lateral SNpc regions shown at 40x magnification in (D, E and F). *Scale bar; 200 µm (in A), 100 µm (in B) and 20 µm (in D - F)*. VTA, ventral tegmental area; SNpc, substantia nigra pars compacta

2.4.7. Fluorescence Immunohistochemistry: Girk2 & eGHSR Co-localization

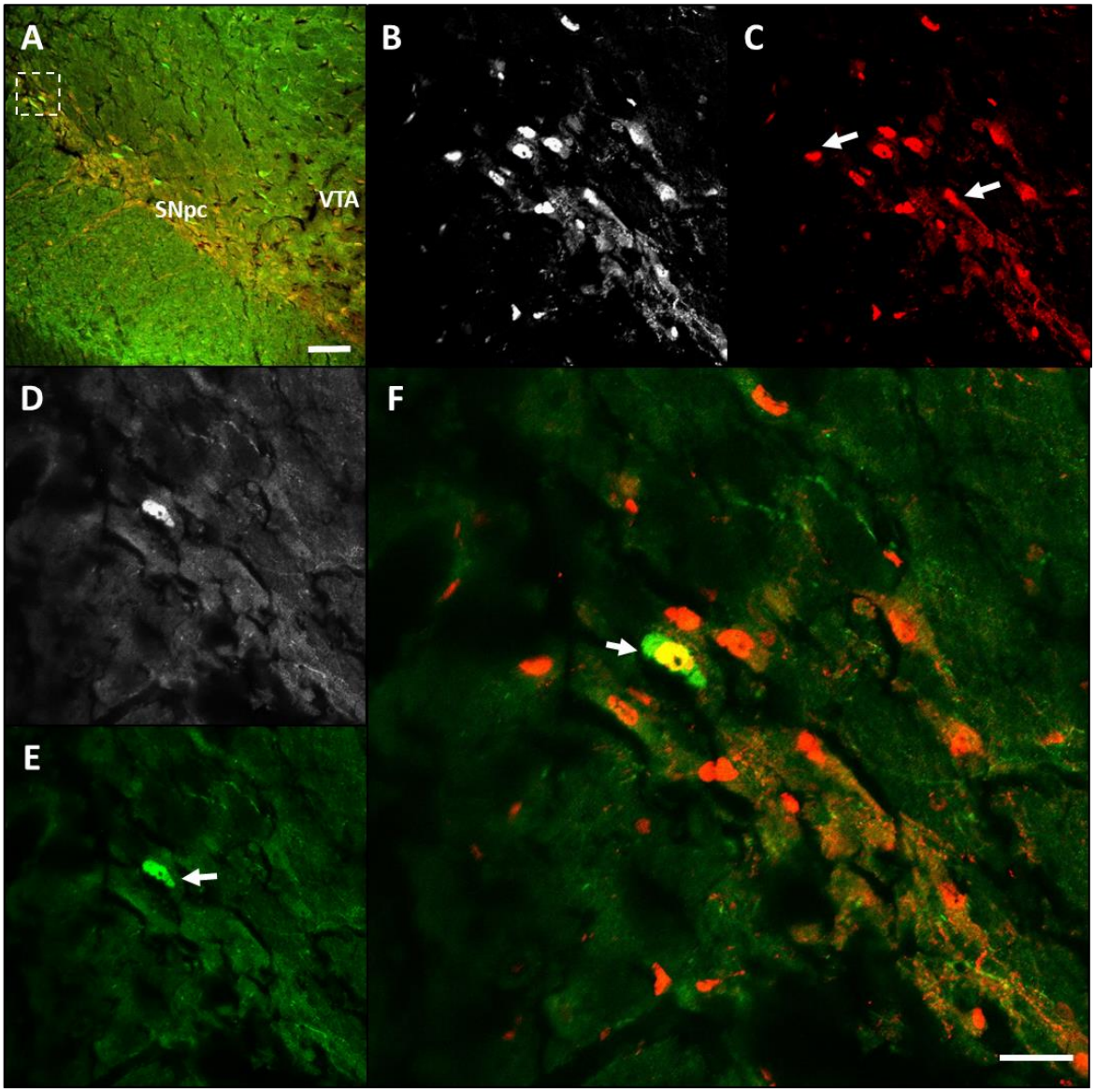

Figure 16: Ghrelin Receptor is Expressed on A9 Dopamine Cells in Adult Mouse Midbrain.

GFP^+ cells in adult mouse GHSR-eGFP co-localized with A9 dopamine cell marker, $Girk2^+$ (F), in the SNpc (F). (A) 10x magnification image demonstrates co-localization in the SNpc. Boxed lateral SNpc regions shown at 64x magnification in (B, C, D, E and F), confirms co-localization (white arrow head in F). B & D show greyscale images of Girk2 and eGFP immuno-reactive cells acquired by confocal microscopy. C & E show pseudo coloured images D & E. SNpc in human and mouse brain with 10x magnification of mouse SNpc (I). Scale bar; 100 µm (in A), 10 µm (F). VTA, ventral tegmental area; SNpc, substantia nigra pars compacta.

2.4.8. SN4741 Fluorescence Immunocytochemistry: Tyrosine Hydroxylase

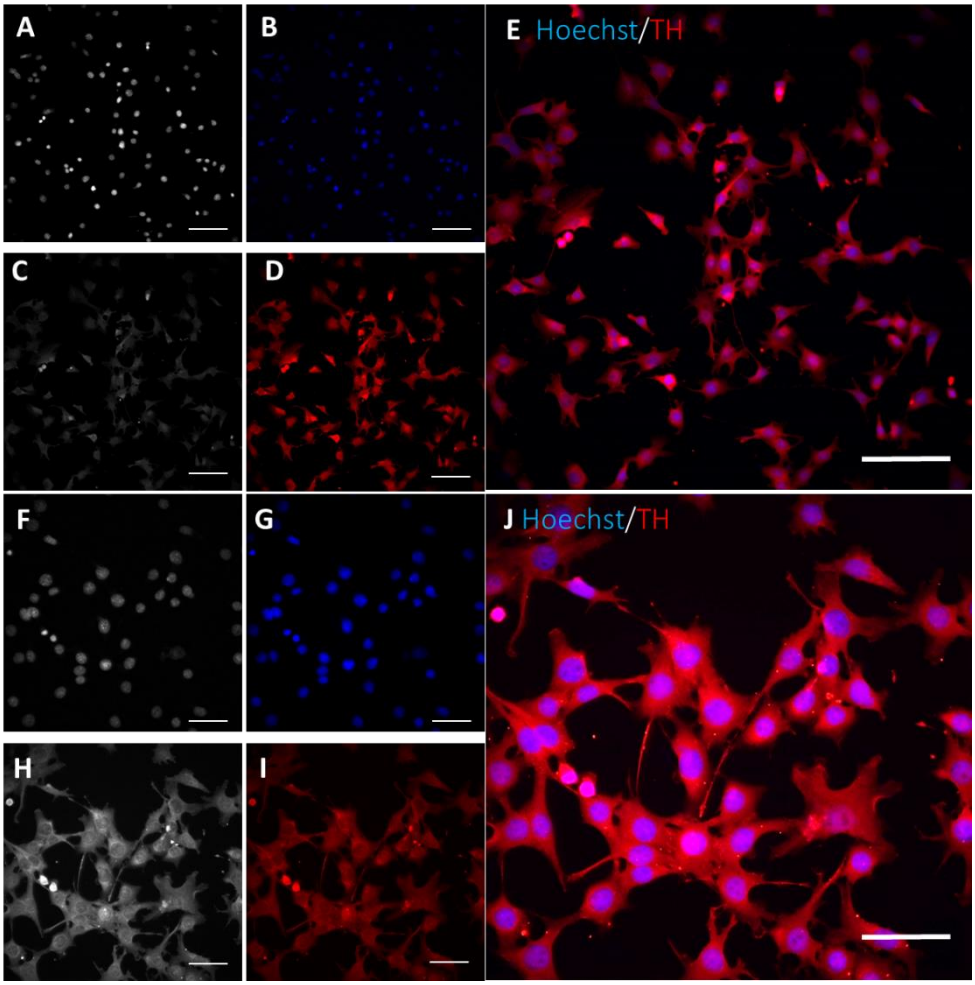

Figure 17: SN4741 Midbrain Derived Neuronal Cell Line Express TH Immunoreactivity

(A & B) x20 magnification greyscale and pseudo coloured images of SN4741 cell nuclei stained with Hoechst (1:10,000). (C & D) x20 magnification greyscale and pseudo coloured images of rabbit-anti TH antibody stained SN4741 cells. (E) Represents a merged image of B & D. (F & G) x40 magnification greyscale and pseudo coloured images of SN4741 cell nuclei stained with Hoechst (1:10,000). (H & I) x40 magnification greyscale and pseudo coloured images of rabbit-anti TH antibody stained SN4741 cells. Merged x20 and x40 magnification images (E & J) show SN4741 cells possess strong TH immunoreactivity. Primary antibody was omitted from control and no TH immunoreactivity was observed. These 20x and 40x magnification Images were acquired using InCell Analyser 2000 (GE, Healthcare).

X20 magnification images cale Bar = 80µm (in E). X40 magnification images scale bar 40µm (in J).

2.4.9. SN4741 Fluorescence Immunocytochemistry: Ghrelin Receptor, GHSR

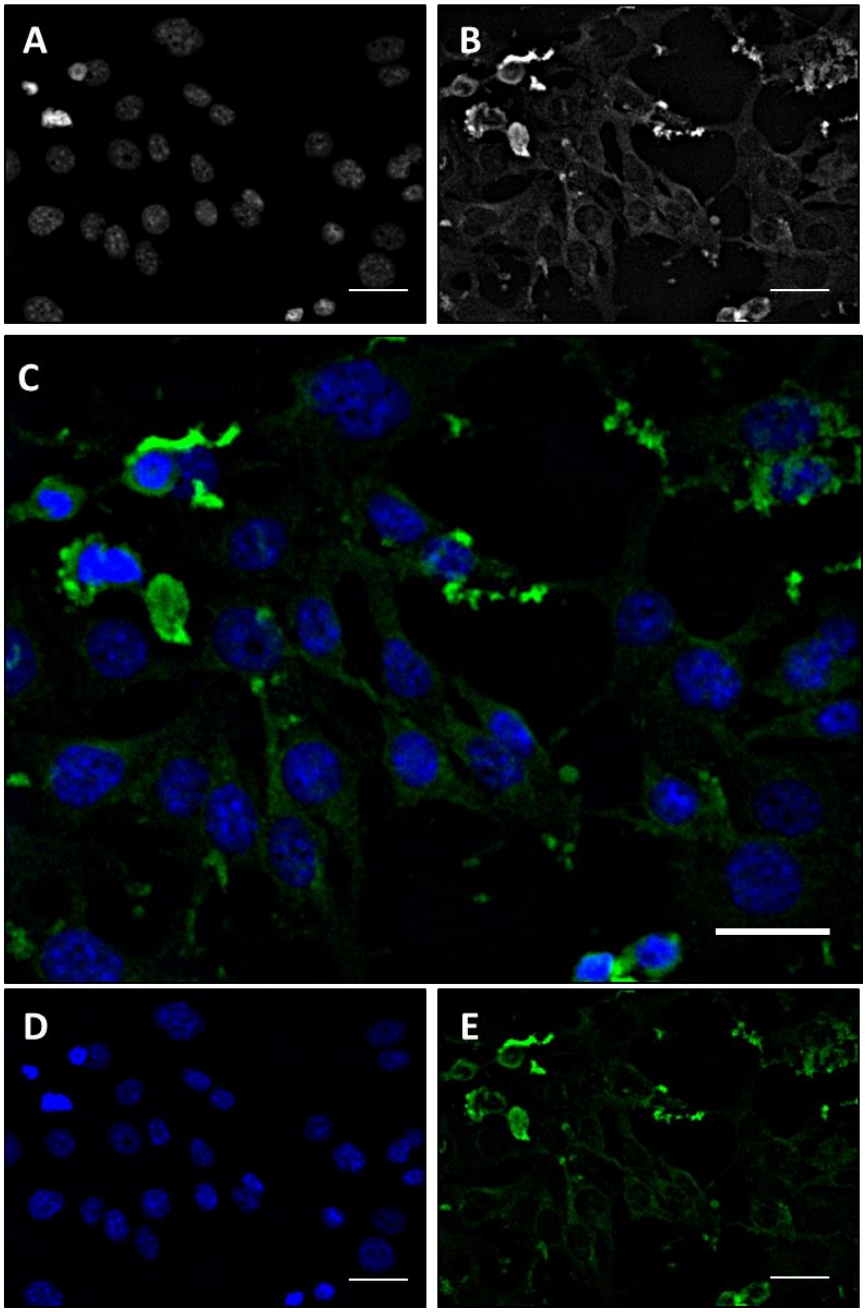

Figure 18: SN4741 Midbrain Derived Neuronal Cell Line Expressed GHSR Immunoreactivity.

(A & B) Greyscale images of SN4741 cells stained with Hoechst (A) and Rabbit-anti GHSR antibody (B). (D & E) are blue and green pseudo coloured versions of A & B. (C) Merged x40 magnification images (D & E) indicate that SN4741 cells are immunopositive for GHSR. Primary antibody was omitted from control and no GHSR immunoreactivity was observed. These 40x magnification Images were acquired using inverted fluorescence microscope, Olympus IX51. Scale Bars = 25μm (in B).

2.4.10. SN4741 Fluorescence Immunocytochemistry: Girk2

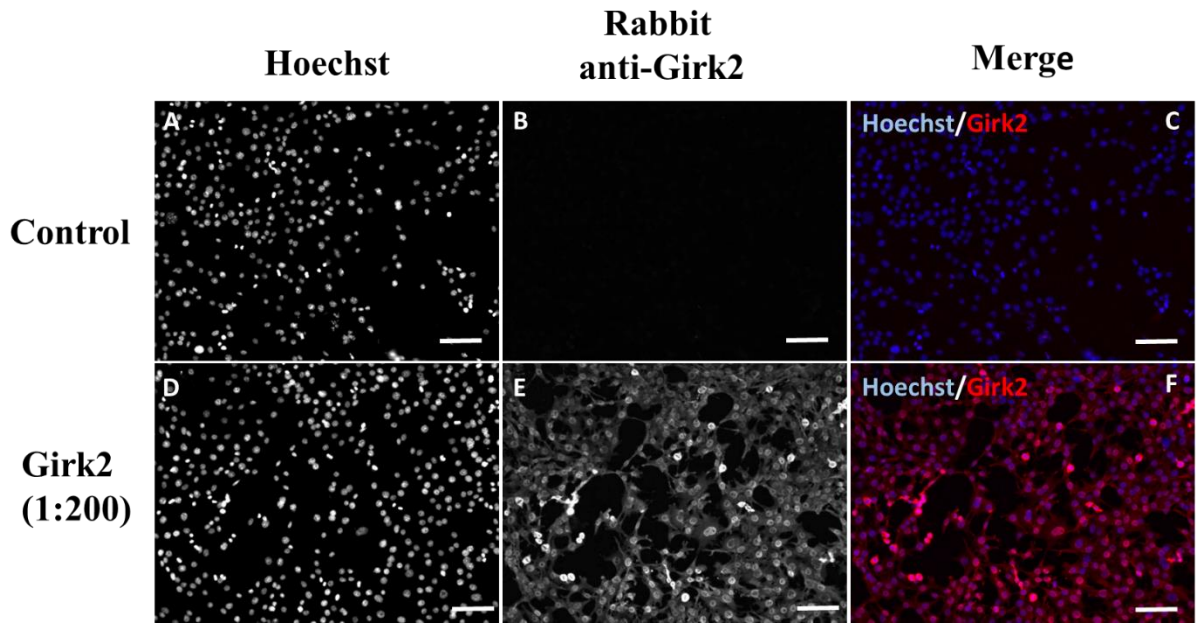

Figure 19: Girk2 is Expressed in Neurones of Midbrain Derived Neuronal Cell Line SN4741

(A & D) Greyscale Hoechst (1:10,000) counterstained SN4741 nuclei. (E) Greyscale image portraying strong Girk2 immunoreactivity in SN4741 cells. Girk2 immunoreactivity was not observed in control group (B & C). Images (C & F) are merged pseudo coloured images (A, B and D, E, respectively.) Primary antibody was omitted from control. These 10x magnification Images were acquired using inverted fluorescence microscope –Olympus IX51. Scale bars = 100µm (A-F)

2.4.11. SN4741 Fluorescence Immunocytochemistry: Calbindin

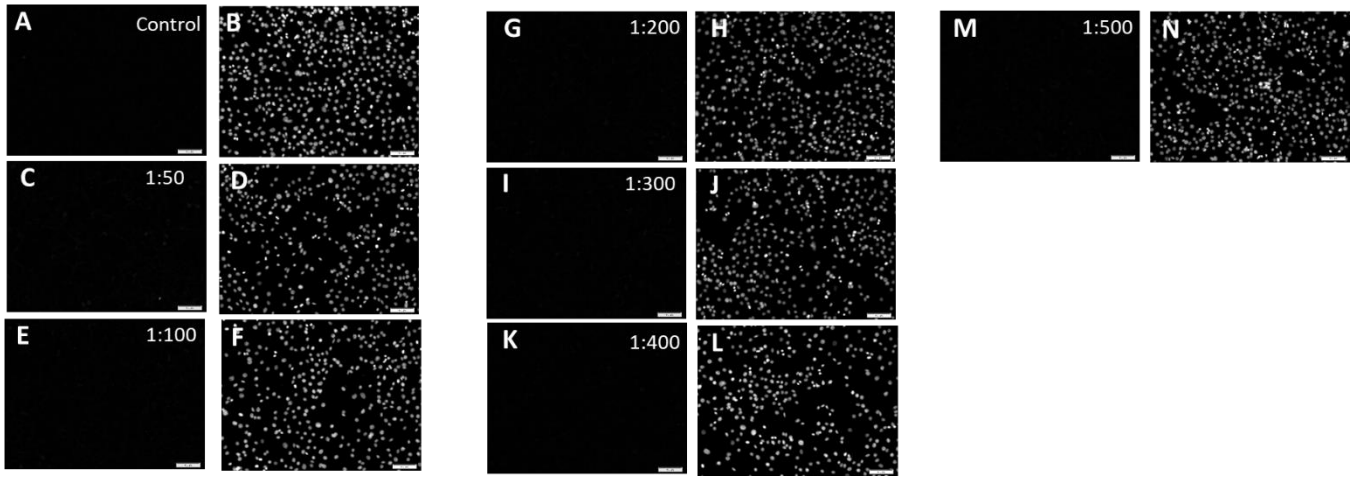

Figure 20: SN4741 Midbrain Derived Neuronal Cell Line Do Not Expressed Calbindin Immunoreactivity.

(B - G) Shows an array of greyscale images of SN4741 cells stained with various dilutions of Rabbit-anti Calbindin antibody. (H-N) show Hoechst (1:10,000) counterstained SN4741 nuclei. (A, C, E, G, I, K, M) indicate that SN4741 cells possess no detectable Calbindin immunoreactivity. Corresponding Hoechst stained nuclei are labelled (B, D, F, H, J, L, N) respectively. Calbindin immunoreactivity on SN4741 cells incubated with Calbindin antibody exhibited immunofluorescence typically observed in control group (A) where primary antibody was omitted. These 10x magnification Images were acquired using inverted fluorescence microscope –Olympus IX51. Scale Bars = 100µm (A-N).

2.4.12. Western Blot & RT-PCR: SN4741 Cell Line Express Key Ghrelin Axis Proteins

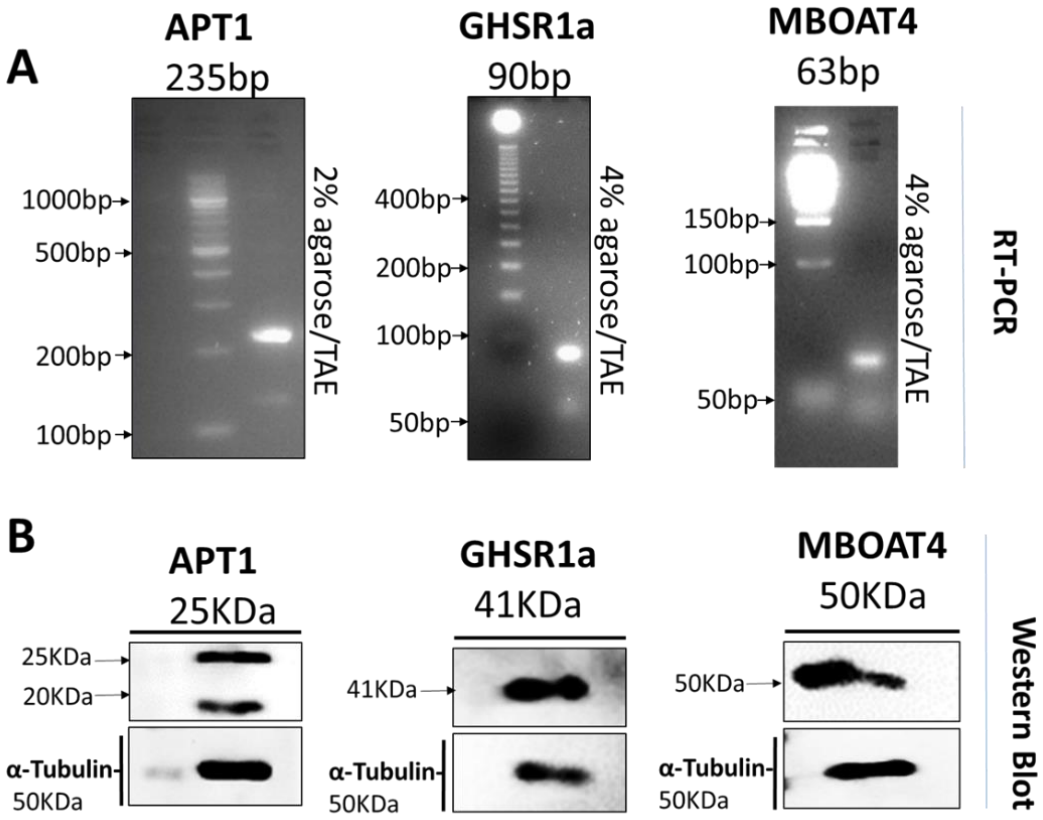

Figure 21: Ghrelin Receptor and Key Ghrelin Axis Enzymes are Expressed in Substantia Nigra Dopamine A9 (Girk2+) Neurones.

RT-PCR (A) and Immunoblotting (B) confirm expression of APT-1, GHSR1a, and MBOAT4 at protein and RNA level in SN4741 cells. MBOAT4, membrane bound O acyl transferase 4; APT-1, acyl-protein thioesterase 1.

2.5. Discussion

SN dopaminergic cell death is a key hallmark of PD pathology and ghrelin's role in neuroprotection is likely mediated via GHSR activation (Andrews, et al., 2009), therefore highlighting the potential for ghrelin's use as a neuroprotective agent on the cells which are degraded in PD. We used immunohistochemistry to confirm the co-localization of TH^+ and GHSR-$eGFP^+$ neurones in the (mouse) SN. Furthermore, we have characterized the midbrain neurones by Girk2 and calbindin immunoreactivity. Consistent with published literature we show that the A9 (SN) subset of dopamine neurones are predominantly Girk2 immunoreactive, and that Calbindin immunoreactivity predominates over Girk2 in the A10 subset of catecholaminergic neurones in the ventral tegmental area (VTA) (Bjorklund & Dunnett, 2007; Reyes, et al., 2012). We conclude that GHSR is expressed in the TH^+/$Girk2^+$ A9 (SN) neurones in-vivo.

Also, we show that the TH^+ mouse midbrain-derived SN4741 cell line (Beynon, et al., 2013; Son, et al., 1999) express Girk2 and GHSR, as well as key ghrelin axis proteins, APT-1 & MBOAT4, thus confirming their suitability in neurotoxicity studies to study direct mechanisms of ghrelin neuroprotection.

In previous literature it is suggested that ghrelin plays a multifaceted role in neuroprotection via GHSR activation and the subsequent down-regulation of pro-apoptotic pathways (e.g. Caspase pathways) and increased mitochondrial function in a UCP-2 dependent manner (Andrews, et al., 2009; Bayliss & Andrews, 2013). This, along with ghrelin's ability to decrease microglial activation and pro-inflammatory factor release, is the proposed method in which ghrelin promotes neuronal protection (Andrews, 2011; Beynon, et al., 2013).

Although the complete mechanism(s) of ghrelin's neuroprotective actions are yet to be elucidated, we will now aim to investigate the effects of known natural and synthetic GHSR activating agents in an *in vitro* PD-toxin model. Our data thus far shows that GHSR is expressed on the sub-population of DA neurones that are preferentially lost in PD (A9 subpopulation, $Girk2^+$) (Damier, et al., 1999a; Damier, Hirsch, Agid, & Graybiel, 1999b). Our results also showed that SN4741 cells do not express Calbindin immunoreactivity. Together, we suggest that the SN4741 share properties of the A9 subpopulation of midbrain neurones rather than the $Calbindin^+$, A10 subpopulation.

Subsequent investigations in Chapter 3, 4 and 5 will focus on testing the neuroprotective potential of GHSR agonists and to characterize the nature of this using both *in vitro* and *in vivo* models.

3.0. Chapter 3: Assessing Ghrelin-Mediated Neuroprotection in the Rat 6-OHDA Parkinson's Disease Model

3.1. Introduction

3.1.1. Parkinson's Disease Animal Models

Animal models of PD are a powerful method for gaining insight into the mechanisms of PD pathogenesis. Etiological (gene-based models) of PD are required to reproduce the adult onset of nigrostriatal DA neurone degeneration which correlates with a measureable alteration in animal behaviour and motor deficits. Gene-based models use transgenic overexpression of mutant genes for autosomal-dominant genes such as α-synuclein and leucine rich repeat kinase 2 (LRRK2) and knockdown models for autosomal-recessive genes such as Parkin, DJ-1, phosphatase and tensin homolog (PTEN)-induced novel kinase 1 (PINK1) (Dawson, Ko, & Dawson, 2010). The measurement of behavioural changes in rodent models of PD may not draw direct parallels with symptoms found in human PD, as the human and rodent motor system organizations vary. However, induced-phenotypes or behavioural changes (or 'symptoms') in rodent models must give a measure correlating a relationship between the degeneration of nigrostriatal DA neurons and striatal function to be of relevance. As rodents do not exhibit typical Parkinsonism as seen in humans, a non-human primate model is best suited to accurately study PD motor symptoms (Dauer & Przedborski 2003).

Besides the use of gene-based models to induce SNpc DA neuron degeneration, pathologic models which utilize neurotoxins to replicate DA neurone degeneration are also well established. The neurotoxins 6-hydroxydopamine (6-OHDA) (Vercammen et al. 2006), (1-methyl-4-phenyl-1, 2, 3, 6-tetrahydropyridine) MPTP (Lee et al. 1992) and more recently, the widely used pesticides, paraquat and rotenone have received attention due to the positive association of human PD cases in users of these pesticides (Tanner et al. 2011).

3.3.2. 6-OHDA Parkinson's Disease Model

6-OHDA is an organic chemical which accumulates in DAergic (and noradrenergic (NAergic) neurons to induce degeneration resulting in loss of motor function in animal models of PD (Ungerstedt, U. 1968). Although the 6-OHDA-induced pathology varies from that of PD; as a result of DA and NAergic transporter uptake, 6-OHDA has been used for over 30 years for its relative selectiveness for monoaminergic neurones (Ungerstedt, U. 1968; Luthman et al. 1989). In this chapter we will focus on replicating selective SNpc DA neuronal degeneration and the resulting motor-deficits in an *in vivo* 6-OHDA unilateral MFB lesion rat model of PD (Simola et al. 2007). Furthermore, we will test the efficacy of acyl-ghrelin neuroprotection against 6-OHDA-induced neurodegenerative phenotype and motor-deficits *ex vivo* and *in vivo* respectively.

6-OHDA is not permeable to the BBB and therefore must be administered by stereotaxic injection into the brain while the animal is under anaesthesia. Stereotaxic injection into the subtantia nigra (SN) or medial forebrain bundle brain (MFB) results in the initiation of DA neurone degeneration without an apoptotic morphology within 24hrs (Jeon et al. 1995). The MFB carries ascending DA and serotonergic projections to the forebrain. Alternatively, the DA nigrostriatal pathway can be targeted by injection into the striatum (Janov et al. 1976). Stereotaxic 6-OHDA injection into the striatum results in a prolonged retrograde degeneration of nigrostriatal cells which lasts for 1-3 weeks (Sauer & Oertel, 1994; Przedborski et al 1995). In unilateral stereotaxic lesions one hemisphere is selectively degenerated, with the contralateral hemisphere then serves as a control (Ungerstedt, U. 1971). Unilateral lesioning results in an asymmetrical rotation in animals when injected with methamphetamine which is proportional to the extent of the nigrostriatal lesion (Przedborski et al 1995). The unilateral lesion can be assessed quantitatively by the number of unidirectional rotations performed by the animal and by quantifying SNpc cells displaying TH immunoreactivity. DA neurone groups in mammalian brains can be identified by staining for tyrosine hydroxylase (TH), the enzyme that catalyzes the rate-limiting step in the synthesis of dopamine (Björklund & Dunnett, 2007). These measurements can be used to assess the success of novel PD treatments such as graft transplantation, gene therapy and novel therapeutics in restoring or protecting nigrostriatal DA neurones (Jiang et al. 1993; Bjorklund et al. 2002).

3.3.3. 6-OHDA Mode of Action to Replicate Progressive Nigrostriatal Dopamine Cell Death of PD

A key pathophysiological hallmark of PD is the progressive degeneration of DA neurons of the nigrostriatal pathway- these are the dopamine neurones which have their soma residing in the SN and their projections extending to the striatum. The nigrostriatal pathway is one of the major dopamine systems in the brain and is part of the basal ganglia motor loop which is involved in the production of movement (Dauer & Przedborski 2003). Loss of DA neurons in the SNpc results in striatal DA deficits and subsequent motor symptoms of PD (Dauer & Przedborski 2003).

The mode of action and mechanism by which 6-OHDA kills DA neurones is not yet fully understood. However, evidence suggests that an amalgamation of many factors contributes to 6-OHDA-mediated cell death. Following neurotoxin uptake via dopamine transporters (Luthman et al. 1989), 6-OHDA resides in the cytosol of DA neurones where it produces reactive oxygen species (ROS) and retards the activity of biological macromolecules (i.e. lipids, nucleic acids, and proteins) by the production of quinones that attach nucleophilic groups (Dauer & Przedborski 2003). The formation of ROS by the autoxidation of 6-OHDA is considered as one of the main underlying DA neurotoxicity mechanisms (Kumar et al. 1995; Seto-Otero et al. 2000). Recent studies have also implicated extracellular oxidation of 6-OHDA in DAergic cell loss and shown high sensitivity of DAergic neurons to oxidative stress which may attribute to the relative selectiveness of DA degeneration versus other monoamine cell types (Berretta et al. 2005; Hanrott et al. 2006). It has also been suggested that 6-OHDA elicits mitochondrial complex 1 inhibition in a mechanism similar to environmental toxins and MPTP-induced neuron degeneration (Glinka et al. 1996; Betarbet et al. 2002; Schober, A. 2004).

To date, there is no evidence demonstrating that 6-OHDA contributes towards the formation of another PD-linked pathology- the intracellular misfolded protein aggregates called Lewy Bodies (LBs).

3.3.4. 6-OHDA in Neuroprotection Studies

6-OHDA has been used extensively to successfully test the efficacy of putative neuroprotective agents to prevent PD neurodegeneration.

For example, resveratrol, curcumin and naringenin are all extracts found in skin of grapes, turmeric and grapefruit respectively. Daily doses (10, 20 and 40 mg/Kg) of

resveratrol were given to rats for 10 weeks following 6-OHDA lesions. Resveratrol alleviated a list of 6-OHDA-induced aberrations, such as chromatin condensation, mitochondrial enzyme complex swelling and DA neurone vacuolization in the rat SNpc. These results were paralleled with a decrease in mRNA expression of inflammatory markers tumour necrosis factor alpha (TNF-alpha) and Cytochrome C oxidase subunit 2 (COX2) (Jin et al. 2008). Curcumin and naringenin also attenuated the loss of TH+ SNpc neurone and striatal levels of DA by anti-oxidative mechanisms (Zbarsky et al 2005). Other food extracts such as polyphenols extracted from green tea, which are known to elicit a potent anti-oxidant scavenging, iron chelating and anti-inflammatory, have been tested against 6-OHDA neurotoxicity in an *in-vitro* setting. Green tea derived polyphenols also showed anti-oxidative mechanisms by inhibiting the 6-OHDA-induced iron-dependent inflammatory redox sensitive transcription factor, nuclear factor-kB (NF-kB) (Levites et al. 2002). Pharmacological agent, edaravone is used to aid neurological recovery following acute brain ischemia and cerebral infarction. Edaravone administered to rats 30 minutes following 6-OHDA unilateral lesioning attenuated the loss of TH+ cells on the SNpc and striatum along with characteristic unidirectional amphetamine-induced rotations. This same study observed edaravone exerted anti-apoptotic and anti-oxidative effects on TH+ neurons cultured *in vitro*. And these effects where paralleled with an increase *in vitro* TH+ neuron survival in a dose-dependent manner (Yuan et al. 2008).

Other treatments shown to attenuate 6-OHDA-induced nigrostriatal lesion include glial cell-line derived neurotrophic factor (GDNF) pre-treatments (24hr) and administration of statins, atorvastatin and simvastatin (Kearns et al. 1995; Kumar et al. 2012). Similarly to edaravone and food extracts the statins' neuroprotective mechanisms involved recovery or attenuation from 6-OHDA-induced inflammation and oxidative stress. Atorvastatin and simvastatin also reversed a plethora of both biochemical and behavioural changes induced by the 6-OHDA lesion. These included impaired body weight, locomotor activity, rota-rod performance, oxidative defence, mitochondrial complex activity and increased levels of pro-inflammatory cytokines TNF-alpha and interleukin-6 (IL-6) (Kumar et al. 2012). An *in vitro* experiment utilising resistin, a cysteine-rich adipose-derived peptide hormone, has shown that inhibition of 6-OHDA-induced apoptotic markers also contributes to neuronal survival. Treatment of MES23.5 cells with resistin resulted in the attenuation of Bcl-2 degradation, BAX expression, PARP degradation and caspase 3 activation whilst decreasing ROS production and restoring perturbed mitochondrial membrane potential (Lu et al. 2013).

This evidence shows the 6-OHDA lesion to be a reproducible and well established method of assessing DA cell neurodegeneration and testing the efficacy of anti-PD therapeutics both *in-vivo* and *in-vitro*. These findings also reiterate that oxidative stress is a key contributor to 6-OHDA induced nigrostriatal DA degeneration. Anti-apoptotic effect are also mechanisms by which DA cell neuroprotection can be achieved. Furthermore, it appears that anti-oxidative and anti-apoptotic effects of naturally occurring and pharmacologically developed compounds are sufficient to attenuate 6-OHDA-induced aberrations *in vivo* and *in vitro*.

3.3.5. Ghrelin in Parkinson's Disease Models

The orexigenic stomach hormone, ghrelin, is known to modulate appetite and metabolic homeostasis (De Vriese & Delporte, 2007). However, acyl ghrelin (AG) has also shown promise as potential neuroprotective agents in models of PD and other disease models (reviewed Andrews Z.B. 2011). In the MPTP mouse model of PD, AG but not UAG promotes SNpc neuron protection in a GHSR1a-dependanet manner (Jiang et al. 2008; Bayliss et al. 2016). AG treatment attenuated an array of pro-apoptotic markers such as the increasing Bcl-2: BAX ratio and activation of Caspase 3. AG-mediated neuroprotection in MPTP-mouse model coincides with a decrease in glial cell activation, glial fibrillary acidic protein and ionized calcium binding adaptor molecule 1 microglia in the SN. No such neuroprotective mechanisms were observed with UAG administration (Bayliss et al. 2016). Thus, supporting the importance of the AG-activated GHSR1a pathway in ghrelin-mediated neuroprotection of SNpc neurons- an effect that is mediated in a mitochondrial uncoupling protein 2 (UCP-2)-dependant manner (Andrews et al. 2009). *In vitro* AG neuroprotection against MPTP radical metabolite, MPP^+, also involved modulation of apoptotic Bcl-2: BAX ratio, anti-oxidative effects and inhibition of NF-KB translocation (Liu et al. 2010). An *in vitro* experiment by (Beynon et al. 2013) also showed anti-inflammatory properties of AG in a lipopolysaccharide (LPS) neuro-inflammatory model using TH and GHSR1a immune-reactive SN4741 midbrain derived neurons. Here, AG attenuated the LPS-mediated release of pro-inflammatory cytokine interleukin-6 (IL-6). An affect which was abolished upon pre-treatment with GHSR1a antagonist [D-Lys3]-GHRP-6 (Beynon et al. 2013).

Work describing the AG-mediated neuroprotection of DA neurons *in vitro* and *in vivo* appears to be governed by GHSR1a activation resulting in an array of downstream effects involving anti-apoptotic, anti-inflammatory and oxidative mechanisms. It

should be noted, however, that the efficacy of AG as a neuroprotective agent has not been tested using the 6-OHDA toxin PD model. Herein, the rat unilateral MFB 6-OHDA lesion model was used in order to assess the effectiveness of AG in prohibiting neurodegeneration.

3.2. Methods and Material

3.2.1. Animal Handling and Stereotaxic 6-OHDA Lesioning

All *in vivo* procedures were performed under licence to the Animal (Scientific Procedures) Act 1986 by Dr Tim Wells and Dr Mariah Lelos in the School of Bioscience, Cardiff University. Male SD rats (weighing 194-241g) were purchased from Charles River (Margate, UK) and housed under conditions of 12h light/12h dark (lights on at 06.00h) with water available *ad libitum*. Rats were fed crushed diet (SDS 801066 RM3(E); 3.64kcal/g) available either *ad libitum* throughout the 24h period or in three 1h periods (at 18.00h, 23.30h and 05.00h) during the dark phase using a Comprehensive Lab Animal Monitoring System (CLAMS). Food intake and body weight was monitored daily. On day 0 one cohort of *ad libitum*-fed rats were surgically implanted with osmotic minipumps (Alzet model 2001) primed to deliver acyl-ghrelin (Phoenix Pharmaceucitals; 80µg/24µl/day) sub-cutaeneously for 7 days. A control group was also monitered where acyl-ghrelin was replaced with saline.

After 1 week on these treatment regimes, rats received an injection of desipramine/pargyline (50mg/kg/i.p), were anaesthetised with isolfluorane and mounted in a Kopf stereotaxic frame. The skull was exposed and a burr hole was drilled to introduce a cannular for a single unilateral medial forebrain bundle (MFB) injection of either vehicle (0.2mg/ml ascorbic acid in 0.9% sterile saline; pH5.0) or 6-OHDA (hydrobromide salt (Sigma Chemicals, UK); 3µg/µl in vehicle). To minimize variability due to degradation of the toxin, the 6-OHDA solutions were freshly made, kept on ice and protected from exposure to light. The solution was injected into the right MFB using the following co-ordinates (relative to bregma) Lateral −1.3; Anterior −4.0 and Ventral 7.0. A total volume of 3µl 6-OHDA was injected at a flow rate of 1µl/min, the cannular was left in place for a further 3 min and then slowly removed. The rats received an injection of analgesic (Metacam, 150µg/s.c) after the skin was sutured and they were allowed to recover before being returned to their home cage.

Rats received injections of BrdU (50mg/kg/i.p) on days 12 and 18 after lesion surgery to birth date dividing cells, whilst on days 27 and 35 (i.e. 3 and 4 weeks post lesioning) they were subjected to drug-induced rotational testing. On the day of testing rats received an injection of methamphetamine (2.5mg/ml/kg/i.p in sterile saline) and immediately placed into individual rotometer bowls. Contralateral and ipsilateral rotations were recorded using Rotorat software for 90 mins.

After rotational testing on day 35 rats were terminally anaesthetised with sodium pentobarbital (200mg/ml) (Euthetal, Merial) until total loss of reflex, nose-anus length measured, and subjected to thoracotomy. After withdrawal of a terminal blood sample by cardiac puncture, rats were killed by transcardial perfusion of 1.5% paraformaldehyde (PFA). After perfusion, brains were excised and post-fixed by immersion in 1.5% PFA in 0.1M PBS overnight at 4ºC. Brains were then cryo-protected by sinking in 30% sucrose at 4ºC until further processing. In addition, pituitaries were dissected and weighed, and right femori and tibiae dissected for quantification of bone length using a handheld micrometer.

3.2.2. Histology: Tissue preparation for Nickel DAB Immunohistochemistry

Whole rat brains were shipped from Cardiff University to the Institute of Life Science, Swansea University and mounted onto a freezing microtome (*Microm HM 450)* (-30◦C) with *JUNG-tissue fixing medium*® for coronal sectioning (30µm thick). Rat brains were sectioned rostro-caudally along the entire brain and sectioned tissue was collected 1:6 in a labelled 12-well plate and immersed in PBS+0.2% Sodium Azide *(Sigma Aldrich).* The tissue sections were stored at 4ºC prior to immunohistochemical preparation.

3.2.3. Tyrosine Hydroxylase DAB Immunohistochemistry

Immunohistochemistry experiments were carried out in CELLSTAR® 12-well plate [665180] (greiner bio-one, UK) at room temperature and with gentle agitation unless stated otherwise. Free-floating tissue sections were removed from storage conditions washed thoroughly (2 x 10 mins) in PBS (Sigma Aldrich) with gentle rocking/agitation at room temperature. PBS was removed prior to permeabilization of tissue sections using 0.03% Triton-x100 in PBS (0.03% PBS-T) for 10mins. Following permeabilization tissue sections were immersed in 1.5% H_2O_2 in PBS for 20 mins in order to remove endogenous peroxidase activity before being washed for another 2 x 10 mins in PBS and 1 x 10 mins in 0.03% PBS-T. Tissue sections were then immersed in 5% Normal Goat serum (5% NGS) (*Sigma Aldrich*) in 0.1% PBS-T for 60 min at room temperature to block non-specific binding sites. Excess block was then removed prior to application of a primary antibody, rabbit anti-TH [ab6211] (1:500, Abcam®, UK), diluted in 2% NGS in PBS-T and incubation at 4ºC overnight (approx. 16-24hrs). Primary antibody stained sections were then washed another 2 x 10 mins in PBS and

1 x 10 mins in 0.03% PBS-T before a 70 minute incubation with biotinylated goat Anti-Rabbit IgG Antibody (Vector Laboratories [BA-1000], with gentle agitation at room temperature whilst being protected from light. All steps from here onwards are carried out with minimum exposure to light as the sample is now light sensitive until the final oxidation reaction occurs and DAB precipitate has formed. Again, the sections were washed 2 x 10 mins in PBS and 1 x 10 mins in 0.03% PBS-T prior to incubation with VECTASTAIN®Elite® ABC Kit [PK-6100] (Vector laboratories, UK) ABC solution (a mix of 0.4% reagent solution A and 0.4% reagent solution B in 0.1% PBS-T). ABC solutions A (Avidin DH solution) & B (biotinylated enzyme) were pre-mixed in 0.1% PBS-T for 30mins, making-up the ABC solution prior to its addition to sample tissues for 90mins. ABC solution was then removed and the tissue sections were washed 2 x 10mins in PBS before a final wash 10 minute wash in 0.1M sodium acetate pH 6.0. Excess sodium acetate solution was then removed prior to initiating the DAB reaction by mixing 1ml Nickel DAB solution with 60ul of glucose oxidase solution (5mg/ml) in the presence of tissue sections. This reaction was performed by 1ml of Nickel DAB solution pipetted into a well of a corner of a weighing boat and 60ul of glucose oxidase was pipetted adjacently but were not mixed. A fine-tipped painting bush was used to transfer tissue sections into the 1ml of DAB solution immediately prior to the mixing with glucose oxidase. The plate was then swirled (3-4 times) to ensure solutions were thoroughly mixed prior to gentle rocking/agitation for nickel DAB staining to develop.

Once sufficient Nickle DAB staining had developed, a paint brush was used carefully to transfer tissue sections from the DAB-glucose oxidase reaction solution into PBS and washed twice for 10 mins in PBS.

3.2.3.1. Sample Dehydration, Delipidation and Slide Preparation

Following 2 x PBS washes tissue sections were suspended in a TBS (*Sigma Aldrich, Gillingham, UK*) filled petri dish. The tissue sections were mounted onto SuperFrost®Plus slides [25 x 75 x 1.0mm] (*VWR International LTD*) and allowed to dry overnight. Once dry, tissue samples underwent dehydration by submerging the slides in increasing concentrations of ethanol (70%, 90%, 100%, and 100 %) for 3 minutes each. Samples were then de-lipified by submerging slides in Histo-Clear [HS-200] (National Diagnostics) twice for 3 minutes. Slides were removed from Histo-Clear and 50ul of Entellan® [107960](MerckMillipore) was pipetted evenly over the slide prior to carefully lowering a MENZEL-GLÄSER 24 x 60mm glass coverslip (Thermo

Scientific, Germany) to complete slide preparation. Sample slides were the left to dry prior to inspection via light microscopy.

3.2.3.2. Light Microscope Imaging

Examination and imaging of tissue sections was performed using a Nikon Eclipse 50i light microscope. X4 magnification .tif/ format images were acquired for spatial orientation and illustration of entire SNpc. 2-3 x10 magnification images (tif format) of the SNpc were then acquired per hemisphere in order to perform TH^+ cell quantification using the open source image analysis software, Image J (Java) (Available to download: http://imagej.net/Welcome). Image J is an image processing program for multidimensional image data with a focus on scientific imaging (imagej.net/Introduction).

3.2.4. Quantification of Tyrosine Hydroxylase-positive SNpc neurons with image J

The protocol below describes the step-by-step image J protocol used to quantify TH^+ SNpc neurones from x10 magnification digital images. Each step includes a description followed by instructions on how to execute the step in image J software (in italic font).

Step 1: Open x10 magnification raw image with image J software.

File > Open. Then select the x10 magnification image to be analysed.

Step 2: Convert raw image to an 8-bit image.

Image > Type > 8-bit

Step 3: Enhance the contrast between foreground and background staining.

Process > Filters > Unsharp Mask. Select 100 radius (sigma); 0.5 mask weight.

Process > Enhance Contrast. Select saturate pixels: 0.4%.

Step 4: Outline the SNpc in x10 magnification image using x4 magnification image for reference and orientation.

Set tool as 'Polygon'. Draw around the SNpc in the x10 image.

Step 5: Convert image to a masked image where there are only two colours, black and white. Then adjust the threshold until only the TH^+ SNpc neurons appear black,

and all image background is white. Use original or contrast enhanced images to ensure TH^+ cells appear black. This is important as threshold values may vary slightly between images, therefore slight adjustments are usually required to ensure correct cell quantification. To minimise the variation in image intensity, all images of the same magnification should be acquired using identical microscope settings (e.g. Acquire all x10 images using an identical exposure time, image type and quality output).

Image > Threshold > Adjust Threshold. Move sliders to 'correct' threshold where only TH immunoreactive cells are visible in black against a white background.

Step 6: Quantify the number of TH immunoreactive cells in the outlined SNpc. Once this step is executed image J will produce a table of results which includes (cell) counts and produce an image of identified cells.

Analyse > Analyse Particles > Set Particle size: 100- Infinity; Circularity: 0.00-1.00; select show: Overlay Masks, select: Display Results and select: Summarise.

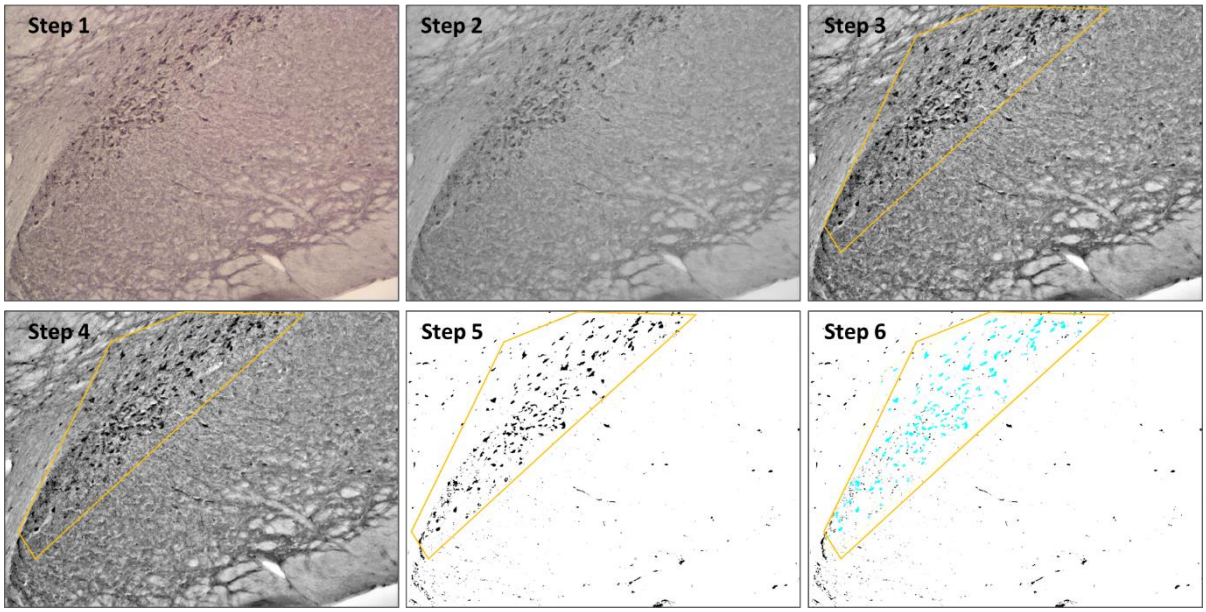

Figure 22: Step by Step Illustration of SNpc DA Cell Identification using Image J Software

This figure illustrates the 7 steps described above in the section titled 'Quantification of Tyrosine Hydroxylase-positive SNpc neurons with image J'.

3.3. Results

3.3.1. Acyl-Ghrelin Treatment Attenuated SNpc Dopamine Cell Loss Induced by 6-OHDA Lesion

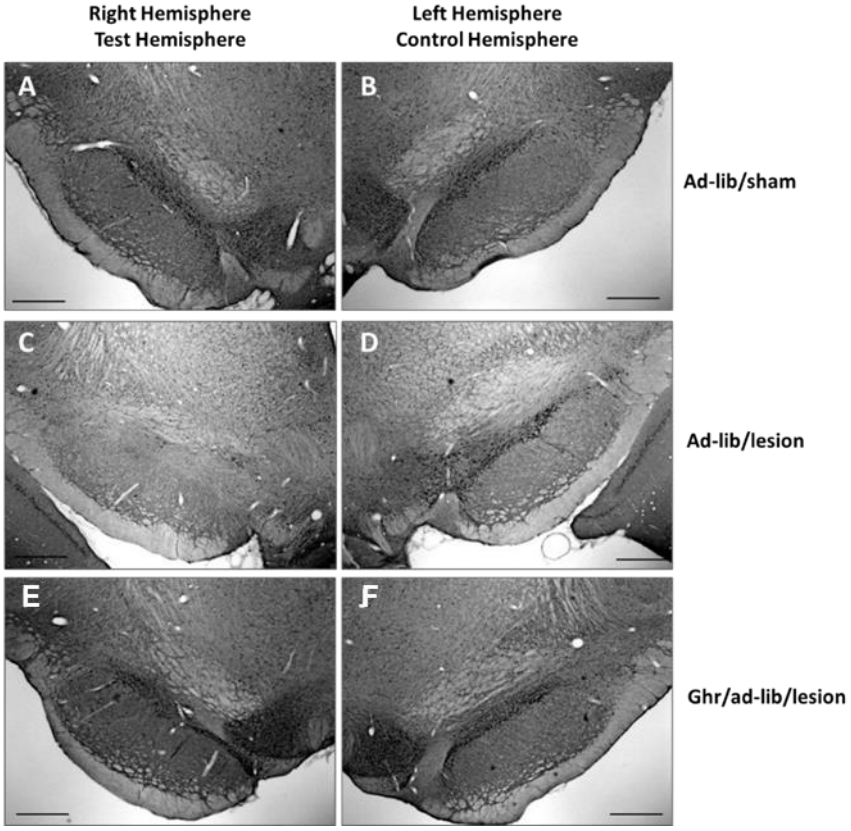

Figure 23: 6-OHDA-Induced SNpc TH+ Neurone Loss is Attenuated in Rats Pre-treated with Acyl-Ghrelin.

A-J show greyscale x4 magnified rat SNpc-containing midbrain tissue sections stained for TH immunoreactivity. (B, D & F) illustrate unlesioned control hemispheres and (A, C & E) illustrate sham or 6-OHDA lesioned rat hemispheres. 6-OHDA lesion results in loss of TH^+ neurones in the SNpc and VTA in ad-lib (C) and meal fed (G) rats. AG pre-treatment attenuated TH^+ cell loss in rat SNpc and VTA. Meal fed, dietary-restricted rats do not prevent 6-OHDA-mediated cell loss. Ad-libitum fed sham/lesioned rat (Ad-lib/sham); Ad-libitum fed/lesioned rat (Ad-lib/lesion); Ghrelin pre-treated/ad-libitum fed/lesioned rat (Ghr/ad-lib/lesion). Scale bar; 500 μm (A-J).

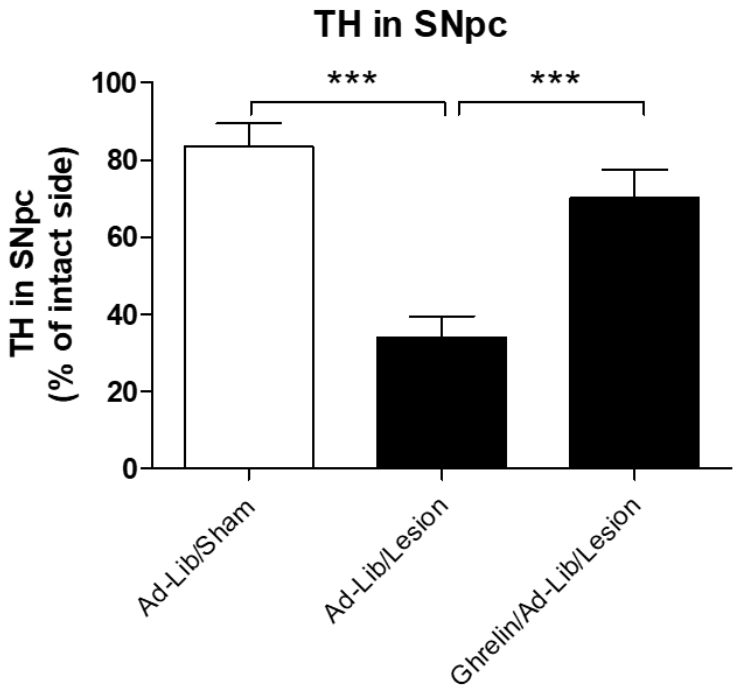

Figure 24: Acyl-Ghrelin Pre-treatment Protects TH+ SNpc Neurones in an In Vivo 6-OHDA Parkinson's Disease Model.

Quantification of TH^+ SNpc neurones in sham or lesioned rat hemispheres (left) as a percentage of intact control hemisphere (left). Image J quantification of rat SNpc TH^+ neurones shows 6-OHDA-induced TH^+ cell loss in lesioned animals. The number of TH^+ SNpc neurones ad-lib fed/6-OHDA lesioned rats was reduced. However, TH^+ SNpc neurone number was protected from 6-OHDA lesioning in acyl-ghrelin pre-treated ad-lib fed rats. Ad-libitum fed sham lesioned rat (Ad-lib/sham) (n=17); Ad-libitum fed/lesioned rat (Ad-lib/lesion) (n=19); Meal fed/sham lesioned rat (Meal/sham) (n=6); Meal fed/lesioned rat (Ad-lib/lesion) (n=8); Acyl-ghrelin pre-treated/ad-libitum fed/lesioned rat (Ghr/ad-lib/lesion) (n=10). Statistical analysis was carried out with Graph Pad Prism 5.0 using one-way-ANOVA and Bonferroni's pot-hoc analysis*, $P<0.05$; **, $P<0.01$; ***, $P<0.001$.

Dietary-restriction (meal –fed) did not protect 6-OHDA-induced dopaminergic cell loss.

3.3.2. Acyl-Ghrelin Treatment Attenuated Amphetamine-Induced Rotations in In Vivo 6-OHDA Parkinson's Disease Model

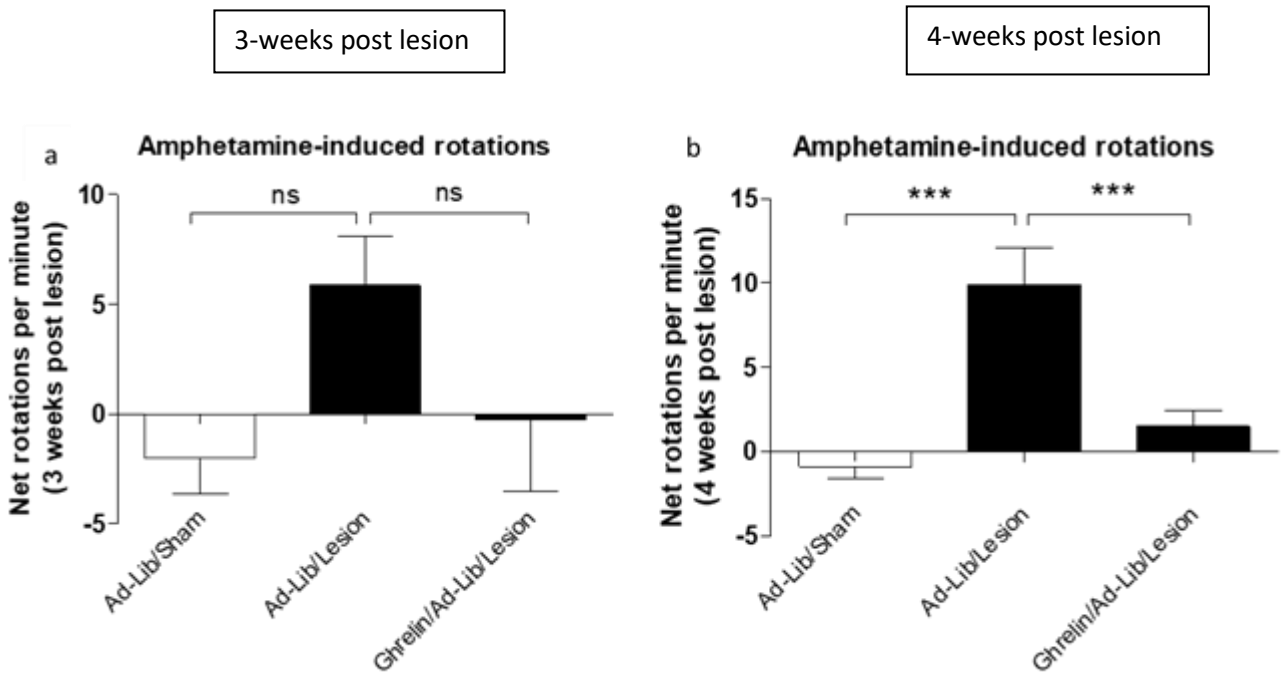

Figure 25: Acyl-Ghrelin Pre-treatment Attenuated Amphetamine-Induced Rotations in In Vivo 6-OHDA Parkinson's Disease Model.

Graphs (a) and (b) demonstrate the average net amphetamine-induced rotations completed by rats in 90 minutes at week 3 and 4 post-lesion, respectively. Graphs (a) and (b) show 6-OHDA-induced unilateral lesion in animals increases the amphetamine-induced rotation versus Ad-Lib/Sham lesioned controls. This effect is significant (***) at 4 weeks post-lesioning. However, 6-OHDA unilateral lesion-induced amphetamine rotation are greatly attenuated in AG-pretreated Ghrelin/Ad-Lib/Lesioned animals. An effect which is statistically significant 4 weeks post-lesioning. Ad-libitum fed sham lesioned rat (Ad-lib/sham) (n=17); Ad-libitum fed/lesioned rat (Ad-lib/lesion) (n=18); Ghrelin pre-treated/ad-libitum fed/lesioned rat (Ghr/ad-lib/lesion) (n=10). Statistical analysis was carried out with Graph Pad Prism 5.0 using one-way-ANOVA and Bonferroni's pot-hoc analysis*, $P<0.05$; **, $P<0.01$; ***, $P<0.001$.

3.4. Discussion

The rat *in vivo* unilateral MFB 6-OHDA lesion is a well-established method used to mimic characteristics of PD pathology - that is the preferential degeneration of midbrain dopaminergic neurons and induction of motor dysfunctions in animal models (Dauer & Przedborski, 2003). Published data suggests the stomach hormone, acyl-ghrelin, as a potential neuroprotective agent against PD neurodegeneration (Andrews et al. 2009). Both *in vitro* and *in vivo* studies propose that increased mitochondrial function, anti-oxidative effects and anti-inflammatory effects underpin the neuroprotective properties of acyl-ghrelin (Lee et al. 2010 & Bayliss et al. 2016). In an effort to test acyl-ghrelin-mediated neuroprotection we raised circulating levels of acyl-ghrelin directly by mini-pump infusion (80ug/kg/day; s.c) and indirectly by subjecting rats to 7 days of dietary restriction prior to unilateral injection of 6-OHDA into the MFB.

As described in previous literature, unilateral 6-OHDA injection into the MFB induced degeneration of dopaminergic SNpc neurons (Bagga et al. 2015), thus replicating aspects of the DA cell death pathology of PD (Brichta et al. 2014). However, it must be noted that our unilateral injection of 6-OHDA also destroyed TH-immunoreactive neurones in the ventral tegmental area (VTA); an area rich in A10 DA neurone sub-type which show relative resistance to degeneration in PD (Dauer & Przedborski, 2003; Björklund & Dunnett. 2007). Direct administration of acyl-ghrelin for 7 days via mini-pump infusion attenuated the 6-OHDA-induced degradation of TH^+ SNpc neurones (Figure 24). However, our indirect attempt to increase circulating acyl-ghrelin levels did not result in dopaminergic cell protection. Acyl-ghrelin has displayed efficacy in the neurone protection MPTP models of PD and other CNS lesions (Bayliss et al. 2016 & Lee et al. 2010). MPTP and 6-OHDA not only share similar uptake mechanisms in DA neurones (Dauer & Przedborski, 2003) but also inhibit mitochondrial complex 1, increase oxidative damage by ROS production and modulate pro-apoptotic events (e.g. release of mitochondrial cytochrome c, increase of Bcl-2: BAX ratio and downstream activation of caspases) (Glinka et al. 1996; Dauer & Przedborski, 2003; Andrews et al. 2009; Lu et al. 2013 & Tobón-Velasco et al. 2013). Since there are similarities in neurotoxic modes of action in DA neurons, it is a possibility that the acyl-ghrelin-mediated neuroprotection observed in both toxin models are governed by similar mechanisms.

Comparable to other agents found to protect against 6-OHDA-induced cell loss, acyl-ghrelin mediated neuroprotection has been attributed to anti-apoptotic (Yuan et al. 2008), ROS-buffering (Andrews et al. 2009) and anti-inflammatory (Levites et al.

2002; Jin et al. 2008) mechanisms. Collectively, the acyl-ghrelin mechanisms could be utilised in treating a range of CNS diseases (Andrews Z, B. 2011) which share underlying perturbations. In the mouse MPTP-PD models, acyl-ghrelin-mediated ROS-buffering (via mitochondrial UCP-2), anti-apoptotic effects (via retention of mitochondrial Cytochrome C and decreased caspase activation) and subsequent survival of SNpc DA neurones is suggested to be GHSR1a mediated (Jiang et al. 2008 & Bayliss et al. 2016). Inflammation is also associated with PD progression. The beneficial effects of acyl-ghrelin on neuronal survival has been associated with a decrease in inflammatory mediators (i.e. microglial activation) (Bayliss et al. 2016) which result in release of pro-inflammatory cytokines such as IL1-1B, TNF-alpha and IL-6 (Hide et al. 2000; Shigemoto-Mogami et al. 2001 & Clarke et al. 2010). The release of the latter (IL-6) was diminished by 4hr acyl-ghrelin pre-treatment on *in vitro* midbrain derived neurons (Beynon et al. 2013). Moreover, upon the addition of ghrelin receptor antagonist these anti-inflammatory effects were abolished. Other unpublished data by our group shows acyl-ghrelin attenuating the activation of microglia-associated protein CD11b.

This data shows that elevating circulating levels of acyl-ghrelin protects SNpc DA neurones from 6-OHDA-induced death and attenuates subsequent amphetamine-induced rotations. These data suggest that acyl-ghrelin may be able to slow or diminish the progression of PD or other diseases that share similar pathological traits. Strides must now be made to identify the underpinning mechanisms of acyl-ghrelin-mediated DA neuroprotection. Elucidation of such mechanisms may aid the development of novel PD therapeutics.

4.0. Chapter 4: In Vitro Parkinson's Disease (PD) Model

4.1. Introduction

4.1.1. In Vitro PD Models

In vitro models of PD are used extensively to study the cellular pathology of PD by attempting to replicate cellular pathophysiological hallmarks such as DAergic cell degeneration and the formation of misfolded protein aggregates that contribute to intracellular inclusions (Gundersen, 2010). Genetic models involve inducing over-expression or under-expression (or knockdown) of key PD-related genes identified from genetic studies in familial PD (Kumaran & Cookson, 2015). Since these PD-related genes are usually associated with a distinct cellular or protein dysfunction, these have been used to investigate specific subcellular PD-associated mechanisms underpinning PD.

Chemicals which induce PD-like cellular phenotypes are also commonly used to study the cellular mechanisms of PD. Moreover, these studies are utilised to test novel anti-PD therapeutics. In this chapter, we use an *in vitro* chemical induced PD model to test the potential neuroprotective effects of AG and a synthetic GHSR1a agonist, JMV 2984.

4.1.2. Chemically Induced PD Models

A range of chemicals have been used to mimic aspects of PD pathology *in vitro*. Among the most frequently used are 1-methyl-4-phenyl-1,2,3,6-tetrahydropyridine (MPTP)(Langston, Ballard, Tetrud, & Irwin, 1983), 6 hydroxydopamine (6-OHDA) (Y. M. Ding, Jaumotte, Signore, & Zigmond, 2004), paraquat (McCarthy, Somayajulu, Sikorska, Borowy-Borowski, & Pandey, 2004) and rotenone (Hao, Li, Duan, & Li, 2017; Pan, Qiao, & Wen, 2016). The mechanism of actions of these *in vitro* PD-inducing chemicals disrupt normal cellular pathways predominantly by increasing production of reactive oxygen species (ROS) resulting in oxidative damage, and inducing mitochondrial dysfunction that perturbs cellular energy homeostasis.

4.1.2.1. MPTP

The metabolic product of MPTP, MPP^+, is a toxin found to cause severe Parkinsonism in humans upon intravenous injection. MPTP is a by-product of the synthesis of 1-methyl-4-phenyl-4-propionoxy-piperidine (MPPP), a synthetic analogue of the opioid

heroin (Langston, et al., 1983). Once inside the cell the active metabolite, MPP^+, inhibits ETC complex 1, impairs mitochondrial respiration and function, and increased ROS production. Moreover, DAergic neurotransmitter DA is relocated from cellular extremities to the cytosol where it becomes oxidised and elicits a further increase in ROS and subsequent oxidative damage. Furthermore, MPP^+ inhibits ATP production and produces oxidative radicals which damage other cellular proteins. Some of the oxidative radicals produced are super oxides, these may react with nitric oxide and for peroxynitrite which is known to cause oxidative damage and nitration of selective proteins (Cleeter, Cooper, & Schapira, 2001). TH, the rate limiting enzyme in the biosynthesis of DA is one such protein. Nitration of TH renders the enzyme inactive and thus DA production is decreased. Nitrating agent peroxynitrite also damages deoxyribonucleic acid (DNA). Peroxynitrite-induced DNA nicks result in the activation of poly-(ADP-ribose)-polymerase (PARP) which itself requires the utilisation ATP. This activity further aggravates cell energy levels which is already stressed by other MPP^+ ETC complex 1 inhibiting mechanisms. Furthermore, there is evidence that nitric oxide enhances the MPP^+ mediated inhibition of ETC complex 1 (Cleeter, et al., 2001). These deleterious cascades result in increased ROS and oxidative stress, decreased mitochondrial efficiency and respiration and energetic failure (Przedborski et al., 2000). Moreover, MPTP mouse models mimic aspects of PD symptoms (Przedborski, et al., 2000).

4.1.2.2. 6-OHDA

6-hydroxydopamine (6-ODHA, also known as oxidopamine) is a DAergic and noradrenergic (NAergic) neurone specific neurotoxin. 6-OHDA is taken up into DAergic and NAergic cells via DA and or NA re-uptake transporters. 6-OHDA is sometimes administered in conjunction with a NA reuptake transporter inhibitor. This ensures the selective uptake and degradation of DA neurones. Once inside neurones 6-OHDA induces an increase in ROS and catecholamine quinone production. The accumulation of 6-OHDA inside the cell results in oxidative stress and cell death. The literature is unclear as to whether 6-OHDA-induced-cell death is a result of inhibition of the ETC complex I and complex IV (Y. Y. Glinka & Youdim, 1995) or that 6-OHDA induces a reduction in cell viability via an increase in ROS production (Storch, Kaftan, Burkhardt, & Schwarz, 2000).

The onset of sporadic PD cases has been linked to farmers working with pesticides such as paraquat and rotenone. A study by (Narayan, Liew, Bronstein, & Ritz, 2017) showed an increased risk of developing sporadic PD amongst individuals who had occupational, residential and household sources of pesticide exposure. An increased

risk of PD is observed in users versus non-users of these pesticides (Tanner et al., 2011).

4.1.2.3. Paraquat

Paraquat is commonly used herbicide which also shown to be toxic to animals and humans. *In vitro* use of paraquat has utilised its oxidative stress-inducing property to stimulate degeneration of neuronal cells in models of PD. In a model used by (Ravi, Narasingappa, Joshi, Girish, & Vincent, 2017) paraquat induced oxidative stress which led to lipid peroxidation, DNA damage and apoptosis.

4.1.2.4. Rotenone

Rotenone is a highly lipophilic compound commonly used as an insecticide which induces PD-like cellular hallmarks including increased oxidative stress, mitochondrial dysfunction and alpha synuclein accumulation, and neurotoxicity in *in vitro* PD models. Moreover, rotenone also produces PD-like motor deficits in animal models of PD (Cicchetti, Drouin-Ouellet, & Gross, 2009; S. Y. Kang et al., 2017; Pan, et al., 2016). Rotenone's link to sporadic PD (Narayan, et al., 2017; Tanner, et al., 2011), *in vivo* selectivity for DAergic neurone degeneration (Sherer, et al., 2003) and its lipophilic properties, which allow it to enter cells directly devoid of transporter assistance, make it a robust PD-like inducing chemical (Sherer, et al., 2003; Testa, Sherer, & Greenamyre, 2005). *In vivo* rotenone treatment in animal models of PD exert PD-like symptoms and motor deficits, and DAergic SNpc neurone degeneration and alpha synuclein and Lewy body proteinous aggregates in both *in vitro* and *in vivo* models. The major limitation of the rotenone model is its variability. There is a variability in terms of the percentage of animals that develop recognizably distinct nigrastatial lesions and the extent of those lesions (Cannon et al., 2009). Although selective degeneration is observed in SNpc in animal models (Sherer, et al., 2003) rotenone's highly lipophilic characteristic allows it to also readily cross the cell membrane of many cell types an induce complex 1 inhibition (e.g. hepatocytes) (Heinz et al., 2017). Thus, the PD-like effects induced in rotenone models may be the result of cumulative cell damage and not specifically the degeneration of nigrostriatal neurones.

PD-like symptoms (e.g. bradykinesias, postural instability and rigidity, loss of TH^+ substantia nigra neurones and subsequent loss striatal dopamine. Rotenone is known to inhibit ETC complex 1, impair mitochondrial respiration and induce an increase in ROS production (Q. Zhang et al., 2014), inhibit the removal of damaged proteins by impairing proteasomal activity (S. Y. Kang, et al., 2017) and increase neurotoxicity.

Besides investigating the neurodegenerative mechanism by which DAergic cells die, *in vitro* models are also used as tools for testing novel anti-PD therapies and elucidating their underpinning mechanism of action. The *in vitro* rotenone PD models is one such tool.

4.1.3. Neuroprotection in In Vitro Rotenone PD models

Published literature identifies the *in vitro* rotenone PD model as a test for new anti-PD therapeutics. Kaempferol inhibits rotenone-induced toxicity by significantly reducing ROS and mitochondrial carbonyls in primary neurones and SH-SY5Y cells. Moreover, this study shows that kaempferol has anti-apoptotic and antioxidative effect, and neuroprotection appears to be related to increased mitochondrial turnover by mitophagy (Filomeni et al., 2012).

Rotenone-induced toxicity was not prevented by quercetin, myricetin and resveratrol (Filomeni, et al., 2012). However, a study by (S. Y. Kang, et al., 2017) shows that rosuvastatin does indeed exert neuroprotection against rotenone-induced neurotoxicity in SH-SY5Y cells. Moreover, rosuvastatin treatment appeared to restore lost cell viability and decrease expression of alpha synuclein. This protection is thought to be mediated by regulation of autophagy related proteins, mTOR and beclin-1, and implicates suppressed autophagy in rotenone-induced neurotoxicity.

The neuroprotective effects of alpha-mangostin on rotenone induced ROS production, caspase 3 and 8 activation, mitochondrial dysfunction and alpha synuclein aggregation was demonstrated by (Hao, et al., 2017). Moreover, alpha-mangostin treated SH-SY5Y cells were protected from the rotenone induced deficit in mitochondrial membrane potential (MMP) and cellular ATP levels.

A study by (Y. Moon, Lee, Park, Geum, & Kim, 2005) showed that pre-treatment of primary rat mesencephalon neurones with coenzyme Q10 reverses rotenone-induced apoptosis and mitochondrial depolarization. This suggests that loss of MMP may be important in rotenone-induced DAergic cell death via apoptosis. *In vitro* rotenone models are commonly used to explore the possible mechanisms behind intracellular PD pathology and mechanisms of action of potential neuroprotective chemicals and agents. Although AG is cited as being neuroprotective in PD models using MPTP *in vitro* and *in vivo*, there is no literature surrounding AG neuroprotection against rotenone-induced neurotoxicity.

4.1.3.1. Acyl-Ghrelin Neuroprotection in Models of PD

An elegant experiment by (Bayliss, Lemus, Santos, et al., 2016) performed on Ghrelin (knockout) KO mice showed that chronic administration of AG attenuated MPTP-induced loss of nigrostriatal TH^+ DAergic neurone number, neurone volume and TH protein expression. Moreover, AG administration reduced the increase in glial fibrillary acid protein (GFAP) and ionized calcium binding adaptor molecule 1 (Iba1) induced by the mouse MPTP PD model. No such effect was observed upon chronic administration of exogenous un-acylated form of ghrelin (UAG) in Ghrelin KO mice. Of note, injection of exogenous AG also increased levels of plasma UAG. Illustrating the un-acylating action of APT-1 in the conversion of AG to UAG. Other studies by this group provide evidence that AG neuroprotection is at least partly dependent on an integral mitochondrial uncoupling protein, mitochondrial uncoupling protein 2 (UCP2), buffering of ROS and increased mitochondrial biogenesis (Andrews, et al., 2009).

In vitro studies indicate that acylated AG protects against MPP^+-induced neurotoxicity in MES 23.5 neuroblastoma cells. In this study ghrelin is seen to reverse a multiplicity of pro-cytotoxic events such as induction of malonaldehyde, increased Bax-Bcl2 ratio and elevated levels of superoxide dismutase and catalase; suggesting that AG's *in vitro* protection against MPTP-induced cytotoxicity must be partly governed by anti-oxidant effects and modulation of cytokines and proinflammatory factors via NF-kB (L. Liu, et al., 2010). A short study by (Beynon, et al., 2013) also shows ghrelin mediating an anti-inflammatory response in lipopolysaccharide (LPS) treated DAergic neurones by inhibiting the release of interleukin-6 (IL-6). This effect was shown to be mediated via AG's endogenous receptor, GHSR1a, which is expressed on these neurones, as inhibition of GHSR1a by [D-Lys3]-GHRP-6 (D-Lys3) abolished these anti-inflammatory effects. This is consistent with an anti-inflammatory and anti-oxidant effect observed in a study showing ghrelin mediated inhibition of pro-inflammatory factors including tumour necrosis factor-alpha (TNF-α), interleukin 1-beta (IL-1β) and nitrite in *in vitro* cultured mesencephalon neurones (Moon, et al., 2009). Furthermore, an *in vivo* aspect to this study showed ghrelin mediating the inhibition of MPTP-induced pro-inflammatory markers and activation of microglia, as well as the attenuation of DAergic neurone death in the SNpc. AG inhibited the expression of TNF-α, IL-1β, activation of inducible nitric oxide synthase and microglial activation in the nigrostriatal pathway. This study states that GHSR1a is not expressed on microglia suggesting that AG-mediated effects are not induced directly at microglia. Instead it is suggested that inhibition of microglia activation, which is associated with

AG neuroprotection (Andrews, 2011), is elicited via the suppression of matrix metalloproteinase-3 in DAergic neurones (M. Moon, et al., 2009).

It has been proposed that AG mediated neuroprotection is the result of GHSR1a binding and activation of 5' adenosine monophosphate activated kinase (AMPK), which shifts cellular energy balance from negative to neutral; enhanced removal of damaged mitochondria (and proteins) via mitophagy (autophagy of mitochondria), which limits the excess production of ROS; and increased mitochondrial biogenesis and function, including the buffering of ROS (Bayliss & Andrews, 2013).

Drawing on insights from the published literature PD-inducing chemicals appear to perturb mitochondrial function, increase ROS production, energetic stress, increased inflammatory response- leading to cytotoxicity and neurodegeneration. Neurodegeneration in animal models manifest in PD-like motor deficits. We propose that AG-mediated neuroprotection is the result of binding with its endogenous receptor, GHSR1a, triggering downstream signalling pathways via phosphorylation of energy homeostasis regulator, AMPK; leading to increased function of the mitophagy/autophagy system and mitochondrial biogenesis to attenuate oxidative damage sustained by neurotoxins and retain metabolic function. In addition, AG may function indirectly as it appears to play an anti-inflammatory role in attenuating the release cytokines and inflammatory factors and suppressing microglial activation.

In this chapter, we aim to:

- Determine growth kinetics of SN4741 cells in full culture medium and substrate restricted medium.
- Define a concentration of mitochondrial complex-1 inhibitor, Rotenone, which results in a decrease of SN4741 cell number and viability and an increase in cell cytotoxicity.
- Test the direct neuroprotective effects of AG and JMV 2894 Pre-treatment against Rotenone-induced cell loss.
- Investigate intracellular mechanisms by which AG treatment protects SN4741 cells from rotenone.

4.2. Methods & Materials

4.2.1. SN4741 Cell Line

SN4741s are a mouse midbrain derived nigral dopaminergic cell line. Establishment of the SN4741 cell line is described fully in (Son et al. 1999) see (http://www.jneurosci.org/content/19/1/10.full.pdf+html). Briefly, DAergic progenitor cells where collected by surgically removing butterfly-shaped mesencephalic regions from transgenic embryos from embryonic day 13.5 (13.5) TA58-#8.

Only DA cells from the transgenic embryos would be immortalized and survived in successive cultivation steps. Mesencephalic butterfly-shaped regions were triturated as described (son et al 1999) and primary pelleted cells were cultured for at least 3-5 weeks. A pure cell population of transgenic primary embryonic cells was produced by repeated passages for 3-4 months. Cloning cylinders were used for cloning purposes. Cells of clonal origin were monitored during colony formation and re-confirmed by TH and SV40Tag immunostaining.

4.2.2. SN4741 Culture Medium and Substrate Restricted Medium

SN4741 cells are routinely cultured in 500mL DMEM without sodium pyruvate (Invitrogen, 41965-039) supplemented with 50ml FBS (10106169, Invitrogen), 5mL Penicillin/Streptomycin (Pen/Strep) (15140122, Gibco, UK), 5mL L-Glutamine (25030081, Gibco, UK) and 15mL 20% Glucose solution, filtered bioultra for molecular biology 20% in water (Sigma, 49163-100ml). Substrate restricted SN4741 cell culture media was also prepared by diluting the above (termed 'Full media') in dilution media in the absence of L-Glutamine, FBS and Glucose supplementation. Full media diluted in dilution media (DMEM without sodium pyruvate, supplemented with Pen/Strep) to prepare a titration of media at various percentages (%). The aim was to mimic caloric restriction *in vitro* as there is growing evidence for the benefits of caloric restriction. Research (Andrews et al.2009) also indicates that the neuroprotective effects of AG, at least in *in vivo* rodent models, require a concomitant reduction in caloric intake. Using our substrate restricted media we investigated the effects of neurotoxin challenge in the presence and absence of GHSR1a agonist pre-treatment. The table below lists the volumes of full medium vs dilution medium used to prepare substrate restricted (SR) media.

Table 13: Volumes of Full Medium and Dilution medium required to Prepare 50mL of Substrate Restricted (SR) SN4741 Cell Culture Media

Percentage of Full Medium	Volume of SN4741 Full Media (mL)	Volume of SN4741 Dilution Media (mL)
0%	0	50
20%	10	40
40%	20	30
60%	30	20
80%	40	10
100%	50	0

SN4741 cells were routinely cultured in full (100%) media. Full media was replaced by a chosen SR medium at the initiation of an experimental procedure. SN4741 cells were seeded in triplicate into corning 3596 flat bottom multi-well plates. Cells were incubated in 0, 20, 40, 60, 80 and 100% of full media for 72hrs. 100µL SN4741 medium was added to each well every 24hrs. At 72hrs cells were screened for cytotoxicity and viability using methods described in *'Development of a Rotenone-induced neurotoxicity/cell loss in vitro PD model'.*

4.2.3. Routine SN4741 Cell Culture

Thawing SN4741 cells: SN4741 cells were stored in liquid nitrogen in cryovials. 18ml of SN4741 full culture medium was pipetted into a T75 flask and incubated at 37◦C (5% CO_2) for 30 mins. SN4741 cryovials were then removed from the liquid nitrogen and thawed by swirling in 37◦C water bath until only a small amount of ice remains. Using a P1000 the contents of the thawed cryovial were placed into the pre-warmed 18ml of SN4741 full culture medium in a T75 flask(s). The flask was then swirled to ensure an even distribution of cells and placed in a cell culture incubator at 37◦C, 5% CO_2 overnight to adhere.

Seeding SN4741 cells: the following morning SN4741 cells should be adhered to the T75 flask- cells were visualised via a light microscope. The SN4741 cell culture media was removed and the cells were washed 1x with 10ml PBS (10010023, Gibco, UK) to

remove excess medium. SN4741 cells were then detached from the cell culture vessel by adding 4ml of trypsin/EDTA, 0.5% (15400054, Gibco, UK) into the flask and incubating (5% CO_2; 37◦C) for 5min. The flask was removed from the incubator and gently tapped to ensure all cells had detached before neutralising trypsin/EDTA by adding 6ml of cell culture medium and resuspending. Using a 10ml pipette, the cell solution was gently pipetted up and down 5-10 times to create a single cell suspension. Prior to seeding cells, 10 µL of cell suspension was mixed with 10 µL Trypan Blue Solution 0.4% (15250061, Gibco, UK) and pipetted onto a Countess™ cell counting chamber slide (Invitrogen). The Trypan Blue Solution is a dye exclusion test where dead cells take up the dye and viable cells do not. The chamber slide was placed into the Countess™ Automated Cell Counter (Invitrogen) and a total cell count, a total live cell count and a total dead cell count was obtained (expressed as cells per ml). Live cell count values were used to quantity cells destined for seeding or sub-culturing/passaging. SN4741 cells were then seeded into experiment vessel of choice and placed into the incubator (5% CO_2; 37◦C) overnight to settle and adhere.

Sub-Culturing SN4741 cells: Following the re-suspension of a 90% confluent T75 flask in cell culture medium:

- Add 0.5ml of SN4741 cell suspension to 19.5ml cell culture medium→90% confluent in 4 days.
- Add 1ml of SN4741 cell suspension to 19ml cell culture medium→ 90% Confluent in 3 days
- Add 2ml of SN4741 cell suspension to 18ml cell culture medium→ 90% Confluent in 2 days
- Add 3ml of SN4741 cell suspension to 17ml cell culture medium→90% Confluent in approx. 24hrs.

Every 2-3 days cell culture medium was removed, cells were washed (PBS) and medium was replenished. All culture vessels and experimental plates were labelled with name, date, contents and passage number.

Making cell stocks: Cell culture medium was removed from a 90% confluent T75 culture flask and SN4741 cells were washed once with 10ml PBS (10010023, Gibco, UK). The PBS wash was removed and 4ml of Trypsin/EDTA (15400054, Gibco, UK) solution was introduced into the culture vessel before being placed in the incubator for 5 minutes whilst SN4741 cells detached. The culture vessel was subsequently checked for cell detachment via light microscope and gently tapped to remove adhered SN4741 cells if necessary. Using a 10ml sterile pipette add 6ml of fresh cell

culture medium to neutralize the trypsin/EDTA solution before pipetting the cell suspension up and down (5-10 times) to produce a single cell solution. The cell suspension was placed into a 50ml falcon/centrifuge tube and centrifuged at room temperature for 300xg for 5 minutes. The supernatant was carefully removed to avoid disturbing the cell pellet and the cells were re-suspended in cryopreservation media (see table 1 below for contents of cryopreservation medium).

Table 14 Contents of Cryopreservation medium

Cryopreservation media			
Reagents	**FBS**	**DMSO**	**SFM (serum free medium)**
Volume	12.5ml	5ml	32.5ml
Ratio	2.5	1	6.5

The resuspension was promptly added to a cryovial and sealed in a Nalgene™ (bottom container holds Isopropanol) container and transferred to a -80ºC freezer overnight (16-24hrs). Cryovials were labelled with cell type, name, date and passage number. The frozen cryovial were then submerged in a tanker filled with liquid nitrogen and a record was made.

4.2.5. SN4741 Cell Growth Curve

To estimate the time required to culture sufficient numbers of SN4741 cells for downstream experiments 1ml of cell suspension (34,000 cells/ml) was added to 19ml of full SN4741 cell culture medium in a T75 flask. Confluency of cells in the T75 was recorded by observation via a light microscope and were then detached and quantified every 24hrs post-seeding- as described in '*Seeding SN4741 cells'* section above. A complete monolayer of cells covering the culture vessel was referred to as 100% confluency and no cells was referred to as 0% confluency.

4.2.6. Development of a Rotenone-Induced Neurotoxicity In Vitro PD Model

The loss of SNpc dopamine neurones is a pathological hallmark of PD. Before testing the direct neuroprotective effect of AG and GHSR1a agonist compound (JMV 2894), SN4741 cells were challenged with a titration of rotenone concentrations over 24hrs. Here we aimed to define a minimum dose (concentration) of rotenone which induced SN4741 cell loss that parallels an increase in cell cytotoxicity and a decrease in cell viability. The optimal dose of rotenone will subsequently be used to test whether AG and GHSR1a agonists exert protective effects on rotenone-induced neurodegeneration.

SN4741 cells were seeded at 3000 cells/well on a 96 well plate (Corning 3596 flat bottom plate) by pipetting 100µL of 30,000 cell/ml of the stock solution into each well (See *SN4741 splitting/subculture* for details on method). Cell culture plates were left to sit on a level surface for 5 minutes before incubation (5% CO_2; 37◦C) – this allowed the cells to distribute evenly onto the bottom of the wells. Following overnight incubation, 100 µL of pre-warmed (37◦C) SN4741 cell culture media was introduced to treatment wells before being returned to the incubator for either 1 hr or 24hrs. Subsequently, SN4741 cells were treated for 24hrs with final well concentrations of rotenone at 0nM (vehicle only), 10nM, 100nM, 1,000nM and 10,000nM. Rotenone was prepared at a 3-fold higher concentration (i.e. 0nM, 30nM, 300nM, 3,000nM and 30,000nM) by thoroughly mixing (vortex) 3 µL of 10mM rotenone stock diluted in Dimethyl Sulfoxide (DMSO) into 10ml culture medium producing a 30,000nM rotenone solution. 3,000nM, 300nM and 3nM rotenone solutions were prepared by performing 1 in 10 dilutions i.e. 100 µL of 30,000nM rotenone solution mixed into 900 µL of cell medium to produce 1ml of 3,000nM rotenone solution. Vehicle treatment was prepared from DMSO using the same dilution method. Finally, 100 µL of 3x concentrated rotenone solution was added to treatment wells performing a 1:3 dilution which resulted in final well concentrations 0nM, 10nM, 100nM, 1,000nM and 10,000nM before 24hr incubation (5% CO_2; 37◦C). 100 µL of a 50:50 solution of DMSO in PBS was used as a positive control to induce cell cytotoxicity. Each treatment was performed in triplicate. Cells were then fixed, imaged and analysed as described in *SN4741 Cell Growth Curve*, *Image acquisition with In Cell 2000* and *Image J cell count analysis macro* for quantification of rotenone-induced cell loss. Rotenone treated cells were also subject to cytotoxicity and viability assessment using the CellTox™ Green Cytotoxicity Assay (Promega, #G8741) and the CellTiter-Blue® Cell Viability Assay (Promega, #G8080) respectively.

4.2.6.1. The CellTox™ Green Cytotoxicity Assay

The CellTox™ Green Cytotoxicity Assay was used according to user manual for endpoint determination of rotenone-induced SN4741 cytotoxicity following 24hr treatments. This assay includes a proprietary asymmetric cyanine dye whose fluorescence properties are amplified upon binding to DNA. The cyanine dye produces no measurable fluorescence intensity in the presence of healthy cells with intact cell membranes. When the cell membrane integrity is compromised, such as that observed in dead or dying cells, the cyanine dye may then bind with DNA and produce appreciably larger fluorescence intensity. The fluorescence intensity measured by the binding of the cyanine dye with DNA of dead cells is proportional to cytotoxicity. A fluorimeter measures the intensity and wavelength distribution of emission spectrum after excitation by a certain spectrum of light.

During 24hr incubation of cells in the presence of rotenone, the CellTox™ Green Cytotoxicity Assay components (CellTox™ Green Dye and Assay Buffer) were thoroughly thawed in a 37°C water bath. Kit components were individually mixed using a vortex to ensure homogeneity, then collected at the bottom of their tubes using a centrifuge. 1 µL CellTox™ Green Dye was added to every 500 µL Assay Buffer, as needed, to produce a 1:500 dilution equivalent to a 2x concentrated staining solution. Following 24hr cell incubation with rotenone, 200 µL of cell medium was removed from each well and 100 µL of 2x concentration of the CellTox™ Green staining solution was added to each well. Samples were protected from light and incubated (5% CO_2; 37◦C) for 15mins before 1 minute of shaking (500-700 RPM). The plate was placed into a microplate-reader for fluorescence intensity measurements using an excitation wavelength of 485–500nm and emission of 520–530nm. Treatments were performed in triplicate. Measurements were exported in a spreadsheet for analysis.

4.2.6.2. CellTiter-Blue® Cell Viability Assay

The CellTiter-Blue® Cell Viability Assay was used according to user manual for endpoint determination of rotenone-induced decrease in SN4741 cell viability following 24hr treatments. This assay utilises the ability of viable cells to convert the redox dye, resazurin, into a fluorescent end product resorufin. The colour change from blue to purple can be observed by eye and therefore the conversion of resazurin to resorufin can be quantified using a plate-reader with fluorimeter and spectrophotometer capabilities. The production of resorufin is hampered in a

population of dead cells as they readily lose metabolic capacity. Thus, the fluorometric intensity and spectrophotometric absorbance measured by the production of resorufin is proportional to cell viability. A spectrophotometer: measures the number of photons (the intensity of light) absorbed after it passes through sample solution. Resazurin is permeable to living cell membranes and is reduced to resorufin once inside living cells. Studies on hepatic subcellular sections show that resazurin (peak absorbance wavelength = 605nm) can be reduced by several redox enzymes found in the cytosol, micro soma and mitochondria. Once reduced, resorufin (peak absorbance wavelength = 573nm) freely diffuses back into the cell culture medium.

During the 24hr incubation of cells in the presence of rotenone, the The CellTiter-Blue® Cell Viability Assay Reagent were thawed in a 37°C water bath. 200 µL of cell culture medium was removed from treatment wells and 20 µL of CellTiter-Blue® Reagent was added. Sample plates were tapped gently to ensure solution homogeneity, before being returned to an incubator (5% CO_2; 37◦C) for 30mins. Absorbance measurements were collected for 1-4 hrs using an OMEGA microplate-reader. Treatments were performed in triplicate. Measurements were exported into an Excel spreadsheet for analysis.

4.2.6.3. SN4741 Counterstaining

To quantify numbers of SN4741 cells following experimental treatments, cells were fixed (as described previously) and counterstained with Hoechst. Hoechst is a blue fluorescent dye with a high affinity to binding with DNA and so is used to counterstain cell nuclei. Following fixation with 4% PFA the fixing solution was removed and a 100 µL of counterstaining solution, consisting of Hoechst diluted 1: 10,000 in PBS, was applied to the cells. The plate was protected from light and incubated for 15 mins at room temperature to counterstain SN4741 cell nuclei. The staining solution was then removed and cells were washed 2 times in 100 µL PBS before applying a final 100 µL of PBS to each well. Samples plates were sealed with parafilm and protected from light with tin foil. Plates containing counterstained cells were kept refrigerated (4◦C) until image acquisition with the In Cell Analyser 2000.

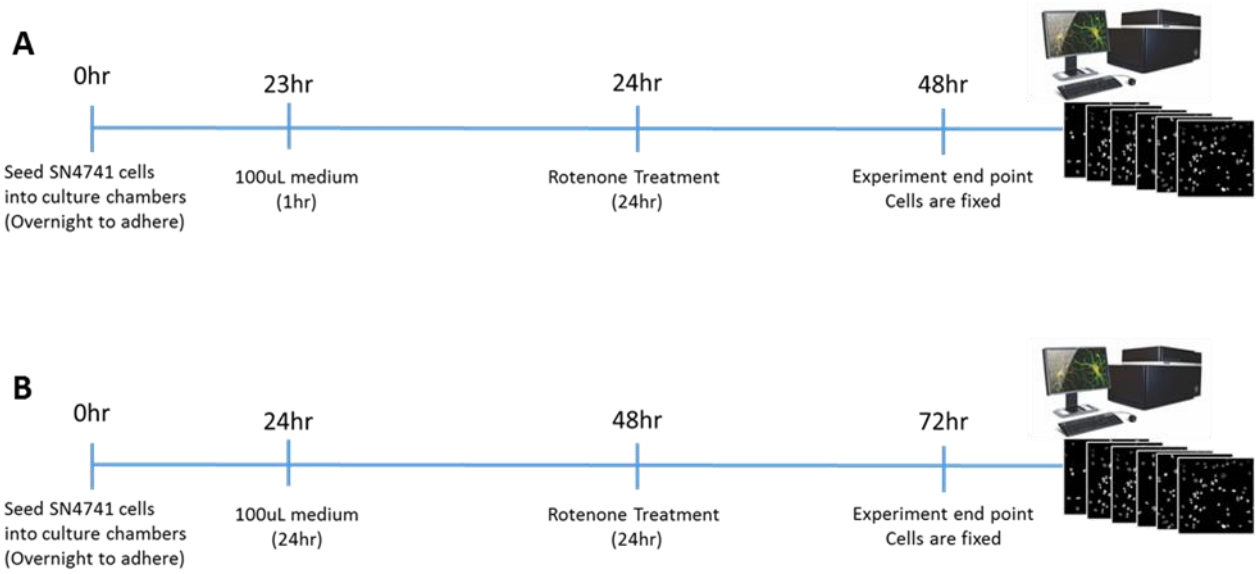

Figure 26: 24hr rotenone treatment timelines

Figure 26 illustrates experimental timeline from seeding SN4741 cells through to rotenone administration and fixation at experimental endpoint prior to cell counterstaining and image acquisition. (A) Illustrated experimental time lines for rotenone treatments in sync with 1hr GHSR1a agonist pre-treatment (A) and 24hr GHSR1a agonist pre-treatments (B).

4.2.6.4. Image Acquisition with In Cell 2000

The In Cell Analyser 2000 is an automated wide-field fluorescence microscope capable of 2D and 3D image capture. The In Cell Analyser 2000 contains a range of fluorescence and bright-field filters and objective lenses. A number of images were acquired per well. These images were termed ‘fields’ or ‘fields of view’. To quantify relative numbers of cells per well, the maximum number of fields per well was selected so that edges of the 96-well plate were not included. Sample plates were left to equilibrate to room temperature before placing into the In Cell Analyser 2000. Images were saved in TIF format to a Seagate (2TB) external hard drive for storage.

4.2.6.5. Image J Cell Count Analysis and Macro Automation

The protocol below describes the step-by-step imageJ protocol used to quantify SN4741 cell nuclei from x20 magnification digital images. Each step includes a description followed by instructions on how to execute the step in image J software (in italic font).

Image J available at (https://imagej.nih.gov/ij/download.html)

Step 1: Open x20 magnification raw image with image J software.

File > Open. Select the x20 magnification image to be analysed.

Step 2: Convert raw image to an 8-bit image and subtract background.

Image > Type > 8-bit

Process > Subtract Background > Set Rolling Ball Radius: 70 pixels.

For rolling ball radius background subtraction method, rolling ball radius must be at least as large as the radius of the largest object. The approximate radius size can be measured by drawing a straight line through the diameter of the largest object (nucleus) using *Set tool as 'Straight"*. Since, Diameter = 2 x Radius; Radius = Diameter/2.

E.g. If the diameter of the largest object (nucleus) measured approximately 120 pixels in length. Since Radius = Diameter/ 2; Radius = 120/2 = 70 pixels. And 60 pixels should be used as minimum Rolling Ball Radius.

Step 3: Enhance the contrast between foreground and background staining.

Process > Enhance Contrast. Select saturate pixels: 0.4%.

Step 4: Convert image to a masked image where there are only two colours, black and white (binary image). Then adjust the threshold until only the SN4741 nuclei appear white, and all image background is black. Use original or contrast enhanced images to ensure cell nuclei appear white. This is important as threshold values may vary slightly between images, therefore images from various treatment groups were selected and tested to before defining a set threshold to be applied to the entire dataset. Variation in image intensity was minimised by acquiring all x20 magnification images using an automated imaging system with identical exposure time and image type output.

Image > Threshold > Adjust Threshold. Move sliders to 'correct' threshold where only cell nuclei are visible in white against a black background.

Step 5: Invert the binary image so that nuclei are black and background is white.

After moving sliders to 'correct' threshold. Select 'Apply' on Thresholding window with 'Dark background' unchecked.

Step 5i: Shows the red box in step 5 (figure 27) zoomed-in shows a cluster of 3 nuclei which would be counted as 1 object by 'Analyse Particles' function in Image J.

Step 6: Separate touching nuclei using the watershed feature. The watershed feature finds the centre of each object and calculates a distance map from the object centre points to the edges of the objects. The algorithm then fills that "topological map" with imaginary water (watershed). A 1 pixel line (dam) is then placed between two objects where their water sheds meet.

Process > Binary > Watershed

Step 6i: Depicts the red box in step 6 (figure 27), zoomed-in region identifies a cluster of 3 nuclei which have been separated using the watershed feature. This cluster of nuclei would be counted as 1 object by 'Analyse Particles' function in Image J but will now be counted as 3 separate nuclei.

Step 7: Quantify the number of cell nuclei in the image. Once this step is executed image J will produce a table of results which includes (cell) counts and produce an image of numbered, identified cell nuclei.

Analyse > Analyse Particles > Set Particle size: 300- 10,000; Circularity: 0.50-1.00; select show: Overlay Outlines, Select: Display Results and select: Summarise.

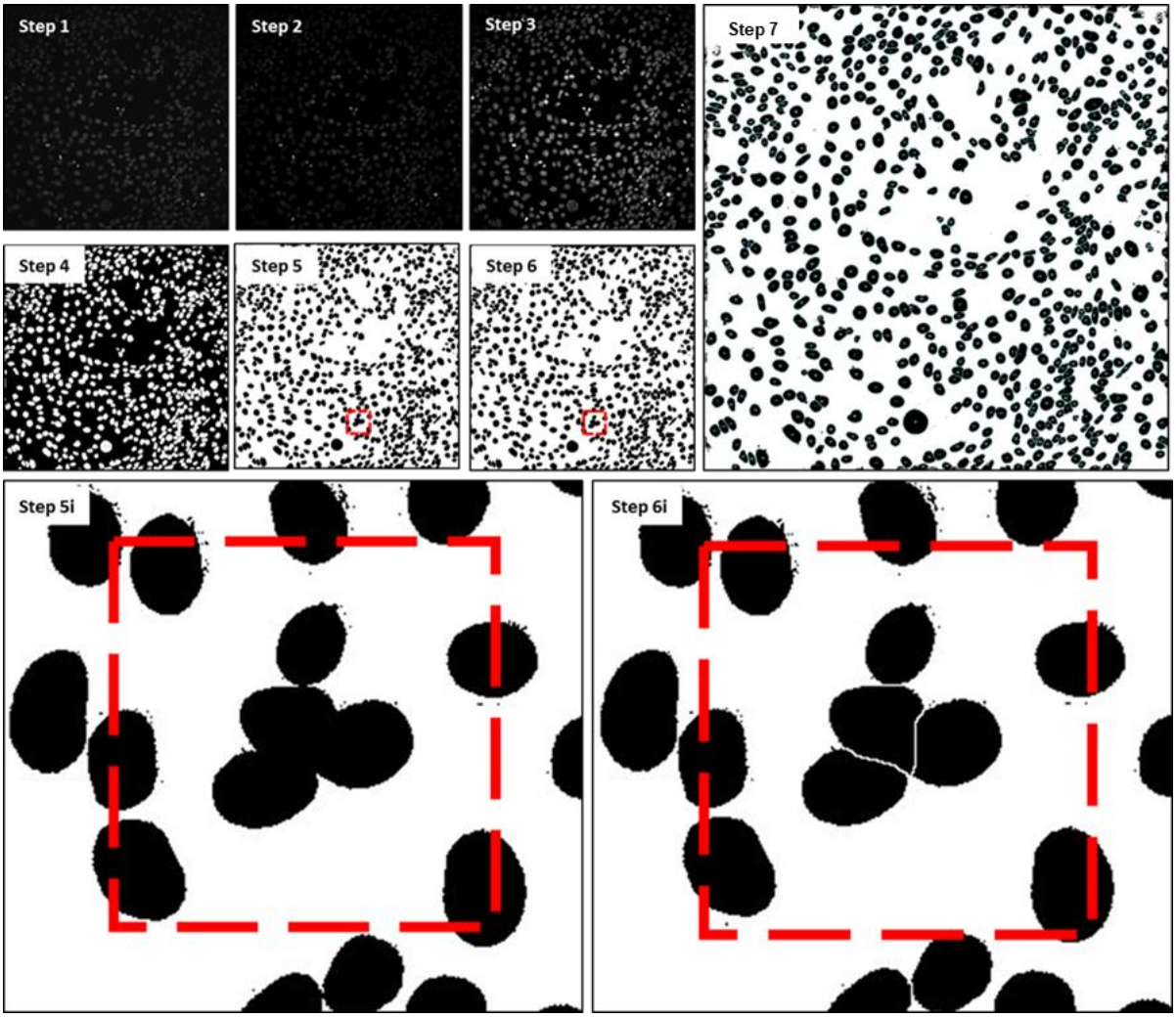

Figure 27: Schematic Illustration of Image J Cell Nucleus Count Protocol Steps 1- 7 as Described Above in "Image J Cell Count Analysis Macro"

Steps 2 through 7 can be automated by creating a macro. Once a macro is created, image J can execute the image processing steps 2-7 on a single image or a collection of images. To create a macro, open one of the images destined for analysis then select: *Plugins > Macros > Record*. When steps 2 to 7 have been completed, click '*Create*' macro and save as 'ijm' file. To run a macro on an image open an image on image J then select *Plugins > Macros> Run*. Select the previously saved macro and steps 2-7 will be executed on a selected image. Selecting and executing a macro for 100s or 1,000s of images is laborious. Image J possessed a batch processing feature which can be utilised to automate the application of an image analysis or image processing macro to an entire image set. This can be done by firstly storing all images

to be analysed into 1 folder. Then select: *Process > Batch > Macro. Select the folder containing images to be analysed into 'Input' and select a folder to store all Overlay Outline images in 'Output'. 'Open' the pre-saved macro containing steps 2-7 and select 'Process'.*

Image J will begin applying the macro in succession to an image set and subsequently populate a table of results which includes object (nuclei) counts. Data produced in image J was transferred to a Microsoft Excel spreadsheet. SN4741 cell nuclei were quantified in 30 fields of view (unless stated otherwise) in each well for each treatment. Treatments were performed in triplicate. Statistical analyses were carried out using GraphPad Prism 5.0 for PC.

4.2.6.6. Live/Dead Assay

LIVE/DEAD ® Viability/Cytotoxicity Kit *for mammalian cells* (L3224, Thermo Fisher Scientific) was also utilised to measure and validate rotenone-induced cytotoxicity across a titration of rotenone concentrations (Vehicle, 0, 10, 100, 1,000 and 10,000nM) with DMSO treatment serving as a positive control for cell cytotoxicity. The LIVE/DEAD ® Viability/Cytotoxicity Kit serve to distinguish viable from cytotoxic cells and with the use of two dyes. Both of which express negligible fluorescence before interacting with cells. The first dye, Ethidium Homodimer-1 (EthD-1) is used as a marker cell cytotoxicity. EthD-1 is impermeable to intact cell membranes. Once compromised EthD-1 enters the cell, binds to nucleic acids and undergoes a 40-fold enhancement of fluorescence. Thus, producing a bright red fluorescence in dead cells. Excitation/emission wavelengths: ~495 nm/~635 nm. Two vials containing 200 µL of EthD-1 (2 mM) was received in DMSO/H2O 1:4 (v/v). The second dye, Calcein AM, is cell permeable and enzymatically converted to the intensity green fluorescent dye calcein. The polyanionic dye calcein is formed in the presence of ubiquitous intracellular esterase activity which produces an intense uniform green fluorescence in live cells. Excitation/emission wavelengths: ~495 nm/~515 nm. Calcein AM (4 mM) was received in anhydrous DMSO.

3,000 SN4741 cell were seeded per well in a 96 well plate and exposed to a titration of rotenone concentrations as described (*Development of a Rotenone-induced neurotoxicity/cell loss in vitro PD model*). 1.25 µL Calcein AM (4 mM) and 5 µL EthD-1 (2 mM) was mixed and vortexed in 5 mL Dulbecco's phosphate-buffered saline (D-PBS) (14040133, Gibco) to produce a LIVE/DEAD staining solution (1µM Calcein AM; 2µM EthD-1). 200 µl of cell culture media was removed and 100µl of staining solution

was applied to the cells for 30 minutes at room temperature and protected from light. Calcein AM is sensitive to esterase activity and esterase activity may be found in FBS supplemented media. Culture media/staining solution was removed and cells were gently washed with 200 µL D-PBS to prevent extracellular fluorescence before fixation in 4% PFA. SN4741 nuclei were then Hoechst counterstained (see *SN4741 Counterstaining*) before 20x objective was used to acquire TexasRed, FITC and DAPI images using In Cell Analyser 2000. FITC stain was not retained well post-fixation and was omitted from analysis. DAPI images were used to identify nuclei as primary objects in the image sets. Mean intensity of nuclear EthD-1 staining in Texas-Red channel images was quantified using cell profiler 'Identify Primary Objects' and 'Measure Object Intensity' modules following image pre-processing. These steps are described fully in chapter 5. Three experimental repeats (n=3) were performed in triplicate and 25 images were acquired per well per treatment. Cell Profiler available at (http://cellprofiler.org)

4.2.6.7. Detection of Rotenone-Induced Activated Caspase 3/7 in SN4741 Neurones

To determine whether rotenone-induced cell loss was mediated via apoptosis, CellEvent™ Caspase-3/7 Green Detection Reagent (Invitrogen, C10423) was applied to cells prior to detection with fluorescence microscopy. Caspase 3 activation is an essential event in apoptosis. Cell Event™ Caspase-3/7 Green Detection Reagent novel fluorogenic substrate for activated caspases 3 and 7. The Caspase-3/7 reagent is a cell permeable compound containing a four amino acid peptide (aspartic acid, glutamic acid, valine and aspartic acid; DEVD) conjugated to a nuclei acid binding dye. In its conjugated form the caspase-3/7 reagent is intrinsically non-fluorescent, however activation of caspase-3 or caspase-7 in apoptotic cells leads to cleavage of DEVD peptide. Cleavage of DEVD peptide leads to the availability of nuclei acid binding dye enabling the dye to bind to DNA and produce a bright green, fluorogenic response inside cell nuclei with an absorption/ emission maximum of ~502/530 nm. This reagent is applicable for live-cell imaging and fixed (3.7% PFA) cell imaging approaches. The dye is well retained post-fixation and detergent permeabilization, making the reagent a candidate for potential multiplexing with other kits or immunostaining for identification of other proteins of interest. Detection reagent was received at 2 mM concentration in DMSO.

3,000 SN4741 cells were seeded per well in a multi-well plate prior to being subject to 24hrs of 10nM rotenone treatment. Rotenone treatment was prepared and administered as described in '*Development of a Rotenone-induced neurotoxicity/cell loss in vitro PD model'.* 50:50 DMSO: PBS solution served as a positive control for activation of apoptosis and DMSO diluted in culture medium served as vehicle. Following 24hrs of 10nM rotenone treatment 0.88 µL of CellEvent™ Caspase-3/7 Green Detection reagent was added and vortexed in 110 µL complete cell culture medium to yield a 16µM stock staining solution (volume was adjusted for number of wells required). 200 µL of was removed from cell culture wells and 100 µL 16µM stock staining solution was applied to cells for 30mins and incubated at 5% CO_2; 37◦C. Application of 100 µL 16 µM stock staining solution into 100 µL of medium present inside cell culture wells produces a 1:2 dilution resulting in a final well concentration of 8 µM Cell Event™ Caspase-3/7 Green Detection reagent. This concentration is within the recommended staining concentration described in CellEvent™ Caspase-3/7 Green Detection reagent user manual, 2 µM - 10 µM. Cell staining solution was removed following a 30 minute incubation with staining reagent. Cells were then fixed in 3.7% PFA and counterstained with Hoechst as described *'SN4741 Cell Growth Curve'* and *'SN4741 Counterstaining'.* Sample plate was sealed with parafilm, stored at 4◦C and imaged using the In Cell Analyser 2000 with 24hrs. 25 x20 magnification images were acquired per well using In Cell Analyser 2000 FITC and DAPI filters. Treatments were carried out in triplicate for two technical experimental repeats. Total cell number (blue Hoechst nuclei) and apoptotic cells (Green Caspase-3/7 Reagent$^+$ nuclei) were quantified in Image J image software as described in '*Image J cell count analysis and macro automation'*. Data is expressed as the percentage of apoptotic cells in the total cell population for each well:

$$\frac{number\ of\ apoptotic\ cells}{total\ number\ of\ cells} x\ 100.$$

Percentage of Caspase 3/7-positive (apoptotic cells) per well(s) was then used in Graph Pad Prism v.5 for statistical analysis.

4.2.6.8. Direct GHSR1a Agonist Neuroprotection in the Rotenone-Induced Neurotoxicity In Vitro PD Model

SN4741 cells cultured in complete medium were treated for 24hrs with 10nM rotenone which resulted in a decrease in the number of midbrain cell number ($P<0.05$) in conjunction with decrease cell viability ($P<0.01$) and increased cytotoxicity ($P<0.001$), as seen in figure 36 (a-c). SN4741 cells cultured in substrate restricted (60% of complete cell culture) medium were treated for 24hrs with 10nM rotenone which resulted in a decrease in the number of midbrain cell number ($P<0.01$) in conjunction with decrease cell viability ($P<0.05$) but no increased cytotoxicity ($P>0.05$), as seen in figure 36 (d-f). 10nM concentration of rotenone was selected to model PD neurodegeneration in our assay due to its efficacy in inducing the loss of SN4741 cells following a 24hr incubation period. To test the potential direct neuroprotective effects of AG and synthetic GHSR1a agonist (JMV 2894) SN4741 cells were treated prior to rotenone challenge. This experiment was carried out on SN4741 cells cultured in 60, 80 and 100% of complete full culture medium. Graphs of results showing significant protection will be displayed in the results section.

SN4741 cells underwent 1hr and 24hr pre-treatment with a titration of AG and JMV 2894 prior to 10nM rotenone challenge. 3,000 SN4741 cells in 100 µL cell culture media were seeded per well and incubated overnight under normal growth conditions (37◦C; 5% CO_2) to adhere. 2x concentrated stocks of AG and JMV 2894 was diluted in cell culture media. 100 µL 2x concentrated AG or JMV 2894 (IC50=0.5+/-0.3nM; EC50=0.6+/-0nM) is applied to treatment wells, performing a 1:2 dilution. Following the addition of 100 µL 2x concentrated stock solutions, final well concentrations of AG pre-treatments were: vehicle (H_2O), 1nM, 10nM, 100nM, 1,000nM. 1mg of lyophilized AG (Tocris, #1465) was reconstituted in 6.0335mL H_2O (Nuclease-Free Water, Ambion® Nuclease-Free Water) producing a 50 µM solution which was stored in single-use aliquots at -20◦C. 40 µL of 50 µM AG stock was mixed with cell culture medium to produce 1mL of 2µM (2,000nM) AG treatment solution. 1 in 10 serial dilutions were performed to produce the remaining 2x concentrated AG treatment solutions (200nM, 20nM and 2nM) e.g. 100µL of subsequent AG treatment solution was added into 900 µL culture medium.

Final well concentrations of JMV 2894 pre-treatment: vehicle (H_2O), 0.6nM, 6nM, 60nM, 600nM. 4.47mg of lyophilized JMV 2894 (molecular weight= 745.79; 10.08mg vial of compound 41 was received from Æterna Zentaris, Germany) was reconstituted in 998.94 µL H_2O (Nuclease-Free Water, Ambion® Nuclease-Free Water) producing a 6mM solution which was aliquoted and stored at -20◦C. 6mM JMV 2894 was then

diluted 1 in 100 (10 µL into 990 µL) in cell culture media to obtain a 600µM JMV 2894 solution. 0.6 µM (600 nM) JMV 2894 stock solution was prepared by mixing 1 µL into 1 mL cell culture medium. 1 in 10 dilutions were performed in cell culture medium to obtain the remaining 2x concentrated JMV 2894 solutions (60nM, 6nM and 0.6nM). SN4741 cells underwent 1hr and 24hr pre-treatment with GHSR1a agonists prior to 24hr rotenone challenge (10nM). Addition of rotenone was as described in '*Development of a rotenone-induced neurotoxicity/cell loss in vitro PD model*'. Cells were subsequently fixed (4% PFA; room temperature for 15mins) and prepared for In Cell Analysis of cell numbers by Hoechst nuclear counterstaining.

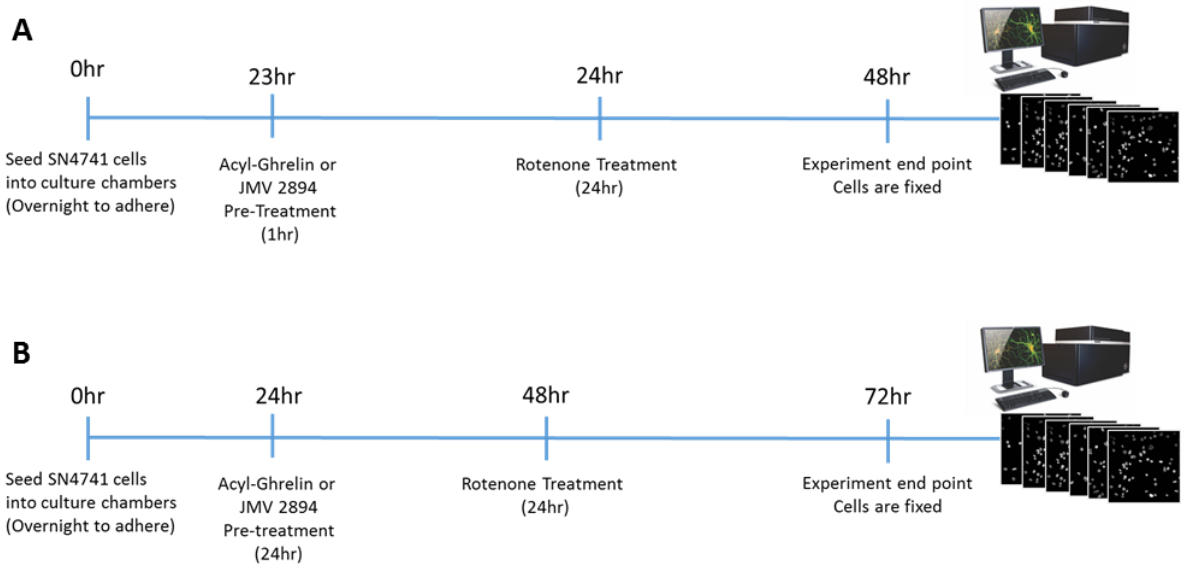

Figure 28: 1hr & 24hr GHSR1a Agonist Pre-treatment Timelines

Figure 28 illustrates experimental timeline from seeding SN4741 cells and GHSR1a agonist pre-treatments through to rotenone administration and fixation at experimental endpoint prior to cell counterstaining and image acquisition for 1hr GHSR1a agonist pre-treatments (A) and 24hr GHSR1a agonist pre-treatments (B).

4.2.6.9. Measurement of Ghrelin-Induced SN4741 Cell Proliferation using EdU (5-Ethynyl-2´-Deoxyuridine) Click-iT Assay

Using our in-vitro PD model, we have shown that acyl-ghrelin pre-treatment attenuates rotenone-induced SN4741 cell loss. To ensure the increase in cell number observed at the endpoint of our assay is the result of AG-neuroprotection and not the result of AG-induced cell proliferation, we employed Click-iT® EdU AlexaFluor®488 HCS Assay (C10351, Invitrogen) to investigate proliferation status of SN4741 cells. The most accurate method of evaluating proliferation is measurement of DNA synthesis. 5-ethynyl-2´-deoxyuridine (EdU) is a thymidine analogue which is readily incorporated into DNA during DNA synthesis occurring in S-Phase of the cell cycle.

Detection of EdU is based on a copper-catalysed covalent reaction between an Alexa Fluor® dye which contains azide and an alkyne contained in EdU. EdU has an advantage over BrDU (also a thymidine analogue) as an efficient detection of the incorporated EdU is possible using standard aldehyde-fixation and detergent permeabilization (e.g. Triton®-X100). The Click-iT® EdU assay is also compatible with nuclear counterstaining (blue fluorescent Hoechst 33342) and multiplexing with immunocytochemistry protocols to identify other cell surface or intracellular markers. Conversely, BrdU detection often requires harsher preparations such as DNA denaturation to expose BrdU antigens for detection via a anti-BrdU antibody. DNA denaturation may disrupt integrity of double-stranded DNA and subsequent nuclear counterstaining. DNA denaturation may also affect cell morphology and affect antigenicity. BrdU antibodies can also exhitbit non-specific binding. This final problem is overcome with the Click-iT® EdU assay using biologically unique (biorthogonal) moieties to ensure minimal background noise and high EdU detection sensitivity.

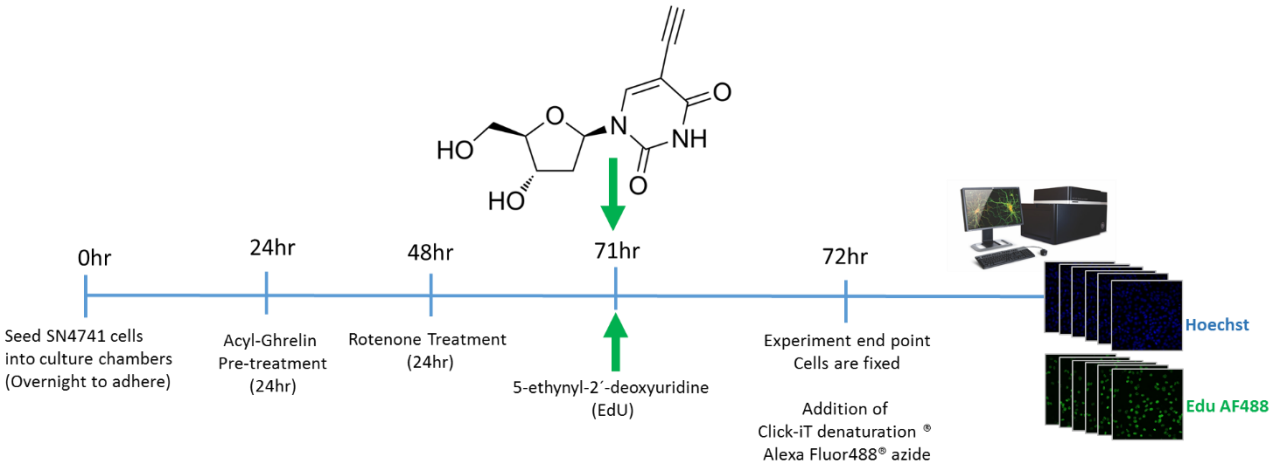

Figure 29:Click-iT EdU Assay Experimental Timeline.

Figure 29 illustrates experimental timeline from seeding SN4741 cells and GHSR1a agonist pre-treatments through to rotenone administration and addition of EdU at 71hrs. Following 1hr incubation, thymidine analogue (EdU) is incorporated into cells undergoing DNA synthesis. At experimental endpoint (72hrs), cells are fixed before the addition of Click-iT detection reagents containing AlexaFluor 488® (AF488) and Hoechst 33342 nuclear counterstain. Images of fluorescently labelled cells are then acquired using the In Cell Analyser 2000.

We selected the following treatments to investigate potential proliferative effects of 1µM AG on SN4741 cells: Vehicle (including water and DMSO diluted accordingly); 1µM AG (diluted in vehicle) and cells exposed to 10nM rotenone in the presence and absence of a 24hr 1 µM AG pre-treatment. Treatments were performed in 100% full culture media and 60% of full culture media. We propose that 1µM AG pre-treatment (24hr) promoted direct neuroprotection from 10nM rotenone-induced cell loss seen in our previous neurotoxicity assay/PD model. Vehicle treated cells and 1µM AG treated cells were inspected to establish whether direct AG promoted proliferation in the absence of neurotoxin challenge. 20µM EdU-media mix was omitted from negative control wells to ensure green EdU fluorescence signal originated from EdU-DNA binding and was not a product of the reaction cocktail alone. All treatments were performed in triplicate for 2 technical repeats (n=2).

SN4741 cells were seeded before undergoing experimental procedure for 24hr 1µM AG pre-treatment. See: '*Direct GHSR1a agonist neuroprotection versus rotenone-induced SN4741 cell loss';* for full description. A 2x concentrated (20µM) EdU staining solution was prepared in cell culture medium. At 71hrs, 200µL of cell culture medium was removed from wells and replaced with 100µL EdU (20µM) staining solution. SN4741 cells were incubated for 1 hr under standard culture conditions (37◦C; 5% CO_2) in EdU (10µM) containing media. Cell medium was removed and cells were fixed (3.7% PFA; room temperature; 15 mins) (see figure 29 for experimental timeline). Fixative was discarded and cells were washed twice in 3% Bovine serum albumin (BSA) (A2153-100G, Sigma) in PBS. Cells were permeabilized in 0.5% Triton® X-100 (X100-500ML, Sigma) in PBS for 20 minutes at room temperature. Fresh 1x Click-iT® EdU buffer additive and Click-iT® reaction cocktail was prepared according to user manual. For optimal results reaction buffer was used within 15 minutes of preparation from kit components: 1X Click-iT® reaction buffer, CuSO4 (Component E), Alexa Fluor® azide and Reaction buffer additive. Permeabilization solution was removed and cells were washed a further 2 times with 100µL 3% BSA in PBS. Click-iT® reaction cocktail was then distributed (50 µL) into each well. Sample plates were protected from light and gently rocked at room temperature for a 30 minute incubation step. All steps were then carried out with minimal direct exposure to light. Reaction cocktail was removed and cells were washed once in 100µL 3% BSA in PBS and once in 100µL PBS. SN4741 cell nuclei were then counterstained by incubation with 100µL of Hoechst 33342 diluted (1:2,000; 5µg/mL) in PBS. Cells were protected from light and incubated for 30 minutes at room temperature. Cells were washed twice in PBS before imaging and analysis using the In Cell Analyser 2000. 25 fields of view (images) were acquired within each well at x20 magnification and 12 images per well were acquired at x40 magnification (for illustrative purposes). Images were acquired for both (blue) Hoechst 33342 and (green) and Click-iT® EdU AlexaFluor®488 fluorescence signals. Approximate fluorescence excitation/emission maxima for AlexaFluor®488 and Hoechst 33342 bound to DNA are 495nm/519nm and 350nm/461nm, respectively. The total number of cells (Blue Hoechst nuclei) and number of actively proliferating cells (Green AlexaFluor®488) in 25 fields of view were quantified using the batch macro process in image J analysis software. Later, datasets were also analysed using Cell Profiler image analysis software to compare data outputs. Higher magnification (x40) images were also analysed by both software. Statistical analysis was carried out in Graph Pad Prism V.5.

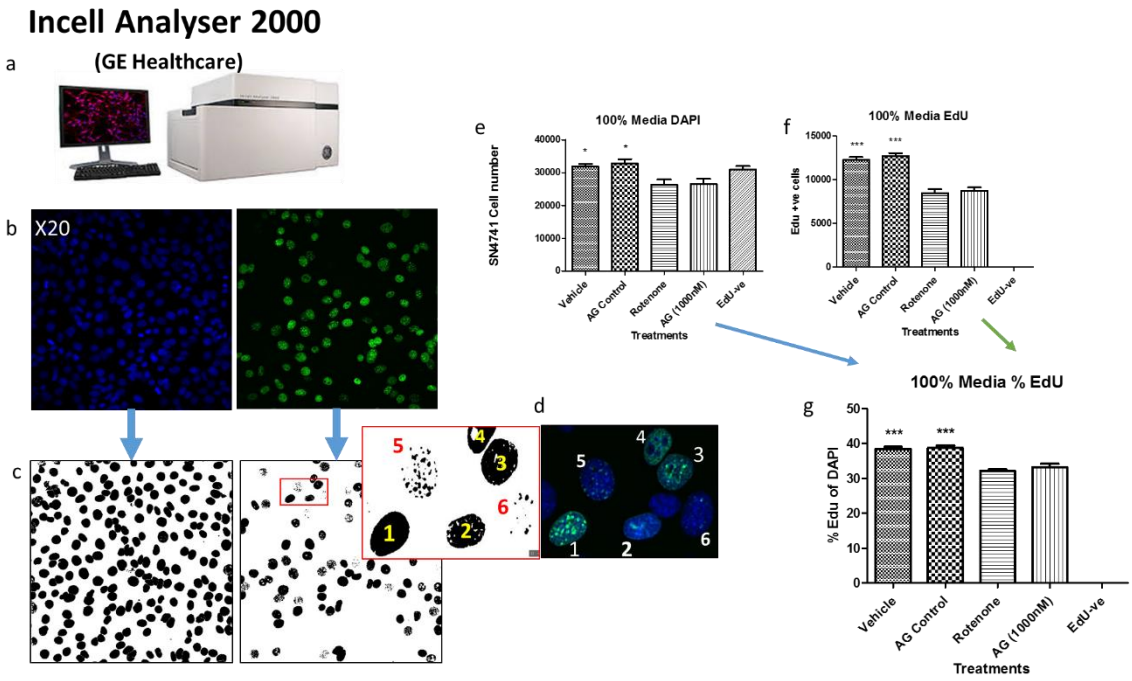

Figure 30: Work Flow Through of EdU Assay and Analysis.

This figure illustrates the step-by-step method use to quantify the percentage of EdU+ve cells. Using the In Cell Analyser (a), images of Hoechst and EdU stained nuclei were acquired (Blue and green respectively) (b). Automated Image J cell scoring was employed to quantify nuclei in both image channels. (C) Illustrates binary masks of scored nuclei, whilst (d) represents numbered nuclei in a zoomed section (red box) of a x20 magnification image (c). Total number (e) and number of EdU+ve nuclei (f) are quantified. These data are used to calculate the percentage of EdU+ve nuclei (g).

4.2.6.10. Ghrelin Receptor (GHSR1a) Antagonist versus Acyl-Ghrelin Neuroprotection

Acyl- Ghrelin (AG) pre-treatment (24hr) significantly attenuates the loss of SN4741 cells in our *in-vitro* rotenone assay. The proposed mechanism of action by which AG exerts neuro-protection is thought to begin extracellularly with the binding of AG to its endogenous receptor, GHSR1a.

Here, we use two known GHSR1a antagonists in order to establish whether AG (1uM) attenuation of SN4741 cell loss during rotenone (10nM) challenge is dependent on GHSR1a. We have previously demonstrated that the SN4741 cell line expresses GHSR1a along with some key ghrelin axis proteins; APT1 and GOAT.

In an attempt to inhibit GHSR1a signalling we pre-incubated (30mins) SN4741s with GHSR1a antagonists at a range of concentrations (10, 100, 1000 and 10,000nM) prior to AG pre-treatment (24hrs) and subsequent rotenone challenge (24hr). D-Lys3 -GHRP-6 (D-Lys3) (500µg, Phoenix Pharmaceuticles, 031-22) is a peptide inhibitor of GHSR1a (IC50= 0.9µM). 500µg D-Lys3 was reconstituted in 10.75mL water to produce 50 µM D-Lys3 solution which was aliquoted and frozen (-20◦C).

Antagonist D-Lys3 stock solutions were added to culture medium in order to prepare 30,000nM antagonist solutions- see table 15 for volumes. This antagonist solution was diluted 1:10 to achieve 30,000, 3000, 300 and 30nM antagonist concentrations. 50µL of each of these were added to cells bathing in 100µL of media (a 1:3 dilution) resulting in final well concentrations of 10,000, 1000, 100, 10nM.

Table 15: Preparation of 30µM GHSR1a Antagonist Solutions

Antagonist	**Volume of Antagonist**	**Volume of Medium**	**Final volume**
D-Lys3	1200ul	800ul	2ml

Vehicle solutions were prepared by adding a volume of water corresponding 'Volume of Antagonist' to full medium.

Antagonists were then added to respective wells and incubated under normal growth conditions (37◦C; 5% CO_2) for 30mins. In this period 4µM (4000nM) AG was prepared from frozen stock (at 50µM) by the addition of 152µL of stock AG into 1748µL of

media. 50µL of this was added to the wells resulting in a 1:4 dilution and a final well concentration of 1000nM AG. SN4741 cells were then incubated under normal culture conditions for 24hrs prior to rotenone challenge (previously described). Cells were fixed, counter stained and analysed as previously described. 25 2-D de-convoluted fluorescence images per well were acquired on the 20x magnification objective of the In Cell Analyser 2000 using the DAPI filters- 100% autofocus; 0.5 second exposure. SN4741 nuclei counts were measured using Cell Profiler image analysis software.

4.2.6.11. 5' Adenosine Monophosphate-activated Protein Kinase (AMPK) Antagonist and Acyl-Ghrelin Neuroprotection

Here we use Compound C (171260, EMD MILLIPORE), a known inhibitor of AMPK, to establish whether AG (1uM) attenuation of SN4741 cell loss during rotenone (10nM) challenge is dependent on the cellular energy homeostasis regulator, AMPK. The phosphorylation of AMPK regulates mitochondrial biogenesis which is thought to result in cellular protection (Reznick & Shulman, 2006).

First, 10mM Compound C stock solution was prepared by dissolving 1mg of powder in 250uL DMSO, aliquoted and stored at 4°C. SN4741 cells were cultured for 48hr in a titration of Compound C concentrations. This was performed in sync with the 24hr AG pre-treatment neurotoxicity experiment, also described in GHSR1a antagonist section, to find a concentration which would not result in SN4741 cell loss. The results of initial test was used to determine the concentration to be used to determine whether AG-mediated neuroprotection is pAMPK dependents.

Compound C Titration: 3,000 SN4741 cells in 100µL of medium were seeded in into a 96-well plate and incubated overnight under standard conditions. On the day of Compound C and AG treatment, 1µL of 10mM Compound C stock was mixed into 1mL of medium producing a 10 µM working stock solution. This working solution was then diluted in 100% or 60% of complete medium to produce 3x concentrated Compound C solutions to apply to cells. The final 1:3 dilution consisted of adding 50µL of 3x concentrated treatments to each well containing 100µL of medium. The final well treatment concentrations were 0nM (vehicle), and 20nM, 40nM, 60nM, 80nM, 100nM, 1000nM Compound C for 30 minutes prior to the addition of 50µL of cell culture medium to simulate the addition of AG treatment in the subsequent neurotoxicity assay. Table below details the volumes of Compound C working solution and medium used to produce concentrated treatments.

Table 16: Preparation of Compound C Solutions.

Compound C Final well Concentration (nM)	Compound C 3x Concentration Solution (nM)	Volume of 10 µM Compound C Working Stock Solution (µL)	Volume of Cell Culture Medium (µL)
0	0	0.00	500.00
25	75	3.75	496.25
50	150	7.50	492.50
75	225	11.25	488.75
100	300	15.00	485.00
250	750	37.50	462.5
20	60	0	500
40	120	6	494
60	180	9	491
80	240	12	488
100	300	15	485
1000	3000	150	350

Following a 30 minute incubation with Compound C, 50µL cell culture medium was added to each well before returning the culture plate to incubate under standard conditions for 24hrs. 100µL of additional medium was then added for the final 24hr prior to fixing, counterstaining and analysis of SN4741 cell nuclei. Treatments were carried out in quadruplicate for 2 experimental repeats (n=2) in both complete (100%) and substrate restricted (60% of complete) medium.

Compound C in neurotoxicity assay: Titration experiment showed that 100nM of potent AMPK phosphorylation inhibitor Compound C did not result in a significant decrease in cell number, as observed in figure 51 (a & b) ($P>0.05$). This concentration was used to test AG-mediated neuroprotection. 3,000 SN4741 cells in 100µL of medium were seeded in a 96-well plate and incubated overnight under standard conditions. Following a 30 minute incubation with 100nM Compound C, 50uL of 4x concentrated AG was applied to SN4741 cells 24hrs prior to rotenone (10nM) challenge (24hr). Cells were then fixed and counterstained for cell count analysis.

Image acquisition: 25 2-D de-convoluted fluorescence images per well were then acquired on the 20x magnification objective of the In Cell Analyser 2000 using the DAPI filters- 100% autofocus; 0.5 second exposure. SN4741 nuclei counts,

corresponding to cell counts, were acquired using a nucleus identifying pipeline in Cell Profiler image analysis software.

The effects of Acyl Ghrelin on SN4741 intracellular metabolic signalling pathways

We propose that the neuroprotection observed in AG pre-treated SN4741 cells is the result of a switch in metabolite utilisation from glucose derivatives to fatty acid derivatives. AG pre-treatment also led to a greater attenuation of rotenone-induced cell loss in substrate restricted (SR) media (60% of full medium) ($P<0.001$) as opposed to 100% medium ($P<0.01$), shown in figure 43 (a-c). Thus, we also queried whether this proposed switch in metabolic regulation was enhanced in SN4741 cells cultured in SR medium.

To investigate the role of metabolic sensor AMPK and fatty acid synthesis and degradation regulator protein, ACC, we collected SN4741 protein lysates from our *in vitro* neurotoxicity PD assay. 24hr AG pre-treatment neurotoxicity timeline (see figure 28 B) was replicated in T25 cell culture flasks with modifications to scale.

$1x10^6$ SN4741 cells were seeded into T25 cell culture flasks (CLS430639, Sigma) in 10mL of cell culture medium and incubated overnight (16-24hr) under normal culture conditions. 5mL of cell culture medium was then removed and replaced with 5mL of fresh medium in the presence of 2µM AG resulting in a 1:2 dilution and a final vessel AG medium concentration of 1µM. AG was omitted from vehicle flasks and replaced with equivalent volumes of H_2O. SN4741 cells were cultured in AG for 24hr prior to the removal of 5mL of culture medium. 5mL of culture medium was subsequently replaced with medium containing 20nM concentration of rotenone resulting in SN4741 cells being cultured in 10nM rotenone. SN4741 in the presence and absence of rotenone were incubated under normal conditions for a further 24hrs. Rotenone was omitted from vehicle flasks and replaced with an equivalent volume of DMSO. SN4741 cell protein lysates were collected from flasks at 24hr intervals prior to the addition of subsequent treatment agents. This allowed us to investigate intracellular targets of interest, step-by-step along our assay timeline, in the presence and absence of AG and rotenone treatments.

At relevant time points, cell culture medium was removed from T25 flasks and cells were washed twice in 10mL of cold PBS (on ice). 250µL of lysis buffer [consisting of 91% deionised H_2O; 150mM Tris HCl, pH7.5; 150mM NaCl; 1% IGEPAL® CA-630;

0.5% sodium deoxycholate (DOC); 0.1% Sodium dodecyl sulfate (SDS); including 1% protease inhibitor and 1% phosphatase inhibitor] was then pipetted onto cells in a T25 flask. Flasks were swirled gently to ensure total coverage of adhered cells in culture vessel before being placed on ice. Cells were scraped from the culture flasks using Greiner cell scrapers (C5981, Sigma) and lysates were transferred to 0.6mL microcentrifuge tubes (E1405-0610, StarLab). Cell lysate was passed 10 times through a 25G needle to mechanically sheared contents and placed on ice for 15 minutes. Following this incubation stage cell lysates were then centrifuged at 14,000 revolutions per minute (RPM) at 4◦C for 10 minutes. Centrifugation ensures that cellular debris is pelleted below protein containing supernatant. Supernatant was transferred into fresh microcentrifuge tubes for estimation of protein concentration and downstream Western blot (described in chapter 2). Cellular debris was discarded.

See experimental timeline (figure 31) and table (table 17) below:

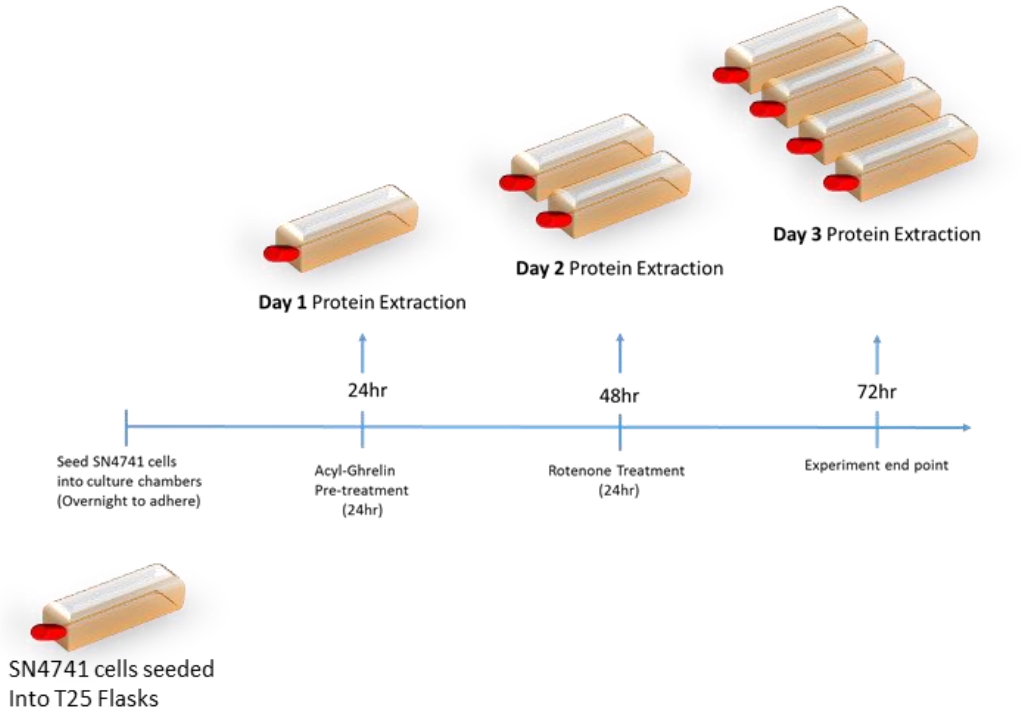

Figure 31:Experimental Timeline for SN4741 Protein Extraction

SN4741 cells were lysed at 24, 48 and 72hour time points post seeding $1x10^6$ SN4741 cells into T25 cell culture flasks.

Table 17: List of Treatment Conditions and Time of SN4741 Protein Extraction

Time point /Day	24hr / Day 1	48hr / Day 2	72hr / Day 3
SN4741 cell treatment(s)	• No Treatment	• Vehicle • 24hr 1µM AG	• Vehicle • 24hr 10nM Rotenone • 24hr 1µM AG pre-treatment & 24hr 10nM Rotenone • 24hr 100nM Rotenone

Relative expression levels of intracellular signalling proteins AMPK and ACC of each treatment group was expressed as a ratio- phosphorylated:non-phosphorylated AMPK (pAMPK:AMPK) and phosphorylated:non-phosphorylated ACC (pACC:ACC). The table below lists details of the primary and secondary antibodies used.

As previously described (Chapter 2: 2.3.4), blots were incubated overnight with primary antibody before the addition of complimentary secondary antibody and subsequent visualisation of chemiluminescence signal using ChemiDoc XRS (Biorad) and Quantity One® 1-D analysis software. 2-D Raw images were transformed using the auto-scale within the Quantity One® software using the transform function and exported. Blot analysis was carried out in Image J software. Data analysis was carried out in Microsoft Excel. Data points were plotted and statistical analysis was carried out in Graph Pad Prims version 5.

Table 18: Primary and Secondary Antibodies Utilised in AMPK/pAMPK & ACC/pACC Western Blot

Target protein	Description	Primary antibody concentration	Secondary Antibody Concentration	Molecular weight kDa
Phospho-AMPKα (Thr172) (40H9) Rabbit mAb. Cell Signalling Technology #2535	Detects endogenous AMPKα only when phosphorylated at threonine 172. The antibody detects both α1 and α2 isoforms of the catalytic subunit. Does not detect the regulatory β or γ subunits.	1:1000 in 5% w/v BSA, 1X TBS, 0.1% Tween® 20	Anti-Rabbit IgG, HRP-linked Antibody (7074S, Cell Signalling Technology). 1:2500 in 5% w/v NFM, 1X TBS, 0.1% Tween® 20	62
AMPKα (D63G4) Rabbit mAb. Cell Signalling Technology #5832	Detects endogenous levels of total AMPKα protein.	1:1000 in 5% w/v BSA, 1X TBS, 0.1% Tween® 20	Anti-Rabbit IgG, HRP-linked Antibody (7074S, Cell Signalling Technology). 1:2500 in 5% w/v NFM, 1X TBS, 0.1% Tween® 20	62
Phospho-Acetyl-CoA Carboxylase (Ser79) Antibody. Cell Signalling Technology #3661	Detects endogenous levels of ACC only when phosphorylated at serine 79. Antibody recognizes both ACC alpha and ACC beta.	1:1000 in 5% w/v BSA, 1X TBS, 0.1% Tween® 20	Anti-Rabbit IgG, HRP-linked Antibody (7074S, Cell Signalling Technology). 1:2500 in 5% w/v NFM, 1X TBS, 0.1% Tween® 20	280
Acetyl-CoA Carboxylase Antibody. Cell Signalling Technology #3662	Detects endogenous levels of all isoforms of acetyl CoA carboxylase protein.	1:1000 in 5% w/v BSA, 1X TBS, 0.1% Tween® 20	Anti-Rabbit IgG, HRP-linked Antibody (7074S, Cell Signalling Technology). 1:2500 in 5% w/v NFM, 1X TBS, 0.1% Tween® 20	280

4.3. Results

4.3.1. SN4741 Cell Growth Curves

To estimate the amount of time required to grow SN4741 cells to a quantity desired to carry out an experiment, confluency and cell concentrations (cells/mL) were measure at 0, 24, 48, 72 and 96 hours post seeding 34,000 SN4741 cells into a T75 culture flask containing 19ml of cell culture medium.

A

Hours	Day	Confluency (%)	Count (cell/ml)
0	0	na	34000
24	1	45	81490
48	2	60	185700
72	3	90	482500
96	4	100	610600

B

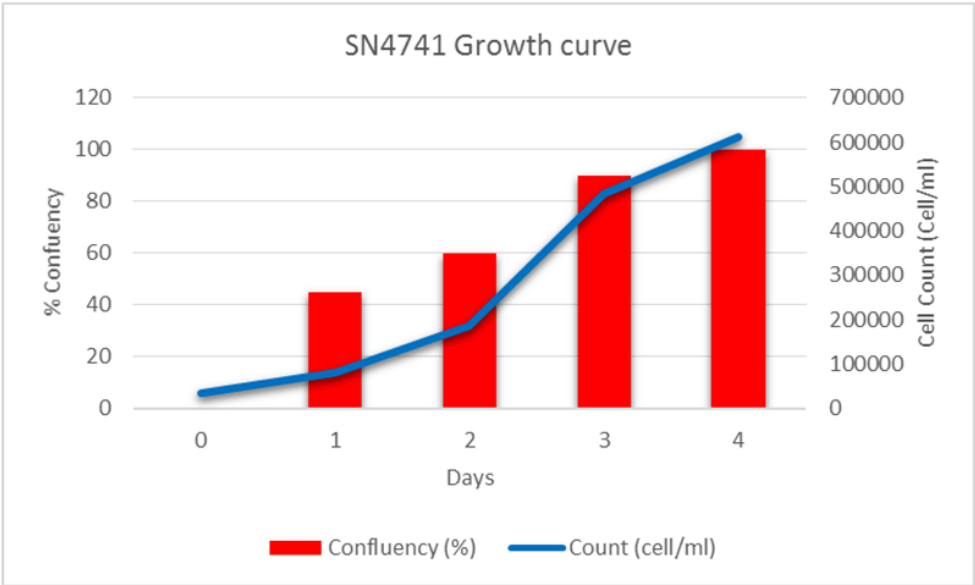

C

$$DoublingTime = \frac{duration * \log(2)}{\log(FinalConcentration) - log(InitalConcentration)}.$$

Where "log" is the logarithm to base 10 or 2 or any other base.

Units : You can use any time unit for duration. Doubling time unit will be the same.

Figure 32: SN4741 growth rate in full culture medium.

34,000 SN4741 cells were seeded into full culture medium and cultured in a T75 flask. Confluency (%) and cell count (Cells/mL) measurements were taken at 0, 24, 48, 72 and 96 hours (A). These measurements (A) are plotted in a graph (B) using MS Excel 2013. SN4741 cell doubling time was quantified by inputting the initial (34,000 cells/ml) and final (610,600 cells/ml) cell concentrations into equation (C). SN474 doubling time calculated as 23.04 hours. Cell doubling equation acquired from Roth

V. 2006 Doubling Time Computing, Available from: http://www.doubling-time.com/compute.php.

This method of calculating SN4741 cell doubling time in (figure 32) utilises 2 data points. Next, in order to generate a cell doubling time using all data points listed in **figure 32a,** a curve fitting equation to fit my data points to a theoretical curve described here : http://mathworld.wolfram.com/LeastSquaresFittingExponential.html was used. This second method applies least square fitting method directly to a dataset and weighs all data points equally.

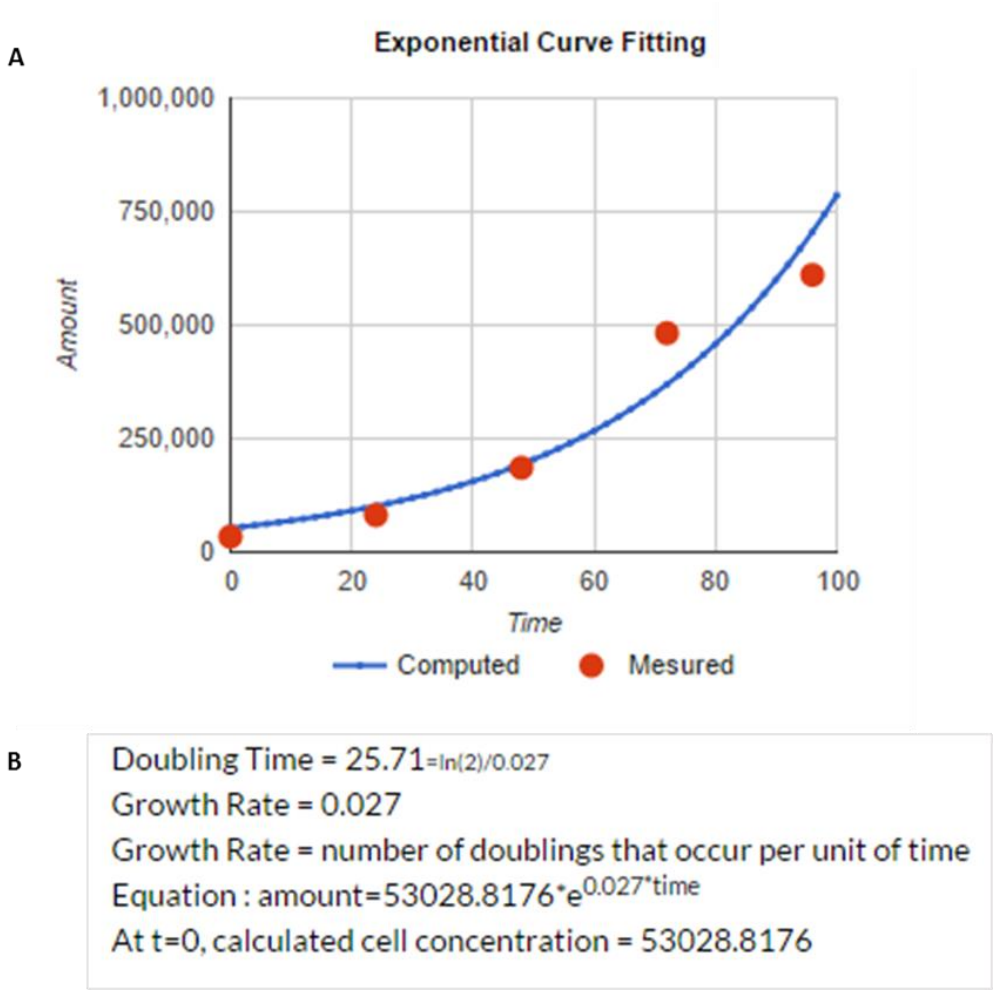

Figure 33: SN4741 Growth Rate in Full Culture Medium Using All Data Points

All data points from **figure 33a** were imputed to a doubling time generator which computes Doubling Time with several data points accessed at: http://www.doubling-time.com/compute_more.php. The online generator generated an exponential curve fitting of all data points (A) and calculated an SN4741 cell doubling time of 25.71 hours (B). This method is with reference to Weisstein, Eric W. "Least Squares Fitting--Exponential." From MathWorld--A Wolfram Web Resource.

Both methods of calculating SN4741 cell doubling time yield slightly different times. The first method utilises initial and final SN4741 cell concentration and does not consider other data points. This method may misrepresent SN4741 cell doubling time as the rate of cell growth may alter during the period between the initial and final time points. The second method fits all data points to a theoretical curve. However, in doing so, alters the initial SN4741 concentration from 34,000 to 53,028.8176 cells/mL. Both methods misrepresent the dataset and a 2.67 hour difference is found between both cell doubling times. SN4741 cell doubling time was approximated by calculating the mean of both values. Mean SN4741 doubling time = 24.375 hours; standard deviation (std.dev) = 1.88798; population std.dev = 1.335).

Finding an approximate population doubling time for SN471 cells is important for experimental design. It will allow us to approximate the time taken for a culture vessel to become confluent and ready for sub-culturing, and avoid over-confluency during cell culture. Changes in the rate of routine SN4741 growth may also indicate a problem within the cell culture system.

4.3.2. Development of a Rotenone-Induced Neurotoxicity/Cell Loss In Vitro PD Model

To define a minimum dose (concentration) of rotenone which replicated the cell loss observed in PD. SN4741 cell line was incubated for 24hr in rotenone of concentrations 0nM, 10nM, 100nM, 1,000nM and 10,000nM. SN4741 cells under the same treatments were assessed for an increase in cell cytotoxicity and a decrease in cell viability. A concentration which replicated DAergic SN4741 cell loss and resulted in increase in cell cytotoxicity and a decrease in cell viability will be selected to test neuroprotective effects of 1hr AG and JMV 2894 pre-treatments.

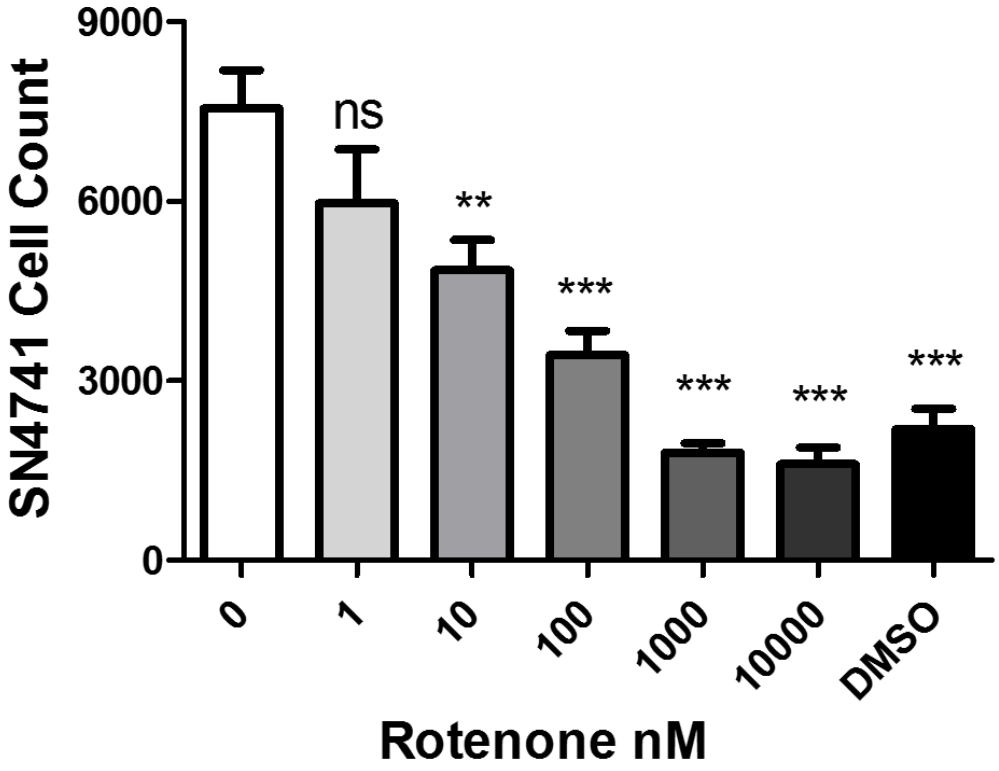

Figure 34: 24hr Rotenone Treatment Causes SN4741 Cell Loss.

24hr rotenone challenge exerts a dose dependant SN4741 cell loss. Rotenone neurotoxicity assay treatments were performed in quadruplicate for each experimental repeat; data shown from 4 experimental repeats (n=4). Statistical analysis was performed by One-way ANOVA with Dunnett's post-hoc analysis, with $P<0.05$ (*), $P<0.01$ (**), $P<0.001$ (***) considered significant when compared to control (0nM Rotenone).

SN4741 cells in sync with 1hr GHSR1a agonist pre-treatment timeline seen in Figure 26a were challenged with a titration of rotenone concentrations. 24h challenge results in a significant (**) SN4741 cell loss (P<0.01) (figure 34) at 10nM rotenone concentration and a dose-dependent decrease in cell number at concentrations thereafter. Next, SN4741cells in sync with 24hr GHSR1a pre-treatment timeline as seen in Figure 26b were subjected to rotenone challenge.

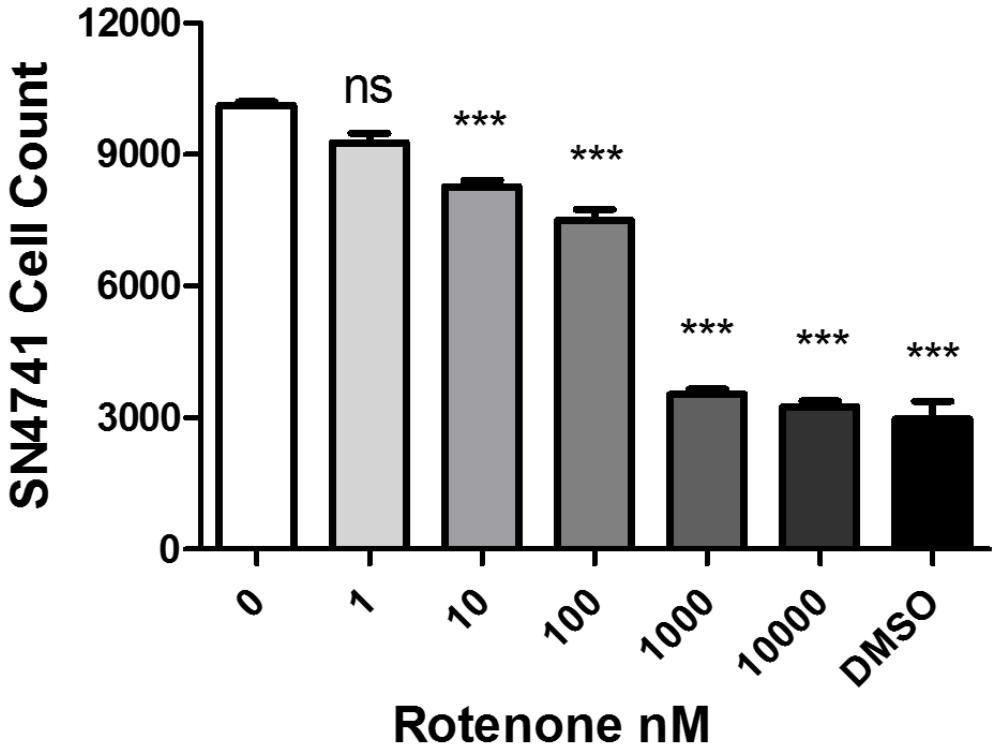

Figure 35: 24hr Rotenone Treatment Causes SN4741 Cell Loss

Rotenone challenge exerts a dose dependant SN4741 cell loss as illustrated. Rotenone neurotoxicity assay treatments were performed as described in timeline figure26b in quadruplicate for each experimental repeat; data shown from 4 experimental repeats (n=4). Statistical analysis was performed by One-way ANOVA with Dunnett's post-hoc analysis on graph pad prism 5 software, with P<0.05 (*), P<0.01 (**), P<0.001 (***) considered significant when compared to treatment control (0nM Rotenone).

SN4741 cells were challenged with a titration of rotenone concentrations for 24hrs in sync with 24hr GHSR1a agonist pre-treatment timeline as seen in Figure 26b. Results show a dose-dependent decrease in SN4741 cell number and a significant (***) cell loss at 10nM rotenone concentration (graphed in figure 35).

We have established that 10nM rotenone is sufficient to ensure a significant and reproducible decrease in SN4741 cell number cultured in 100% of full medium following a 24hr incubation. We will use 10nM rotenone to assess SN4741 cell viability and cytotoxicity.

4.3.3. The CellTox™ Green Cytotoxicity & CellTiter-Blue® Cell Viability Assays

SN4741 cells in 100% and 60% of full medium were assessed for cell numbers, cytotoxicity and cell viability following 24hr rotenone treatment (in sync with 24hr GHSR1a pre-treatment). Hoechst counterstained nuclei were quantified using In Cell Analyser 2000 whilst cytotoxicity and viability measurements were carried out on POLARstar® Omega (BMG Labtech) microplate reader.

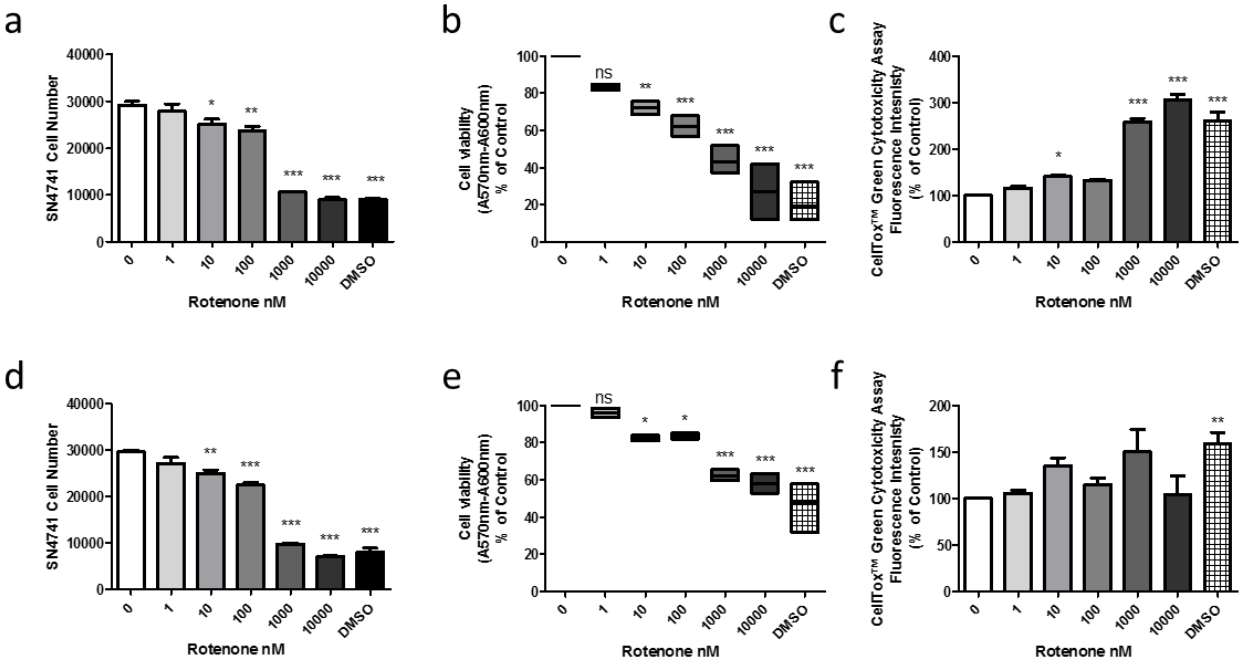

Figure 36: 24hr Rotenone Treatment Cell Loss, Decreases Viability and Increases SN4741 Cell Cytotoxicity.

Figure 36 (a), (b) and (c) represent SN4741 cell count, viability and cytotoxicity data respectively from cells cultured in complete (100% of full) culture medium. Figure 36 (d), (e) and (f) represent SN4741 cell count, viability and cytotoxicity data respectively from cells cultured in 60% of full culture medium. Rotenone exerts a dose dependant decrease in SN4741 cells in both complete (100%) and substrate restricted (60% of full) cell culture medium, (a) and (d) respectively. A dose dependant decrease in cell viability is observed in rotenone treated SN4741 cells cultured in complete (b) and substrate restricted medium (e).10nM,1000nM and 10,000nM rotenone treatment induces a significant increase in cell cytotoxicity in complete medium (c). No significant increase in cell cytotoxicity was observed in rotenone challenged SN4741 cells cultured in substrate restricted medium (f). SN4741 cell count data (a & d) expressed as mean cell count from cells treated in triplicate for 4 experimental repeats (n=4). SN4741 cell viability (b and e) and cytotoxicity (c and f) data represents data from treatments performed in triplicate for 3 experimental repeats (n=3) and is

expressed as percentage of control (0nM). Statistical analysis Statistical analysis was performed by One-way ANOVA with Bonferroni's post-hoc analysis (a and d) and with Dunnett's post-hoc analysis (in b, e, c and f) on graph pad prism 5 software, with $P<0.05$ (*), $P<0.01$ (**), $P<0.001$ (***) considered significant when compared to treatment control (0nM Rotenone).

4.3.4. SN4741 Counterstaining and Quantification

In order to speed up the tedious task of manual scoring of nuclei, images of SN4741 nuclei were run through image analysis software Image J or Cell Profiler to automate cell counting. This short section aims to i) validate that automated cell counting accurately quantifies nucleus (cell) numbers versus manual scoring and ii) ensure transferability in nuclei counting between Image J and Cell Profiler. The accurate identification of nuclei is not only integral for correct quantification of cell number; it also provides a 'seed' (digital coordinates) which can be utilised as a primary object to build image analysis protocols to extract quantitative data on changes in morphology of the nucleus or other fluorescently (or non-fluorescently) probed cellular organelles. The construction of an image analysis protocol to measure several cellular features will be discussed further in chapter 4.

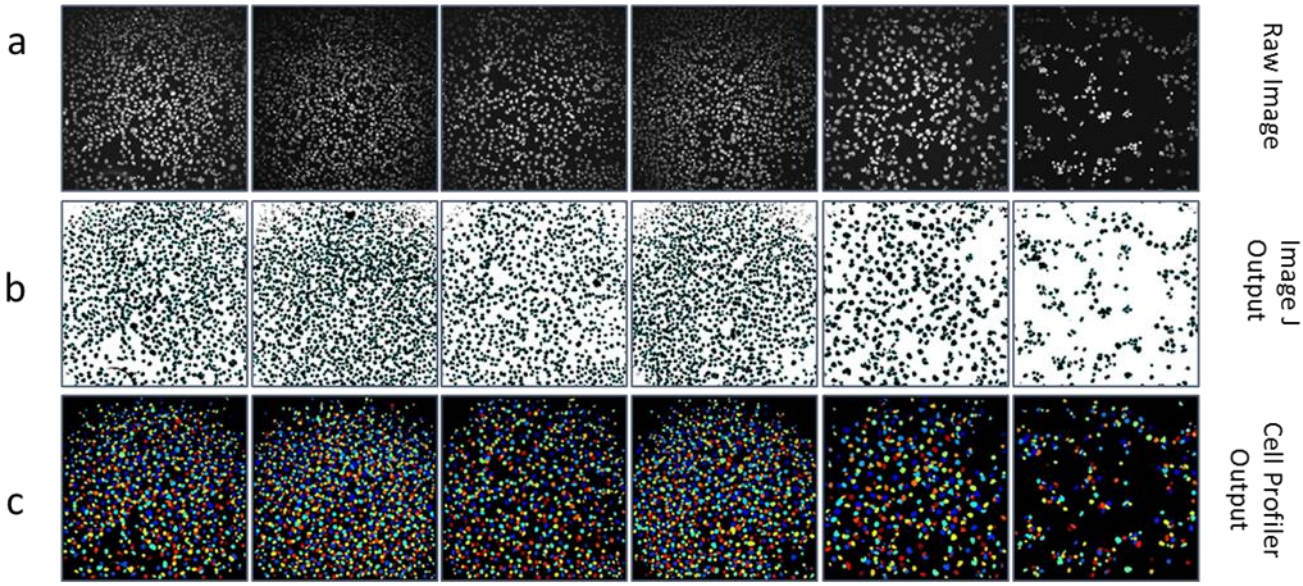
a
b
c
Raw Image
Image J Output
Cell Profiler Output

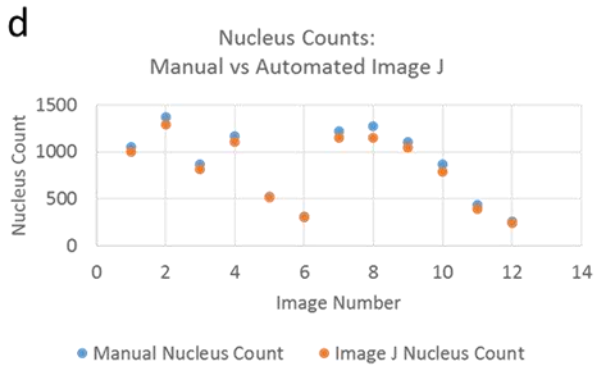
d
Nucleus Counts:
Manual vs Automated Image J
Nucleus Count
1500
1000
500
0
0 2 4 6 8 10 12 14
Image Number
Manual Nucleus Count
Image J Nucleus Count

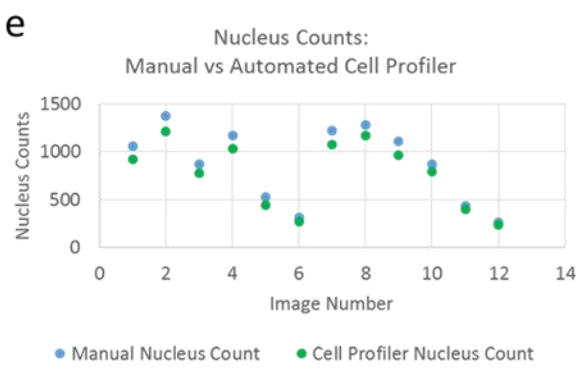
e
Nucleus Counts:
Manual vs Automated Cell Profiler
Nucleus Counts
1500
1000
500
0
0 2 4 6 8 10 12 14
Image Number
Manual Nucleus Count
Cell Profiler Nucleus Count

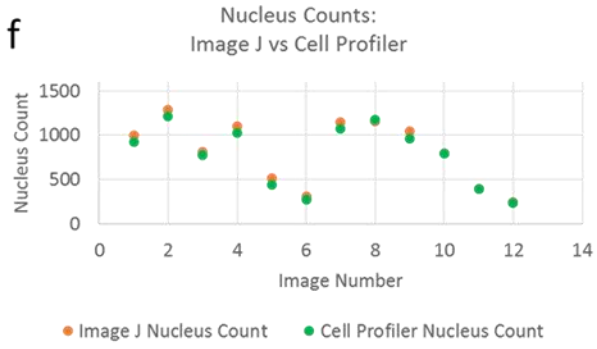
f
Nucleus Counts:
Image J vs Cell Profiler
Nucleus Count
1500
1000
500
0
0 2 4 6 8 10 12 14
Image Number
Image J Nucleus Count
Cell Profiler Nucleus Count

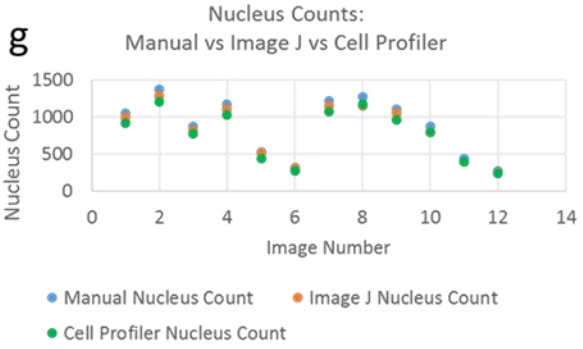
g
Nucleus Counts:
Manual vs Image J vs Cell Profiler
Nucleus Count
1500
1000
500
0
0 2 4 6 8 10 12 14
Image Number
Manual Nucleus Count
Image J Nucleus Count
Cell Profiler Nucleus Count

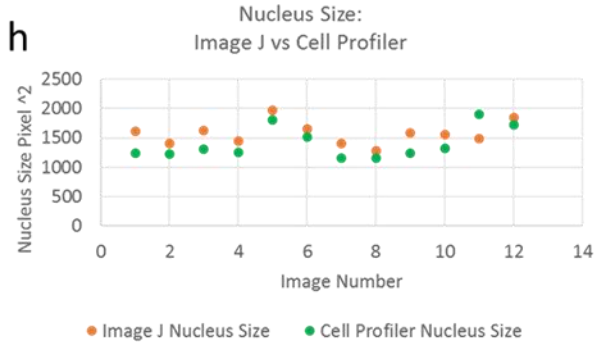
h
Nucleus Size:
Image J vs Cell Profiler
Nucleus Size Pixel ^2
2500
2000
1500
1000
500
0
0 2 4 6 8 10 12 14
Image Number
Image J Nucleus Size
Cell Profiler Nucleus Size

i

Nucleus Count: Manual vs Automated Image J												
MEAN	1027	1332	842.5	1137	522.5	309.5	1186	1215.5	1075	830	411.5	255
STDEV	39.59798	59.39697	41.7193	48.08326	7.778175	7.778175	52.3259	86.97413	41.01219	55.15433	28.99138	12.72792
SEM	28	42	29.5	34	5.5	5.5	37	61.5	29	39	20.5	9

j

Nucleus Count: Manual vs Automated Cell Profiler												
MEAN	988.5	1292.5	821.5	1100.5	483.5	292	1149	1224	1033.5	829.5	413.5	249
STDEV	94.0452	115.2584	71.41778	99.70206	62.9325	32.52691	104.6518	74.95332	99.70206	55.86144	26.16295	21.2132
SEM	66.5	81.5	50.5	70.5	44.5	23	74	53	70.5	39.5	18.5	15

k

Nucleus Count: Automated Image J vs Automated Cell Profiler												
MEAN	1019	1310.5	812	1139.5	494.5	292	1187.5	1242	1040.5	822	406	236
STDEV	28.28427	28.99138	1.414214	51.6188	31.81981	16.97056	54.44722	124.4508	7.778175	43.84062	21.2132	14.14214
SEM	20	20.5	1	36.5	22.5	12	38.5	88	5.5	31	15	10

l

Nucleus Count Manual vs Automated Image J vs Automated Cell Profiler												
MEAN	1031	1331.667	832	1150	505.6667	299.6667	1199.333	1253.667	1061.667	837.6667	414.6667	245.3333
STDEV	28.84441	42.00397	34.65545	40.7799	29.67041	17.89786	43.61575	90.29027	37.072	41.19871	21.22106	19.00877
SEM	16.65333	24.251	20.00833	23.54428	17.13022	10.33333	25.18156	52.12911	21.40353	23.78608	12.25198	10.97472

m

Nucleus Area (Pixels ^2) : Automated Image J vs Automated Cell Profiler												
MEAN	1425.74	1313.216	1463.665	1347.156	1887.472	1584.359	1276.919	1221.264	1406.239	1438.762	1694.058	1781.867
STDEV	264.8254	131.2159	229.5769	141.2001	113.8831	90.00207	169.8204	85.89327	241.4923	158.7285	287.1677	92.11161
SEM	187.2599	92.78362	162.3354	99.84354	80.52754	63.64107	120.0812	60.73571	170.7609	112.238	203.0582	65.13274

Figure 37: Validating Transferability of Manual vs Automated Nuclei Scoring.

12 x20 magnification images of Hoechst stained SN4741 nuclei were selected from a dataset to compare manual versus automated nucleus scoring. Nucleus size (area in Pixel^2) was also acquired via automated approaches. Image 1-6 represent nuclei following 24hr incubation 0, 1, 10, 100, 1000 & 10,000nM rotenone treatment cultured in full (100%) culture medium. Image 7-12 represent nuclei following 24hr incubation 0, 1, 10, 100, 1000 & 10,000nM rotenone treatment cultured in SR (60%) culture medium. Tiles (a) represent raw images used for manual counting (scoring) of SN4741 nuclei. (b) And (c) represent masked images of automated computer software scored nuclei from raw images (a) using Image J and Cell Profiler respectively. Graphs: (d) displays nuclei counts scored per image by manual and automated Image J method; (e) displays nuclei counts per image scored by manual versus automated Cell Profiler methods; (f) compares nuclei counts per image for both automated approaches- Image J versus Cell Profiler; (g) compares nuclei counts per image for all 3 scoring methods. Graph (h) displays a comparison of the mean nucleus area per image measured using automated methods, Image J and Cell Profiler. Data is graphed using MS Excel 2013. Mean values, standard deviation (STDEV) and standard error of means (SEM) were calculated for each comparison (d-h). Means, STDEV and SEM for each comparison (d-h) is displayed in form of tables (i-m).

4.3.5. Live/Dead Assay

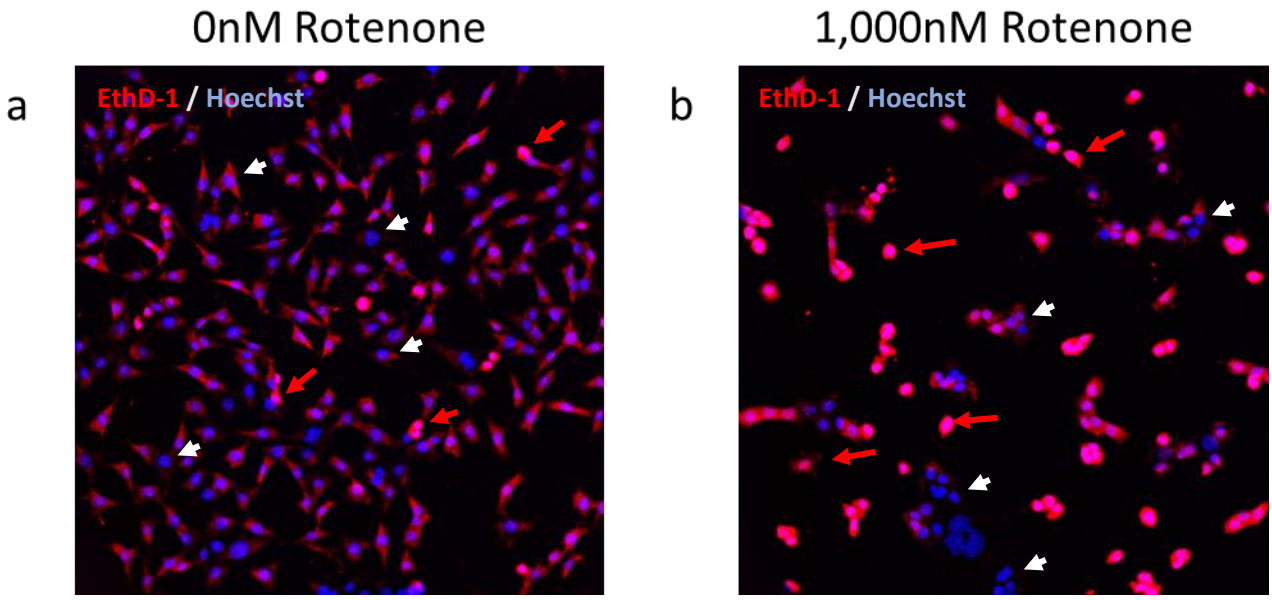

Figure 38: Ethidium homodimer-1 & Hoechst stained SN4741 cells.
(a) & (b) Represent merged x20 magnification images of EthD-1 and Hoechst stained SN4741 cells following 0nM and 1,000nM rotenone challenge (24hrs). These images clearly illustrate an increase in nuclear EthD-1 staining intensity upon rotenone challenge (1,000nM). Images (a) and (b) were acquired by In Cell Analyser 2000. White and red arrows delineate nuclei containing low and high EthD-1 fluorescence intensity, respectively. Nuclei were identified by Hoechst counterstaining and mean EthD-1 fluorescence was measure in each nucleus using Cell Profiler image analysis software.

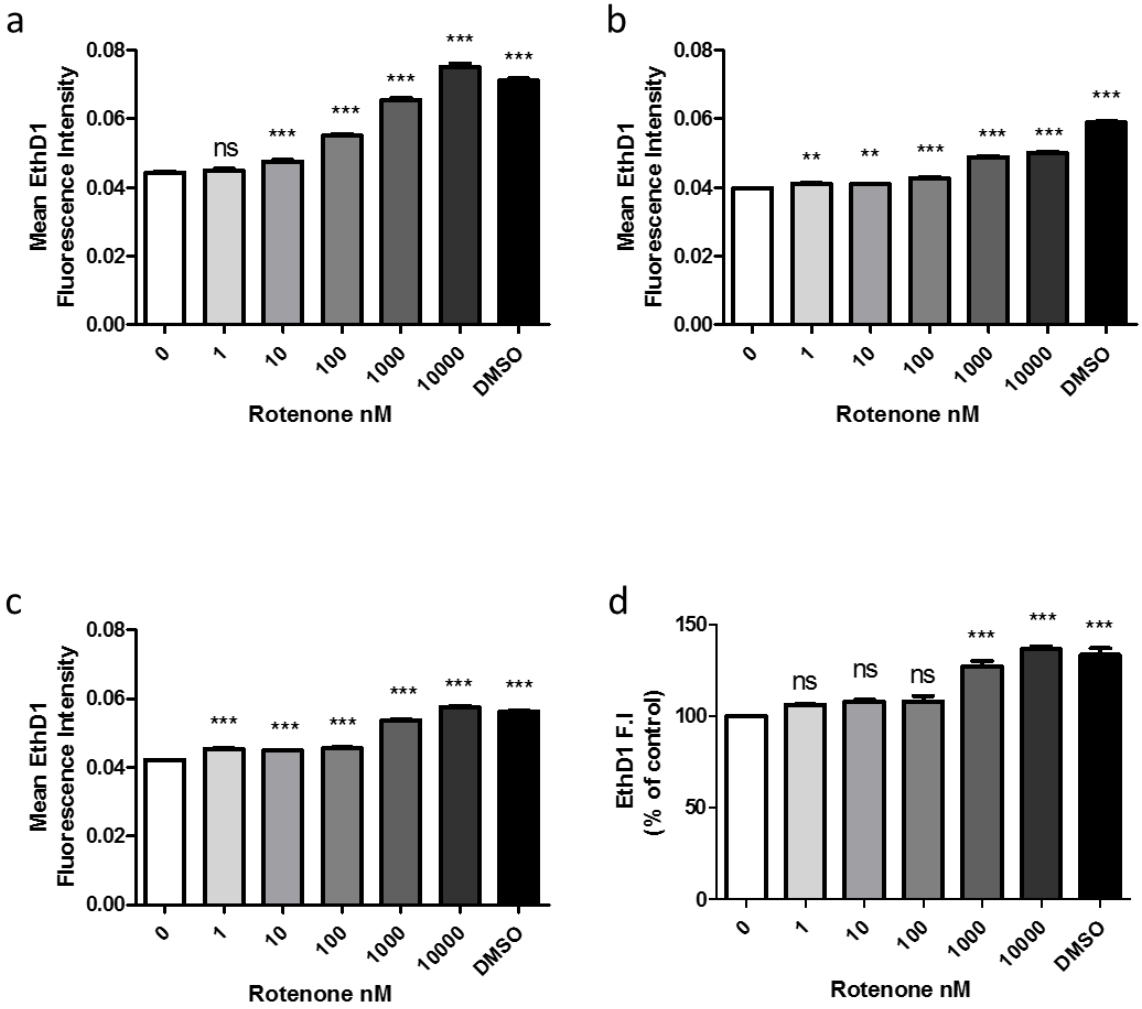

Figure 39: 24hr Rotenone Challenge Induces Cell Death Measured by EthD-1

24hr rotenone challenge induces an increase in cell death measure by an increase in nuclear EthD-1 fluorescence intensity (AU). Pooled mean nuclear EthD-1 fluorescence intensity of 100 images per treatment group. Treatments were performed in quadruplicate per technical repeat. Technical repeats 1, 2 & 3 (n=3) are represent by (a), (b) & (c). EthD-1 fluorescence intensity was calculated as a percentage of control (0nM rotenone) for each dataset (a-c). Percentage of control for all 3 technical repeats were plotted in (d). Statistical analysis was performed by One-way ANOVA with Dunnett's post-hoc analysis on graph pad prism 5 software, with $P<0.05$ (*), $P<0.01$ (**), $P<0.001$ (***) considered significant when compared to control (0nM Rotenone).

4.3.6. Detection of Rotenone-Induced Activated Caspase 3/7 in SN4741 Neurones

We have established that treating SN4741 cells for 24hrs with 10nM rotenone induces an increase in cell cytotoxicity, a decrease in cell viability and cell loss. Published literature shows rotenone mediated cell death is possible via caspase 3/7-dependant pathways (N. Li et al., 2003). In this section we aim to investigate whether challenging SN4741 cells with 10nM rotenone for 24hrs results in increased caspase 3/7 expression. As seen in figure 40 (a), there is no detectable increase in caspase 3/7 fluorescence intensity in SN4741 nuclei following 24hr incubation with 10nM rotenone, when compared to control. Conversely, DMSO treated cells exhibit a large increase in nuclear fluorescence intensity.

As expected, wells where Caspase-3/7 Green Detection Reagent was omitted- Caspase 3/7 positive nuclei were not detectable by visual inspection (not shown), nor via software analysis. Caspase 3/7-positive nuclei counts, acquired by automation of Image J software, show a significant increase in percentage of Caspase 3/7-positive cells following DMSO treatment; however, no increase is observed following treatment with 10nM rotenone. This indicates that the loss of SN4741 cells is not the result of Caspase 3/7 activation and therefore must be attributed to an alternative cell death pathway.

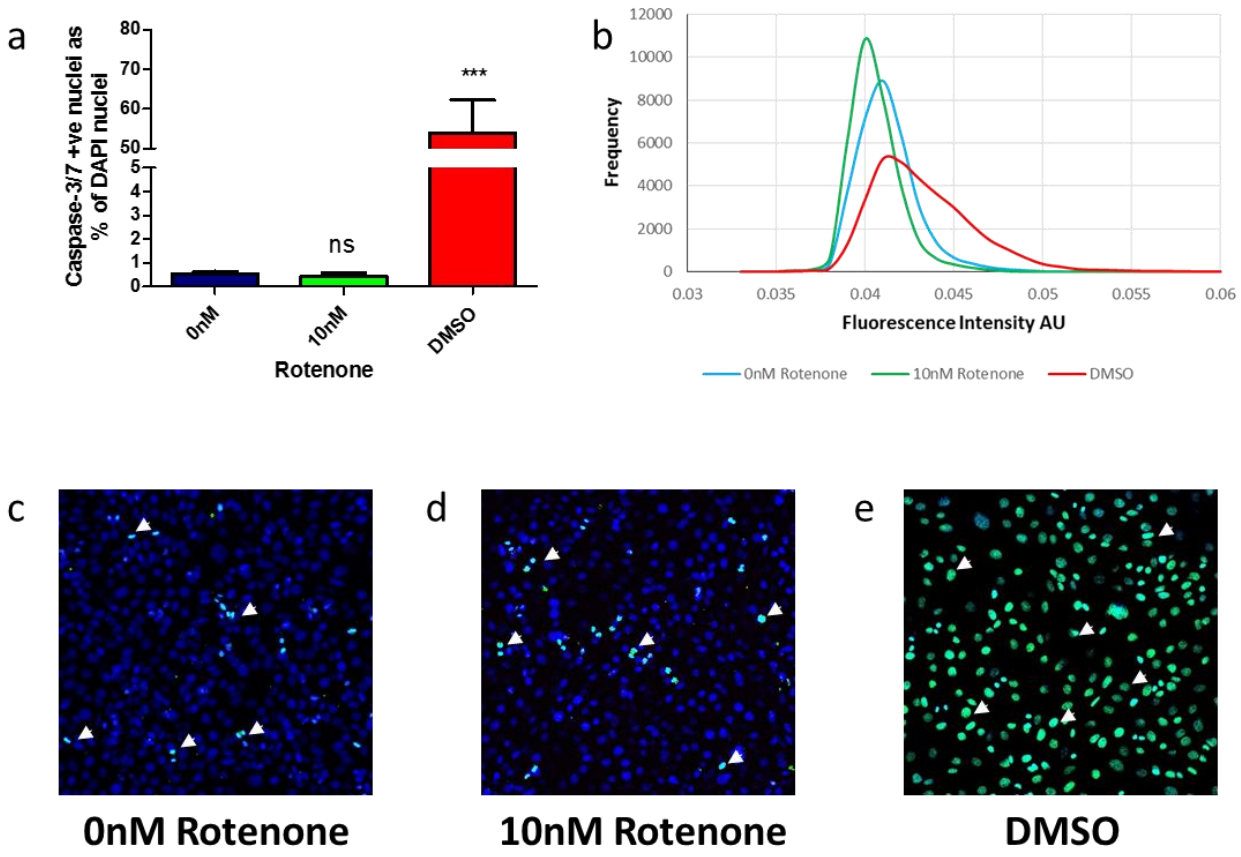

Figure 40:Rotenone (10nM) Does Not Increase Active Caspase 3/7 Activity in SN4741s Cells

Graph a) shows the number of Caspase 3/7-positive SN4741 nuclei as a percentage of total nuclei counterstained with Hoechst. Statistical analysis was performed by One-way ANOVA with Dunnett's post-hoc analysis on graph pad prism 5 software, with $P<0.05$ (*), $P<0.01$ (**), $P<0.001$ (***) considered significant when compared to control (0nM Rotenone). An intensity histogram of nuclear SN4741 Caspase 3/7 fluorescence intensities b). 10,000 nuclei were selected per well and measured for Caspase 3/7 fluorescence intensity. Merged DAPI (blue) and FITC (green) channel images c), d) and e) represent 0nM rotenone (control), 10nM rotenone and DMSO treated SN4741 cells (as labelled) stained with Hoechst and Caspase-3/7 Green Detection Reagent. White arrows indicate examples of Caspase 3/7-postive nuclei (c-e).

4.3.7. GHSR1a Agonists Protect Against Rotenone-Induced SN4741 Cell Loss

SN4741 cells incubated for 24hr in 10nM rotenone results in a significant cell loss, an increase in cytotoxicity and a decrease in cell viability with respect to controls. Here we aim to test the effectiveness of 1hr and 24hr GHSR1a agonist pre-treatment in reversing the observed SN4741 cell loss. Cells were treated directly with a titration of known GHSR1a agonists acyl-ghrelin and JMV-2894 for 1hr or 24hr prior to 10nM rotenone challenge (24hrs). Here we also investigate whether ghrelin-mediated neuroprotection is enhanced or diminished in SN4741 cell growing and treated in 0, 20, 40, 60, 80 and 100% of full (complete) medium.

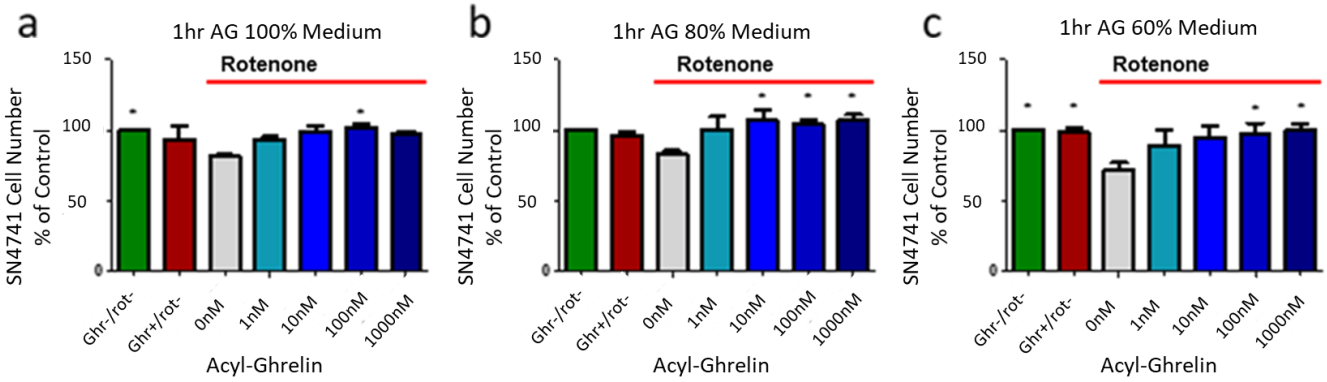

Figure 41: 1hr Acyl-Ghrelin Pre-treatment Attenuates Rotenone-Induced SN4741 Cell Loss.

SN4741 cells were cultured in 100%, 80% or 60% of full medium. Cells were grown in respective media before 1hr AG pre-treatments followed by a 24hr rotenone (10nM) challenge. (a) In 100% of full medium, 1hr pre-treatment with 100nM AG prevented rotenone (10nM) induced dopamine cell loss; (b) In 80% of full medium, 1hr pre-treatment with 10nM, 100nM and 1000nM AG prevented rotenone (10nM) induced dopamine cell loss; (c) in 60% of full media 1hr pre-treatment with 100nM and 1000nM AG prevented rotenone (10nM) induced dopamine cell loss. Statistical analysis was performed by One-way ANOVA with Dunnett's post-hoc analysis on Graph Pad Prism 5 software, with $P<0.05$ (*), $P<0.01$ (**), $P<0.001$ (***) considered significant compared to control (0nM). Ghr-/rot- signifies cells treated with neither AG nor rotenone. Ghr+/rot- signifies cells treated with 1,000nM AG without rotenone challenge. Red bar above graph indicates 24hr 10nM rotenone treatments.

As shown in figure 41a we see that in cells cultured in 100% medium 100nM AG pre-treatment for 1hr attenuates rotenone-induced cell loss significantly with P<0.05. Figure 41b shows that in cells cultured in 80% of full medium 10nM, 100nM and 100nM AG pre-treatment for 1h attenuates rotenone-induced cell loss significantly with P<0.05. We see in Figure 41c that in cells cultured in 60% of full medium 100nM and 1000nM AG attenuates rotenone-cell loss significantly with P<0.05. This suggests that our crude substrate restriction (80% and 60% of complete cell culture media) increases the efficacy of AG neuroprotection against rotenone-induced cell loss.

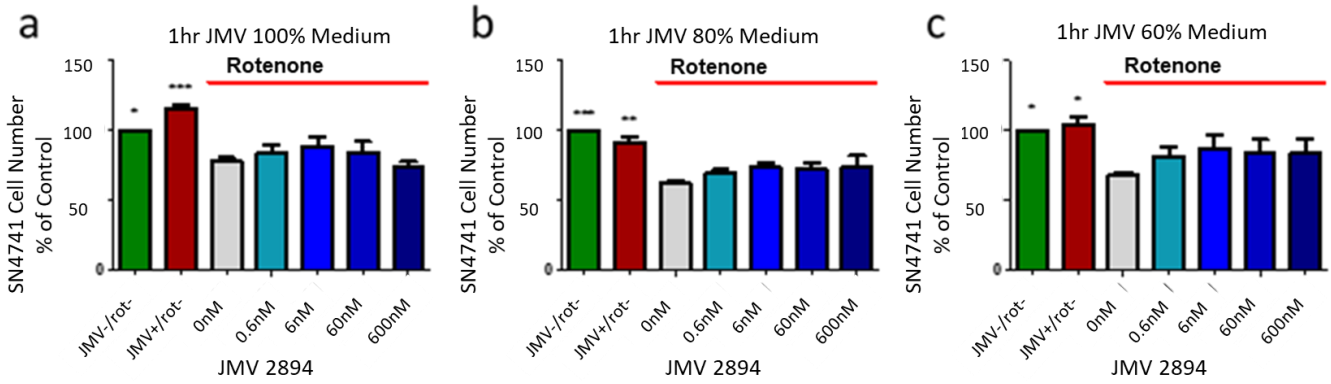

Figure 42: 1hr JMV2894 Pre-Treatment Does Not Significantly Attenuate Rotenone-Induced SN4741 Cell Loss.

SN4741 cells were seeded into respective 100%, or 80% and 60% of complete media to simulate substrate restriction prior to 1hr pre-treatments with GHSR-agonist (JMV2984) followed by rotenone (10nM) challenge. 1hr pre-treatment with JMV2984 did not prevent rotenone (10nM) induced dopamine cell loss in full media (a), 80% media (b) or 60% media (c). Treatments were performed in triplicate and in three separate experiments. Statistical analysis was performed by One-way ANOVA with Dunnett's post-hoc analysis on Graph Pad Prism 5 software, with P<0.05 (*), P<0.01 (**), P<0.001 (***) considered significant when compared to control (0nM). JMV-/rot- signifies cells treated with neither JMV2894 nor rotenone. JMV+/rot- signifies cells treated with 600nM JMV2894 only. Red bar above graph indicates treatments including 24hr 10nM rotenone.

As seen in Figure 42 (a-c), none of the JMV 2894 pre-treatments resulted in attenuation of rotenone-induced cell loss in cells cultured in 100%, 80% or 60% media (P>0.05).

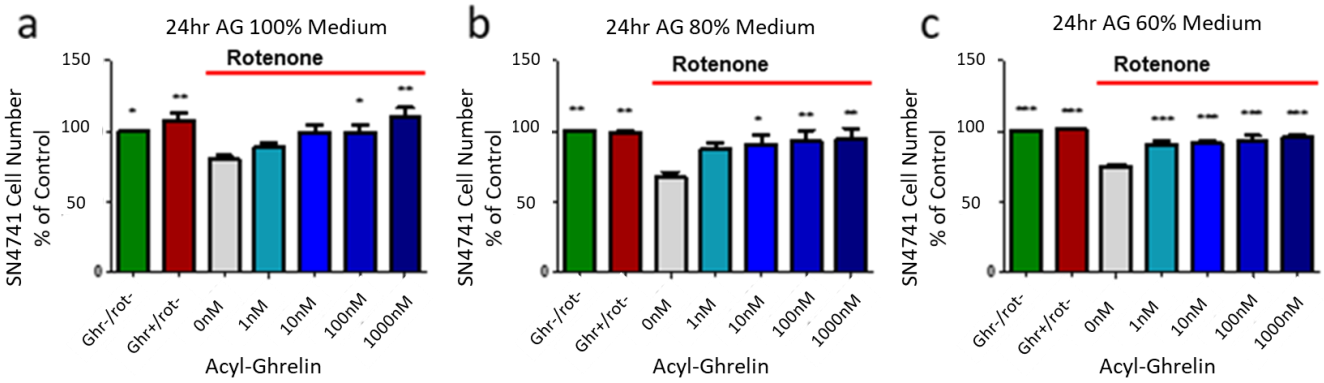

Figure 43: 24hr Acyl-Ghrelin Pre-Treatment Attenuates Rotenone-Induced SN4741 Cell Loss.

SN4741 cells were cultured in 100%, 80% or 60% of full medium. Cells were grown in respective media before 24hr AG pre-treatments followed by a 24hr rotenone (10nM) challenge. (a) In 100% of full medium, 24hr pre-treatment with 100nM and 1000nM AG prevented rotenone (10nM) induced dopamine cell loss; (b) In 80% of full medium, 24hr pre-treatment with 10nM, 100nM and 1000nM AG prevented rotenone (10nM) induced dopamine cell loss; (c) in 60% of full media 24hr pre-treatment with 1nM, 10nM, 100nM and 1000nM AG prevented rotenone (10nM) induced dopamine cell loss. Treatments were performed in triplicate and in three separate experiments. Statistical analysis was performed by One-way ANOVA with Dunnett's post-hoc analysis on Graph Pad Prism 5 software, with $P<0.05$ (*), $P<0.01$ (**), $P<0.001$ (***) considered significant compared to control. Ghr-/rot- signifies cells treated with neither AG nor rotenone. Ghr+/rot- signifies cells treated with 1000nM AG without rotenone challenge. Red bar above graph indicates treatments including 24hr 10nM rotenone.

As observed in Figure 43a, cells cultured in 100% medium 100nM AG attenuates rotenone-induced cell loss significantly with $P<0.05$ and 100nM attenuates AG more significantly with $P<0.01$. Figure 43b shows that in cells cultured in 80% media, 10nM AG attenuates rotenone-induced cell loss significantly with $P<0.05$ and 100nM AG and 1000nM AG do so more significantly with $P<0.01$. As seen in Figure 43c, in cells cultured in 60% medium 1nM, 10nM, 100nM and 1000nM AG all attenuated rotenone-induced cell loss very significantly with $P<0.001$. This further proves that our crude substrate restriction increases the efficacy of AG neuroprotection against rotenone-induced cell loss.

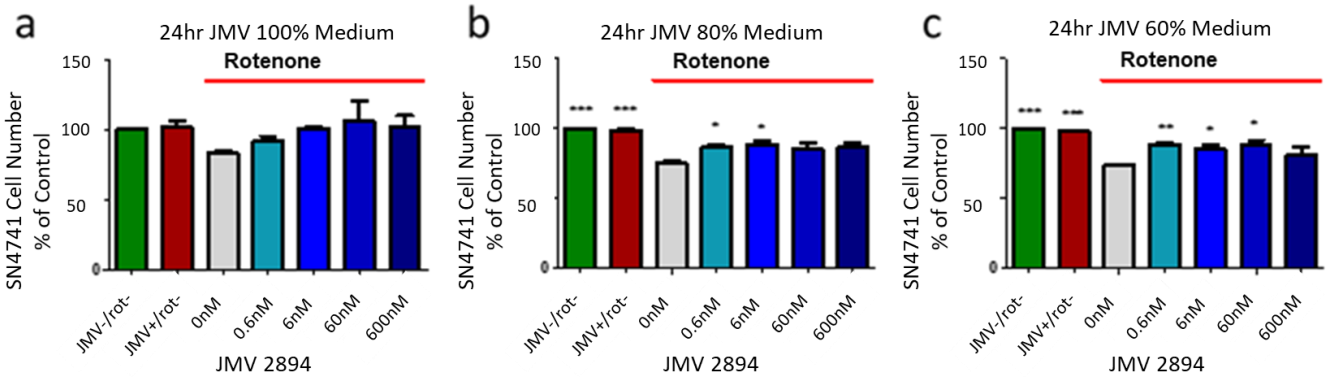

Figure 44: 24hr JMV2894 Pre-Treatment Attenuates Rotenone-Induced SN4741 Cell Loss

SN4741 cells were cultured in 100%, 80% or 60% of full medium. Cells were grown in respective media before 24hr JMV 2894 pre-treatments followed by a 24hr rotenone (10nM) challenge. (a) In 100% of full medium, 24hr pre-treatment with JMV 2894 did not prevented rotenone (10nM) induced dopamine cell loss; (b) In 80% of full medium, 24hr pre-treatment with 0.6nM and 6nM JMV 2894 prevented rotenone (10nM) induced dopamine cell loss; (c) in 60% of full media 24hr pre-treatment with 0.6nM, 6nM and 60nM JMV 2894 prevented rotenone (10nM) induced dopamine cell loss. Treatments were performed in triplicate and in three separate experiments. Statistical analysis was performed by One-way ANOVA with Dunnett's post-hoc analysis on Graph Pad Prism 5 software, with $P<0.05$ (*), $P<0.01$ (**), $P<0.001$ (***) considered significant when compared to control (0nM). JMV-/rot- signifies cells treated with neither JMV-2894 nor rotenone. JMV+/rot- signifies cells treated with 600nM JMV-2894 without rotenone challenge. Red bar above graph indicates treatments including 24hr 10nM rotenone.

Figure 44a shows that cells cultured in 100% medium for 24hrs showed no significant attenuation in cell loss. As seen in Figure 44b, in cells cultured in 80% medium 0.6nM and 6nM JMV 2894 significantly attenuated rotenone-induced cell loss with $P<0.05$. Figure 44c shows that in cells cultured in 60% medium, 0.6nM JMV 2894 attenuated rotenone-induced cell loss more significantly with $P<0.01$ and 6nm and 60nm JMV 2894 attenuated rotenone-induced cell loss less significantly with $P<0.05$. This suggests that our crude substrate restriction increases efficacy of JMV 2894 neuroprotection against rotenone-induced cell loss, with the most significant protection with 0.6nM in 60% medium.

4.3.8. Acyl-Ghrelin Does Not Induce SN4741 Cell Proliferation

AG pre-treatment attenuates rotenone-induced SN4741 cell loss *in-vitro*. The mode of AG's neuroprotective mechanism is yet to be fully elucidated with this cell line. Prior to investigating the potential molecular mechanisms underpinning AG-mediated neuroprotection, it is necessary to establish that the observed protection of SN4741 cell number is not the result of an AG-mediated increase in cell proliferation. Ghrelin is reported as an inducer of cell proliferation (e.g. cardiomyocytes) (Pettersson et al., 2002), but also an inhibitor of cell proliferation in other cells (e.g. mouse T lymphocytes) (Pettersson, et al., 2002; Q. Xia et al., 2004). To determine whether the attenuation of cell loss is a result of increased cell proliferation, SN4741 cells were incubated in the presence of thymidine analogue EdU which was incorporated in to actively dividing cells, giving us a relative measure of cell proliferation.

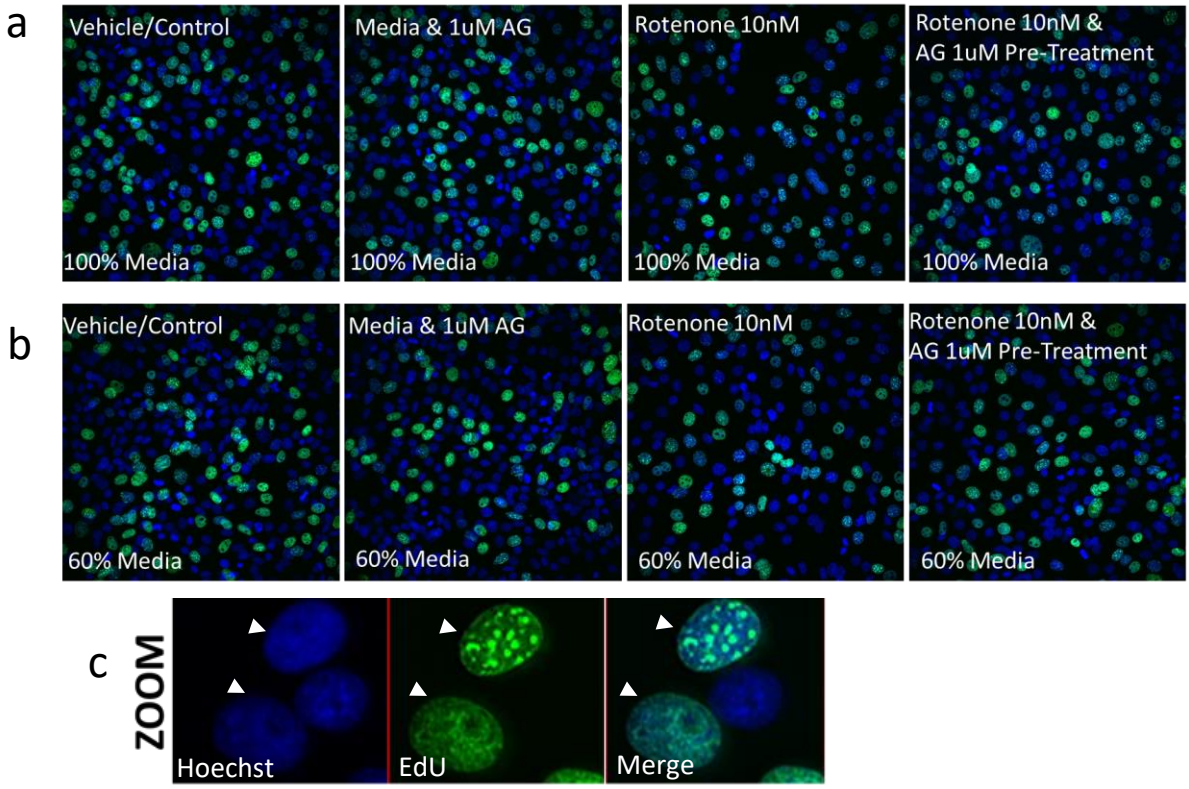

Figure 45: Hoechst and EdU as an Indicator of SN4741 Cell Proliferation

Image tiles (Figure 45 a and b) illustrate Hoechst (blue) and EdU-Click-iT (green) stained SN4741 nuclei of treated in full media and 60% media, respectively. From left to right (in tile panels a and b), image tiles represent the nuclei of vehicle, 1µM AG, 10nM rotenone and 1µM AG+10nM rotenone treated SN4741 cells, as labelled. (c) Shows zoomed-in examples of Hoechst and EdU stained nuclei, as labelled. White arrows on zoomed image tile (c) indicate examples of EdU^{+} neurones.

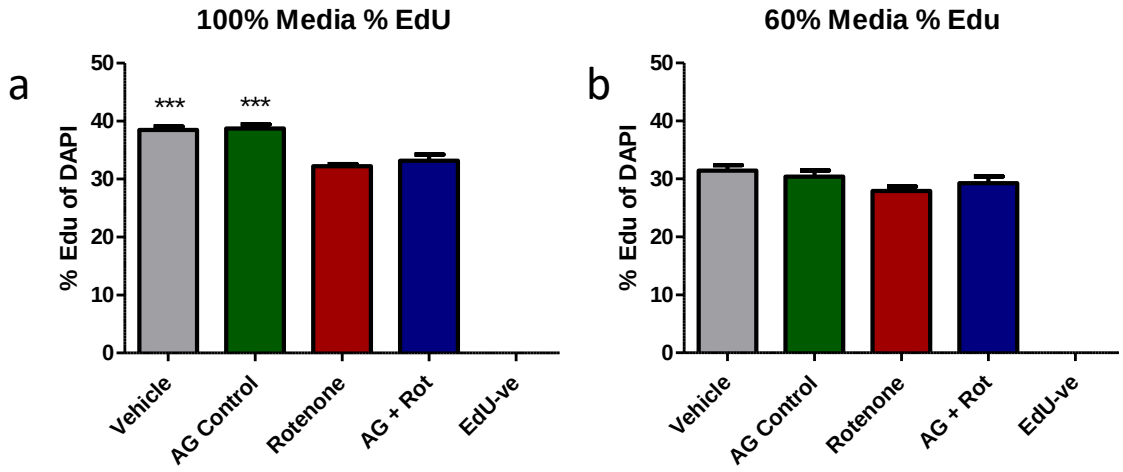

Figure 46:Rotenone Reduces SN4741 Proliferation in Full Media but Not in Substrate Restricted Media.

The percentage of proliferating (EdU-positive) nuclei per total nucleus count for SN4741 cells challenged with 10nM rotenone in the presence and absence of 24hr 1µM AG pre-treatment. 10nM rotenone was omitted from AG control treatment where cells were incubated with 1µM AG only. EdU was omitted from EdU-ve well and no EdU-positive nuclei were detected upon image analysis. Treatments were carried out on cells seeded in 100% and 60% of full media and percentage of proliferating cells are shown in graphs (a) and (b) respectively. 24hr Rotenone challenge induces a significant decrease in cell proliferation in both presence and absence of 24hr 1µM AG pre-treatment in SN4741 cells cultured in complete medium (a). This is not observed in SN4741 cells cultured in SR (60%) media (b). Treatments were performed in triplicate and in two separate experiments. Statistical analysis was performed by One-way ANOVA with Dunnett's post-hoc analysis on Graph Pad Prism 5 software, with $P<0.05$ (*), $P<0.01$ (**), $P<0.001$ (***) considered significant when compared to rotenone (10nM).

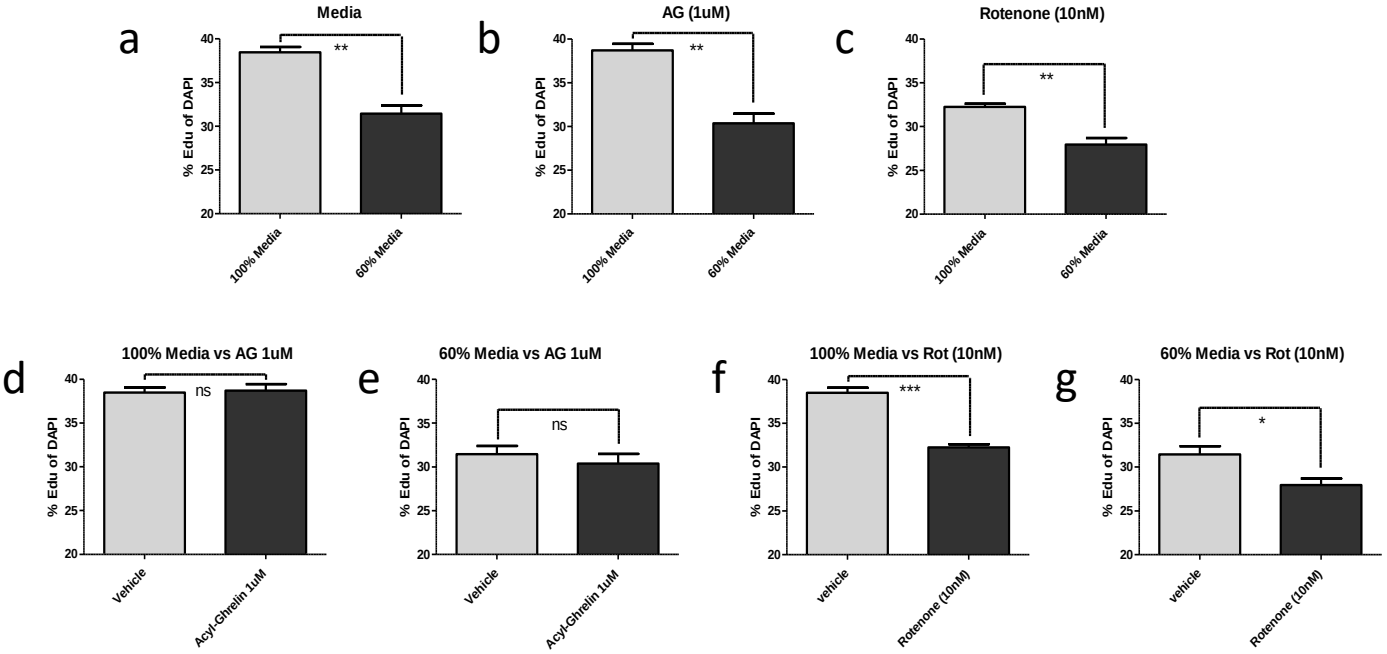

Figure 47: Substrate Restriction (SR) (60% of full medium) and Rotenone Challenge Reduces SN4741 Cell Proliferation Whilst AG Does Not Effect Cell Proliferation.

Graph (a) compares the proliferation of vehicle treated SN4741 cells seeded in 100% and 60% of full media; (b) compares proliferation of 1µM AG treated SN4741 cells cultured in 100% and 60% of full media. Graph (c) compares proliferation of SN4741 cells seeded in 100% and 60% of full media followed by 10nM rotenone challenge. Graph (d) and (e) compare the proliferation of SN4741cells treated with 1µM AG versus vehicle treatment following cell seeding in 100% and 60% of full media respectively. Graph (f) and (g) compare the proliferation of SN4741cells treated with 10nM rotenone versus vehicle treatment following cell seeding in 100% and 60% full media, respectively. Statistical analysis was performed by unpaired one-tailed t-test on Graph Pad Prism 5 software, with $P<0.05$ (*), $P<0.01$ (**), $P<0.001$ (***) considered statistically significant.

In each treatment group, the percentage of EdU-positive (indicated with white arrows, figure 45c) per total nuclei was calculated. The proliferation of SN4741 cells seeded in full media was significantly reduced following 10nM rotenone challenge (figure 46a), an effect which was not observed in SN4741 cells seeded in SR (60%) media (figure 46b). Moreover, 24hr pre-treatment with 1µM AG did not result in increased SN4741 cell proliferation in full or SR media in the presence or absence of rotenone (figure 46a and b). Results shown in figure 47(a-c) shows a decrease in SN4741 cell proliferation in vehicle (a), AG only (b) and rotenone (c) treated cells cultured in SR media compared to full media. Data shown in graphs (figures 47 d & e) illustrate no significant increase in SN4741 cell proliferation following 1µM AG treatment. Data represented in graphs (figure 47 f & g) show a significant decrease in SN4741 cell proliferation following rotenone challenge in both full media (figure 47 f) and SR media (figure 47g). A significant decrease in cell proliferation was observed in vehicle treated SN4741 cells cultured in SR media compared to full media (figure 47a);

4.3.9. GHSR1a Antagonist Inhibits Ghrelin-Mediated Neuroprotection

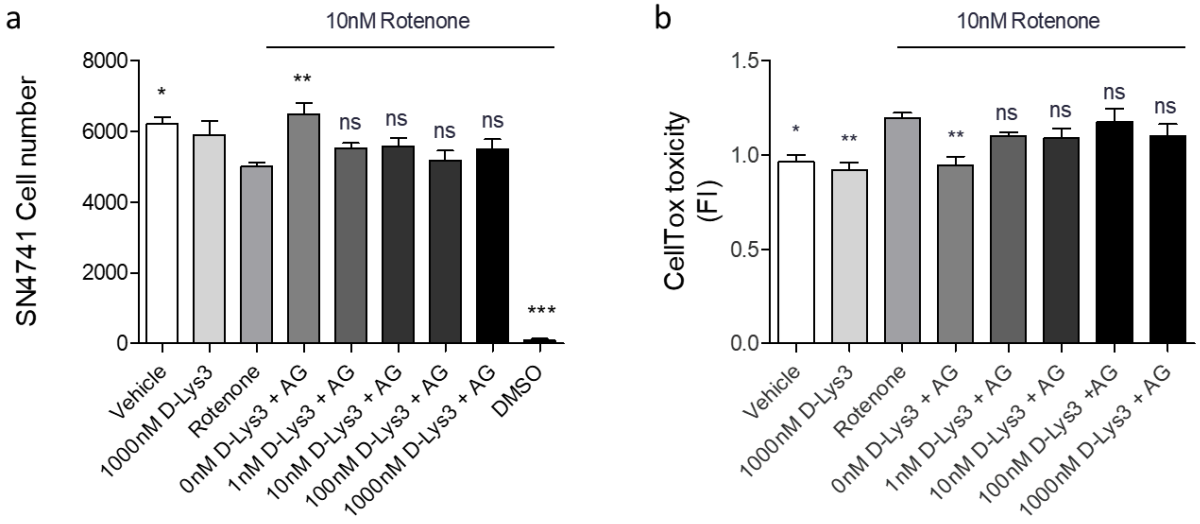

Figure 48: GHSR1a Antagonist D-Lys3 Inhibits Acyl-Ghrelin's Effect on Rotenone-Induced Cell Loss and Cytotoxicity in Full Medium

Graph (a) shows SN4741 cell counts at endpoint in each treatment group acquired by automated cell counting. Graph (b) illustrates CellTox™ Green fluorescence intensity (FI) captured at experimental endpoint. FI intensity is normalised to cells per well. Graph (a & b) shows that 1,100 and 1000nM of D-Lys3 attenuated 1µM AG-mediated cell survival and decrease in cell viability. Statistical analysis was performed by One-way ANOVA with Dunnett's post-hoc analysis on Graph Pad Prism 5 software, with $P<0.05$ (*), $P<0.01$ (**), $P<0.001$ (***) considered significant when compared to rotenone (10nM). Each treatment was performed in triplicate for two experimental repeats (n=2).

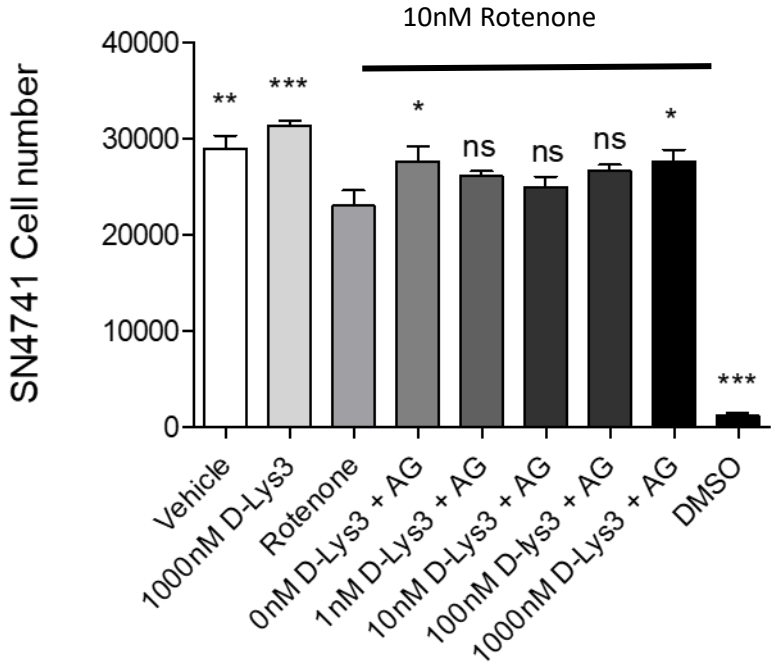

Figure 49: GHSR1a Antagonist D-Lys3 Inhibits Acyl-Ghrelin's Effect on Rotenone-Induced Cell Loss in SR (60% of Full) Media.

Graph shows that 1,100 and 1000nM D-Lys3 attenuated 1μM AG-mediated cell survival. Statistical analysis was performed by One-way ANOVA with Dunnett's post-hoc analysis on Graph Pad Prism 5 software, with $P<0.05$ (*), $P<0.01$ (**), $P<0.001$ (***) considered significant when compared to rotenone (10nM). Each treatment was performed in triplicate for two experimental repeats (n=2).

4.3.10 Is AG-Mediated Neuroprotection Dependent on AMPK?

Optimisation of Compound C concentration: as shown in figure 50a, no reduction in SN4741 cell number was observed following Compound C treatment at 0nM, 20nM, 40nM, 60nM, 80nM, 100nM and 1000nM in 100% medium in compound C optimisation. However, a decrease in SN4741 cell number was observed following 1000nM ($P<0.001$) Compound C treatment. Moreover, in Figure 50b no reduction in SN4741 cell number was observed following Compound C treatment at 20nM, 40nM, 60nM, 80nM and 100nM ($P>0.05$) in substrate restricted (60% of full cell culture) medium. However, a decrease in SN4741 cell number was observed following 1000Nm ($P<0.001$) compound C treatment. Treatments were carried out in quadruplicate for 2 experimental repeats (n=2) in each media.

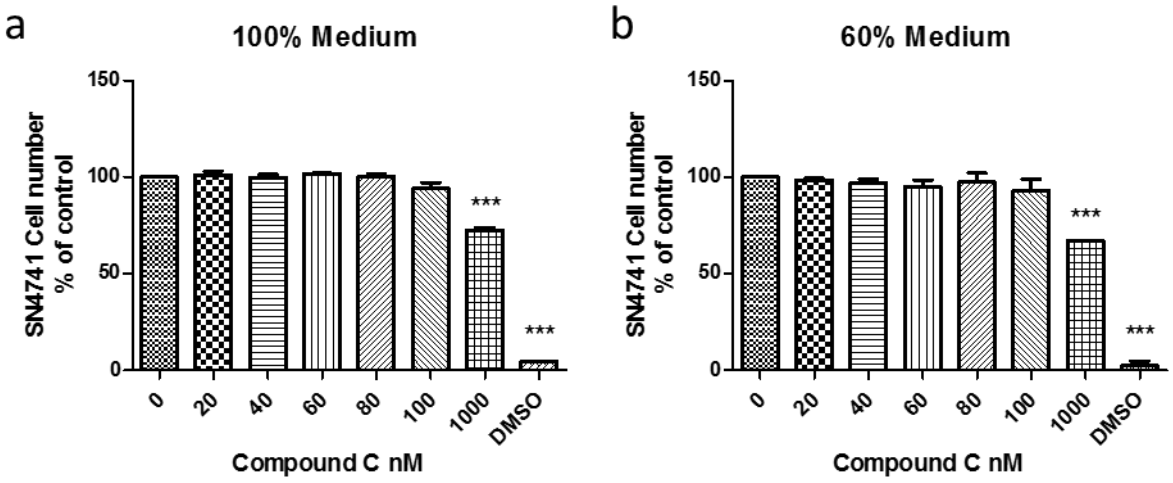

Figure 50: 1000nM AMPK Phosphorylation Inhibitor Compound C Produces SN4741 Cell Loss.

Compound C decreases SN4741 cell number following 48hr incubation. Treatment with Compound C at the initial concentration of 1000nM resulted in a significant loss of SN4741 cells cultured in 100% (a) and 60% (b) of full culture media. Treatments were carried out in quadruplicate across two experimental repeats (n=2) for cells cultured in complete and SR media. Mean cell number was quantified in each replicate (n=2) and expressed in graphs (a) and (b). Statistical analysis was performed by One-Way-ANOVA with Dennett's post-hoc test in Graph Pad Prism 5, with $P<0.05$ (*), $P<0.01$ (**), $P<0.001$ (***) considered statistically significant.

In both full and SR (60% of full cell) culture media, 100nM Compound C was the highest concentration that did not significantly reduce SN4741 cell number. This concentration of compound C was used to pre-treat SN4741 cells prior to AG-pre-treatment and rotenone challenge.

Compound C in neurotoxicity assay: SN4741 cells seeded in complete and SR media were incubated with 100nM and 200nM Compound C for 30mins prior to 24hr AG (1µM) treatment and subsequent 24 hr 10nM rotenone challenge.

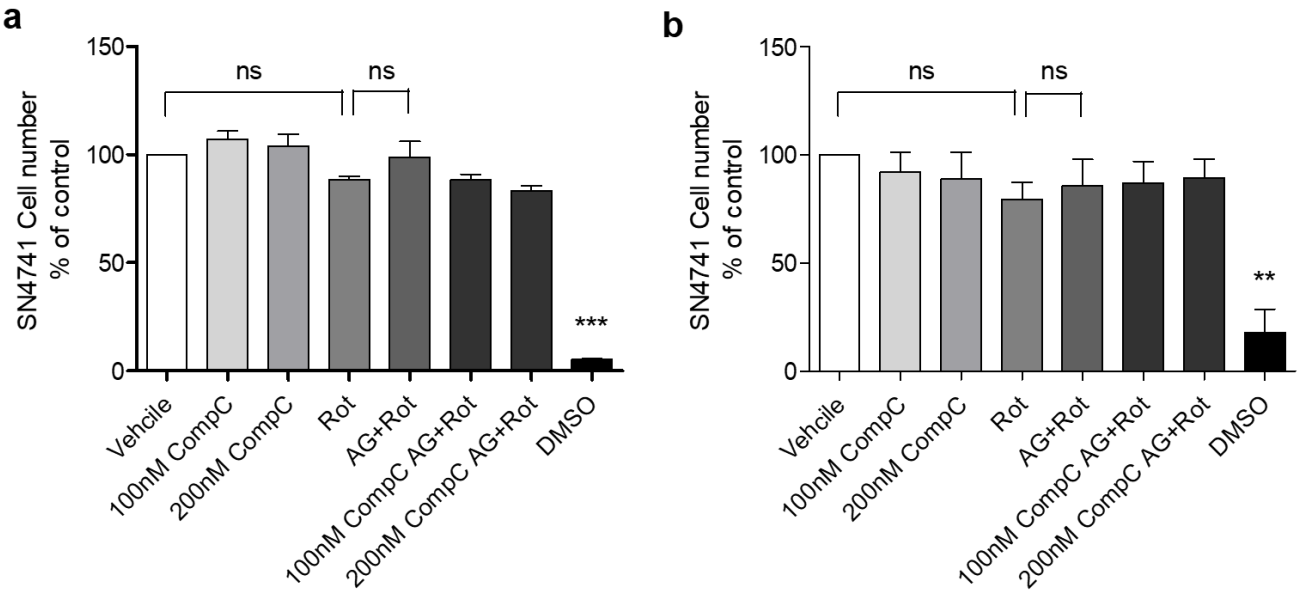

Figure 51: SN4741 Cell Number Does Not Decrease with Rotenone Treatment in Neurotoxicity Assay.

(a) Graph showing the SN4741 cell counts expressed as percentage of the control (vehicle treated cells) in 100% media. This graph shows that a significant rotenone-induced SN4741 cell loss is not observed in cells cultured in full medium in n=2 experimental trials. (b) Graph showing the SN4741 cell counts expressed as percentage of the control (vehicle treated cells) in SR (60%) media. This graph shows that significant rotenone-induced SN4741 cell loss was not observed in cells cultured in complete medium in n=2 experimental trials. Therefore, AG-mediated neuroprotection was not observed. Treatments were performed in triplicate and in two separate experiments. Statistical analysis was performed by One-way ANOVA with Dunnett's post-hoc analysis on Graph Pad Prism 5 software, with $P<0.05$ (*), $P<0.01$ (**), $P<0.001$ (***) considered significant when compared to rotenone (10nM).

SN4741 cell loss was not induced by rotenone and therefore, we were not able to test the efficacy of Compound C as an inhibitor to the neuroprotective effects of AG.

4.3.11 The effects of Acyl Ghrelin on SN4741 Metabolic Signalling Pathways

Protein lysate was collected from SN4741 cells at 5 minutes and 24h post-AG and JMV2894 agonist treatment as described in the method. Expression of phosphorylated versus non-phosphorylate AMPK and ACC was determined.

4.3.11.1. AG and GHSR1a agonist (JMV2894) phosphorylates the cellular energy sensor AMPK and catalytic enzyme ACC at 5 minutes.

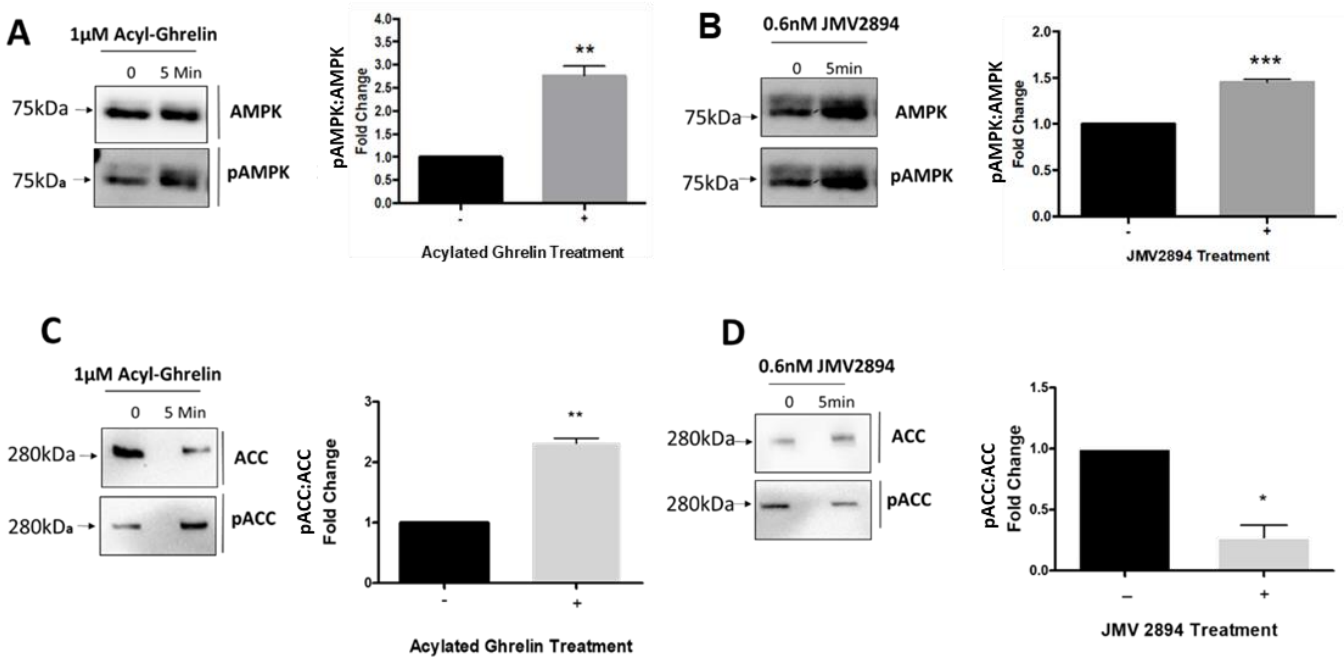

Figure 52: Acyl-Ghrelin and GHSR1a Agonist JMV2894 Induce Phosphorylation of Metabolic Sensor AMPK & Inhibits Phosphorylation of ACC

(A) & (B) Immunoblot data shows that 5-minute treatment with both acyl-ghrelin (AG) (1uM) and GHSR1a agonist JMV2894 (0.6nM) induced phosphorylation of metabolic sensor AMPK ($P<0.01$), ($P<0.001$). (C) & (D) Immunoblot data shows that 5-minute treatment with (C) AG (1uM) induced phosphorylation of fatty acid biosynthesis regulator ACC ($P<0.01$) whilst (D) GHSR agonist JMV2894 (0.6nM) decreased phosphorylation of ACC ($P<0.05$). These data demonstrate that SN4741 cells are responsive to ghrelin-GHSR1a signalling.

4.3.11.2. Phosphorylation of cellular energy sensor AMPK and catalytic enzyme ACC during neurotoxicity experiment following treatment with GHSR1a agonist AG.

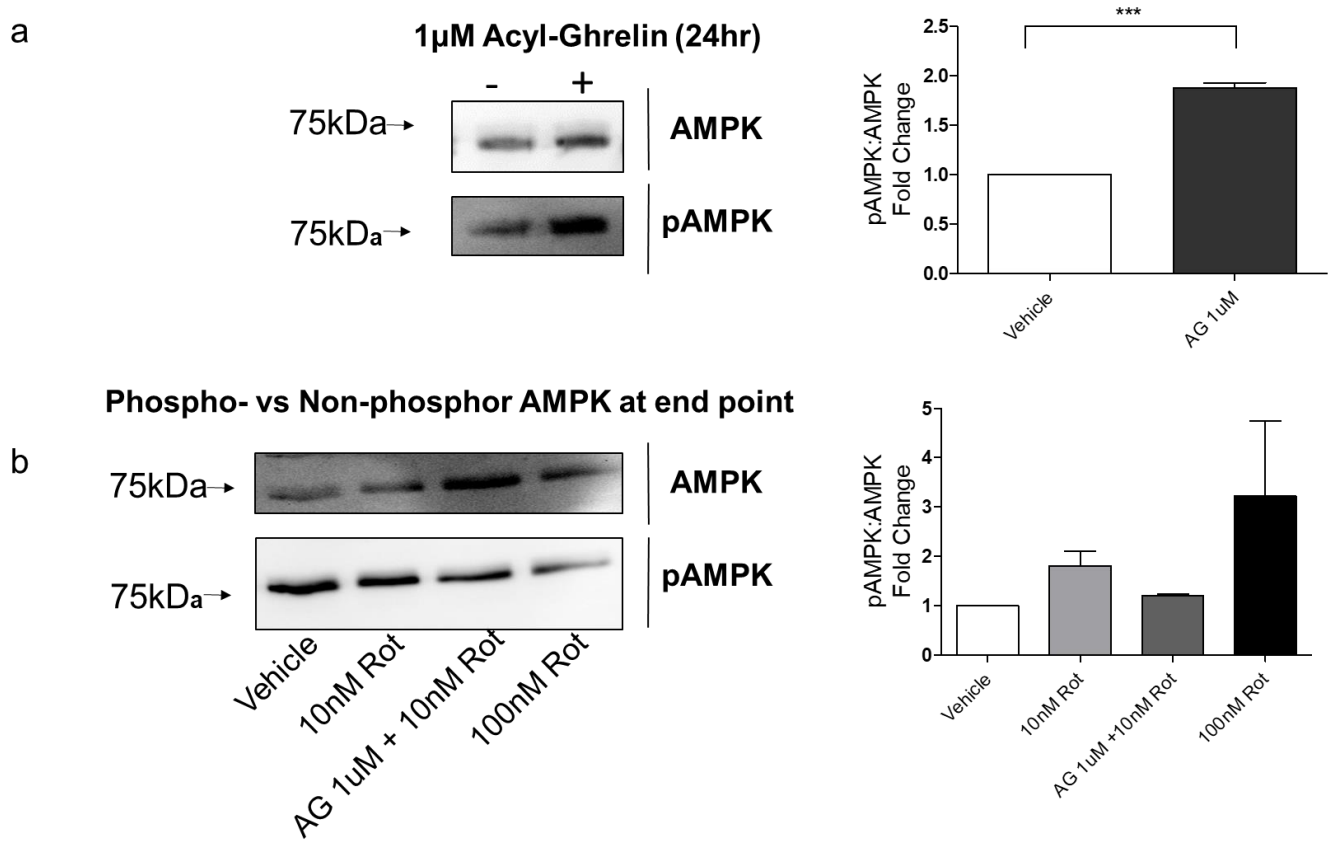

Figure 53: Phosphorylation of Metabolic Sensor AMPK During Neurotoxicity Experiment.

(a) Immunoblot data shows that 24 hr treatment of SN4741 cells with AG (1uM) induced phosphorylation of metabolic sensor AMPK ($P<0.001$). (b) Immunoblot data shows that AG (1uM) induced phosphorylation of AMPK does not persist to experimental endpoint. SN4741 cells in the presence of rotenone (10nM and 100nM) showed an increase in pAMPK at experimental endpoint. However, the increase was not statistically significant. Graphed data represents the mean fold change of phosphorylated AMPK versus non-phosphorylated AMPK for 3 technical experimental repeats. Statistical analysis was carried out using Graph Pad Prism version 5 using an unpaired Two-tailed T-test for (a) and one-way ANOVA with Bonferroni's Multiple Comparison Test for (b).

Experimental paradigm for the protein extractions above is illustrated in Figure 31 & table 17.

4.3.11.3. Phosphorylation of catalytic enzyme ACC during neurotoxicity experiment following treatment with GHSR1a agonist AG.

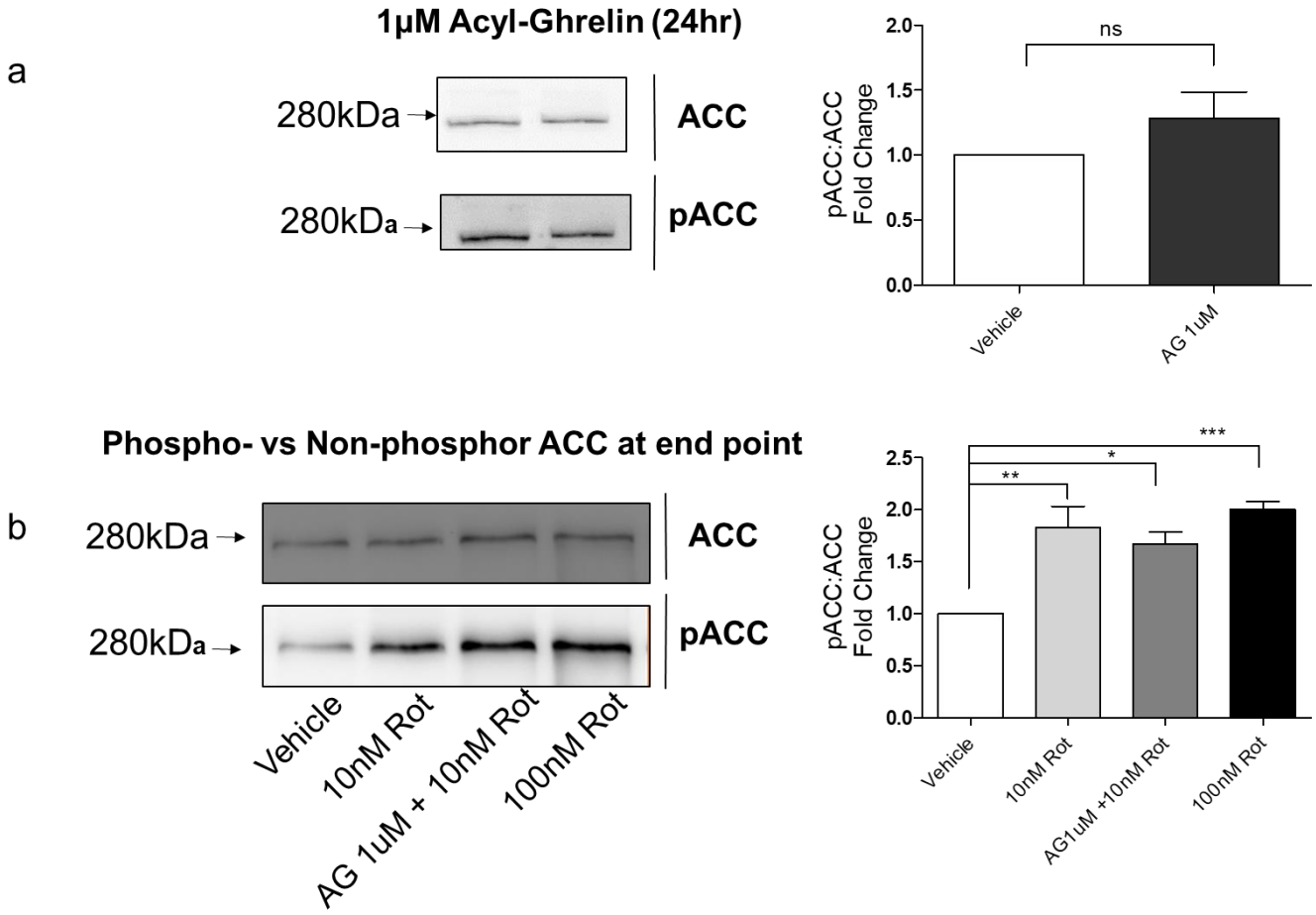

Figure 54: Phosphorylation of Fatty Acid Biosynthesis Enzyme ACC During Neurotoxicity Experiment.

(A) & (B) Immunoblot data shows that AG (1uM) induced phosphorylation of ACC is not retained at 24hr post treatment. (b) Analysis of SN4741 cell protein lysates from experimental endpoint shows that cells treated with 10nM rotenone, AG and 10nM rotenone, and 100nM rotenone all expressed significantly higher levels of phosphorylated ACC compared to vehicle. Graphed data represents the mean fold change of phosphorylated ACC versus non-phosphorylated ACC for 3 technical experimental repeats. Statistical analysis was carried out using Graph Pad Prism version 5 using an unpaired two-tailed t-test for (a) and one-way ANOVA with Bonferroni's Multiple Comparison Test for (b).

Experimental paradigm for the protein extractions above is illustrated in Figure 31 & table 17.

4.4 Discussion

In this chapter, we show that Girk2-positive mouse SN derived DAergic neurones are sensitive to rotenone-induced cell loss and cytotoxicity. The origin of the SN4741 cell line is important as the nigrostriatal subpopulation DAergic neurones show a selective degeneration in *in-vitro* (Y. M. Ding, et al., 2004) and *in vivo* models (Andrews, et al., 2009) of PD that attempt to mimic the degeneration observed in human PD (Damier, et al., 1999a). We find that treatment of SN4741 cells for 24hr with rotenone (10nM) results in a significant decrease in cell number which parallels an increase in cytotoxicity and loss of viability. These data suggest that SN4741 cells are particularly sensitive to the mitochondrial perturbing effects of ETC complex 1 inhibition.

The rotenone-induced cell loss was observed in SN4741 cells cultured in full media and SR (60% of complete) media. SN4741 cells cultured in SR media solely did not show increased tolerance to 10nM rotenone challenge. This may have been expected as caloric restriction in a range of organisms shows there to be evolutionarily conserved mechanisms seen in bacteria, flies and mammals which increase life span, longevity and the ability to overcome the effects of cellular stressors in both healthy and diseased conditions (Longo & Mattson, 2014). It is possible that depletion of a particular substrate, and not the total restriction of cell nutrients used in this chapter may result in enhanced cellular resilience. This may be an avenue for further investigation. However, restriction of cellular substrates did enhance the neuroprotective effects of AG at lower concentration, suggesting that SR in SN4741 cells may, at least partly, act as a mechanism to prime cells to buffer cell stress. The mechanism of rotenone induced cell loss did not appear to be mediated via caspase 3/7 activation, which has been linked to cytotoxicity, mitochondrial dysfunction and oxidative stress (Balakrishnan et al., 2018).

SN4741 neurones pre-treated with a titration of AG concentrations (0, 10, 100, 1000nM) for 24hr in full cell culture media showed attenuated rotenone induced cell loss with 1000nM AG. However, SN4741 cells cultured in SR media showed a significant increase in cell survival following AG pre-treatments at lower concentrations. Similar effects were observed in SN4741 cells following 24hr pre-treatment with the GHSR1a agonist JMV2894. The period of pre-treatment may also play an important role in the mechanism of SN4741 neuroprotection. 1hr pre-treatment with AG resulted in less pronounced AG-mediated SN4741 protection compared to those pre-treated for 24hr. Moreover, unlike the 24hr JMV2894 pre-treatment, no neuroprotection was observed following 1hr pre-treatment. Therefore, it is possible that the resulting intracellular signalling events induced via GHSR1a

agonism by AG and JMV2894 requires more than 1hr to substantiate changes in cellular phenotype to enhance resilience to mitochondrial toxins.

Furthermore, our data suggests that AG neuroprotection in our assay was GHSR1a-mediated. This is consistent with data by (Beynon, et al., 2013), who show that ghrelin's effects are at least partly mediated via it's endogenous receptor, GHSR1a. The study also utilised SN4741 cells and showed that the inhibition of GHSR1a receptor abolished pro-inflammatory IL-6 production. Here, we show that inhibition of GHSR1a by D-Lys3 abolishes the AG-mediated SN4741 cell survival and decrease in cytotoxicity in full and SR media. Further studies should be performed to determine whether the JMV2894-mediated neuroprotection was GHSR1a-dependent.

The changes observed in SN4741 cell number could be the result of alterations to cell proliferation rates. Indeed, AG has been reported to increase cell proliferation in beta-cells and T-cells) (Bando et al., 2013; Granata et al., 2007; J. H. Lee et al., 2014). However, our results show no significant increase in cell proliferation (EdU^{+}) following AG treatment. Rotenone treatment attenuated cell proliferation in cells cultured in both full and SR media. Interestingly, a significant increase in proliferation was observed in SN4741 cells cultured in full media when compared with cells cultured in SR media. This suggests that reduced availability of nutrients in SR media results in cells preserving nutrients for survival/growth rather than utilise them in mitosis. Moreover, these data suggest that 40% depletion of total culture nutrients is sufficient to induce changes in SN4741 cell growth and division kinetics.

Recent work in a mouse MPTP-model of PD demonstrated that ghrelin-mediated neuroprotection was dependent on activation of the cellular energy homeostasis regulator AMPK (Bayliss, Lemus, Stark, et al., 2016). Since SN4741 treated with 1µM AG showed a rapid increase in AMPK activation at 5 mins, which was still observed at the 24hr time point, it is reasonable to suggest that the AG effects observed in our model may also be attributed to a molecular pathway involving AMPK activation. Studies of PD link AMPK with increased mitochondrial function and mitophagy as contributors to the maintenance of cellular homeostasis and survival under stressed conditions. For a comprehensive review see (Bayliss & Andrews, 2013) ; (Andrews, 2011).

We also investigate the phosphorylation of ACC along the time course of our neurotoxicity assay. ACC is one of many downstream substrates of activated/phosphorylated-AMPK (Berg, Tymoczko, & Stryer, 2002). When active, ACC increases utilisation of fatty acid stores as an energy source (Berg, et al., 2002).

ACC becomes phosphorylated 5 minutes post-AG treatment, suggesting that pAMPK is active. As pACC is increased at the experimental endpoint in all treatment groups we cannot define pACC phosphorylation as a contributor to AG-mediated neuroprotection. However, since expression of pACC appears to be greater in SN4741 cells treated with 100nM rotenone versus 10nM rotenone, with and without AG, the phosphorylation of ACC might be a molecular response to cellular stressors. Further experiments are required to elucidate the role of ACC in AG-mediated neuroprotection. These might involve studies of AMPK and ACC phosphorylation events in conjunction with the use AMPK-phosphorylation inhibitors such as compound C/dorsomorphin (Vucicevic et al., 2011). As shown in figure 51 (a-b) 100nM and 200nM compound C did not prevent the expected AG-mediated neuroprotection in full or SR media, respectively. Although in full medium (a), there appears to be an attenuation of SN4741 cell loss in AG & rotenone treated cells, the rotenone induced SN4741 cell loss was not significant.

Importantly, our data does not elucidate whether compound C inhibits the neuroprotective effects of AG as rotenone did not induce a significant reduction in SN4741 cell number, possibly due to decreased efficacy as a result of oxidation of rotenone stocks. Therefore, we can conclude that AG-mediated neuroprotection in SN4741 cells treated with rotenone is GHSR1a-dependant. However, we cannot conclude whether this effect is AMPK-dependent.

Phosphorylation of AMPK is linked to neuroprotective events involving mitochondrial function and dynamics. The next chapter in this thesis will investigate AG-mediated neuroprotection using our *in vitro* rotenone assay in the context of mitochondrial health and function.

5.0. Chapter 5: Investigating Mitochondrial Dynamics using Automated Cell Profiler Image Analysis Pipeline and Electron Microscopy

5.1. Introduction

5.1.1. Mitochondrial Dynamic: Fission, Fusion and Motility

In healthy cells and tissues mitochondria are an essential organelle which generate adenosine triphosphate (ATP) through metabolic reactions that convert nutrients such as glucose, fatty acids and amino acids into biochemical energy (ATP) and waste products. The emphasis placed on their metabolic activity relies heavily on the type of tissue the mitochondria reside in (Wai & Langer, 2016). Mitochondria, commonly referred to as the powerhouse of the cells, are dynamic cellular organelles which are continuously undergoing morphological changes depending on cellular demands and environment. Mitochondrial dynamics including mitochondrial fusion and fission and mitochondrial motility are integral to the regulation of mitochondrial morphology, quality, apoptosis regulation, thermogenesis and homeostasis to ultimately ensure cell survival (Detmer & Chan, 2007; Okamoto & Shaw, 2005; Yamashita & Kanki, 2017) The quality of mitochondria is tightly regulated by pathways designed to retain healthy subset of these organelle whilst segregating the dysfunctional subset for degradation (Yamashita & Kanki, 2017).

There appear to be 6 main mechanisms by which mitochondria regulate homeostasis. First, mitochondria have their own proteolytic system which degrades misfolded or oxidatively damaged dysfunctional mitochondrial proteins to avoid mitochondrial disruption (Anand, Langer, & Baker, 2013; Marcillat, Zhang, Lin, & Davies, 1988). Second, mitochondrial proteins found on the outer membrane (OM) of the mitochondrion can be degraded via the proteasome (Karbowski & Youle, 2011). Third, during oxidative stress parts of the mitochondria may bud-off and form mitochondrial-derived vesicles (MDV) which are subsequently fused with digestive enzyme containing lysosomes that degrade the oxidised mitochondrial material contained in the MDVs (Soubannier et al., 2012). Fourth, mitochondrial spheroids can form under certain conditions. These spheroids are tagged with lysosomal markers suggesting that this may be an alternative removal pathway for damaged mitochondria (Cook, Soto-Pantoja, Jin, Abu-Asab, & Clarke, 2014). The fifth mechanism, as mentioned previously, is the continuous mitochondrial fission-fusion dynamics which attempt to

repair damaged mitochondrial components. Fission results in the segregation of damaged mitochondria, whilst fission allows for the inter-mitochondrial exchange of healthy mitochondrial components. These dynamic mitochondrial events are broadly integral to ensure cell survival, cell growth, adaptation to changes in conditions and overcome mitochondrial disruption during differentiation (Ni, Williams, & Ding, 2015). And finally, another mode by which dysfunctional mitochondria are cleared for degradation is by a mitochondrial specific autophagy pathway, named mitophagy (H. Chen & Chan, 2009). The presence of damaged mitochondria along with deficits and genetic mutations in the cellular machinery orchestrating the clearance of sub-optimal mitochondria for degradation have been associated with neurodegenerative diseases such as Alzheimer's (Moreira, Carvalho, Zhu, Smith, & Perry, 2010), Huntington's (Quintanilla & Johnson, 2009) and Parkinson's disease (Sha, Chin, & Li, 2010).

5.1.2. Mitochondrial Fusion

Fusion is a coordinated event which entails the merger of two outer membranes and two inner membranes of two separate mitochondria. In mammals, three large GTPases are required for this function. The first two are mitofusins (Mfns), Mfn1 and Mfn2, which are integral outer-membrane proteins with most of their polypeptide chain facing the cytoplasm. Mfn1 and Mfn2 can form protein complexes with themselves or each other (H. Chen et al., 2003). This interaction between the Mfns on fusing mitochondria physically tethers the outer membranes of merging mitochondria (Koshiba et al., 2004) and if the Mfns are omitted, fusion of the outer-membrane fusion nor inner-membrane fusion does not occur (Song, Ghochani, McCaffery, Frey, & Chan, 2009). The presence of GTPase domains in Mfns suggests that they actively promote membrane merger via GTP hydrolysis (H. Chen & Chan, 2010). The third integral in mammalian mitochondrial fusion is a dynamin-related guanosine triphosphatase mutated in dominant optic atrophy, OPA1 (Song, Chen, Fiket, Alexander, & Chan, 2007; Song, et al., 2009). In mice and humans, the posttranslational proteolytic cleavage by peptidase produces long isoforms of OPA1 from eight messenger RNA (mRNA) splice variants- integral inner-membrane proteins which transverse the membrane once (Del Dotto et al., 2017). The long form of OPA1 becomes destabilised upon the loss of mitochondrial membrane potential which enhances cleavage at two protease sites. Cleavage at S1 and S2 protease sites generates short forms of OPA1- short isoforms reside in the intermembrane space and are thought to be peripherally associated with the inner membrane (Del Dotto, et al., 2017). Individually, the long and short forms of OPA1 substantiate little

mitochondrial fusion activity. However, co-expression of short and long OPA1 isoforms complement each other's fusion activity. These results from (Song, et al., 2007) suggest that mammalian cells have multiple pathways to control mitochondrial fusion by the processing of OPA1 variants that are regulated by mRNA splicing, membrane potential, and Yme1L (a ATPase Associated with diverse cellular Activity, a i-AAA protease) (Song, et al., 2007).

In mammals, these three major proteins are necessary for mitochondrial fusion of the outer mitochondrial membrane (Meeusen et al., 2006) and the inner mitochondrial membrane (Song, et al., 2009). The importance of these proteins is highlighted by the mitochondrial dysfunction and embryonic lethality observed in mice containing knockouts of each of these three genes (Alavi et al., 2007; H. Chen, et al., 2003; Davies et al., 2007).

5.1.3. Mitochondrial Fission

Mitochondrial fission involves the recruitment of a dynamin-related protein 1 (DRP1), a member of the dynamin superfamily of GTPases. Although DRP1 an integral regulatory protein in the process of mitochondrial fission it is also involved in a range of other cellular functions inclusive of vesicle and organelle fission, viral resistance, and intracellular trafficking (Praefcke & McMahon, 2004).

In mammalian cells DRP1 is an important driver in the change observed in mitochondrial morphology, peroxisomal fission and mitochondrial fission (Koch, Yoon, Bonekamp, McNiven, & Schrader, 2005; Mishra & Chan, 2014; Taguchi, Ishihara, Jofuku, Oka, & Mihara, 2007). During mitochondrial fission, DRP1, which usually resides in the cytoplasm, utilises power from GTP hydrolysis to facilitate its translocation to four protein receptors on the outer mitochondrial surface (Cribbs & Strack, 2007). Four mitochondrial outer membrane receptor proteins are associated with DRP1 include fisson 1 (Fis1), mitochondria fission (Mff), mitochondrial dynamics protein of 49 kDa (MID49) and mitochondrial dynamics protein of 51 kDa (MID51) (Westermann, 2010). These act as tethers for DRP1 during the scission (the cutting) of mitochondria (Mishra & Chan, 2014).

DRP1 is recruited to the mitochondrial membrane to facilitate in the segmentation of mitochondrial structure by constriction of the mitochondrial membranes which eventually results in two separate organelle. In mammals, the DRP1- Mff (Gandre-Babbe & van der Bliek, 2008; Otera et al., 2010), DRP1-MiD49 and DRP1-

MiD51interactions (Palmer et al., 2011) appear to play a more prominent role in fission than that of the interaction between DRP1- Fis1 which plays a minor role (Loson, Song, Chen, & Chan, 2013; Westermann, 2010). Moreover, DRP1 is also known to localize at the close contact site between the endoplasmic reticulum (ER) and mitochondria, suggesting that ER might contribute to mitochondrial fission (Friedman et al., 2011).

Studies in yeast cells suggest that during fission, DRP1 molecules self-assemble on the mitochondrial outer membrane in a multimeric ring-like spiral structure surrounding an area on the mitochondria destined for fission (Knott & Bossy-Wetzel, 2008; Knott, Perkins, Schwarzenbacher, & Bossy-Wetzel, 2008). This process is also thought to be conserved in mammalian cells (Smirnova, Griparic, Shurland, & van der Bliek, 2001) and is an important step in apoptosis, as well as normal cell growth and development. These cellular events which rely on mitochondrial fission and are regulated by the phosphorylation of DPR1 at *Serine 616 (Ser616)* and at *Serine 637 (Ser637).* Ser616 and Ser637 are phosphorylated by Cdk1/cyclin B and protein kinase A (PKA), respectively (Knott, et al., 2008; Taguchi, et al., 2007). The phosphorylation of DPR1 at Ser616 during mitosis leads to increased mitochondrial fission. However, mitochondrial fission is inhibited upon Ser637 phosphorylation (Knott, et al., 2008). Interestingly, this is an effect which can be reversed by dephosphorylation of Ser637 by a calcium and calmodulin dependent serine/threonine protein phosphatase, calcineurin (Cereghetti et al., 2008). Moreover, a mitochondrial E3 ubiquitin ligase, MARCH5, has also been identified as a critical regulatory switch of mitochondrial fission as MARCH5 RING mutants and MARCH5 RNA interference induced elongated and interconnection mitochondrial morphology synonymous of an inhibition of mitochondrial fission in HeLa cells (Karbowski, Neutzner, & Youle, 2007). In addition to phosphorylation, sumoylation of DRP1 by SUMO-1 is also an enhancer of mitochondrial fission (Zunino, Schauss, Rippstein, Andrade-Navarro, & McBride, 2007).

5.1.4. Mitochondrial Motility

Mitochondria are dynamic and mobile organelle. The movement of mitochondria is supported by the intracellular cytoskeleton and is essential for mitochondrial distribution/localization and turnover (Kislin et al., 2017). Mitochondrial motility/transport is facilitated by microtubules, consisting of (+) plus and minus (-) ends, and motored by kinesin and dynamic protein motors. Kinesis interacts with

adaptor protein Milton (also called TRAK1/2) which binds with the E-F hand motifs of Miro (Mitochondrial Rho GTPase, also called RhoT1/2), a protein associated with the mitochondrial OM which forms a mitochondrial motor/adaptor complex (Schwarz, 2013). There is an important interaction between the outer membrane associated proteins Mfn1 and Mfn 2 with both Miro and Milton during mitochondrial motility. Such that, the knockout of Mfn2 in neuronal cultures results in interrupted mitochondrial motility/transport which is also observed in Mfn2 knockout mice (Misko, Jiang, Wegorzewska, Milbrandt, & Baloh, 2010). The mitochondrial motility complex involving kinesis is like that involving dynein. Dynein and kinesin differ in their direction of mitochondrial motility. Dynein aids in the transport of mitochondria towards the minus microtubule end (that is towards the centre of the cell); whilst kinesin motors mitochondria towards the positive end of microtubule (that is away from the centre of the cell) under the regulation of a series of mitochondrial adaptor proteins (Schwarz, 2013). In neurons, the localisation of mitochondria is integral as they produce ATP and Ca^{2+} for synaptic transmission homeostasis at synapses (J. S. Kang et al., 2008; Tang & Zucker, 1997).

Studies on mouse axons have shown that most mitochondria are fixed to kinesin by the static axonal mitochondrial specific anchor, syntaphilin (SNPH) (Y. M. Chen, Gerwin, & Sheng, 2009). An increase in calcium ions (Ca^{2+}) leads to the release of kinesin from the Miro resulting in increased axonal mitochondrial motility. Mitochondrial movement is then stalled at axonal SNPH sites. Mouse neurons containing mutant SNPH show a marked increase in axonal mitochondrial motility and a reduced mitochondrial density. SNPH has been suggested to be part of a ‘stop-start engine’ mechanism which propels mitochondria along microtubules. Studies suggest that elevated levels of Ca^{2+} induce the release of Kinesin from tethering with adaptor protein Miro of the mitochondrial OM which releases the ‘brakes’ on the mitochondria allowing for mobility along a microtubule. Miro subsequently interacts with SNPH to inhibit mobilisation (Y. Chen & Sheng, 2013; Y. M. Chen, et al., 2009; J. S. Kang, et al., 2008). Mitochondrial motility can also be stalled by the effects of an increase in extracellular glucose. Studies in neurones that O-GlcNAc Transferase-mediated GlcNAcylation of adaptor protein Milton results in decreased mitochondrial motility and therefore tailors mitochondrial dynamics based on nutrient availability (Pekkurnaz, Trinidad, Wang, Kong, & Schwarz, 2014).

The balancing of fission, fusion and motility events which are essential for proper mitochondrial function appear to be tightly regulated by intracellular signals to maintain proper cellular function. Research studies have demonstrated mitochondrial

defects in a variety of neurodegenerative diseases including Alzheimer's disease, Parkinson's disease, and Huntington's disease (Knott, et al., 2008). A greater understanding of the subcellular implications of perturbation and mutations in key proteins regulating mitochondrial dynamics and function could highlight therapeutic pathways.

5.1.5. Mitochondrial Quality Control and Degradation

Oxidative stress, the imbalance between the production of free radicals, such as Reactive Oxygen Species (ROS) and the ability to neutralise them to avoid damage to mitochondria (or other cellular organelles). The overproduction of ROS, which are produced as a by-product of ATP synthesis, are implicated in several neurodegenerative diseases, including Huntington's, Alzheimer's and Parkinson's disease (Hwang, 2013; Manoharan et al., 2016).

Mild mitochondrial damage triggers a proteolytic mediated process resulting in the inactivation of OPA1 (Alavi & Fuhrmann, 2013), resulting in a decrease in inner-mitochondrial membrane fusion without effecting fusion of the OM. As the OM fusion is associated with Mfn1 and Mfn2. Severe mitochondrial damage may lead to events which are dependent on a mitochondrial serine/threonine-protein kinase encoded for by gene PINK1, PTEN-induced putative kinase 1 (Pink1) and Parkin (Shimura et al., 2000). The protein Parkin is encoded for by gene PARK2 and is a component of a E3 ubiquitin ligase complex which plays an integral part of the ubiquitin-proteasome system (Pickrell & Youle, 2015). In the event of mitochondrial damage Pink1 activity causes the parkin protein to bind to outer membrane of the depolarized mitochondria and induces a mitophagy which ultimately leads to its degradation. Initiation of Pink1-Parkin events can trigger the degradation of Mfn1 and Mfn2 via pathways involving the proteasome or ubiquitination resulting in mitophagy (Alavi & Fuhrmann, 2013). Although, fragmentation of mitochondria is key for processing damaged mitochondria towards mitophagy, as engulfment my autophagosome is easier, evidence shows that mitochondrial fission is not the lone factor in the initiation of mitophagy (Yamashita & Kanki, 2017). Mitochondrial fragments must also be depolarised and autophagy adaptor protein must also be assembled. Of note, the overexpression of Parkin and Pink1 proteins can lead to increased ubiquitination and degeneration of adaptor protein Miro- linking the adaptor protein with a role in regulation of Pink1-Parkin mediated mitophagy (Twig et al., 2008). For example, the loss of Miro in *in-vitro* HeLa cells results in increased clustering of mitochondria in the area immediately

surrounding the nucleus- the peri-nuclear area- and mitophagy (S. Liu et al., 2012). The exact role of Miro in mitophagy is yet to be fully elucidated. However, the role of Miro in mitophagy is postulated to involve two mechanisms. The first is that Miro-tethering acts as a process of inhibiting the mitochondria to the fate of mitophagy by the tethering of mitochondria to microtubule (via Mitochondria-Miro-Milton-Kinesin-Microtubule) (S. Liu, et al., 2012). The other is that Miro acts as a mitophagy receptor, attracting mito/autophagy associated proteins to mitochondria destined for degradation (X. Wang et al., 2011).

Oxidative stress can result in mitochondrial DNA mutations, damage to the mitochondrial respiratory chain, permeabilise mitochondrial membranes and alter Ca^{2+} homeostasis. It is these perturbations which has seen oxidative stress being implicated in the development of these neurodegenerative diseases, mediating or amplifying neuronal dysfunction and triggering or exacerbating neurodegeneration (Guo, Sun, Chen, & Zhang, 2013).

5.1.6. Parkin-Dependant Mitophagy

Mitophagy can occur in a Parkin-dependent or independent manner (Grenier, McLelland, & Fon, 2013). Upon mitochondrial insult in the context of Parkin-dependent mitophagy, the mitochondrial membrane becomes depolarised and Parkin translocates from cytosolic position to the mitochondrial OM and is regulated by Pink1. Pink1 is stabilised on the depolarised mitochondrial membrane due to the inactivation of mitochondrial protease, Presenilins-associated rhomboid-like protein (PARL) which resides in the inner mitochondrial membrane. Upon mitochondrial damage Pink1 is also stabilized by the outer mitochondrial membrane protein, Translocase of the Outer Mitochondrial Membrane 7 (TOMM7) and de-stabilised by another resident mitochondrial protein SIAH3 (siah E3 ubiquitin protein ligase family member 3) which inhibits Pink1 accumulation (Hasson et al., 2013).

Pink1 is thought to regulate Parkin by either directly phosphorylating Parkin or phosphorylating ubiquitin to promote translocation or ligase activity. The translocation of Parkin to Pink1 from the cytosol is also regulated by two cytosolic proteins- HSPA1L (Heat Shock Protein, 70KDa, A1L) and BAG4 (BAG family molecular chaperone regulator 4) (Takayama, Xie, & Reed, 1999). HSPA1L promotes and BAG4 inhibits parkin translocation. Once Parkin is bound to Pink1 at the mitochondria (Parkin-Pink1), selective Parkin-dependent mitophagy is promoted by mitochondrial ubiquitination and subsequent recruitment of autophagy receptor proteins (e.g. p62

and optineurin) which in turn recruits Microtubule-associated protein 1A/1B-light chain 3-positive (LC3+ve) autophagosomes to engulf targeted mitochondrial cargo (Tanida, Ueno, & Kominami, 2008).

5.1.7. Parkin- Independent Mitophagy

Mitophagy can also be initiated in the absence of Parkin translocation. In the absence of Parkin recruitment, a range of autophagy receptor proteins can localise on the mitochondria which tether directly to LC3 to recruit autophagosomes to orchestrate engulfment of the damaged organelle. These LC3 binding proteins include BNIP3, NIX, FUNDC1 and Cardiolipin (Shi et al., 2014; Tagaya & Arasaki, 2017; Yuan et al., 2017). Autophagosomes may also be recruited to the mitochondria via mitochondrial OM associated E3 ligase, MUL1 (J. Li et al., 2015) and cytosolic E3 ligase smurf1 promotes ubiquitination of mitochondria and recruitment of autophagy receptor protein P62 which targets the mitochondria for mitophagy (Orvedahl et al., 2011).

5.1.8. Mitochondrial-Derived Vesicles and Spheroids

Other mechanism by which damaged mitochondria are degraded include the formation of Mitochondrial-Derived Vesicles (MDV) and Spheroids. During MDV formation, small vesicles containing subsets of damaged mitochondrial proteins are formed. Pink1 and Parkin mediate the segregation of dysfunctional components and encapsulates them into MDVs. MDVs subsequently fuse with late-endosomes and the cargo/contents are delivered to the lysosome for degradation (McLelland, Soubannier, Chen, McBride, & Fon, 2014). Thus, reinforcing the importance of Pink1 and Parkin proteins in the regulation of mitochondrial quality and trafficking of cargo-filled vesicles for degradation. Mitochondrial spheroid formation is regulated by mitofusins and ROS (W. X. Ding et al., 2012). Here, Parkin acts as a reversible switch to mitochondrial spheroid formation. Spheroid formation can occur in the absence of Parkin which is demonstrated in cells treated with a reversible mitochondrial un-coupler, carbonyl cyanide m-chlorophenylhydrazone (CCCP). CCCP triggers a unique form of mitochondrial dynamic process involving the subsequent acquisition of lysosomal markers (W. X. Ding, et al., 2012). The formation of the mitochondrial spheroids and MDV are pathways independent of the canonical autophagy pathway (McLelland, et al., 2014; Samardzic & Rodgers, 2017).

The fission-fusion dynamics and clearance mechanisms surrounding mitochondrial homeostasis has implications in quality control to maintain a healthy intra-cellular mitochondrial network. Fission works to segregate and exclude regions of the mitochondria with a collapsed/low mitochondrial membrane potential (MMP) which is associated with damaged or unhealthy mitochondria. Alternatively, fusion works to preserve healthy mitochondria and its components that typically form organelles with a high MMP. Thus, changes in MMP are associated with cell health and the resulting perturbations are manifested in a range of diseases such as cancer, cardiovascular diseases, diabetes, and various neurodegenerative diseases (Pieczenik & Neustadt, 2007). As such, MMP is used as a measure for mitochondrial toxicity, cell health and apoptosis (Sakamuru, Attene-Ramos, & Xia, 2016), making MMP a key parameter for evaluating mitochondrial function.

5.1.9. Mitochondrial Dynamics in Parkinson's Disease

The cell types with the greatest demand for mitochondrial metabolism are particularly sensitive to mitochondrial dysfunction as this results in decreased function and concomitant ROS production and damage. Moreover, the dynamic mitochondrial fission-fusion interplay facilitates effective motility of mitochondria to their cellular destinations such as dendrites or axons via polarised microtubules. The abnormal inhibition of mitochondrial fission, fusion or motility are suggested to contribute to occur as early events during the neuro-pathogenesis of many neurodegenerative diseases (H. Chen & Chan, 2009).

Approximately 10% of PD cases are thought to be the result of genetic inheritance of mutations in genes including SNCA (PARK1-4) (Polymeropoulos et al., 1997), LRRK2 (PARK 8) (Brice, 2005), DJ-1 (PARK7) (Pankratz et al., 2006), ATP13A2 (PARK9) (Ramirez et al., 2006), as well as Parkin (PARK2) (Lucking et al., 2000) and PINK1 (PARK6) (Bonifati et al., 2005), which are important for the maintenance of mitochondrial integrity (Dodson & Guo, 2007).

There has been a lack of success in replication of common PD symptoms (such as a reduced lifespan, dysfunction of brainstem and sympathetic nerves, visible aggregates of alpha synuclein-positive Lewy bodies or nigrostriatal neuronal degradation) in PINK1 and Parkin knockout mouse studies. These techniques are adequate to produce potential underlying causes of the common PD symptoms. These genetic mutants resulted in symptoms including increased mitochondrial dysfunction (Gautier, Kitada, & Shen, 2008), decreased respiration and ATP

production, and an increased sensitivity to oxidative stress (Gautier, et al., 2008), decreased DA neurotransmitter firing and synaptic plasticity in the nigrostriatal circuit (Kitada et al., 2009; Kitada et al., 2007) (Gispert et al., 2009). Although the loss of DAergic neurons was not directly observed, these perturbations may be a precursor to nigrostriatal neurodegeneration.

In vitro studies using mouse-derived primary neuronal cultures and human DAergic neuron cultures show that loss of protein PINK1 induces, oxidative stress, alterations to mitochondrial morphology and a decrease in long-term cell viability (Wood-Kaczmar et al., 2008). Genetic manipulation studies in drosophila and mammal derived cell lines show that an overexpression of Pink1 promotes fission which is possibly facilitated by Fis1 acting as the intermediator between Pink1 and the fission promoting action of Drp1 (Y. Yang et al., 2008).

In HeLa cells, RNA interference induced downregulation of PINK1 leads to dysfunctional mitochondrial morphology and abnormal membrane potential. These observations are reversed upon reintroduction of wildtype PINK1. Furthermore, primary human patient-derived fibroblasts containing two different PINK1 mutants partly mirrored these observation in mitochondrial morphology. Interestingly, human Parkin rescued this altered morphology, which is associated with cellular stress, in the human cells; an effect which was not seen with PD-associated mutants. This study also suggests that the induced abnormal mitochondrial phenotype may be rescued by increased expression of parkin (Exner et al., 2007).

Fragmented mitochondrial morphology is associated with cells derived from PD patients (Exner, et al., 2007). The importance of Pink1 in replication of PD-like mitochondrial morphology has been shown in studies using HeLa and SH-SY5Y human cell lines as the knockout of Pink1 leads to a fragmented mitochondrial morphology (Dagda et al., 2009; Exner, et al., 2007). Moreover, the overexpression of wild-type Pink1 in SH-SY5Y cells increased mitochondrial interconnecting networks and attenuated toxin-induced mitophagy. In this context mitophagy serves a neuroprotective role by limiting cell death. (Dagda, et al., 2009).

Whereas mouse Parkin and Pink1 loss of function mutants show a very mild phenotype, studies show that drosophila mutants express a more pronounced phenotype inclusive of multi-tissue mitochondrial dysfunction, DAergic neurone and flight muscle degeneration (Y. Yang et al., 2006). This severe phenotype derived from mutant Pink1 flies can be rescued by overexpression of Parkin (Park et al., 2006). Drosophila mutant studies also show that mitochondrial morphology is regulated by a

balance between fusion, which is regulated by Mitofusin (mfn) and opa1, and fission, which is regulated by drp1. Interestingly the severe phenotypes observed in Pink1 and Parkin mutant flies can be ameliorated by the knockdown of mfn or opa1 or overexpression of drp1. The Pink/Parkin pathway is thought to promote the fragmentation of mitochondria via promotion of fission or inhibition of fusion by the positive regulation of drp1 and negative regulation of fusion proteins mfn and opa1.

These results implicate Pink1 and Parkin in a common pathway that regulates mitochondrial physiology and cell survival in drosophila via regulation of mitochondrial fission and fusion (Y. Yang, et al., 2006). However, mitochondrial morphology and phenotypes of Pink1 and Parkin mutant flies are unique from the mitochondrial phenotypes from drp1 mutant flies. Moreover, flies containing heterozygous mutation in drp1 enhance the severity of the Pink1-knockout phenotype, resulting in lethality. These results suggest that Pink1 and Parkin are probably chief constituents of the drp1-mediated mitochondrial fission machinery (Deng, Dodson, Huang, & Guo, 2008). Together this suggests that Pink1/Parkin regulation of mitochondrial fission and fusion dynamics is not a straightforward linear pathway. Although Pink1 and Parkin appear to promote mitochondrial fission and/or inhibition of fusion, other fusion and fission machinery play their own integral roles. An RNAi experiment which screened 719 genes predicted to code for mitochondrial proteins were screened for alterations in Caenorhabditis elegans mitochondrial morphology. The knockdown of over 80% of the targets resulted in altered mitochondrial morphologies such as abnormal mitochondrial fragmentation and elongation. This study implies that maintenance of normal tubular/networked mitochondrial morphology and fission/fusion dynamics is dependent on a range of fundamental mitochondria functions including oxidative phosphorylation and metabolism (Ichishita et al., 2008).

Cell health can be evaluated by investigating mitochondrial health, a marker of which is MMP. Of note, mitochondria in smaller fragmented networks are preferentially chosen for degradation if they also possess a collapsed mitochondrial membrane potential (Pieczenik & Neustadt, 2007).

In this chapter, we investigate the effect of complex-1 inhibitor, rotenone challenge on mitochondrial health by measuring mitochondrial membrane potential and fragmentation as markers of cell health. Furthermore, we study whether AG pre-treatment attenuates rotenone SN4741 neurone loss and ameliorates impairment in MMP and fragmentation. For ease of use and replicability the open-source image analysis software, Cell Profiler was employed to measure mitochondrial health and

fragmentation. Cell Profiler is used to extract meaningful quantitative measurements in an automated pipeline of pre-set computer algorithms for 100s of multi-channel images and export data in the form of a user-friendly spreadsheet format (e.g. MS Excel). We will also utilise Transmission Electron Microscopy (TEM) to investigate the effects of our AG-rotenone neurotoxicity assay to provide greater morphological detail.

5.1.10. Cell Profiler: a High Throughput Image Analysis Software

The examination of cellular function has long been carried out by visual analysis and microscopy following appropriate cellular staining. However, the mid-1990s saw the advancement of technology towards automation of light and fluorescence microscopy hardware. This provided the researcher with a method of rapidly capturing 1000s of high quality images for analysis. The result was a bottleneck in the experimental protocol between image capture and data acquisition due to the laborious and time-consuming task of manual image analysis. Now, both open-source and commercial software is available to decrease the time required for high-quality image acquisition, image analysis and subsequent output of results. Cell Profiler is an example of an open-source software streamline the experimental process.

Cell Profiler: Cell Profiler is a free open-source modular image analysis software capable of handling hundreds of thousands of images (Carpenter et al., 2006).The Cell Profile Project was developed by a collaboration between the 'Broad Institute' and MIT (**www.cellprofiler.org/about/**). The software is available for download at: http://cellprofiler.org/. The Cell Profiler software was developed to allow biologists to investigate cellular phenotypes of interest using a user-friendly, module-based interface. Although some tweaking of Cell Profiler modules is necessary, there is no requirement for the user to have previous experience in computer vision or computer programming in order to successfully construct a Cell Profiler image analysis pipeline (a string of modules) (Carpenter, et al., 2006). Pre-developed modules (algorithms developed by computer scientists) cover a range of features for image analysis including image pre-processing, object segmentation and a list of data exportation options to suit downstream quantitative data management and statistical analysis (Kamentsky et al., 2011).

The automated nature of this software enables the extraction of quantitative data on a large, high-throughput scale, making it an ideal tool for the investigation of multiple parameters within a large image dataset. The Cell Profiler project and software is

bridging the gap between advanced image analysis algorithms and scientists who lack knowledge in computer science. Moreover, carefully designed strings of algorithms and features, named pipelines, can be saved and re-used by the individual or by colleagues running the same experiment

Why use Cell Profiler? Microscopy has long been the go-to method for trained biologists to observe and analyse cellular events and phenotypes. Manual microscopy is a feasible method for imaging small sample sizes. The subsequent qualitative or quantitative manual analysis of a small sample sizes are relatively practical and non-labour intensive. However, recent years (mid-1990s) have seen the development of more sophisticated and automated microscope technologies to analyse samples on a larger scale (Shariff, Kangas, Coelho, Quinn, & Murphy, 2010). The automation of light, wide-field and confocal fluorescence microscope systems allows for the possibility of large scale image acquisition without the laborious task of constant manual user input (e.g. re-focusing microscope between images and manual adjustment of microscope to subsequent samples etc.).

Although, these automated high content analysis (HCA) systems allow scientists to acquire vast image datasets sufficient for robust statistical analysis across a range of samples and treatments, a common bottleneck in the experimental pipeline often occurs during image analysis and data acquisition (Carpenter, et al., 2006; Shariff, et al., 2010).

The automation of image analysis steps which allows the screening of chemical libraries to identify perturbants useful as research tools or drugs (T. R. Jones et al., 2009) can both facilitate and build on the knowledge of a researcher by providing quantitative data outputs which are not possible by eye- even by a trained and experienced cell biologist.

Example uses of Cell Profiler:

As the demand for experimental process automation and High Content Screening and analysis grows (for example in drug discovery and RNA interference screens), the use of image analysis software capable of extracting quantitative data and scoring cellular events from image datasets is increasing. In the 4 years following its

publication, Cell Profiler has been cited in over 250 articles (Kamentsky, et al., 2011) and is used in a variety of methods to extract data from image datasets.

Cell Profiler can be used at many levels of complexity, from simply identifying primary objects such as nuclei for cell counting (see chapter 4), to segmentation of cellular compartments of interest to extract cell-by-cell quantitative information, to more complex methods including particle tracking and the use of machine learning to score specific cell phenotypes (T. R. Jones, et al., 2009). Cited research papers show the application of Cell Profiler in the analysis of a variety of in-vitro and ex-vivo experiments.

In this research chapter we focus on identifying cellular compartments, a method commonly termed segmentation. This method involves designating groups of pixels in a 2-dimentional (2D) image as cellular compartments of interest, such as nuclei, cell bodies and cytoplasm. Once these areas of interest have been identified, information in the form of quantitative data is easily extracted using Cell Profiler's intuitive user interface, object measurement features and variety of data output tools.

5.2. Methods and Materials

5.2.1 SN4741 Mitochondrial Health Analysis

SN4741 cells were seeded and treated in a neurotoxicity assay as described in chapter 4 (see figure 28 B for experimental timeline). Following incubation in test compounds for a designated period of time under normal cell culture conditions, 175 µL was removed from each well resulting in 125 µL remaining.

As described in the HCS Mitochondrial Health Kit (Invitrogen, Cat.No #H10295) (referred from here on as MitoHealth Kit) protocol manual, a 50 µL mixture of MitoHealth stain and Image-iT® DEAD Green™ viability stain in complete medium should be added and incubated under normal condition for 30 mins at this point. Although both stains included in this kit are well retained following formaldehyde fixation and detergent permeablization, for our application Image-iT® DEAD Green™ viability stain was omitted as we have explored SN4741 cell cytotoxicity in this context and we were now predominantly focussing on mitochondrial health and fragmentation. Mitohealth staining solution was prepared by the addition of 2 µL of Mitohealth stain into 650 µL of cell culture medium (1:350 dilution) as required. Following 30 minute incubation with Mitohealth stain, the medium was removed and 100 µL of counterstain/fixation solution was added to each well. Cells were protected from direct light using tin foil and incubated for 15 minutes at room temperature to ensure fixation and counterstaining of SN4741 cells and nuclei. The counterstain/ fixative solution was prepared by adding 3 mL 16% paraformaldehyde (PFA) and 6 µL of Hoechst 33342 (included in HCS Mitochondrial Health Kit) to 9 mL PBS. This ratio of counterstain/fixation solution (PFA: Hoechst 33342: PBS) was prepared fresh in the ratio of 1mL PFA: 2 µL Hoechst 33342: 3 mL PBS as required prior to addition to cells. SN4741 cells were then washed once in 100 µL PBS before the addition of 200 µL PBS to each well and stored overnight at 4°C (protected from light) or proceeding directly to imaging and analysis.

5.2.2. HCS Mitochondrial Health Kit

The MMP, Δψm, is a feature of healthy mitochondria. The Δψm is essential for generation and detoxification of reactive oxygen species (ROS), the uptake and storage of Ca^{2+}, and synthesizing ATP by oxidative phosphorylation (Nicholls, 2004). Since the retention of a Δψm is a good indicator of mitochondrial health and its depolarization is a good indicator of mitochondrial dysfunction, it is utilised as a measurable parameter in high-content analysis cytotoxicity assays (Abraham, Towne, Waring, Warrior, & Burns, 2008).

In recent years, fluorescent dyes for measuring the MMP (Δψm) have become commonly used tools for monitoring changes in this important physiologic mitochondrial parameter as it relates to cells' capacity to generate ATP by oxidative phosphorylation (Perry, Norman, Barbieri, Brown, & Gelbard, 2011). To assess the effects of treatments on SN4741 cell mitochondrial health the MitoHealth Kit was employed. The MitoHealth kit consists of two stains which can be used can be used to quantitatively assess two cell health parameters: Mitotoxicity (or Mitochondrial Health) and cytotoxicity. HCS Mitochondrial Health Kit also includes Hoechst 33342 DNA counterstain.

The MitoHealth stain, accumulates in functional mitochondria proportional to mitochondrial membrane potential. The fluorescence intensity (FI) staining observed with the MitoHealth stain corresponds to MMP and gives a measure of mitochondrial health (mitotoxicity) i.e. The FI observed in healthy mitochondrial is greater than that observed in damaged mitochondria because they have a higher MMP.

Hoechst 33342 is a fluorescent DNA counterstain which can be applied to live and dead cells. Approximate fluorescence excitation/emission maxima: Hoechst 33342: 350/461 nm bound to DNA; Image-iT® DEAD Green™ viability stain: 488/515 nm; MitoHealth stain: 550/580 nm. All dyes included in this kit are applicable for live cell imaging and have sufficient FI retention following formaldehyde fixation and permeablization for endpoint assays.

Image acquisition was carried out using the InCell Analyser 2000 (GE Healthcare) to capture 52 x40 magnification tiff format images from each well. Treatments were carried out in duplicate for 5 experimental repeats (n=5). Treatments included vehicle, 1µM AG-treatment, 10nM rotenone challenge, 1µM AG-treatment prior to 10nM rotenone challenge, 100nM rotenone challenge and DMSO. Treatments were carried out in full medium in synchronicity with the 24hr neurotoxicity assay, as described in Chapter 4. A Cell Profiler pipeline was developed to i) identify cell nucleus from Hoechst 33342 staining intensity; ii) measure MitoHealth staining intensity in each cell peri-nuclear region (area surrounding the nucleus) and iii) quantify extent if mitochondrial fragmentation by counting and measuring areas of Mitohealth stained mitochondrial fragments.

5.2.3. CellProfiler Protocol for the Identification of Cell Nuclei, measurement of Mitochondrial Membrane Potential and Mitochondrial Fragmentation.

A variety of example image analysis pipelines and tutorials are available at: CellProfiler.org. These include pipelines for various levels of image analysis complexity and purpose. Basic Cell Profiler pipelines see relevant application in the analysis of human cells, fruit fly cells, tumours and comet assays.

More Advanced Pipelines include examples which can be applied to Human cytoplasm-nucleus translocation assays, Speckle Counting, Object Tracking and Metadata Management, and Sequencing RNA molecules in situ.

Although CellProfiler software and corresponding website does contain pre-made computer algorithms (modules) and example analysis pipelines respectively, this does not mean that Cell Profiler is a simple out-of-the-box, plug-and-play image analysis software. Rather, these pre-made modules and example pipelines are used to teach the everyday biologist, with little computer programming or macro script writing experience, how to design and assemble an image analysis pipeline to fit the specific needs of their experimental question. Interestingly, CellProfiler also allows for ImageJ (NIH) software input of macro scripts to aid image analysis. Taken together, CellProfiler is relatively flexible, user-friendly platform on which to conduct image analysis.

The protocol below describes the step-by-step Cell Profiler pipeline for the identification of nuclei, measurement of MitoHealth staining intensity and quantification of mitochondrial fragmentation protocol used to quantify SN4741 cell mitochondrial measurements from x40 magnification digital images. This protocol was developed by optimising a range of modules and example protocols. Each step includes a description, Cell Profiler-derived notes and rationale followed by instructions on how to execute the step in Cell Profiler software (in italic font). ‘Notes’ are heavily reference from **CellProfiler.org/manuals.**

Cell Profiler Pipeline: Measuring MMP.

The fluorescence intensity of the mitochondrial health stain corresponds with MMP. The fluorescence intensity was measured in the area/ ring around the nucleus of each identified SN4741 cell, as is described in the HCS Mitochondrial Health Kit [H10295, Molecular Probes]. The area of the ring surrounding the nucleus is also calculated. Here we describe a step-by-step method used to segment this area of interest from the remainder of the image to extract measurements.

Step 1: Upload Image set, Image Sorting and Image Pre-processing and Illumination Correction

First, it is necessary to open Cell Profiler Software and select the experimental image set.

Open Cell Profiler Pipeline > Select 'Images' in 'Input Module' window > Right click inside empty 'File list' window > Browse and select image set.

Here, our image set is composed of two channels, Cy3 and DAPI, which account for x40 magnification images containing MitoHealth stained mitochondria and Hoechst stained nuclei of SN4741 cells respectively (see figure 55). To filter the images according to filename:

Select 'Names and Types' in pipeline Input modules > Select 'Images Matching Rules' then select 'File', 'Does', 'Contain' from dropdown box selections > Type 'DAPI' into input box to group DAPI channel images.

Select 'Add another image' and repeat the process with exception to entering 'Cy3' into input box to group Cy3 channel images. Assign a (user-defined) name for grouped files > Select 'Update'.

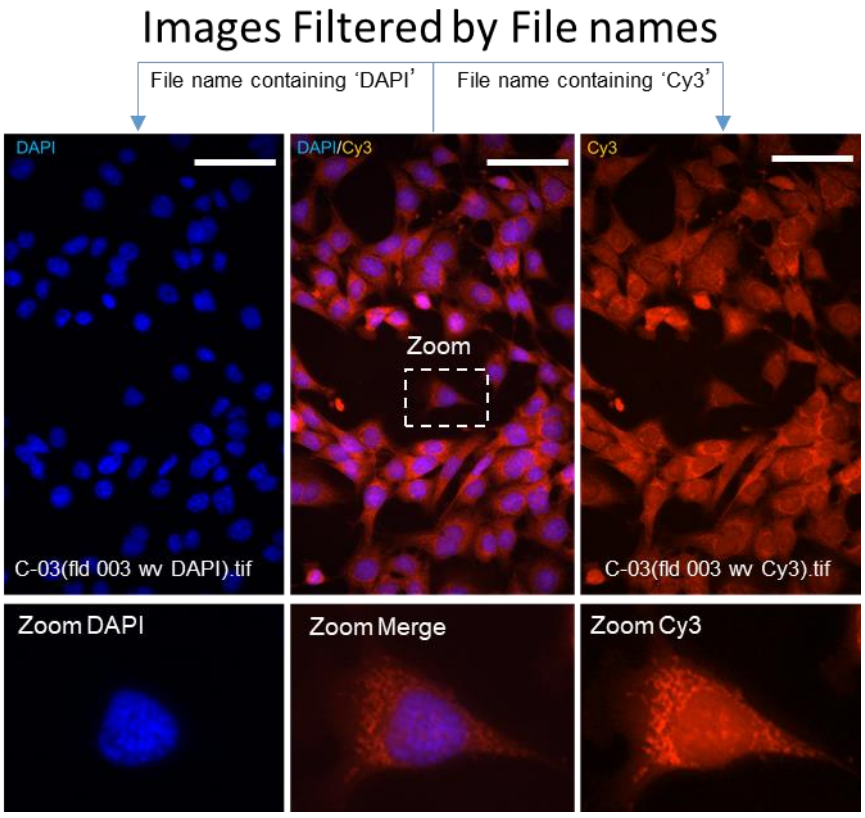

Figure 55: Images are Filtered into Groups by File Names.
This diagram illustrates an image set containing DAPI and Cy3 images being separated into groups (DAPI and Cy3) based on their file names. Cropped image tile labelled DAPI/Cy3 represents a pseudo-coloured composite of both channels. Blue arrows illustrate the separation of DAPI and Cy3 channels based on contents of their file names. Example image filenames are given on pseudo-coloured DAPI and Cy3 images. DAPI, merged and Cy3 x40 magnification images scale bar 40µm. Each pseudo-coloured image has a representative Zoomed image for graphical purposes. MitoHealth-stained mitochondrial networks are visible in Zoom Cy3 image.

Note: Care must be taken when filtering image sets by common phrases in filenames, such as 'DAPI' and 'Cy3', as phrases are case-sensitive. Inconsistency in spelling or case-sensitivity results in failure to identify files and sub-group images. Experimental image set should now be grouped in two file lists under user-defined group titles e.g. DAPI and Cy3 and ranked in numerical order.

During the analysis of images taken with a fluorescence microscope it is common for the images to be pre-processed prior to analysis. The most common reason for this is uneven illumination across a field of view as the light source does not evenly

illuminate across the entire area. This results in areas with greater illumination than other areas, usually the corners of the image.

A limitation of many High-Content Screening (HCS) platforms, such as the InCell Analyser 2000, is that a flat field correction (FFC) function cannot easily be implemented into the imaging process. There is the option to modify the images taken during a post-processing stage; however, this leaves the quality control of the FFC to the imaging software without any further input or quality control from the end user. Without a FFC application we can see that the intensity of an images varies widely from the centre to its edges (illustrated in figure 56). This spread of illumination intensity within an image will deter the accuracy of downstream image analysis. For example, regions of a cell body may appear shaded and therefore segmentation of image into biologically-relevant compartments (i.e. identification of cell body boundary) may be deterred.

The illumination pattern will change if a different staining reagent(s) is used for a batch of samples or if there is a change in the components or setting in the optical path of the microscope. For example, the illumination pattern may change throughout the same day or analysis as the lamp changes temperature. Therefore, in this protocol illumination is measured and correction applied for each image channel- that is Hoechst and Cy3.This illumination pattern must be corrected to ensure correct and comparable measurements in intra and inter image analysis. Cell Profiler software has built-in modules to deal with these issues. The ***CorrectIlluminationCalculate*** module is used to measure the intensity pattern of a single or set of images and produces an intensity function which is to be applied across the entire image set. The ***CorrectIlluminationApply*** module then applies the calculated intensity function to the images prior to analysis. Correction of intensities can be important for segmentation and intensity measurement functions. In this method of illumination correction, we create and save an illumination function and apply this correction to images before segmentation. This can be performed using a separate Cell Profiler pipeline to create an 'average' illumination function for a specific fluorescence channel in a data set. Alternatively, as it is performed in this instance, the pre-processing (illumination correction) can be implemented at the start of an image analysis pipeline. This illumination function is saved as an image and is applied to the entire data set. The drawback of implementing illumination correction as part of a working pipeline, especially when dealing with large quantities of image files, is that calculation of the illumination function can add a considerable amount of time to the automated analysis process.

Cell Profiler users recommend calculating different Illumination correction for each multi-well experiment and for each wavelength measured within the experiments as there is variability in illumination between experimental plates and samples.

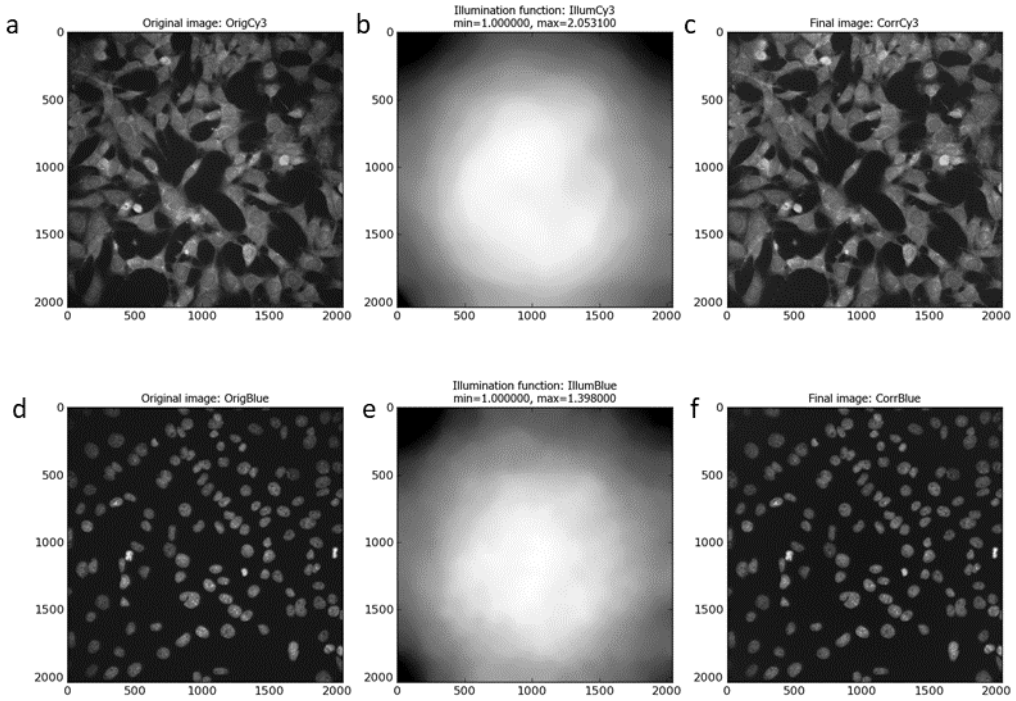

Figure 56: Cy3 Image and DAPI Channel Images Before and After Illumination Correction.

Figure 56 (a) and (c) show representative x40 magnification greyscale images acquired using In Cell 2000 Cy3 filters before (OrigCy3) and after (CorrCy3) illumination correction via, respectively. (Figure 56 b) illustrates the Illumination function (IllumCy3) produced from entire Cy3 image set. Figure 56 d & f show representative x40 magnification greyscale images acquired using In Cell 2000 DAPI filters before (OrigBlue) and after (CorrBlue) illumination correction, respectively. Figure 56 e (IllumBlue) illustrates the Illumination function produced from entire image set This illumination correction is carried out by Cell Profiler modules *CorrectIlluminationCalculate* and *CorrectIlluminationApply* Images (a-f) are micro pictograms acquired and saved from the Cell Profiler Software.

To calculate correct illumination function:

Select **Correct Illumination Calculate** *module > Select input image (name assigned from Names and Types)*

Insert a (user-defined) Name the Output Image e.g. 'IllumCy3'

Select 'Regular' option in How the illumination function is calculated.

Note: The option 'Regular' is selected if stained objects (e.g. cell bodies, nuclei) are evenly dispersed across your image(s) and cover most of the image. This is true in the case of Cy3 and DAPI channel images. Regular intensities make the illumination function based on the intensity at each pixel of the image (or group of images if you are in All mode) and applied by division using **Correct Illumination Apply module.**

Select 'Median Filter' > Select 'Manual' method to calculate filter size > input smoothing filter size '325'.

Note: Illumination function was calculated across the entire image set prior to initiation of object identification and subsequent data measurements.

To apply the illumination function calculated by **Correct Illumination Calculate**:

Select ***Correct Illumination Apply*** *module*

Input > a user defined name into 'Name the output image' box e.g. 'CorrCy3'

Select illumination function from drop down box (as defined in **Correct Illumination Calculate** module *e.g. IllumCy3)*

Select 'Divide' as method for how the illumination function is applied

Note: Divide is the recommended method of illumination function application by Cell Profiler users if the illumination correction function was created using 'Regular' in the **Correct Illumination Calculate** module.

Figure 56 illustrates the shading seen on edges of Cy3 and DAPI channel images acquired images before and after application of illumination function as described above.

Step 2: Identification of Nuclei

Here we identify cell nuclei (a feature) based on their high contrast background to foreground staining intensity. In Cell Profiler software, a primary object is defined as an object or feature (usually a cellular sub-compartment e.g. nucleus) which can be

Nuclei are commonly selected as the primary object (or the seed) of an image analysis pipeline due to their relatively uniform morphology and high background to foreground staining intensity ratio which makes them easily identifiable.

Select > ***'Identify Primary Objects'*** *module*

Input > (user named illumination corrected) DAPI image(s)

Input > Typical Nucleus diameter range (pixels). Min: 50 and Max: 135

Discard objects outside the diameter range > Yes

Discard objects touching the border of the image > Yes

Note: Estimate nucleus diameter using Cell Profiler by selecting a DAPI image by *'Right click'* on DAPI image and selecting *'Show Selected Image';* and selecting *'Tools > Measure length'.*

For thresholding select 'Global' Thresholding Strategy with 'Otsu' method and 'Two Classes' thresholding. Set threshold correction factor of '1.0'; and lower and upper bounds to '0.0' and '1.0', respectively.

Note: Global thresholding strategy uses the pixel intensities in each un-masked image to calculate a single threshold value to classify pixels as foreground (brighter/more intense than threshold value) or background (with intensity below the threshold value). This thresholding strategy is fast and robust and commonly applied to images that have a uniformly illuminated background. Since foreground-to-background pixels are easily distinguishable using Hoechst, DAPI channel images showing counterstained SN4741 cell nuclei, this 'Global' thresholding strategy is a sensible choice for this primary object identification. Otsu is a method of automatically finding thresholds by splitting image pixels into two (foreground and background) or three classes (foreground, mid-level and background) by minimizing the variance within each class. Lower bounds on threshold can be set at 0.0 as there is an object (Nucleus) in each image. Otherwise, an empirically determined lower threshold bound as automatic methods of thresholding may miss-assign pixels in a blank image to the foreground class, potentially yielding false-positive results.

Select > 'Shape' for de-clumping of primary object which are touching or in close proximity and 'Shape' for drawing dividing lines between objects.

Select > 'Yes' to 'Automatically calculate size of smoothing filter for de-clumping'

Select > 'Yes' to 'Automatically calculate minimum allowed distance between local maxima'

Select > 'No' to 'Retain outlines of the identified objects

Fill in identified objects > 'After both thresholding and de-clumping'

Note: By selecting 'shape' for de-clumping method, cases in which there are definite indentations separating objects. The image is converted to a binary (black and white) image and the resulting shape determines whether clumped objects will be distinguished.

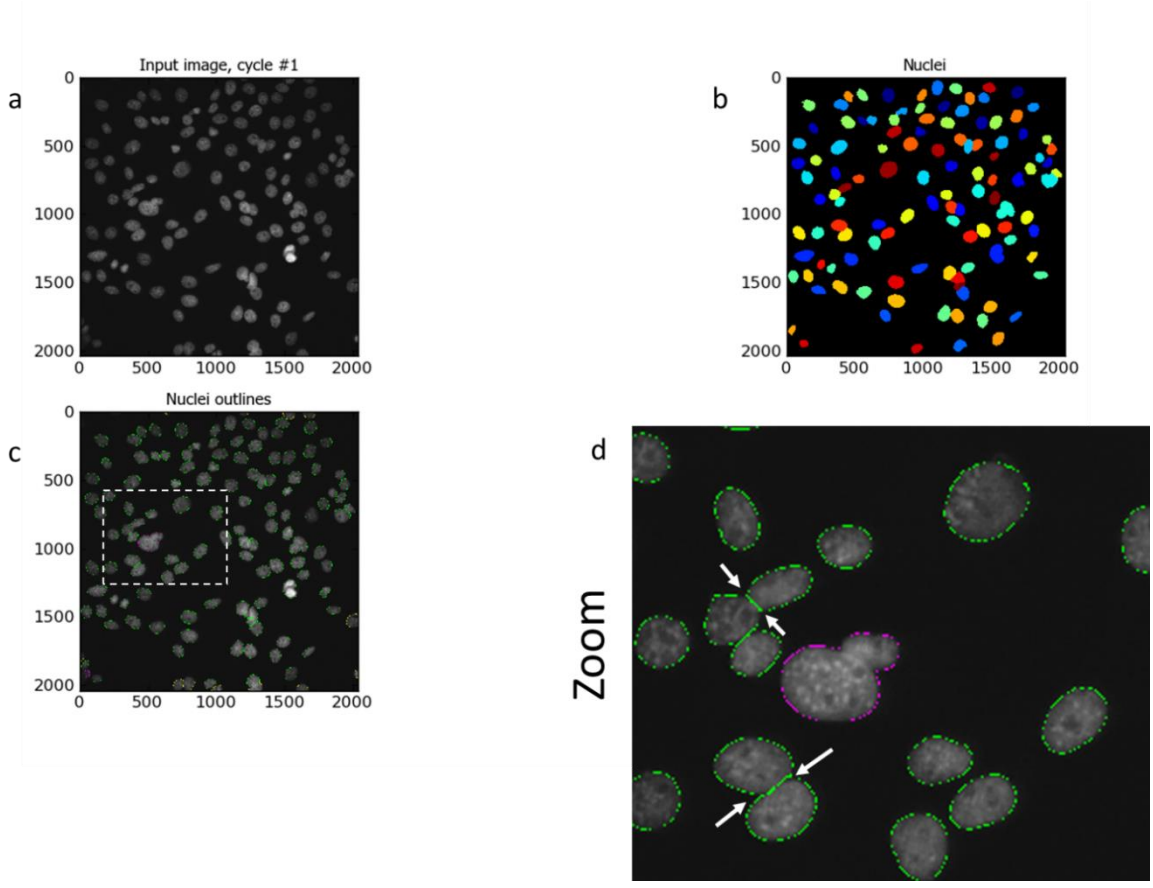

Figure 57: Identify Nuclei as Primary Objects.

Figure 57(a) shows a representative illumination corrected x 40 magnification image of Hoechst counter-stained nuclei acquired using In Cell Analyser 2000 DAPI channel filters. (b) illustrates identified primary objects using object coloured masks. (c) shows nuclei fitting to protocol input criteria (outlined in green); nuclei filtered out by size

criteria (outlined in magenta); and nuclei filtered out for touching the image border (outlined in yellow). Dashed white line shows zoomed area (d). (d) shows the Zoomed area with white arrows indicate indentations used to de-clump objects (nuclei). Images (a-d) are micro pictograms acquired and saved from Cell Profiler.

Step 3: Identify Secondary Objects: Ring shaped Cell Body

The next module in Cell Profiler pipeline is **Identify Secondary Objects.** This module identifies objects by using the object identified by another module as a starting point. In this example, the primary object (nuclei) identified in the Identify Primary Object will act as the seed for the identification of SN4741 peri-nuclear area (doughnut shaped ring around the nucleus) in the corresponding Cy3 images. This will be executed by dilation of the previously identified nuclei- this dilated nucleus area is named 'Full Doughnut' in figure 58 (c) A subsequent module in this pipeline will remove the nucleus, and a ring like object will be remaining (a doughnut shaped-perinuclear region). This is referred to as 'True Doughnut' in figure 59 (f). Other modules will the collect measurements such as area and intensity of peri-nuclear regions.

To expand nucleus and create 'Full Doughnut' shape:

*Select > '**Identify Secondary Object'** module*

Input > Illumination function corrected Cy3 image ''CorrCy3'

Input (primary) objects > Select 'Nuclei'. These were identified by Identify Primary Object module.

Insert the name of objects to be identified > 'FullDoughnut'

Select > 'Distance- B' as method to identify the secondary objects

Note: By selecting Distance as the method to identify the secondary objects ('Full Doughnut') the primary object (nucleus) is expanded to identify a 'doughnut' (or 'annulus') shaped region in the cell, usually in the cytoplasm. Cell Profiler provides two methods of identifying the secondary object. The first, 'Distance-N' does not utilise staining intensity in the image of the second stain- in this instance Cy3. This entails expanding the nucleus a set distance. However, this may include areas of image background as well as cell cytoplasm. Our protocol on the other hand utilises 'Distance- B' method. This second 'Distance' method expands the nucleus a set distance however, this method uses the thresholding of the secondary staining image

to eliminate background regions. Thus, the nucleus is only expanded in to areas of foreground staining intensity to identify Full Doughnut secondary object without including background image regions.

Select > 'Automatic' threshold method.

Input > '25' as number of pixels to expand the primary object (nucleus)

Fill holes > Select 'Yes'

Discard Objects touching the border of the image > Select 'Yes'.

Retain outlines of the identified secondary objects > Select 'No'

Note: the 'Automatic' thresholding method is the default setting in Cell Profiler and is robust. As this strategy is automatic it does not allow user to select the threshold algorithm or to apply additional corrections to the threshold. The 'Automatic' strategy calculated the threshold using maximum correlation thresholding (MCT) for the whole image. The threshold is then applied to the image and smoothed with a Gaussian filter with a sigma of 1, this blurs or obscures smaller than an entered diameter and spreads bright or dim features larger than the entered diameter. The MCT method is described by (Padmanabhan, Eddy, & Crowley, 2010) as computationally efficient and accurate without relying on assumptions of the statistics of the image. This algorithm has been trialled and tested on neuroscience images in the presence and absence of illumination correction to accurately aid in automated image analysis.

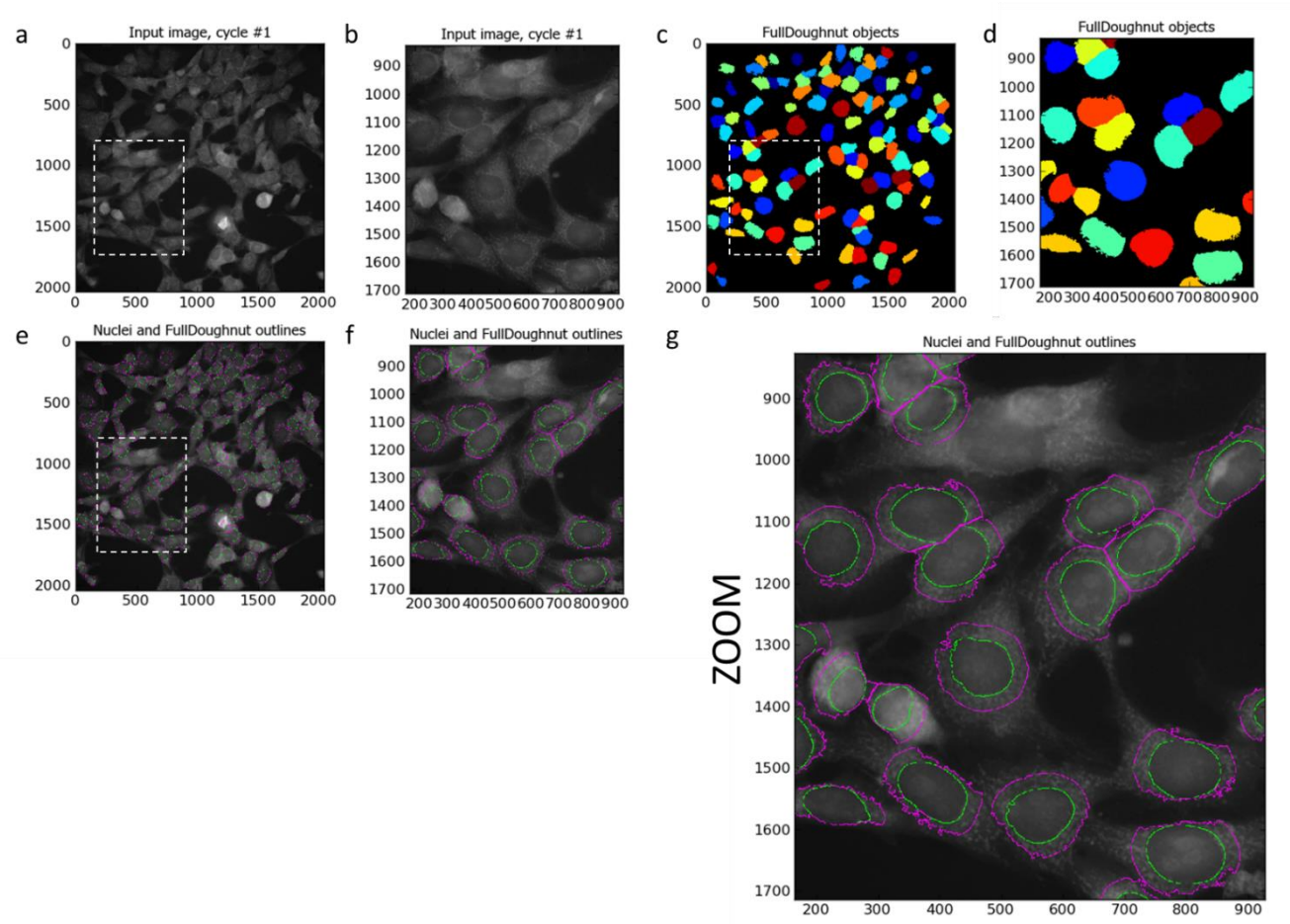

Figure 58: Identification of Secondary Object- Full Doughnut

Figure 58a shows the Illumination Corrected Cy3 image (a); the result of a 25-pixel distance dilation in nucleus size with respect to Cy3 image staining intensity thresholding. Identified secondary objects/Full Doughnuts are illustrated in the form of coloured masked objects. Dashed white line boxes in (a), (c) and (e) highlight the area(s) which are zoomed-in and illustrated in (b), (d) and (f) respectively. Zoomed images show the image segmentation more clearly. Image (g) is a larger version on (f), illustrating the nuclear area/primary object with a green outline and the edges of the Full Doughnut/secondary object with a magenta outline. Images (a-g) are micro pictograms acquired and saved from the Cell Profiler Software.

Step 4: Identify Tertiary Objects: Cell Cytoplasm or True Doughnut

Following the identification of the 'Full Doughnuts' (secondary objects), the **Identify Tertiary Objects** module is then used to remove the smaller objects (nuclei) from the larger secondary objects (Full Doughnuts) to leave a ring shape around the nucleus, referred to here as 'True Doughnut'.

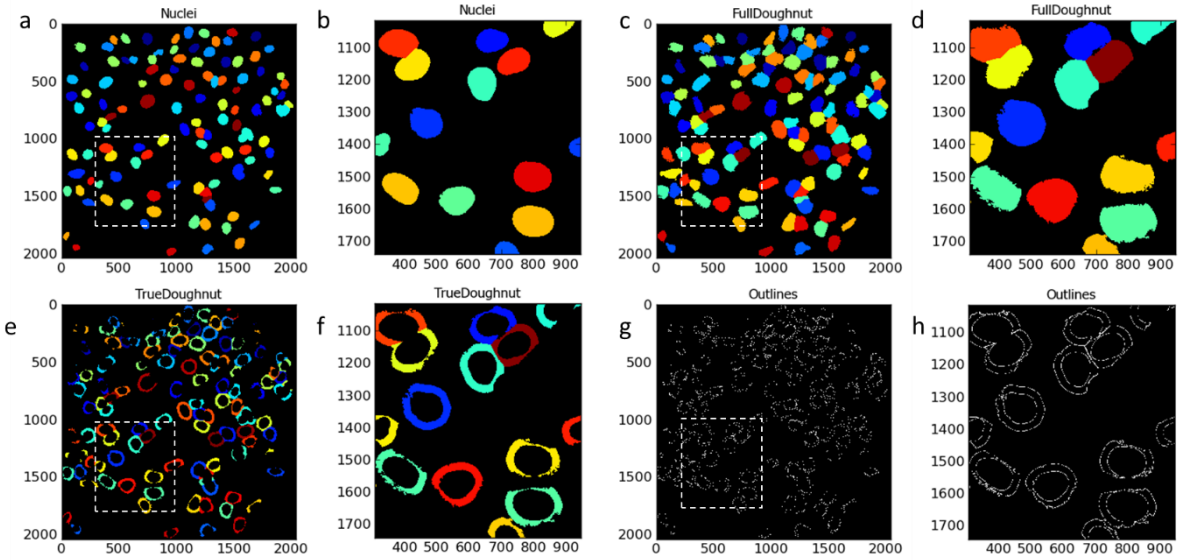

Figure 59: Identify Tertiary Objects

Images (a), (c) and (f) illustrate the masked image result of sequential steps/modules from identification of primary object (Nuclei), identification of secondary object (Full Doughnut) and tertiary object (True Doughnut), respectively. The ring shaped True Doughnut is the result of removing the Nuclei areas from the areas of Full Doughnuts. Micro-pictograph (g) highlights the outlines of the resulting True Doughnut. Dashed white boxed in images (a), (c), (e) and (g) indicated the areas which have been zoomed-in for illustrative purposes and are represented by images (b), (d), (f) and (h) respectively. Images (a-h) are micro pictograms acquired and saved from the Cell Profiler Software.

To identify tertiary objects (ring shaped 'True Doughnuts'):

*Select > **'Identify Tertiary Objects'** module*

Select > 'FullDoughnut' as larger identified objects (output from Identify Secondary Object module)

Select > 'Nuclei' as smaller identified objects (Output from Identify Primary Object)

Select > 'Yes' to shrink smaller object prior to subtraction.

Note: Nuclei will now be subtracted from Full Doughnut area to produce a ring shaped 'True Doughnut' in the peri-nuclear region of the identified SN4741 cells. By selecting 'Yes' to shrink the smaller object the nucleus is shrunk by 1 pixel before subtracting the objects. This ensures a tertiary object is produced. Measurements such as area and fluorescence intensity of the segmented area can be acquired subsequently.

Cell Profiler Pipeline: Measure SN4741 Mitochondrial Fragmentation

Abnormal fragmentation of mitochondria is a trait observed in cells derived from patients afflicted with neurodegenerative diseases such as PD (Pieczenik & Neustadt, 2007). Pesticides such as rotenone are commonly used to generate PD models (Knott & Bossy-Wetzel, 2008). In in-vivo rat models, systemic exposure to rotenone induces neurochemical, behavioural and neuropathological features of PD. These PD-like features are inclusive of nigrostriatal dopaminergic degeneration which is associated with the behavioural traits of hypokinesia and rigidity. The systemic exposure of rotenone in this rat model also resulted in other PD-associated neurochemical hallmarks such as the accumulation of ubiquitin and alpha-synuclein containing cytoplasmic inclusions (Betarbet et al., 2000). Moreover, evidence shows that cells exposed to rotenone, a mitochondrial Electron Transport Chain (ETC) complex-I inhibitor, results in a fragmented mitochondrial morphology *in-vitro*. An affect which is appears to be dependent on metabolic energy sensor, AMPK (Toyama et al., 2016).

Here we describe a protocol variation on the 'Cell Profiler Pipeline: Measuring MMP', previously described, which allows for identification of entire mitochondria in SN4741 cell body and subsequent quantification of mitochondrial fragments and measurement of fragment size. This Cell Profiler pipeline utilises aspects of the Cell Profiler website's 'Speckle Counting' example pipeline with alterations to complement the analysis of x40 magnification image of SN4741 cells for mitochondrial fragments stained by the mitochondrial health stain. The basic pipeline is similar to that described above, however, there are adjustments at i) 'step 3' as Cell Profiler software is tweaked to identify SN4741 cell body; and ii) 'step 4' as the edges of entire SN4741 cell cytoplasm are identified as opposed to only the ring shaped 'True Doughnut' in the peri-nuclear region of the cell. Alterations are described in a step-by-step method below.

Step 3: Identify Secondary Objects: SN4741 Cell Body

Following the identification of SN4741 nuclei using **Identify Primary Object module** the **Identify Secondary Object** module is used again. However, this time the module and method must find the edge of SN4741 cell bodies as secondary objects using cell body-specific Cy3 staining intensity. Again, this module involves a thresholding step which assigns pixels in the input image to foreground and background. To identify cell body:

*Select > **'Identify Secondary Objects'** module*

Input Image > Selects 'CorrCy3'

Select > Input Objects 'nuclei' (identified in Identify Primary Object module)

Input > 'CellBody' as name for identified objects

Select > 'Propagation' as method to identify secondary objects

Select > 'Automatic' as threshold method

Input > '0.00' as regularization factor.

Select > 'No' to fill holes in identified objects

Select > 'Yes' to discard objects touching the image border

Select > 'Yes' to discard associated primary objects

Select > 'No' to retain the outlines of the identified secondary objects

Note: This module uses 'propagation' as the method to identify dividing lines between clumped cell bodies (secondary objects) where there is a local change in staining intensity (i.e. cell bodies having different staining intensities; and foreground and background have different staining intensities). This algorithm varies from the watershed method (used in Image J macro) as the dividing lines between objects (cell bodies) are determined by both the changes in local image intensity (intensity gradient) and distance to the nearest primary object (nucleus). Dividing lines are placed in the image where the images local intensity changes perpendicular to the boundary (T. R. C. Jones, A. Golland, P., 2005)**.** Therefore, this method is considered an improved method of object segmentation. Since 'propagation' is selected a regularization factor (given the symbol λ) must be user-defined to inform the execution of the propagation algorithm. Propagation takes 1) the distance to nearest primary object and 2) intensity of the secondary object image into account when defining the

dividing lines between objects. The regularization factor is used to decide the balance and weight placed on each factor during propagation and can be anywhere in the range 0 to infinity. If a regularization value >1 is selected, the image intensity is almost completely ignored. Whilst selecting a regularization value of 0, means that the distance to the nearest primary object is ignored and propagation relies on image intensity. The larger the regularization value the more image intensity is ignored and dividing lines drawn become more reliant on distance to the nearest primary object.

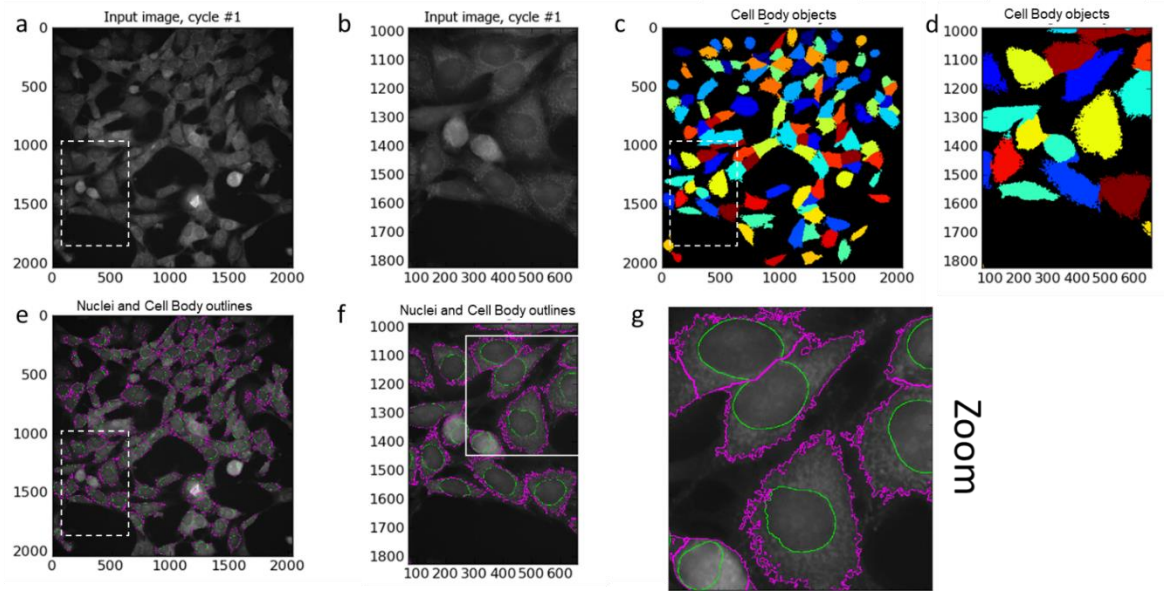

Figure 60: Identify SN4741 Cell Body as Secondary Object

Figure 60 (a) shows the input Illumination Corrected x40 magnification Cy3 channel image; (C) Illustrated the result of propagation method of identifying cell (body) edge with respect to Cy3 image staining intensity thresholding. Identified secondary objects/Cell bodies are illustrated in the form of coloured masked objects. Image (e) shows the input Cy3 channel image with identified cell body outlines in magenta and nuclei outlines in green. Dashed white line box in (e) highlights the area zoomed to produce image (f). White box in image (f) indicates area which is zoomed in to produce image (g). Zoomed in images (f) and (g) were generated to illustrate image segmentation. Dashed white line boxes in (a) and (c) highlight the area(s) which are zoomed and illustrated in (b) and (d) respectively. Images (a-g) are micro pictograms acquired and saved from the Cell Profiler Software.

Step 4: Identify Tertiary Objects: SN4741 Cytoplasm

Similarly, to that described in 'Step 4' of MMP Protocol, the **Identify Tertiary Objects** module subtracts the shape of the smaller object (nucleus) from that of the larger identified object (i.e. cell body). Once removed the segmented area identified is the cell cytoplasm.

To identify Mitohealth stained SN4741 cytoplasm using Cell Profiler modules:

Select > ***Identify Tertiary Objects*** *module*

Select > 'Cell Body' as input for larger identified objects

Select > 'Nuclei' as input for smaller identified objects

Input > 'Cytoplasm' as name for tertiary objects to be identified

Select > 'Yes' to shrink smaller object. Ensuring a cytoplasm is created for each nucleus

Select > 'No' to Retain outlines of tertiary objects as these will not be utilised downstream

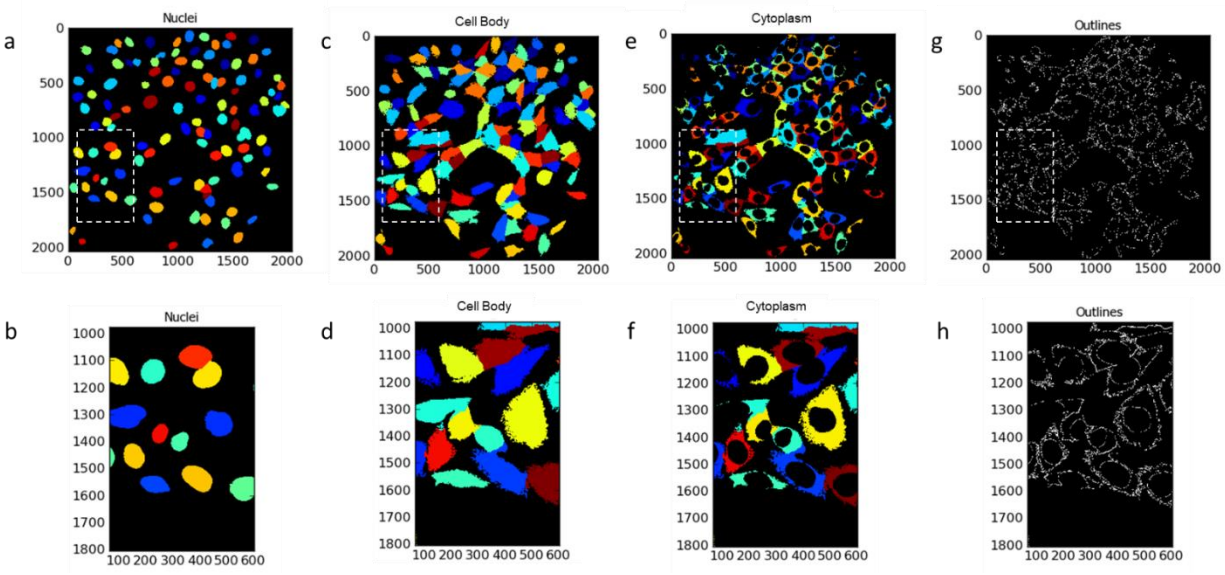

Figure 61: Identify SN4741 Cytoplasm as Tertiary Object

Images (a), (c) and (f) illustrate the masked image result of sequential steps/modules from identification of primary object a (Nuclei), identification of secondary object c (cell body) and tertiary object f (cell cytoplasm), respectively. SN4741 cytoplasm is the result of removing the Nuclei areas from the areas of entire cell bodies. Micro-pictograph (g) highlights the outlines of the resulting SN4741 cell cytoplasm. Dashed white boxed in images (a), (c), (e) and (g) indicated the areas which have been zoomed-in for illustrative purposes and are represented by images (b), (d), (f) and (h) respectively. Images (a-h) are micro-pictograms acquired and saved from the Cell Profiler Software.

Step 5: Enhance Mitochondrial Speckles

The **Enhance Or Suppress Feature** module is a Cell Profiler module that suppresses or enhances selected image features such as speckles, ring shapes and neurites) to improve the subsequent object identification by an Identify module. In this case it is used to make the punctate mitochondrial staining pop out by applying image processing filters to the input image and giving a grayscale image output. Following the execution of this module the Identify Primary Object module is used again to identify mitochondrial puncta.

Select > 'CorrCy3' as input image (image is illumination function corrected)

Input > 'FilteredRed' (or other user-defined name) for output grayscale image

Select > 'Enhance' as operation type

Select > 'Speckles' as feature type to be 'Enhanced'

Input > '20' as feature size.

Note: The enhance operation is used to create an output image which predominantly contains user defined features. In this pipeline, the module produces a grayscale image largely composed of mitochondrial puncta. Feature size was determined by measurement of mitochondrial puncta using the *Tools > Measure length* Cell Profiler function. Cell Profiler suggests that when enhancing (or subtracting) the largest feature size in the image(s) should be selected. In these MitoHealth stained x40 magnification images the largest mitochondrial puncta measured were approximately 20 pixels in diameter. Speckle feature type was selected to enhance mitochondrial puncta in image. Cell profiler defines a speckle as an area of enhanced pixel intensity relative to its immediate neighbourhood using a tophat filter. This filter used grayscale image erosion within a set radius (Approx. object diameter = 20 pixels; therefore radius = 10 pixels), and then dilation. The speckles are enhanced by this module making them easier to identify with the **Identify Primary Object** module. See figure 56 (e-g) & figure 57 for example of identified puncta.

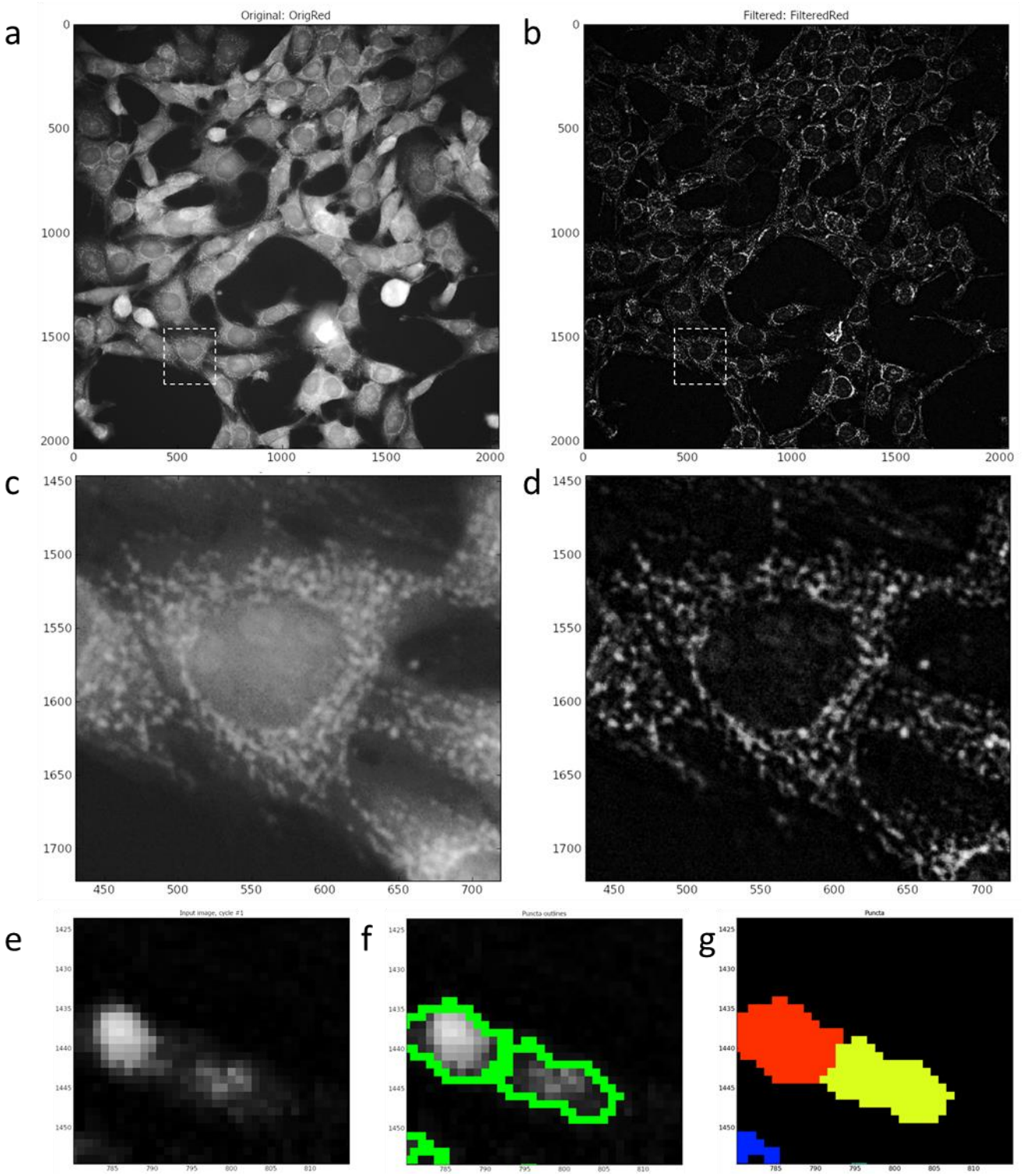

Figure 62: Enhance Mitochondrial Fragments and Identification.

Figure 62 (a) shows an input 'CorrCy3' image prior to speckle enhancement; (b) shows image (a) post-enhance module. Dashed white line box in (a) and (b) highlight the area displayed in (c) and (d) which are pre- and post- enhancement module,

respectively. (e), (f) and (g) show zoomed input image; outlined mitochondrial puncta; and marks of identified objects.

Step 6: Identify Primary Objects: Mitochondrial Fragments

This step utilises the **Identify Primary Objects** module to identify the mitochondrial puncta in the images enhanced in step 5. To identify mitochondrial puncta in enhanced x40 objective Cy3 channel images of MitoHealth stained SN4741 cells we:

Select > ***Identify Primary Objects module***

Select > FilteredImage (output image from previous module) as input image

Input > 'Puncta' (or other user-defined name) to assign to identified objects

Select object diameter range > Min= 2; Max= 35

Select > 'Yes' to discard objects outside the diameter range

Select > 'Yes' to discard objects touching the bored of the image

Select > 'Per Object' as Thresholding strategy and 'Otsu' as thresholding method

Select > 'Cytoplasm' (previously identified tertiary objects) as masking objects

Select > 'Three classes' thresholding and minimize the 'weight variance'

Assign> Middle intensity pixels to 'Foreground'

Note: Using 'Per object' thresholding strategy relies on the identification of a cellular compartment in a previous Cell Profiler module. In this example, SN4741 cell 'Cytoplasm' is identified by **Identify Tertiary Object** module. Using this strategy means each individual cell cytoplasm has its own applied threshold. Pixels outside of the object are considered background. Cell Profiler suggests this as a useful method for identifying particles is cellular sub-compartments if staining varies between objects/cell-to-cell. Otsu method of thresholding (named after Nobuyuki Otsu) calculates image threshold by minimising the variance within the pixel that are considered to be classed and assigned to foreground or background (Otsu, 1979; Sezgin & Sankur, 2004). Cell Profilers' application of Otsu thresholding method can be applied to assign pixels to either two-classes (foreground and background), or three-classes (foreground, mid-ground and background). Two-class is selected as foreground (regions of interest i.e. puncta) background are easily distinguishable following enhancement module.

Select > 'Automatic' smoothing method for thresholding

Input > '1.0' as Threshold correction factor with '0.001' lower and '0.005' as upper bounds on threshold

Select > 'No' to automatically calculate size of smoothing filter for object de-clumping

Input > '5' as size of smoothing filter

Select > 'No' to automatically calculate allowed distance between local intensity maxima

Input > '5' to suppress local maxima that are closer than this minimum allowed distance

Select > 'No' to retain outlines of identified puncta

Select > 'Never' to fill holes in identified objects

Select > 'Continue' to handling of excessive number of identified objects- as puncta are small and therefore the number of puncta identified per image is usually high.

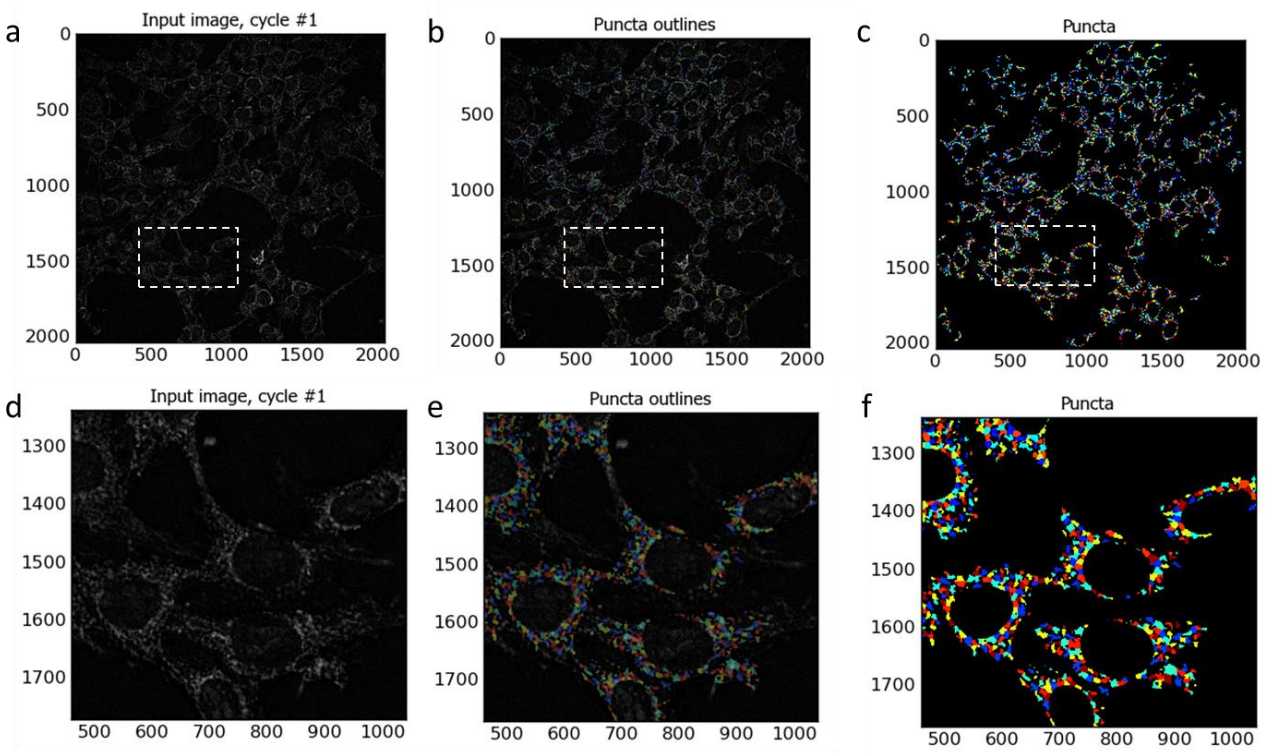

Figure 63: Identification of Mitochondrial Puncta

Images illustrating mitochondrial puncta identified with automated image analysis Cell Profiler pipeline. Image (a) is an example input image to the Identify Primary Objects module; (b) illustrated the outlines of identified mitochondrial puncta, and (c) shows object masks of identified mitochondrial puncta. Dashed boxes on (a), (b) and (c) indicate where Cell Profiler zoom function has been utilised to generate images (d), (e) and (f) respectively for illustrative purposes.

Measurement Modules

Step 7: Measure Object Size and Shape

Although the **Measure Object Size and Shape** module can measure a vast array shape and area features, I will use this module to measure object size (area in pixels) of each cells mitochondrial puncta, cytoplasm and True Doughnut respective to Cell Profiler pipeline.

To measure size and shape of object using **Measure Object Size and Shape:**

Select > ***Measure Object Size and Shape*** *module*

Select > 'Cytoplasm' or 'Puncta' or 'True Doughnut' or any combination of identified objects

Note: Specific shape or size measurements (e.g. area) to output into spreadsheet is defined in a later module. This module simply selects which objects the measurements should be taken from.

Step 8: Measure Object Intensity: True Doughnut or Cytoplasm

To measure the intensity of identified objects we use the **Measure Object Intensity** Cell Profiler module. To do so;

Select > 'CorrCy3' illumination corrected image as image to measure.

Select > 'True Doughnut' or 'Cytoplasm' (or other object) identified in previous modules to measure

Note: CorrCy3 image, as opposed to a Raw Image, is selected to acquire intensity measurements as this image has previously undergoes illumination correction during the pre-processing stage. Specific object intensity measurements (e.g. mean, median, minimum, maximum intensity) to output into spreadsheet is defined in a later module. This module simply selects which objects the measurements should be taken from.

Step 9: Relate Objects: assign mitochondrial fragments to cell cytoplasm.

The **Relate Objects** Cell Profiler module is used here to assign a relationship between 'children' objects (e.g. puncta) with 'parent' objects (e.g. cytoplasm). This module can be utilised in order to count the number of puncta per SN4741 cytoplasm and calculate a mean measurement value for all 'children' objects which are associated with each 'parent' object. Objects (e.g. mitochondrial puncta) are considered 'children' of a 'parent' object (e.g. a cell cytoplasm) if the child object is found within or at the edge of a 'parent' object. To assign the relationship between mitochondrial puncta and a cell cytoplasm:

Select > 'Puncta' as input child objects (identified in second Identify Primary Objects module)

Select > 'Cytoplasm' as input parent objects (Identified in Identify Tertiary Objects module)

Step 10: Mask Objects to relate puncta to cytoplasm of origin

The **Mask Objects** module hides regions of the input image which are not regions of interest. This then aids in the assignment of puncta to a cell cytoplasm of interest and allows for cell-by-cell puncta counts. In this example only SN4741 cell cytoplasm is selected as a region of interest and subsequently aids in exporting the Parent-Child (Cytoplasm- Puncta) data in the **Export to Spreadsheet** module which follows. To create a mask from previously identified objects (i.e cytoplasm):

*Select > 'Filtered Red' (the output of **Enhance or Suppress Feature** module) as input image*

Input > 'Mask Red' as (user defined) name for output image

Select > 'objects' and 'Cytoplasm' to select object (cytoplasm) for mask.

Select > 'No' to invert mask to ensure mask is produced from the foreground area within the masking objects (cytoplasm).

Step 11: Export to Spreadsheet: Output data into MS Excel Spreadsheet

The final module in these Cell Profiler protocols is the Export to Spreadsheet. Here we assign a folder/file destination and name for the output data.

Select > 'Elsewhere' and then 'browse' for desired output file location.

Select > 'Yes' to add prefix to file output file name

Input > 'Name' (user-defined) prefix for output filename (e.g. MitoMMP or MitoPuncta)

Select > 'No' to overwrite without warning (Does not affect protocol- decided by end user)

Select > 'No' to add metadata columns to object data file (Does not affect protocol)

Select > 'Yes' to limit output to a size that allowed in Excel. If 'no' is selected, then upon exceeding limit on Excel spread sheet the pipeline will be terminated without data outputted.

Select > 'NaN' to represent data points which are numerical values are 'infinite' or 'undefined' in output spreadsheet

Select > 'Yes' to select the measurements to export. The user can define which data are outputted to spread sheet. By selecting 'No' all data types will be outputted.

Select the following data outputs from drop down box 'select measurement to export'.

To export number of nuclei (cell count) and puncta per image:

Image > Count > Nuclei;

Image > Count > puncta;

To export area of the objects True Doughnut and Cytoplasm:

True Doughnut > Area Shape > Area;

Cytoplasm > Area Shape > Area;

To export intensity of mitohealth staining intensity in S4741 peri-nuclear area:

True Doughnut > Intensity > Mean Intenisty

To export cell-by-cell puncta counts:

Cytoplasm > Children > Puncta > Count

Select > 'Yes' to calculate the per-image mean values for object measurement. Cell Profiler will calculate mean intensity, mean area, mean number of puncta per cell etc. for each image will then be exported into spreadsheet. Median and standard deviation measurements per image can also be calculated if desired.

File > Save Project As > input user defined project name. to save the Cell Profiler image analysis pipeline for future use.

Cell profiler protocol can now be opened and used on image set. To allow modules to run in sequence in an automated fashion select:

File > Analyze Images. A spreadsheet will be populated and saved as an output upon termination of all executable algorithms/modules in the Cell Profiler pipeline. This pipeline can be applied to experimental repeats.

Below is a table (Table 19) containing the names and functions of the Cell Profiler algorithm modules used in the above protocol(s).

Table 19: Cell Profiler Modules and Functions

Cell Profiler Module	Function
Correct Illumination - Calculate	Calculates an illumination function that is used to correct uneven illumination/lighting/shading or to reduce uneven background in images.
Correct Illumination - Apply	Applies an illumination function, usually created by Correct Illumination Calculate, to an image to correct for uneven illumination (uneven shading).
Identify Primary Objects	Identifies biological components of interest in grayscale images containing bright objects on a dark background (e.g. nuclei or speckles).
Identify Secondary Objects	Identifies objects (e.g., cell body) using objects identified by another module (e.g., nuclei) as a starting point, or seed.
Identify Tertiary Objects	Identifies tertiary objects (e.g., cytoplasm) by removing smaller primary objects (e.g. nuclei) from larger secondary objects (e.g., cell body), leaving a ring shape.
Enhance Or Suppress Features	Enhances or suppresses certain image features (e.g. speckles, ring shapes, and neurites), which can improve subsequent identification of objects (such as mitochondrial fragments).
Measure Object Size Shape	Measures several area and shape features of identified objects.
Measure Object Intensity	Measures several intensity features for identified objects.
Relate Objects	Assigns relationships; all objects (e.g. speckles) within a parent object (e.g. nucleus) become its children.
Export To Spreadsheet	Exports measurements into one or more files that can be opened in Excel or other spreadsheet programs.

Once these Cell Profiler pipelines (Cell Profiler Pipeline: Measuring Mitochondrial Membrane Potential and Cell Profiler Pipeline: Measure SN4741 Mitochondrial Fragmentation) have been constructed it is then possible to automate image analysis for hundreds or thousands of images.

5.2.4. Cell Preparation for Electron Microscopy

SN4741 cells were treated as described in (Chapter 4) and fixed using a mix of para- and glutaraldehyde at experimental endpoint prior to analysis via electron microscopy. The only exceptions were that the SN4741 cells were seeded at 30,000 cells per well in 1 mL of culture medium in specialised six well plates containing filters (received from Prof Christian). Identical treatment concentrations to those in (Chapter 4- see figure 28 B for experimental timeline) were applied to the SN4741 cells with the exception that the reagents were administered in 1mL additions rather than the 100 µL previously described.

At the experimental endpoint, well filters were rinsed once with PBS then promptly immersed in fixative solution to avoid drying of cells and minimise exposure to air, and left to fix at room temperature for 2 hrs. For transit to Professor Helen Christian, University of Oxford, fix was gently removed and replaced with 10-fold weaker dilution of final fixative solution diluted in PBS. Wells were filled and the lid was sealed onto the culture vessel using parafilm before being placed into polystyrene box containing ice blocks (4°C). Samples were transported to our collaborator, Professor Helen Christian from the Department of Physiology, Anatomy and Genetics at the University of Oxford to perform morphological analysis using TEM.

For preparation of fixative: Fresh 12% paraformaldehyde and 25% glutaraldehyde solution (Grade I, 25% in H_2O, specially purified for use as an electron microscopy fixative) was purchased from SIGMA-ALDRICH (Cat no. G5882). 12% PFA and 25% glutaraldehyde were diluted in PBS to produce the final fixing solution comprising of 2.5% glutaraldehyde and 2% PFA. Final fixing solution was adjusted to pH 7.2 using 1M sodium hydroxide (NaOH), a basic compound used to increase pH level, and 1M Hydrogen Chloride (HCl) acid, used to acidify the solution as necessary. This mixture of fixatives was advised by Professor Christian to achieve the best ultrastructure preservation for TEM analysis of mitochondria morphology.

5.3. Results

5.3.1. 24hr Acyl-Ghrelin Pre-treatment Attenuates the Loss of MMP Induced by Rotenone

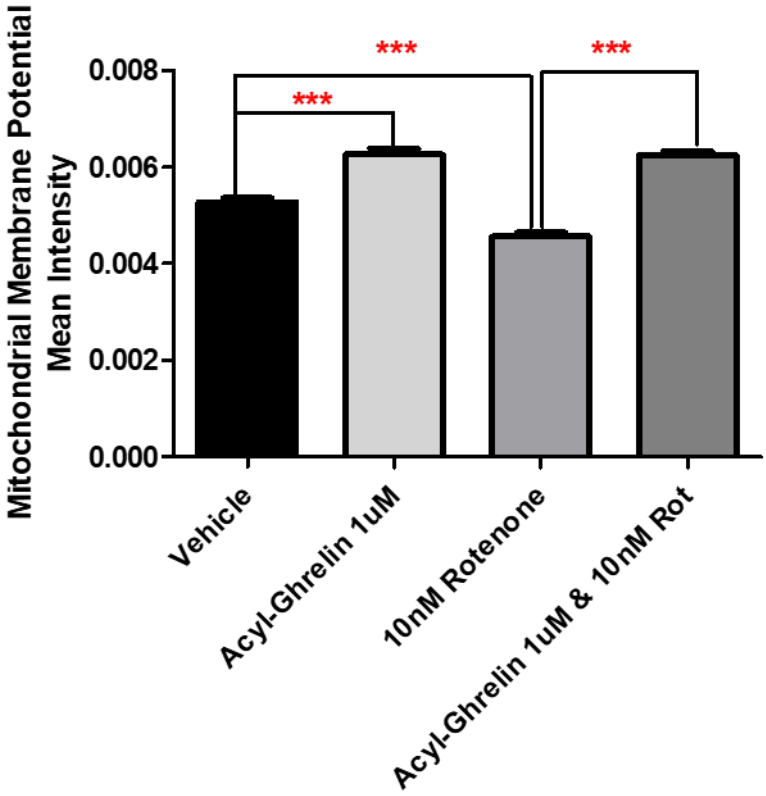

Figure 64 :Acyl-Ghrelin Pre-Treatment Attenuates the Rotenone Induced Loss of MMP Intensity.

SN4741 cells were stained using Mitochondrial Health HCS stain following treatment regimen described in Chapter 4 (figure 28B). 52 x40 magnification images were acquired per well using the In Cell Analyser 2000 (GE Healthcare). Perinuclear mitochondria staining intensity was measured by an automated image analysis pipeline developed in Cell Profiler. 24hr AG treatment significantly increases mean fluorescent intensity and attenuates the complex 1 induced loss of MMP in SN4741 cells. Statistical analysis was performed by One-way ANOVA with Bonferroni's Multiple Comparison Test post-hoc analysis on Graph Pad Prism 5 software, with $P<0.001$ (***).

5.3.2. 24hr Acyl-Ghrelin Pre-treatment Attenuates Rotenone-induced Mitochondrial Fragmentation.

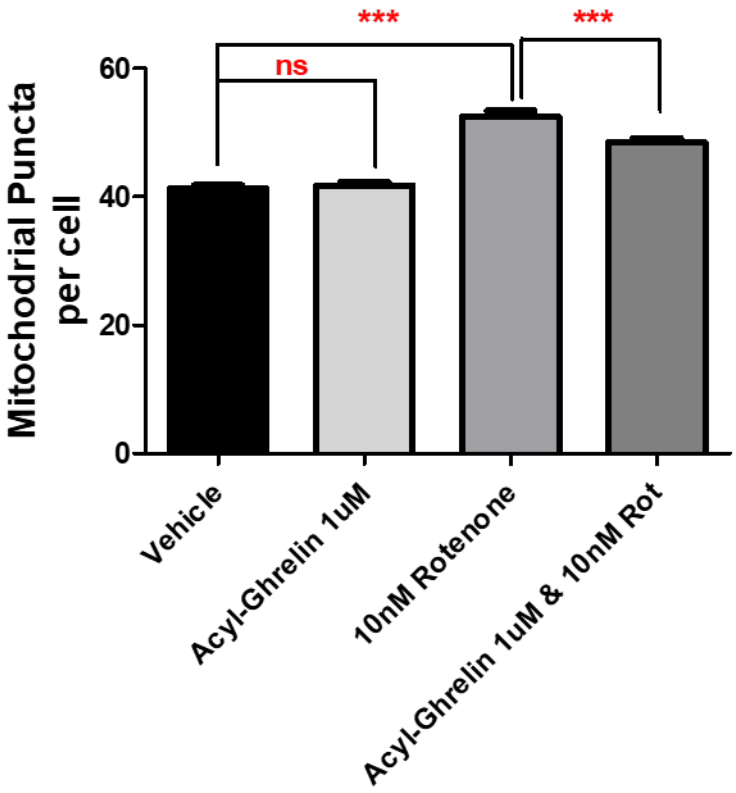

Figure 65: Acyl-Ghrelin Pre-Treatment Attenuates the Rotenone Induced Mitochondrial Fragmentation.

SN4741 cells were stained using Mitochondrial Health HCS stain following treatment regimen seen in Chapter 4 (figure 28B). 52 x40 magnification images were acquired per well using the In Cell Analyser 2000 (GE Healthcare). Cytoplasmic mitochondrial fragmentation was measured by an automated image analysis pipeline developed in Cell Profiler. AG treatment significantly decreases mean mitochondrial fragmentation induced by complex 1 inhibitor rotenone in SN4741 cell. Statistical analysis was performed by One-way ANOVA with Bonferroni's Multiple Comparison Test post-hoc analysis on Graph Pad Prism 5 software, with $P<0.001$ (***).

5.2.3. Electron microscopy analysis of mitochondria

Treatment and fixation of SN4741 cells with vehicle, 24hr AG, 10nM rotenone and 10nM rotenone with 24hr AG pre-treatment was performed at Swansea University. SN4741 cells were also treated with 100nM rotenone as a positive control for mitochondrial fragmentation. Following preparation, duplicate samples were transported to Professor Helen Christian's Laboratory in St. Mary's College, Oxford University for analysis using TEM. Professor Christian, who has extensive knowledge and expertise in TEM and mitochondrial analysis kindly carried out the TEM analysis on our behalf and provided descriptions of mitochondrial morphology and health.

TEM images acquired of vehicle treated SN4741 cell show mitochondria that appear healthy, quite electron-dense with compact cristae (figure 66a). TEM images of SN4741 cell mitochondria treated with AG (1µM) also appear healthy, quite electron-dense with compact cristae. Whereas, rotenone (10nM) treatment causes mitochondrial swelling and loss of mitochondrial cristae indicated by asterisk symbol (*) in (figure 66b). TEM images of SN4741 cells following 24hr 1µM AG pre-treatment prior to 10nM rotenone treatment appear electron dense and contain compact cristae. AG appears to protect mitochondria from rotenone induced damage (figure 66d). TEM images of SN4741 cells treated with a higher dose of rotenone (100nM) appear stressed, swollen and show a loss of cristae. Stressed mitochondria which are swollen and show a loss of cristae are indicated with asterisk symbols (*) in figure 66c)

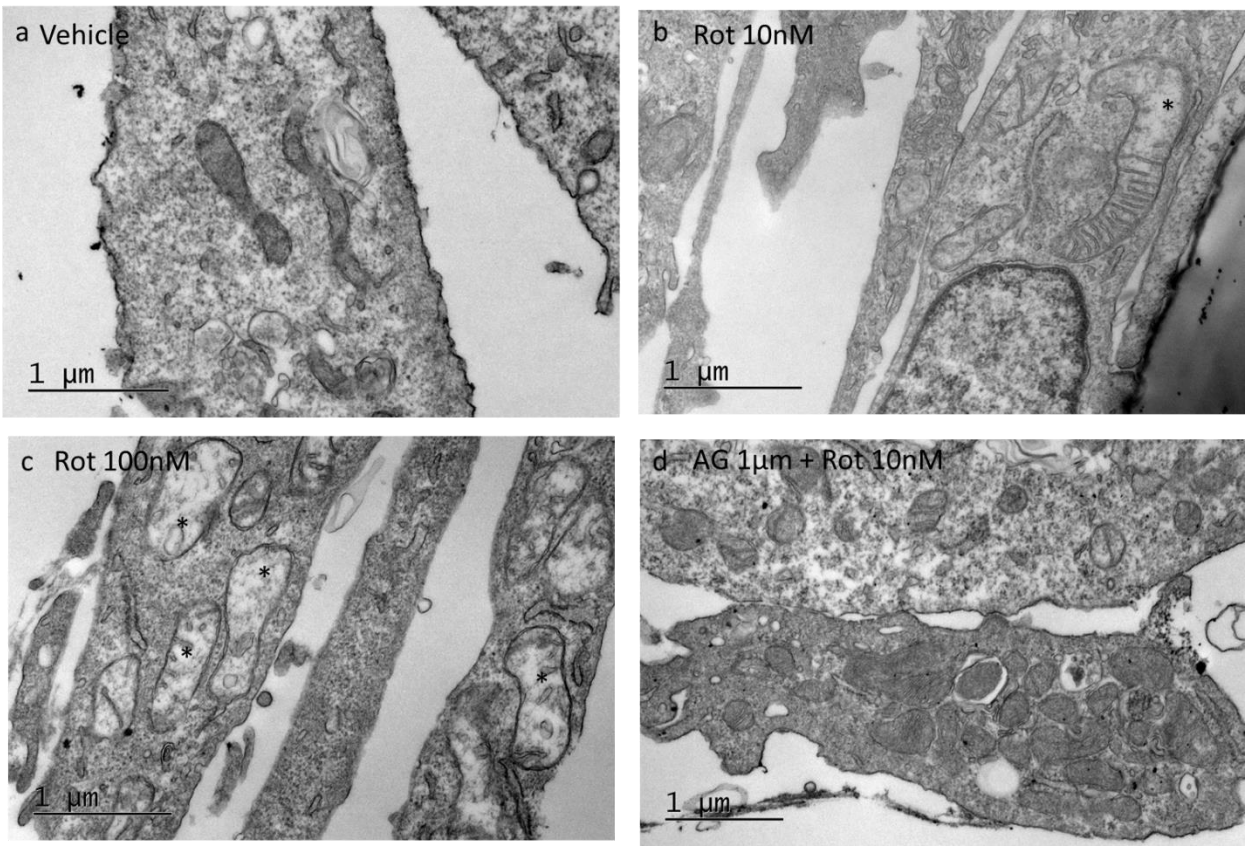

Figure 66: TEM Images of SN4741 Cells suggests AG Pre-Treatment Protects Mitochondria from Rotenone Induced Damage

(a-d) are representative TEM images of SN4741 cells acquired by Professor Helen Christian, Oxford University following vehicle treatment (a); 10nM rotenone treatment (b); 100nM rotenone treatment (c) and 1µM AG pre-treatment followed by 10nM rotenone treatment (d). Images are arranged side by side to compare altered mitochondria ultrastructure between groups; AG appears to protect mitochondria from rotenone induced damage. SN4741 cell mitochondria appear healthy, electron dense and compact with cristae following vehicle (a) and 1µM AG pre-treatment followed by 10nM rotenone treatment (d). SN4741 cell mitochondria appear stressed, swollen and show a loss of cristae in rotenone treated samples (b and c). Swollen mitochondria expressing a loss of cristae are indicated with asterisk symbols (*) in images (b) and (c). Image (c) shows evidence of rotenone induced mitophagy. Example SN4741 nuclei are labelled ‘Nucleus’ in image (a).

Table 20 Results of EM Image Analysis on 10 SN4741 Cells per Treatment group. Mean Number of Mitochondria Scored per Unit Area and Standard error of the mean (SEM)

Treatment Group	Mitochondrial Number / Area (μm^2)			
	Longitudinal Sections/Area	**Transverse Section/Area**	**Total Mitochondria/Area**	**Mitophagy events/Area**
Vehicle	0.13 +/-0.02	0.27 +/- 0.05	0.4 +/- 0.07	0
1μM AG	0.15 +/-0.02	0.31 +/- 0.05	0.45 +/- 0.07	0
10nM Rotenone	0.1 +/-0.03	0.2 +/- 0.06	0.3 +/-0.07	0.13 +/- 0.06 * increase vs vehicle
1μM AG + 10nM Rotenone	0.05 +/-0.01 ** decrease vs vehicle	0.45 +/- 0.06* increase vs rotenone only	0.51+/- 0.075 NS vs vehicle	0.026 +/- 0.004 ** increase vs 10nM rotenone group
100nM Rotenone	0.068 +/-0 .02 * decrease vs vehicle	0.18 +/- 0.046* decrease vs vehicle	0.25 +/-0.06 * decrease vs vehicle	0.24 +/- 0.08 ** increase vs vehicle

Longitudinal Mitochondrial Sections per Unit Area

No significant difference in longitudinal mitochondria per unit area was observed in 1μM AG and 10nM rotenone treated SN4741 cells versus vehicle treated cells. However, a significant (**) decrease in number of longitudinal mitochondria per unit area was observed in SN4741 cells treated with 1μM AG + 10nM rotenone versus control. Moreover, SN4741 cells treated with 100nM rotenone also showed a significant (*) decrease in longitudinal mitochondria per unit area versus vehicle treated cells.

Transverse Mitochondrial Sections per Unit Area

No significant difference in longitudinal mitochondria per unit area was observed in 1μM AG, 10nM rotenone, and 1μM AG + 10nM rotenone treated SN4741 cells versus vehicle treated cells. However, a significant (*) increase in number of transverse mitochondrial sections per unit area was observed in SN4741 cells treated with 1μM AG + 10nM rotenone versus 10nM rotenone treated cells. Moreover, SN4741 cells

treated with 100nM rotenone also showed a significant (*) decrease in longitudinal mitochondria per unit area versus vehicle treated cells.

Total Mitochondria per Unit Area

No significant difference in total counts of mitochondria per unit area was observed in 1µM AG, 10nM rotenone, and 1µM AG + 10nM rotenone treated SN4741 cells versus vehicle treated cells. However, a significant (*) decrease in the overall number of mitochondria per unit area was observed in SN4741 cells treated with 100nM rotenone versus vehicle treated cells.

Mitophagy/Degenerating Mitochondria per Unit Area

The number of mitochondria undergoing mitophagy was also scored. No significant difference in mitophagy events per unit area was observed in 1µM AG treated SN4741 cells versus vehicle treated cells. A significant (*) increase in mitophagy events was observed in SN4741 cells treated with 10nM rotenone versus control. This number of mitophagy events is increased as the dose of rotenone is increased from 10nM rotenone to 100nM rotenone. With 100nM rotenone treatment, a more significant (**) number of mitophagy events per unit area are observed in SN4741 cells. Interestingly, 1µM AG + 10nM rotenone treated SN4741 cells do not show a significant increase in mitophagy events per unit area versus control. However, there is a significant (**) increase in the number of mitophagy events observed per unit area in 1µM AG + 10nM rotenone treated SN4741 cells versus SN4741 cells solely treated with 10nM rotenone.

Statistical analysis

10 SN4741 cells per group were analysed for mitochondrial counts and morphology. Statistical analysis was carried out in Graph Pad prism version 5 using one-way ANOVA with Bonferroni post-hoc test. Experiment was performed in duplicate.

TEM images show that rotenone treatment causes mitochondrial stress, swelling and loss of mitochondrial cristae. The observed degeneration is not apparent when SN4741 cells are pre-treated with AG (figure 66d).

The total number of mitochondria per area (μm^2) is significantly decreased (*) in 100nM rotenone treated SN4741 cells versus control group. 10nM rotenone or AG pre-treated SN4741 cells do not show a significant increase or decrease in total mitochondria versus vehicle.

Mitophagy events are significantly elevated in both 10nM rotenone and 100nM rotenone treated SN4741 cells versus vehicle. There is no significant difference in mitophagy events in rotenone treated SN4741 cells following AG pre-treatment relative to vehicle treatment. However, there is a significant difference between the number of mitophagy events versus samples treated with only 10nM rotenone suggesting that mitophagy might be playing a role in the upkeep of healthy mitochondria in rotenone challenged SN4741 cells that have undergone AG pre-treatment.

5.4. Conclusions

The experimental procedures carried out in this chapter allows us to conclude the following.

- Cell profiler can be used to automate the identification of nuclei/ the seed of the experiment upon which an automated image analysis pipeline may be constructed for cell-by-cell analysis.
- Experimental pipeline to measure mitochondrial health staining intensity in peri-nuclear area has been developed.
- 24hr AG treatment reverses rotenone-induced decrease in MMP.
- Cell Profiler protocol has been extended by the application of add-on software modules to identify and measure mitochondrial fragmentation.
- Rotenone-induced mitochondrial fragmentation is inhibited in cells pre-treated (24hrs) with AG.
- Electron microscopy and analysis performed by Professor Helen Christian at St. Mary's College, Oxford University showed (n=2) that rotenone induced mitochondrial swelling and ultrastructural cristae deformities is attenuated by 24hr AG pre-treatment. Furthermore, 100nM rotenone treatment exacerbated the detrimental effects of rotenone treatment, inducing an increased incidence of mitochondrial perturbations

5.5. Discussion

In this results chapter, we have described and constructed an automated image analysis pipeline developed in Cell Profiler software which identifies, measures and quantifies cellular characteristics from 2D images. Like the paper by (Sakamuru, et al., 2016); we outline, step-by-step, an automated images-based MMP assay which we utilise to measure and quantify the effects of AG and rotenone on SN4741 cell MMP. Image analysis plays a vital role in the study of PD models, with the need for it at an all-time high. This demand can be attributed to two major contributing factors. The exponential rise in microscope power provides researchers with a key insight into cell behaviour and neurotoxin effects. The ability of TEM to provide images of such significantly higher resolution than light microscopy makes it a key tool in analysis of PD models. TEM is also utilised in various other fields, with the prevailing notion being that it is among the most effective forms of microscopy available today. Another considered factor is the rise in human cell models, an example being iPSC derived neurons from PD patients, a more reliable model for testing neuroprotection against PD in humans. The need to study these models on a graphic platform is of integral importance to further the understanding of PD in humans, its symptoms and potential neuroprotective therapies. Image analysis led to some crucial findings within the current study, detailed in the conclusions above.

As cellular powerhouses, mitochondria are integral in the production of ATP (Agarwal, 2011; Mitchell, 1961) and the generation of a MMP which can be measured as a critical parameter for the evaluation of mitochondrial integrity and function (L. B. Chen, 1988). Moreover, mitochondrial dysfunction, inclusive of collapsed MMP, have been linked with neurodegenerative diseases such as PD (Knott & Bossy-Wetzel, 2008; Pieczenik & Neustadt, 2007) and cell death via apoptosis, necrosis and autophagy (Lemasters et al., 2002).

Rotenone is an inhibitor of Complex I of the ETC. Rotenone inhibits mitochondrial electron transport by acting at complex I (NADH CoQ1 reductase) of the respiratory chain and preventing the transfer of electrons from iron-sulphur centres and subsequent reduction of ubiquinone. Inhibition results in an interference with NADH in the process of generating ATP (Treberg, Quinlan, & Brand, 2011). Moreover, as coenzyme Q is unable to accept electrons from inhibited mitochondrial electron transport chain complex I, an overload of electrons is backed-up in the mitochondrial matrices. An excessive pool of electrons can result in increased reduction of cellular

oxygen and subsequent reduction to ROS. ROS can damage local mitochondrial proteins, mitochondrial DNA and other non-mitochondrial cellular components (Mehta & Li, 2009).

Rotenone is utilized to replicate cellular and physiological features in *in vitro* and *in vivo* models of PD and is known to contribute to cell/neuron death by mitochondrial membrane depolarization (Y. Moon, et al., 2005); increasing ROS production (Nataraj, Manivasagam, Thenmozhi, & Essa, 2017) unbalancing cellular antioxidant mechanisms (H. Ding, Gao, Zhu, Xiong, & Liu, 2008); and facilitating the opening of mitochondrial permeability pore which results in the release of cytochrome-C (Cyt-C) into the cytoplasm - an event associated with activation of pro-apoptotic pathways (Doran & Halestrap, 2000; Ott, Robertson, Gogvadze, Zhivotovsky, & Orrenius, 2002).

Inhibition of complex I (NADH: Ubiquinone oxidoreductase) by rotenone induced oxidative stress is thought to be the key contributor to its toxicity in DAergic neurones by decreasing MMP (Testa, et al., 2005). Rotenone reduces MMP, which enhances mitochondrial permeability. The increase in mitochondrial permeability leads to an increased movement of Cyt-C, from its anchoring at the inner mitochondrial membrane to the cytosol. This event can initiate programmed cell death by apoptosis (X. Liu, Kim, Yang, Jemmerson, & Wang, 1996). Once in the cytosol, Cyt-C complexed with other pro-apoptotic factors such as Apaf-1, dATP, Caspase 3 and Caspase 9 to drive apoptosis (X. Jiang & Wang, 2004). In line with this, our data shows that mild (10nM) rotenone treatment is sufficient to cause SN4741 cell loss. The cell loss observed following 24hr treatment with 10nM rotenone coincides with a significant reduction in SN4741 MMP which may be mediating the effect.

TEM imaging and analysis showed vehicle treated SN4741 cell mitochondria as tightly packed cristae-dense and electron-rich. However, following rotenone treatment, mitochondria appeared large and swollen, often with irregular cristae distribution throughout - some of which were completely lacking in cristae in large areas. AG treatment alone showed no significant difference in mitochondrial morphological ultrastructure compared to vehicle samples. Analysis of AG pre-treated SN4741 cells followed by rotenone challenge show a reverse in perturbed mitochondrial cristae and mitochondrial swelling. Adverse rotenone-induced ultrastructural alterations are also apparent in the substantia nigra neurones of PD model rats following a 42-day treatment regimen with the complex I inhibitor. In this *in vivo* PD rat study, ultrastructural mitochondrial perturbation by rotenone, coincided

with increased apoptosis, and cleaved caspase 3 index; and a decreased complex I activity and ATP production level - effects which were attenuated upon increasing concentrations (0 to 400mg/kg) of baicalein treatments. The same study showed baicalein induced mitobiogenesis in *in vitro* rotenone treated SH-SY5Y cells (X. Zhang et al., 2017). It may be possible that AG pre-treatments exert similar cellular mechanisms of protection as the bioactive flavone, baicalein. These mechanisms include retention of MMP - reducing the decrease in MMP brought about by rotenone – and the inhibition of Cyt-C release. (X. Zhang, et al., 2017). Studies by (Andrews, et al., 2009) suggest that increased mitochondrial biogenesis is a key contributor to AG mediated neuroprotection in an MPTP model, highlighting that the AG mediated protection in both models may be working in similar ways.

The rotenone PD model has also been used extensively to investigate potential novel neuroprotective treatments which are thought to contribute to cell survival via mitochondrial-related mechanisms. Many studies have shown that neuroprotective effects of their chosen test agent have attenuated rotenone-induced perturbances via sustainment of MMP (Seoposengwe, van Tonder, & Steenkamp, 2013), (Filomeni, et al., 2012; Hao, et al., 2017; Mendivil-Perez, Velez-Pardo, & Jimenez-Del-Rio, 2016). Data from our *in vitro* rotenone PD model shows that 24hr pre-treatment with AG prevents rotenone-induced cell loss and reduction in MMP. These matched observations made by (Yu, Xu, Shen, & Jiang, 2016) in their rotenone PD model which used MES23.5 DAergic cells. This study showed ghrelin mediating protective effects by preventing mitochondrial dysfunction and inhibiting the release of Cyt-C to MES23.5 cytosol and subsequently decreasing the induction of apoptosis. In non-neuronal cells, ghrelin treatment decreases markers of oxidative stress and retains their MMP which is considered one of the key contributors to doxorubicin induced cell death in cardiomyocytes (Z. Xu et al., 2008).

Interestingly, ghrelin mediated anti-apoptotic and cyto-protective effects were not observed in fresh human neutrophils. Ghrelin treated neutrophils had no effect on apoptotic events such as regulation of BAX: Bcl-2 ratio or cleavage of caspase 3 and did not appear to modulate factors involved in regulating apoptosis. The opposite was observed upon lipopolysaccharide treatment of neutrophils. Moreover, pre-treatment with physiological levels (100nM) of ghrelin in this study did not exert any effect on human neutrophil MMP nor did it extend human neutrophil lifespan *in vitro* (B. Li et al., 2016). Although rotenone is used widely to generate *in vitro* and *in vivo* PD models, there are few detailing the effects of AG neuroprotection and MMP retention in the context of a rotenone induced-PD models.

SN4741 cell exhibited increased mitochondrial fragmentation following 24hr rotenone (10nM) challenge. This result is in line with literature showing that rotenone does indeed induce mitochondrial fragmentation in other cultured cells. For example, rotenone-induced AMPK-dependant mitochondrial fragmentation is observed in U20S osteosarcoma cells and mouse embryonic fibroblast (MEF) cells following a 30-minute treatment. In this study, an ETC complex III inhibitor also induced a fragmented mitochondrial phenotype which was AMPK-dependant. This paper suggests that the fragmented morphology, induced by the ETC inhibitors, is a result of cellular stress rapidly activating AMPK which in turn phosphorylates a number of downstream substrates including ACC, Raptor and ULK within 15-minutes. This effect was shown to be AMPK-dependant as mitochondrial fragmentation was significantly attenuated when AMPK signalling was abolished (Toyama, et al., 2016). The mitochondrial fragmentation observed was dependent on recruitment and localization of GTPase dynamin-related protein-1 (DRP-1) to the outer mitochondrial membrane. Moreover, the phosphorylation of serine 155 and serine 172 of mitochondrial fission factor (MMF) was essential for recruitment of DRP-1 to mitochondrial surface (Toyama, et al., 2016).

A dose-dependent increase in fragmented mitochondrial phenotype was also observed when COS-7 fibroblast-like cells were treated with increasing doses of rotenone. In this study involving COS-7 cells, increasing concentration of rotenone resulted in an increased formation of mitochondria with spherical morphology (Passmore, Pinho, Gomez-Lazaro, & Schrader, 2017). This decrease in MMP and concomitant increase in mitochondrial fragmentation has also been identified in an *in vitro* 6-OHDA PD model utilising SH-SY5Y neuroblastoma cells (Gomez-Lazaro, Bonekamp, Galindo, Jordan, & Schrader, 2008). In this model, the fragmentation was also DRP1-dependent. Therefore, decreased MMP and concomitant increase in mitochondrial fragmentation, appears to be a common cellular response observed in at least two i*n vitro* PD models which are associated with increased cell toxicity- as is observed in our model.

It is generally considered that the accumulation of mitochondrial dysfunction is associated with mitochondrial fragmentation, neurodegenerative disease and ageing (Ferguson, Mockett, Shen, Orr, & Sohal, 2005). Interestingly, a study in drosophila melanogaster (fruit fly) show that mild induction of Drp1-induced mitochondrial fission during the fly midlife promotes a longer and healthier lifespan. The upregulation of Drp1 and subsequent initiation of mitochondrial fission in young adult flies (day 0- 30) had no effect on longevity. However, when Drp1-induced mitochondrial fragmentation

was initiated in flies during their mid-life period (day 30-37) a significant increase in lifespan and health-span was observed. The study suggests that this effect observed is the result of improved mitochondrial function; attenuation of age-associated losses in mitochondrial proteins and a decrease in the accumulation of ubiquitin inclusions in fly flight muscles and increased facilitation of autophagy/mitophagy (Rana et al., 2017).

Studies appear to indicate that, at least in some cells, AMPK is activated by mitochondrial stressors which trigger mitochondrial fission and fragmentation, at least partly, as a result of MFF phosphorylation and DRP-1 recruitment to the mitochondrial membrane. Moreover, a rapid AMPK-dependent initiation of mitochondrial fission and fragmentation might serve as a protective method to prepare mitochondria and cells for clearance via mitophagy (Youle & van der Bliek, 2012). Together these observations highlight that a deeper understanding of mitochondrial dynamics and mitophagy must be developed to address age related neurodegenerative diseases.

6. Chapter 6: Discussion

This thesis has aimed to develop our understanding of the orexigenic stomach hormone AG as a potential neuroprotective agent against Parkinson's Disease.

The first results chapter (chapter 2) characterized the mouse midbrain, and more specifically identified co-localisation of TH^+ and GFP-$GHSR^+$ neurones in the (mouse) SN using IHC. We conclude that that GHSR is expressed in $Girk2^+$ (SN) neurones *in vivo*. We also characterised key protein markers that are important to the study. Using immunofluorescence (IF) techniques, we show SN4741 midbrain derived neurones express TH^+, $Girk2^+$, $Calbindin^-$ and $GHSR^+$ immunoreactivity. The SNpc contain a mix of neurone types of which A9 and A10 subtypes of dopamine neurones predominate (Bjorklund & Dunnett, 2007). Our IF analysis show that SN4741 cells are of the A9 ($Girk2^+$) subtype which are preferentially degenerated in PD (Codrich et al., 2017; Hirsch, Graybiel, & Agid, 1988). Furthermore, we show that the SN4741 cells, on which we modelled our *in-vitro* rotenone-based neurotoxicity PD model, expressed detectable levels of key ghrelin axis proteins, GHSR1a, APT-1 & MBOAT4, thus confirming their suitability. This was confirmed using PCR and Western blot techniques. Literature eludes to AG mediating neuroprotection by decreasing neuroinflammation and microglial activation, increased mitophagy, as well as enhanced mitochondrial function and biogenesis. Although the exact mechanisms are yet to be elucidated GHSR1a agonists hold potential to be utilised as therapies (Andrews, 2011). Efficacy of AG as a neuroprotective agent was then tested using experimental models of PD.

Data (chapter 3) showed that the administration of AG via minipump attenuated 6OHDA-induced loss of TH^+ neurones in the rat SNpc and amphetamine-induced rotations. Other data (not included) extracted from the same photo-micrographs showed a significant decrease in the size of DAergic (TH^+) SNpc neurone size following lesioning.

In chapter 4, we report the development of an *in-vitro* rotenone-induced neurotoxicity PD model using midbrain-derived SN4741 neurones. We show that 24hr treatment of SN4741 neurones with rotenone (10nM) induced a significant decrease in SN4741 cell number and cell viability and increased cell cytotoxicity in complete (full) and substrate restricted (SR) (60%) cell culture media. The cytotoxic effect of rotenone was not mediated via Caspase 3/7 activity, at least in neurones cultured in full

medium. Building on these observations we show that direct treatment of SN4741 neurones with AG and GHSR1a agonist, JMV2894, exerted a protective effect. This effect was amplified in SN4741 neurones cultured in SR media. Furthermore, we showed that inhibition GHSR1a by D-Lys3 attenuated AG-mediated neuroprotection. This suggest that the direct binding AG to GHSR1a and resulting downstream events are integral for AG-mediated neuroprotection in our model. Subsequently, a thymidine analogue (EdU) pulse chase experiment was utilised to confirm that the resulting cell survival was not the result of an AG-induced increase in cell proliferation.

Interestingly, SN4741 protein lysates following 5-minute treatment with AG increased protein expression of pAMPK and fatty acid metabolism regulator pACC. SN4741 cells treated with GHSR1a agonist JMV2894 for 5 minutes also showed an increase in AMPK phosphorylation but a decreased phosphorylation of ACC.

At the 24hr timepoint post-AG treatment, SN4741 cells expressed a significant increase in AMPK phosphorylation and despite an increase in ACC phosphorylation the fold change was not statistically significant. These data suggest, along with other literature, that AG-mediated neuroprotection may be the result of GHSR1a agonism and subsequent downstream signalling via phosphorylation of AMPK (Bayliss, Lemus, Stark, et al., 2016) resulting in enhanced mitochondrial function (Andrews, et al., 2009). Since mitochondrial dysfunction and its associated mechanisms (e.g. mitophagy) are implicated in a range of age-related disorders such as PD, we studied AG-mediated neuroprotection in the context of mitochondrial health.

In chapter 5 we investigated the effects of AG treatment on mitochondrial function, specifically MMP and dynamics (i.e. fragmentation phenotype). We concluded that the rotenone treatment administered in our *in vitro* model was sufficient to induce a depolarization of MMP and an increase in mitochondrial fragmentation. These cellular events were reversed in cells pre-treated with AG, suggesting that AG's neuroprotection may be the result of maintaining mitochondrial membrane potential. Other studies indicate increased mitochondrial biogenesis and function (particularly the buffering of ROS by UCP-2) as a key mechanism by which AG protects DAergic neurones from neurotoxin insult (Andrews, 2011; Andrews, et al., 2009). To obtain measurements on mitochondrial health, we developed an automated image analysis pipeline using open-source CellProfiler software to measure fluorescence intensity of a mitochondrial health marker in the perinuclear area of treated SN4741 cells. This protocol was expanded to quantify the mitochondrial fragments in the SN4741 cell soma.

To conclude, we show that AG prevents DAergic cell loss *in vivo* and *in vitro.* GHSR1a agonist, JMV2894, also promotes SN4741 cell survival in our *in vitro* rotenone induced model of PD. Therefore, our data support a role for GHSR1a agonists as potential neuroprotective agents against PD.

6.1. Proposed Mechanisms and Pathways of Ghrelin Neuroprotection in PD Models

Studies by (Bayliss, Lemus, Santos, et al., 2016; Bayliss, Lemus, Stark, et al., 2016) highlight a potential mechanism by which AG mediates neuroprotection on DAergic neurones on the SNpc. These studies identify AMPK activation and increased mitochondrial function that is dependent on the action of an integral mitochondrial protein, UCP-2 in buffering the excessive production of ROS and ultimately reducing the pro-apoptotic Bax-Bcl2 ratio. Although we did not investigate the effect of AG-mediated increase in mitochondrial MMP on the buffering of ROS; we did however show AG's direct protective effects on SN4741 cells to be dependent on the GHSR1a receptor.

The exact mechanism by which rotenone-induced SN4741 cytotoxicity and cell loss is yet to be elucidated. Published literature propose that rotenone induces cell death by apoptotic events both *in vitro* and *in vivo* (Ahmadi et al., 2003; Sonia Angeline, Chaterjee, Anand, Ambasta, & Kumar, 2012). Our *in vitro* investigations failed to link SN4741 cell loss and increased cytotoxicity with the increase in activity of pro-apoptosis marker, Caspase-3/7. These data suggest that rotenone-induced SN4741 cell loss and cytotoxicity is either governed by an alternative mechanism or that apoptotic events (involving caspase 3/7 activity) may have occurred prior to our analysis. To investigate this further, we could analyse caspase 3/7 translocation to the nucleus and measure its fluorescence intensity (FI) along our experimental timeline and at earlier timepoints.

Ghrelin is produced by X/A cells in the stomach at times of negative energy balance. It is post-transcriptionally modified to AG by enzymatic activity of GOAT which catalyses the addition of an acyl side chain to the nascent ghrelin peptide at serine 3 (Kojima, et al., 2016; Kojima, et al., 1999). The acylation of ghrelin is integral for its ability to activate GHSR1a by binding to the exposed receptor on cell surfaces (J. Yang, Brown, Liang, Grishin, & Goldstein, 2008). Activation of GHSR1a by AG regulates growth hormone release, initiation of feeding, and regulation of energy homeostasis (Lall, Tung, Ohlsson, Jansson, & Dickson, 2001; Tschop, Smiley, &

Heiman, 2000), which is governed activation of orexigenic neuropeptide Y (NPY) and agouti-related protein (AgRP) neurones (H. Y. Chen et al., 2004) in the arcuate nucleus of the hypothalamus (Dickson, Leng, & Robinson, 1993; Kojima, et al., 1999). Both acylated and un-acylated forms of ghrelin are BBB permeable and upon release from the stomach, travel via the bloodstream to the brain (Banks, Tschop, Robinson, & Heiman, 2002) to exert hypothalamic and extra-hypothalamic effects (Andrews, 2011). Aside from regulation of metabolic homeostasis, ghrelin plays a role in many non-metabolic functions such as enhancing learning and memory via increased hippocampal synaptic plasticity (Diano, et al., 2006), modulating anti-anxiety and anti-depression like behaviour (Lutter et al., 2008). But importantly, its neuroprotective mechanisms have been observed in many neurodegenerative disease models. Examples of this include decreasing microglial activation in amyotrophic lateral sclerosis (S. Lee, Kim, Li, & Park, 2012) and neuroprotection, memory consolidation and learning in models of Alzheimer's disease (Gahete, Cordoba-Chacon, Kineman, Luque, & Castano, 2011). Suggesting that AG-mediated neuroprotection may be utilised across a range of diseases, possibly by the similar mechanism of action as that observed in models of PD (Andrews, 2011).

The neuroprotective effects of AG may be multifaceted. Studies show that AG-mediated neuroprotection on DAergic neurones in neurotoxin-induced models of PD is governed by (i) attenuating the pro-inflammatory effects of microglial activation (M. Moon, et al., 2009), (ii) attenuating the activation of pro-apoptotic events by caspase activation (H. Jiang, Li, Wang, & Xie, 2008; X. Jiang & Wang, 2004) and (iii) increasing mitochondrial function (Andrews, et al., 2009). PD-inducing neurotoxins such as MPTP (Meredith & Rademacher, 2011), 6-OHDA (Y. Glinka, Tipton, & Youdim, 1996; Y. Y. Glinka & Youdim, 1995) and rotenone (Xiong et al., 2012) appear to replicate the degenerative pathology of PD via inhibition of mitochondrial function (at least partly via complex 1 inhibition) which result in increased ROS production and deficits in the production of ATP.

A considerable amount of literature has placed emphasis on metabolic energy sensor AMPK as an integral link in a pathway between neuroprotective agents and cellular events associated with neuroprotection. AMPK is a highly evolutionarily conserved regulator of energy homeostasis which is predominantly regulated allosterically by the binding of cellular energy molecules on its gamma subunit (Jeon, 2016). The allosteric competition is between ATP, which allows access of a phosphatase enzyme to Threonine 172, and AMP or ADP which blocks phosphatase access (Hawley et al., 1996). Therefore, AMPK phosphorylation is dependent on the ratio of cellular energy

molecules AMP/ATP and ADP/ATP (Jeon, 2016). Upon activation at times of negative energy balance, AMPK phosphorylates acetyl-Coenzyme-A carboxylase (ACC) or sterol regulatory element-binding protein (SREBP). Phosphorylation of these downstream targets results in inhibition of fatty acid, cholesterol and triglyceride synthesis and activates the cellular uptake and utilisation of fatty acids as an energy source by β-oxidation (Jeon, 2016). AMPK also appears to have tissue specific roles, such as $GLUT4^{+}$ mediated glucose uptake in skeletal muscle via phosphorylation of Rab-GTPase activating protein; stimulation of glycolysis and inhibition of glycogen synthesis via activation of 6-phosphofructo-2-kinase/fructose-2,6-bisphosphatase 2/3 and glycogen phosphorylase and inhibition of glycogen synthase (Jeon, 2016). In liver hepatocytes, AMPK mediated inhibition of hepatocyte nuclear factor 4 (HNF4) and CREB regulated transcription coactivator 2 (CRTC2) reduced gluconeogenesis (Jeon, 2016). AMPK activation is also known to upregulate autophagy via downstream signalling through ULK1 and upregulate mitochondrial biogenesis (J. Kim, Kundu, Viollet, & Guan, 2011) via PGC-1α which contribute to buffering of excessive ROS (Deas, Wood, & Plun-Favreau, 2011; Shin et al., 2011).

AMPK consists of three subunits with various isoforms; these are α1, α2, β1, β2, γ1, γ2 and γ3 (Carling et al., 1994). The alpha subunit plays a catalytic role whilst beta and gamma subunits are engaged in regulatory roles (Crute, Seefeld, Gamble, Kemp, & Witters, 1998). The integrity of AMPK is paramount in maintenance of cellular energy homeostasis and AMPK dysfunction or loss of activity has implications in diseases such as diabetes (Jorgensen et al., 2004; O'Neill et al., 2011; Wahlqvist et al., 2012) as well as PD (J. Kim, et al., 2011). In line with metabolic alterations of type 2 diabetes, whole body deletion of the AMPK α2 subunit in mice showed increased insulin resistance and impaired glucose tolerance (Jorgensen, et al., 2004). Furthermore, a study by (O'Neill, et al., 2011) showed the deletion of beta subunits (β1 and β2) specifically in the muscles of mice showed an increased insulin resistance and a dysfunctional mitochondrial phenotype. Interestingly, the anti-diabetes type 2 drug metformin is thought to decrease the risk of developing PD as diabetes patients provided with metformin show a reduced risk of developing PD (Wahlqvist, et al., 2012). Taken together, we postulate that activators of AMPK could be used to tackle a range of diseases with associated mitochondrial dysfunctions. Thus, highlighting a potential for re-purposing of AMPK-specific type-2 diabetes to act as neuroprotective PD therapeutics, and vice versa. Another important downstream event occurring as a consequence of AMPK activation is autophagy of damaged cellular organelles (or mitophagy for damaged mitochondria). A negative energy balance, which can occur

as a result of perturbed mitochondrial function, results in AMPK phosphorylation and downstream inhibition of mTOR and phosphorylation of ULK1 which are integral in the induction of autophagy (J. Kim, et al., 2011).

The mechanism for ghrelin neuroprotection in DAergic neurones in PD models can be linked to the attenuation of pro-inflammatory effects of microglia (M. Moon, et al., 2009) and effects of downstream GHSR1a signalling. (Andrews, et al., 2009) shows AG-mediated enhancement in mitochondrial function and reduction of neurotoxin (MPTP) induced ROS production via UCP-2. Phosphorylation of the metabolic sensor AMPK, downstream of GHSR1a activation via AG, was found to be integral in the neuroprotective effects of exogenous AG administration as depletion of β1 and β2 subunits of AMPK abolished DAergic neurone protection in mice (Bayliss, Lemus, Stark, et al., 2016). This strongly suggests that intracellular energy sensor AMPK is key to eliciting neuroprotection in PD models. AMPK was also shown to play a key role in mitigating mitochondrial and DAergic neurone dysfunction in a drosophila model of PD (Ng et al., 2012) where a parkinsonian phenotype was observed in parkin and LRRK2 null flies. This phenotype was abolished upon activation of AMPK supporting the idea that AMPK plays a role in neuroprotection in PD (Ng, et al., 2012). Other *in vivo* studies have shown activation of AMPK via pharmaceuticals, such as resveratrol (Jin, Wu, Lu, Gong, & Shi, 2008) and guanidinopropionic acid (GPA), mediated AMPK-dependant increases in mitochondrial function and biogenesis (Horvath et al., 2011). The anti-diabetes drug metformin is also a known activator of AMPK (Meng et al., 2015). The activation of AMPK in an *in vitro* alpha synuclein model of PD attenuated SH-SY5Y cell loss (Dulovic et al., 2014). However, not all studies show AMPK activation to be associated with beneficial effects. A study by (P. Jiang et al., 2013) reported that overactivation AMPK resulted in facilitation of alpha synuclein accumulation and inhibition of neurite outgrowth. AMPK activation has also been associated with enhanced mitophagy/autophagy (Wu et al., 2011) and enhanced mitochondrial biogenesis (Reznick & Shulman, 2006). AMPK activation inhibits downstream mTOR and phosphorylated Ulk1 to enhanced autophagy (J. Kim, et al., 2011). Mitochondrial biogenesis increases the mass and number of individual mitochondria to deal with cellular demands such as the requirement for increased ATP (energy) expenditure, buffering of excessive ROS production and to compensate for dysfunctional mitochondria (Sanchis-Gomar, Garcia-Gimenez, Gomez-Cabrera, & Pallardo, 2014; Valero, 2014).

As neurodegenerative diseases are strongly associated with mitochondrial dysfunction and oxidative stress, DNA damage, proteins and membrane lipids (Lin &

Beal, 2006) the buffering of oxidative species and regulation of healthy mitochondrial turnover via autophagy (mitophagy) is integral to maintain viable cellular homeostasis by removal of damaged cellular components. Damaged mitochondria are targeted by PINK1 which recruits cytosolic Parkin to surround the damaged organelle. The accumulation of PINK1 leads to an increase in Parkin's E3 ubiquitin ligase activity, and recruitment of Parkin to the outer membrane of the dysfunctional mitochondrion. Parkin ubiquitinates outer mitochondrial membrane proteins to trigger selective autophagy (mitophagy) (Pickrell & Youle, 2015; Vives-Bauza et al., 2010). The defective clearance of damaged mitochondria (and other cellular organelles) are associated with hereditary PD (Kitada, et al., 2009). These genetic defects lead to perturbed PINK1 and Parkin function which ultimately affects the clearance of damaged mitochondria by mitophagy leading to an accumulation of dysfunctional mitochondria, a restriction in ATP production and increased ROS production which predisposes cells to degeneration (Deas, et al., 2011; Wood-Kaczmar, et al., 2008). In DAergic cells Parkin is also involved in reducing the quantity of PARIS which is an inhibitor of PGC-1α and its target gene NRF-1 (Scarpulla, 2011). A study by (Shin, et al., 2011) shows that Parkin is integral for modulating optimal mitochondrial biogenesis as the overexpression of PARIS in DAergic SNpc neurones results in cell death. Furthermore, the study suggests that the Parkin–PARIS–PGC-1α pathway may be important in regulating mitochondrial biogenesis which is implicated in neuroprotection as it maintains optimal levels of mitophagy (Bayliss & Andrews, 2013; Shin, et al., 2011). Another downstream substrate of AMPK activation is SIRT1. Increasing SIRT1 activity increases the activity of its downstream target PGC-1α the master regulator of mitochondrial biogenesis. The importance of the AMPK-SIRT1-PGC-1α pathway in increasing mitochondrial biogenesis to maintain function and avoid metabolic decline is shown in *in vivo* and *in vitro* SIRT1 KO experiments (Price et al., 2012) where the maintenance of mitochondrial integrity and function, as well as the increased mitochondrial biogenesis exerted by neuroprotective agent, resveratrol, is abolished with SIRT1 KO. Notably, published work has shown resveratrol exert neuroprotection in a rotenone model of PD via AMPK-SIRT1-autophagy pathway (Wu, et al., 2011) to protect against rotenone-induced apoptosis. These data suggest that the upregulation of PGC-1α through AMPK and PARIS and /or SIRT1 (AMPK-PARIS-PGC-1α pathway and / or AMPK-SIRT1-PGC-1α pathway) is integral to the maintenance of mitochondrial function and mitophagy under normal cellular conditions. Furthermore, the increased mitochondrial damage, excessive ROS production and swamping of autophagy and degradative systems caused by mitochondrial neurotoxins used in PD models increase the cells reliance on such

pathways. In this instance neuroprotective agents such as resveratrol and AG may induce intracellular signalling via AMPK and its downstream targets and effector proteins to increase mitochondrial turnover by Parkin and Pink mediated autophagy and degradation; increased mitochondrial biogenesis to cope with increased cellular energy demand to buffer excessive ROS and thus prevent damage to cellular organelle. Together this illustrates that ghrelin-mediated neuroprotection observed in models of PD may be the direct effect of reduced oxidative stress via enhanced mitochondrial biogenesis and UCP2 action and the enhancement of autophagy (mitophagy) to clear damaged organelles (e.g. mitochondria). AMPK appears to be an important intracellular signalling molecule capable of governing ghrelin-mediated neuroprotection through these pathways. Further research will be required to determine whether ghrelin-GHSR1a signalling is linked to the enhancement of mitophagy via the PINK1/Parkin pathway.

6.2. Future Investigations

Although our studies find that AG exerts neuroprotection on DAergic neurones in our *in vivo* 6-OHDA PD model and *in vitro* rotenone PD model further investigation is required to identify the cellular mechanism underpinning the neuroprotection observed.

Here, using pharmacological inhibition of GHSR1a, we show that AG's direct neuroprotective effects are mediated via this receptor. However, due to the failure of rotenone to induce cell loss in our later neurotoxicity assay, we were not able to determine whether AG-mediated neuroprotection was dependent on activation of AMPK. To elucidate whether AMPK is essential for this effect the experiment should be repeated with a new stock of rotenone, as current vials may have lost efficacy due oxidation. Alternatively, siRNA could be utilised to knockdown AMPK expression in SN4741 neurones. A Western blot could be run to confirm target knockdown before performing the assay. It is important to remember that AMPK is a master regulator of many downstream signalling cascades as described earlier in this chapter. Therefore,

caution must be taken when interpreting data as the effects observed may be the result signalling via other cellular pathways. In this case, it might be benefitial to KO or inhibit effector proteins such as PGC-1a further down the signalling pathway to limit off-target effects. The same would be true for the development of PD-therapeutics.

Here in our studies we utilise two different neurotoxin models to investigate AG-mediated neuroprotection. There is potential to use a range of toxin models *in vitro* and *in vivo.* Such studies are warranted to identify whether there is a common AG signalling pathway that would provide a common mechanism to target potential therapies.

Rotenone is a robust PD-inducing neurotoxin for modelling aspects of PD. Besides the degeneration of DAergic neurones, the accumulation of intracellular protein aggregates which are inclusive of miss-folded proteins such as alpha synuclein and poly-ubiquitin is another key hallmark of human PD pathology. In *in vitro* and *in vivo* tests; rotenone causes both DAergic cell degeneration and accumulation alpha-synuclein aggregates (Giráldez-Pérez, Antolín-Vallespín, Muñoz, & Sánchez-Capelo, 2014; Hao, et al., 2017). As such we could investigate whether alpha-synuclein accumulation is modulated in our *in vitro* rotenone-induced neurotoxicity assay as a marker of pathogenesis.

Our data shows that treatment with rotenone induces a fragmented SN4741 mitochondrial phenotype compared to vehicle treated cells and also that AG pre-treatment is sufficient to inhibit the degree of fragmentation. To provide more detail and understanding of the mitochondrial fission/fusion dynamics surrounding the detrimental effects of neurotoxin treatment and neuroprotective effects of AG pre-treatments, we should utilise live fluorescence or confocal microscopy to enable us to follow the events in real-time through treatment periods as opposed to only analysing at experimental endpoints. Moreover, the emergence and utilisation of high- or super-resolution microscopy such as the DeltaVision systems developed by GE Healthcare should be used to gain further insight. The DeltaVision systems are a flexible platform that caters for a wide range of cell imaging including live cell imaging- which is one of the fastest growing areas in cell biology imaging. DeltaVision systems combine modern imaging technologies with the ability to analyse acquired high- or super-resolution images to provide qualitative and quantitative data outputs. A super-resolution would allow us to gain a greater understanding of the underlying mechanisms of AG neuroprotection in our PD model and others. With the correct fluorophores it would be possible to track mitochondrial fission and fusion dynamics

and mitophagy/autophagy in the context of our *in vitro* rotenone neurotoxicity assay, in live SN4741 cells in real-time. Two examples include the role of dynamin-related protein-1 (Drp1) which is shown to localize and cluster at areas of the mitochondrial network and form a multimeric ring around the area undergoing fission (Smirnova, et al., 2001). A technique described by (Smirnova, et al., 2001) where Drp1 is fused to green fluorescent protein (GFP) and transfected into mammalian cells from time-lapse photography is a possible avenue to explore with SN4741 cells. Since Drp1 is critically associated with mitochondrial fission in healthy and pathological cell biology (Hu, Huang, & Li, 2017) it may be a valuable target to investigate the effects of rotenone-induced mitochondrial fragmentation and subsequent reversal of this phenotype in AG-pre-treated SN4741 cells. It is possible that rotenone increases Drp1 recruitment to the mitochondrial membrane whilst AG inhibiting this recruitment or increases the activity of proteins that increase mitochondrial fusion events - such as mitofusin and OPA (Benard & Karbowski, 2009).

Another proposed neuroprotective mechanism is enhanced mitophagy (autophagy) (Bayliss & Andrews, 2013). Microtubule-associated protein 1A/1B-light chain 3 (LC3) is recruited to the autophagosome membrane during the clearance of cellular material destined for degradation during autophagy (Tanida, et al., 2008). This could also be analysed using real-time super resolution microscopy with co-labelling of mitochondria along with this GFP-LC3 (Premo™ Autophagy Sensor LC3B-GFP BacMam 2.0, P36235 Thermo Fischer). The use of different fluorophores would allow us to investigate whether AG pre-treatment in SN4741 cells enhances the rate of autophagic clearance of mitochondria in our assay. A recently performed pilot study supports a role for AG in promoting LC3-GFP autophagosome formation in SN4741 cells (see figure 67 below).

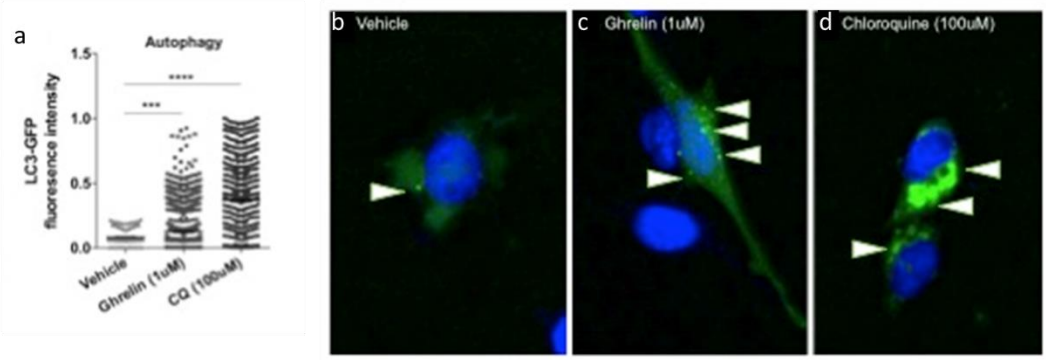

Figure 67: AG Enhances LC3-GFP Formation in SN4741 Cells.

Graph (a) shows 24hr treatment with 1µM AG significantly increases cytoplasmic LC3-GFP fluorescence intensity versus vehicle treated cells (P<0.001). Positive control for autophagosome formation, chloroquine (100µM) induces a greater significant increase in cytoplasmic LC3-GFP fluorescence intensity. Images and represent illustration of LC3-GFP cytoplasmic accumulations (b) vehicle, (c) 1µM AG and (d) 100µM chloroquine treated SN4741 cells. Each treatment was performed in quadruplicate with only 1 experimental repeat and therefore must be repeated. One-way ANOVA with Bonferroni's post-hoc analysis on graph pad prism 5 software, with P<0.05 (*), P<0.01 (**), P<0.001 (***) and P<0.0001 (****) considered significant.

Autophagy mediates the clearance of damaged or dysfunctional organelle (including mitochondria) for lysosomal degradation (Tanida, et al., 2008). This pilot data suggests that up-regulation of autophagy system could aid in turnover of damaged organelle for lysosomal degradation and potentially be a mechanism underpinning AG-mediated SN4741 cell survival. Moreover, a study by (Mizushima, 2009) describe methods for monitoring LC3-GFP transgenic mice, thus, it would be possible to investigate the role of AG-mediated neuroprotection and autophagy in *in-vitro* models and *in vivo* models. Notably, a recent report suggests that AG-mediates an increase in autophagy via AMPK (Ezquerro, Fruhbeck, & Rodriguez, 2017) and others show AG-stimulated autophagy in cortical rat neurones(Ferreira-Marques et al., 2016).

Our PD model shows that direct AG pre-treatment attenuates rotenone-induced SN4741 cell loss and cytotoxicity. However, we are yet to test the utilisation of AG treatments post neurotoxin insult. By doing so we may investigate the AG's (or GHSR1a agonist) efficacy as a neuroprotective agent for PD patients. Therefore, it is

integral that further work seeks to elucidate the action of direct AG treatment on cells once the PD-like insult has already been administered. This is important as PD patients show no overt phenotype until a large proportion of SNpc DAergic neurones have degenerated. Our experimental paradigms administered AG prior to neurotoxin administration. This means that AG mediated neuroprotection may work as a preventative method for PD onset. However, this does not inform us whether any AG neuroprotective effects will be observed if AG is administered after the onset of lesion or incubation with neurotoxin. Therefore, with our current data it is not possible to determine whether AG can reverse or slow detrimental effects induced by neurotoxins. As 6-OHDA is a potent and rapidly-acting DAergic neurotoxin (Simola, et al., 2007), post-lesion treatment may prove challenging. An alternative model is the intra-striatal 6-OHDA lesion which produces a slower progression of dopaminergic cell loss in SNpc as 6-ODHA is carried retrogradely from nigrostriatal projections in the striatum to the SN and depletes nigrostriatal dopamine concentrations. This delayed onset of nigrostriatal DAergic neurone degradation provides progressive depletion of DA in SN and striatum which is more characteristic of the human disease. A drawback of this technique is the 6OHDA lesion-induced motor dysfunctions and behavioural changes appear to be reversible (Alvarez-Fischer et al., 2008).

Since the reason for the onset of sporadic PD is still unknown, genetic models in animals expressing known familial PD mutations may provide the most effective tool for understanding the mechanisms underpinning PD progression and testing of novel therapeutics.

PD models based on genetic/familial PD include LRRK, SNCA, A53T, PINK1 and PARKIN. Leucine-rich Repeat Kinase 2 LRRK2 is encoded for by the PARK8 gene in humans and is associated with an increased risk of developing PD (Paisan-Ruiz et al., 2004). Mutations in the PARK8 gene are associated with autosomal dominant inheritance of familial PD and appears to be the most prevalent familial PD gene mutation (Q. Xu, Shenoy, & Li, 2012). Transgenic mouse models expressing mutant LRRK2 develop dysfunctional motor symptoms which progress with age. LRRK2 mutant models also exhibit deficient DA signalling, DAergic nigrostriatal axonopathies (Sepulveda, Mesias, Li, Yue, & Benson, 2013) and hyperphosphorylation of protein tau (Guerreiro et al., 2016). Collectively, LRRK2 animal models robustly replicate behavioural, neurochemical and pathological features of PD (Q. Xu, et al., 2012).

Alpha-synuclein (α-Synuclein) is a 140-amino acid protein coded for by the SNCA gene in humans (Y. Xia et al., 2001). Alpha-Synuclein is thought to contribute to PD pathogenesis by forming soluble oligomeric conformations that are toxic and result in neuronal death (Stefanis, 2012). It is thought that secreted alpha-synuclein exerts deleterious effects on surrounding cells and by depositing and aggregating in neighbouring cells and contributing to disease propagation. Animal models of alpha-synuclein show the aggregates may be deposited in various brain areas. Evidence shows that DAergic metabolism may be related to alpha-synuclein and its conformational plasticity which suggests there may be a parallels between dopaminergic neurodegeneration and Lewy body (LB) formation- the two major hallmarks of PD (Giráldez-Pérez, et al., 2014). The aggregation of alpha-synuclein in PD is also associated with the two-point mutations, A53T and A30P, which are linked with familial early-onset PD. These mutant alpha-synuclein exhibited an increased propensity to aggregate with other mutant synuclein and wild-type α-synuclein, which is thought account for the correlation of these mutations with Parkinson's disease (J. Li, Uversky, & Fink, 2001).

PTEN-induced putative kinase 1 (PINK1) is a mitochondrial serine/threonine-protein kinase encoded by the PINK1 gene (Narendra et al., 2010). PINK1 protein acts upstream of Parkin. Parkin, also named Parkinson juvenile disease protein 2, is a 426amino acid enzyme protein, encoded by PARK2 gene and located on the 6q chromosome (Miklya, Goltl, Hafenscher, & Pencz, 2014). Studies in drosophila show that KO of PINK1 results in major indirect flight muscle and dopaminergic neuronal degeneration accompanied by locomotive defects related to mitochondrial dysfunctions (Clark et al., 2006). Drosophila lacking PINK1 or Parkin exhibit swollen mitochondria and reduced ATP levels. Moreover, parkin knockout mice showed deficits in nigrostriatal DA neurotransmission and striatal synaptic plasticity (Kitada, et al., 2009). This suggests that any of the resulting physiological symptoms in drosophila and rodent models of PINK1 or Parkin. Which is to be expected as they are integral in protecting cells from stress-induced mitochondrial dysfunction (Gautier, et al., 2008).

Although the underpinning mechanism of familial PD pathology in humans and in their animal model counter parts are not fully elucidated it is not irrational to propose that a therapeutic could be deemed anti-PD if it reversed the dysfunctional effects observed in the animal models of PD. Furthermore, since the entire mechanistic pathway of mutant (or sporadic) PD pathology is not elucidated, a PD therapeutic

could work to upregulate compensatory mechanisms such as mitophagy or mitochondrial biogenesis to compensate for impaired energy (ATP) production.

Induced Pluripotent Stem Cells (iPSC) experimental techniques developed by (Takahashi et al., 2007; Takahashi & Yamanaka, 2006) allow adult dermal fibroblast cells to be reprogrammed to their pluripotent stem cells state by use of the four factors Oct3/4, Sox2, Klf4, and c-Myc, where they may then be pushed down a lineage towards any cell phenotype such as DAergic neurones. Thus, it is possible to generate DAergic neurones from iPSC lines derived from PD patient fibroblasts (Byers, Lee, & Reijo Pera, 2012) to more effectively model PD *in vitro.* A study using two iPSC lines from PD patients with p.G2019S mutation in LRRK2 gene and another carrying a full gene triplication of the SNCA gene was produced by (Byers, et al., 2012). Their studies compared wild-type DAergic iPSC lines with PD patient-derived iPSC lines and showed increased sensitivity to hydrogen peroxide, MG-132 and 6-OHDA-induced capsase-3 activation in the patient derived line. IPSCs which were derived from SNCA mutant patients exhibited increased sensitivity to hydrogen peroxide-induced stress. These cells also showed an increased the rate of early ubiquitin-positive puncta/accumulations. Since these iPSC derived DAergic neurones produce a clinical resemblance of patients afflicted with genetic and sporadic PD, these models may be used to elucidate the molecular pathology underpinning PD and be used to generate of novel therapeutic agents for alleviation of relevant disease phenotypes. Moreover, the multifaceted investigation into the electrical activity, DA release kinetics, energy metabolism and other cellular and molecular fundamentals in PD patient-derived iPSC will increase knowledge of PD pathology and aid in approaches to develop new PD therapies. The use of human cells may also prove particularly useful for delineating disease pathogenesis given the species-specific differences in dopamine metabolism (Burbulla et al., 2017).

6.3. Other perspectives: Drug re-purposing for neuroprotection

There is a current demand for the re-purposing of therapeutically approved drugs for other disease. The efficacy and application of re-purposed drugs relies heavily on the elucidation of the mechanisms underpinning PD pathology which can be investigated using genetic models of PD which recapitulate specific aspects of pathology associated with familial PD. The purposing of pharmaceuticals as opposed to development of new drugs has the benefit of being subsequently approved by FDA and other health and safety administrative bodies for patient use. Once such example is the anti-diabetic drug metformin, currently used to restore insulin sensitivity in type 2 diabetics, is known to activate AMPK (Meng, et al., 2015). Since AMPK activation and downstream signalling elicits a range of neuroprotective effects in PD models (Hang, Thundyil, & Lim, 2015), there is potential for re-purposing this pharmaceutical for the treatment of PD. Moreover, the fact that patients undergoing metformin treatment are at a decreased risk of developing PD reinforces this view (Wahlqvist, et al., 2012).

Other compounds such as Guanidinopropionic acid (GPA), a creatine monohydrate analogue which is a common additive in dietary supplements used by body builders and athletes have shown strong anti-hyperglycemic effects in hyperglycemia in KKAy and C57BL6Job/ob mice and increases blood glucose uptake in rhesus monkeys (Meglasson et al., 1993). Other studies have also shown GPA to induce an AMPK-dependant increases in mitochondrial function and biogenesis (Horvath, et al., 2011). Moreover, this same study showed that GPA-fed mice in an MPTP mouse model of PD exhibited no loss of TH neurones versus mice that were fed with chow not containing GPA. This highlights the potential for GPA to be studied as a potential protective agent in PD. Collectively, it is reasonable to propose that any pharmaceutical capable activating AMPK and downstream increases in autophagy and mitochondrial function would find efficacy as an anti-PD therapeutic.

There is growing evidence that another anti-type 2 diabetes drug, exenatide, may be re-purposed as a treatment for PD patients as they may share some common underlaying cellular mechanisms of disease pathology such as mitochondrial dysfunction (Athauda & Foltynie, 2016). There is a body of evidence that indicates that insulin is BBB-permeable and plays a role in influence a range processes in the brain including neuronal survival and growth, dopaminergic transmission, maintenance of synapses and pathways involved in cognition and that insulin signalling pathways may contribute to the development of the pathological features of Parkinson's disease. As such, exenatide, a glucagon-like peptide 1 (GLP-1) receptor

agonist has been highlighted as drug for possible re-purposing to PD patients. *In vitro* and *in vivo* tests suggest that exenatide may act via the GLP-1 receptor to influence neuronal insulin signalling to activate intracellular protein kinase B (AKT) and its downstream substrates which include mTOR and glycogen synthase 3β (GSK3β) to influence neuronal survival pathways, increase mitochondrial function and reduce neuroinflammation (Athauda & Foltynie, 2016). Other data also suggests that downstream GLP-1 signalling induced by exenatide effects Mitogen Associated Protein Kinase (MAPK) activity (Baggio & Drucker, 2007). The activation of MAPK is thought to induce long term potentiation, synaptic plasticity (Thomas & Huganir, 2004) and also stabilization of dendritic spines (Goldin & Segal, 2003; Thomas & Huganir, 2004). Current literature suggests that exenatide-mediated PD neuroprotection is mediated via perpetuation of striatal dopamine neurotransmission (Harkavyi et al., 2008; Ventorp et al., 2017) which is thought to be the result of intracellular cyclic AMP (K. S. Kim et al., 1993).

Finally, other chemicals may be utilised to enhance the cognitive decline associated with neurodegenerative diseases such as PD. Non-peptide ghrelin mimetics such as GSK894490A and CP-464709-18 used by (Atcha, et al., 2009) improved performance in the novel object recognition and modified water maze tests in male Lister hooded rats. This study demonstrated that these BBB-permeable small-molecule GHSR1a agonists improve cognition and enhance learning and memory substantiating their potential as novel therapeutics for PD.

6.4. Other beneficial side effects of acyl-ghrelin and GHSR1a receptor agonists for PD patients

GHSR1a agonists such as AG hold potential for treating cachexia and impaired gastric motility typical observed in PD patients. Cachexia is also termed a wasting syndrome is characterised by loss of weight, muscle atrophy, fatigue, weakness, and significant loss of appetite in someone who is not actively trying to lose weight. This is one such symptom observed in the late stages of diseases such as cancer and Parkinson's disease (D'Amelio et al., 2006). GHSR1a agonism by AG stimulates appetite and feeding behaviour (Wren et al., 2000). This is also true for a range of small-molecule synthetic peptide and non-peptide ligands of the GHSR1a (Bresciani, Tamiazzo, et al., 2008). A study by (Moulin, et al., 2007) investigated *in vitro* binding and *in vivo* biological activity effect of trisubstituted 1,2,4-triazole structured GHSR1a receptor ligands. They concluded that a number of these ligands held potent

stimulation of food intake *in vivo* (e.g. JMV2894); whilst others GHSR1a ligands held potential as potent inhibitors of hexarelin-induced food intake (e.g. JMV2959 and JMV3021). Hexarelin is a potent synthetic GHSR1a agonist and inducer of food intake (Bresciani, Pitsikas, et al., 2008). Thus, highlighting the potential for utilising GHSR1a agonists such as AG and its synthetic counterparts as initiators of feeding activity. However, this study did show that *in vitro* binding of agonists to GHSR1a is not a predictor of their *in vivo* endocrinological effects and that other receptors may play a role in regulating these endocrinological and extra-endocrinological effects. Moreover, a study using the same GHSR1a agonist as we utilised in our rotenone-induced PD model, JMV2894, antagonized cisplatin-induced weight loss in a rat model of cachexia (Bresciani et al., 2016). Again, highlighting the modulatory effects of GHSR1a agonists as a potential treatment of cachexia.

Another symptom typical of PD is reduced gastric motility and gastrointestinal (GI) dysfunction at the early stages of disease progression (Anselmi, Toti, Bove, Hampton, & Travagli, 2017). It is postulated that disruption of the nigro-vagal nerve pathway, which is thought to control gastric tone and motility, might be involved in the prodromal gastric dysmotility observed in early-stage PD. The extent of the impairment in gastric motility seen in PD patients occurs in approximately 42% of PD patients who experience complications in motor function (Bestetti, Capozza, Lacerenza, Manfredi, & Mancini, 2017). This study suggests that common PD treatment, L-DOPA, may contribute to the delay in gastric emptying by effecting DAergic neurones in the stomach. Moreover, the study suggests that dosage of Aromatic L-amino acid decarboxylase inhibitor (dopa-decarboxylase inhibitor) and increasing concentration of L-DOPA may contribute to the GI dysfunctions and thus effects the efficacy of their treatment. Ghrelin promotes gastric motility via the GHSR1a in a direct pathway from the arcuate nucleus of the hypothalamus which regulates gastric motility via stimulation of the vagus nerve (Bestetti, et al., 2017).

Therefore, there appears to be potential in re-purposing and utilising molecules and pharmaceuticals which agonise GHSR1a in the arcuate nucleus to increase gastric motility and feeding behaviour to alleviate patient symptoms and improve quality of PD patient life.

In summary, the work presented here support a role for AG and GHSR1a agonists as potential therapeutics to treat PD. Further work is needed to delineate the mechanisms of action and neuroprotective efficacy in more diverse models of disease.

7.0. Bibliography

Abraham, V. C., Towne, D. L., Waring, J. F., Warrior, U., & Burns, D. J. (2008). Application of a high-content multiparameter cytotoxicity assay to prioritize compounds based on toxicity potential in humans. *Journal of Biomolecular Screening, 13*(6), 527-537. doi: 10.1177/1087057108318428

Agarwal, B. (2011). A role for anions in ATP synthesis and its molecular mechanistic interpretation. *Journal of Bioenergetics and Biomembranes, 43*(3), 299-310. doi: 10.1007/s10863-011-9358-3

Ahmadi, F. A., Linseman, D. A., Grammatopoulos, T. N., Jones, S. M., Bouchard, R. J., Freed, C. R., . . . Zawada, W. M. (2003). The pesticide rotenone induces caspase-3-mediated apoptosis in ventral mesencephalic dopaminergic neurons. *J Neurochemistry, 87*(4), 914-921.

Alavi, M. V., Bette, S., Schimpf, S., Schuettauf, F., Schraermeyer, U., Wehrl, H. F., . . . Wissinger, B. (2007). A splice site mutation in the murine Opa1 gene features pathology of autosomal dominant optic atrophy. *Brain, 130*(Pt 4), 1029-1042. doi: 10.1093/brain/awm005

Alavi, M. V., & Fuhrmann, N. (2013). Dominant optic atrophy, OPA1, and mitochondrial quality control: understanding mitochondrial network dynamics *Molecular Neurodegeneration* (Vol. 8, pp. 32).

Albarran-Zeckler, R. G., Sun, Y., & Smith, R. G. (2011). Physiological roles revealed by ghrelin and ghrelin receptor deficient mice. *Peptides, 32*(11), 2229-2235. doi: 10.1016/j.peptides.2011.07.003

Alvarez-Fischer, D., Henze, C., Strenzke, C., Westrich, J., Ferger, B., Hoglinger, G. U., . . . Hartmann, A. (2008). Characterization of the striatal 6-OHDA model of Parkinson's disease in wild type and alpha-synuclein-deleted mice. *Experimental Neurology, 210*(1), 182-193. doi: 10.1016/j.expneurol.2007.10.012

Anand, R., Langer, T., & Baker, M. J. (2013). Proteolytic control of mitochondrial function and morphogenesis. *Biochimca et Biophysica Acta, 1833*(1), 195-204. doi: 10.1016/j.bbamcr.2012.06.025

Andersson, U., Filipsson, K., Abbott, C. R., Woods, A., Smith, K., Bloom, S. R., . . . Small, C. J. (2004). AMP-activated protein kinase plays a role in the control of food intake. *Journal of Biological Chemistry, 279*(13), 12005-12008. doi: 10.1074/jbc.C300557200

Andrews, Z. B. (2011). The extra-hypothalamic actions of ghrelin on neuronal function. *Trends in Neuroscience, 34*(1), 31-40. doi: 10.1016/j.tins.2010.10.001

Andrews, Z. B., Erion, D., Beiler, R., Liu, Z. W., Abizaid, A., Zigman, J., . . . Horvath, T. L. (2009). Ghrelin promotes and protects nigrostriatal dopamine function via a UCP2-dependent mitochondrial mechanism. *Journal of Neuroscience, 29*(45), 14057-14065. doi: 10.1523/jneurosci.3890-09.2009

Anselmi, L., Toti, L., Bove, C., Hampton, J., & Travagli, R. A. (2017). A Nigro-Vagal Pathway Controls Gastric Motility and is Affected in a Rat Model of Parkinsonism. *Gastroenterology* doi: 10.1053/j.gastro.2017.08.069

Atcha, Z., Chen, W. S., Ong, A. B., Wong, F. K., Neo, A., Browne, E. R., . . . Pemberton, D. J. (2009). Cognitive enhancing effects of ghrelin receptor agonists. *Psychopharmacology, 206*(3), 415-427. doi: 10.1007/s00213-009-1620-6

Athauda, D., & Foltynie, T. (2016). Insulin resistance and Parkinson's disease: A new target for disease modification? *Progress in Neurobiology, 145-146*, 98-120. doi: 10.1016/j.pneurobio.2016.10.001

Baggio, L. L., & Drucker, D. J. (2007). Biology of incretins: GLP-1 and GIP. *Gastroenterology, 132*(6), 2131-2157. doi: 10.1053/j.gastro.2007.03.054

Balakrishnan, R., Elangovan, N., Mohankumar, T., Nataraj, J., Manivasagam, T., Justin Thenmozhi, A., . . . Abdul Sattar Khan, M. (2018). Isolongifolene attenuates rotenone-induced mitochondrial dysfunction, oxidative stress and apoptosis. *Frontiers in Bioscience, 10*, 248-261.

Bando, M., Iwakura, H., Ariyasu, H., Koyama, H., Hosoda, K., Adachi, S., . . . Akamizu, T. (2013). Overexpression of intraislet ghrelin enhances beta-cell proliferation after streptozotocin-induced beta-cell injury in mice. *American Journal of Physiology, 305*(1), E140-148. doi: 10.1152/ajpendo.00112.2013

Banks, W. A. (2012). Role of the blood-brain barrier in the evolution of feeding and cognition. *Annals of the New York Academy of Sciences, 1264*, 13-19. doi: 10.1111/j.1749-6632.2012.06568.x

Banks, W. A., Tschop, M., Robinson, S. M., & Heiman, M. L. (2002). Extent and direction of ghrelin transport across the blood-brain barrier is determined by its unique primary structure. *Journal of Pharmacol Experimental Therapeutics, 302*(2), 822-827. doi: 10.1124/jpet.102.034827

Bayliss, J. A., & Andrews, Z. B. (2013). Ghrelin is neuroprotective in Parkinson's disease: molecular mechanisms of metabolic neuroprotection. *Therapeutic*

Advances in Endocrinology and Metabolism, 4(1), 25-36. doi: 10.1177/2042018813479645

Bayliss, J. A., Lemus, M., Santos, V. V., Deo, M., Elsworth, J. D., & Andrews, Z. B. (2016). Acylated but not des-acyl ghrelin is neuroprotective in an MPTP mouse model of Parkinson's disease. *Journal of Neurochemistry, 137*(3), 460-471. doi: 10.1111/jnc.13576

Bayliss, J. A., Lemus, M. B., Stark, R., Santos, V. V., Thompson, A., Rees, D. J., . . . Andrews, Z. B. (2016). Ghrelin-AMPK Signaling Mediates the Neuroprotective Effects of Calorie Restriction in Parkinson's Disease. *Journal of Neuroscience, 36*(10), 3049-3063. doi: 10.1523/jneurosci.4373-15.2016

Benard, G., & Karbowski, M. (2009). Mitochondrial fusion and division: Regulation and role in cell viability. *Seminars in Cell & Developmental Biology, 20*(3), 365-374.

Berg, J. M., Tymoczko, J. L., & Stryer, L. (2002). *Acetyl Coenzyme A Carboxylase Plays a Key Role in Controlling Fatty Acid Metabolism* (Vol. 5): W H Freeman.

Bertram, L., & Tanzi, R. E. (2005). The genetic epidemiology of neurodegenerative disease. *Journal of Clinical Investigation, 115*(6), 1449-1457. doi: 10.1172/jci24761

Bestetti, A., Capozza, A., Lacerenza, M., Manfredi, L., & Mancini, F. (2017). Delayed Gastric Emptying in Advanced Parkinson Disease: Correlation With Therapeutic Doses. *Clinical Nuclear Medicine, 42*(2), 83-87. doi: 10.1097/rlu.0000000000001470

Betarbet, R., Sherer, T. B., MacKenzie, G., Garcia-Osuna, M., Panov, A. V., & Greenamyre, J. T. (2000). Chronic systemic pesticide exposure reproduces features of Parkinson's disease. *Nature Neuroscience, 3*(12), 1301-1306. doi: 10.1038/81834

Beynon, A. L., Brown, M. R., Wright, R., Rees, M. I., Sheldon, I. M., & Davies, J. S. (2013). Ghrelin inhibits LPS-induced release of IL-6 from mouse dopaminergic neurones. *Journal of Neuroinflammation, 10*, 40. doi: 10.1186/1742-2094-10-40

Bezard, E., Yue, Z., Kirik, D., & Spillantini, M. G. (2013). Animal models of Parkinson's disease: limits and relevance to neuroprotection studies. *Movement Disorders, 28*(1), 61-70. doi: 10.1002/mds.25108

Bjorklund, A., & Dunnett, S. B. (2007). Dopamine neuron systems in the brain: an update. *Trends in Neuroscience, 30*(5), 194-202. doi: 10.1016/j.tins.2007.03.006

Bonifati, V., Rohe, C. F., Breedveld, G. J., Fabrizio, E., De Mari, M., Tassorelli, C., . . . Oostra, B. A. (2005). Early-onset parkinsonism associated with PINK1 mutations: frequency, genotypes, and phenotypes. *Neurology, 65*(1), 87-95. doi: 10.1212/01.wnl.0000167546.39375.82

Bove, J., Prou, D., Perier, C., & Przedborski, S. (2005). Toxin-induced models of Parkinson's disease. *NeuroRx, 2*(3), 484-494. doi: 10.1602/neurorx.2.3.484

Bresciani, E., Pitsikas, N., Tamiazzo, L., Luoni, M., Bulgarelli, I., Cocchi, D., . . . Torsello, A. (2008). Feeding behavior during long-term hexarelin administration in young and old rats. *Journal of Endocrinological Investigation, 31*(7), 647-652. doi: 10.1007/bf03345618

Bresciani, E., Rizzi, L., Molteni, L., Ravelli, M., Liantonio, A., Ben Haj Salah, K., . . . Torsello, A. (2016). JMV2894, a novel growth hormone secretagogue, accelerates body mass recovery in an experimental model of cachexia. *Endocrine* doi: 10.1007/s12020-016-1184-2

Bresciani, E., Tamiazzo, L., Torsello, A., Bulgarelli, I., Rapetti, D., Caporali, S., . . . Locatelli, V. (2008). Ghrelin control of GH secretion and feeding behaviour: the role of the GHS-R1a receptor studied in vivo and in vitro using novel non-peptide ligands. *Eat Weight Disorders, 13*(3), e67-74.

Brice, A. (2005). Genetics of Parkinson's disease: LRRK2 on the rise. *Brain, 128*(Pt 12), 2760-2762. doi: 10.1093/brain/awh676

Burbulla, L. F., Song, P., Mazzulli, J. R., Zampese, E., Wong, Y. C., Jeon, S., . . . Krainc, D. (2017). Dopamine oxidation mediates mitochondrial and lysosomal dysfunction in Parkinson's disease. *Science, 357*(6357), 1255-1261. doi: 10.1126/science.aam9080

Byers, B., Lee, H. L., & Reijo Pera, R. (2012). Modeling Parkinson's disease using induced pluripotent stem cells. *Current Neurology and Neuroscience Reports, 12*(3), 237-242. doi: 10.1007/s11910-012-0270-y

Camina, J. P. (2006). Cell biology of the ghrelin receptor. *Journal of Neuroendocrinology, 18*(1), 65-76. doi: 10.1111/j.1365-2826.2005.01379.x

Cannon, J. R., Tapias, V., Na, H. M., Honick, A. S., Drolet, R. E., & Greenamyre, J. T. (2009). A highly reproducible rotenone model of Parkinson's disease. *Neurobiology of Disease, 34*(2), 279-290.

Carling, D., Aguan, K., Woods, A., Verhoeven, A. J., Beri, R. K., Brennan, C. H., . . . Scott, J. (1994). Mammalian AMP-activated protein kinase is homologous to

yeast and plant protein kinases involved in the regulation of carbon metabolism. *Journal of Biological Chemistry, 269*(15), 11442-11448.

Carlini, V. P., Perez, M. F., Salde, E., Schioth, H. B., Ramirez, O. A., & de Barioglio, S. R. (2010). Ghrelin induced memory facilitation implicates nitric oxide synthase activation and decrease in the threshold to promote LTP in hippocampal dentate gyrus. *Physiology & Behaviour, 101*(1), 117-123. doi: 10.1016/j.physbeh.2010.04.026

Carpenter, A. E., Jones, T. R., Lamprecht, M. R., Clarke, C., Kang, I. H., Friman, O., . . . Sabatini, D. M. (2006). CellProfiler: image analysis software for identifying and quantifying cell phenotypes. *Genome Biology, 7*(10), R100. doi: 10.1186/gb-2006-7-10-r100

Cereghetti, G. M., Stangherlin, A., Martins de Brito, O., Chang, C. R., Blackstone, C., Bernardi, P., & Scorrano, L. (2008). Dephosphorylation by calcineurin regulates translocation of Drp1 to mitochondria. *Proceedings of the National Academy of Sciences of the United States of America, 105*(41), 15803-15808. doi: 10.1073/pnas.0808249105

Chen, H., & Chan, D. C. (2009). Mitochondrial dynamics--fusion, fission, movement, and mitophagy--in neurodegenerative diseases. *Human Molecular Genetics, 18*(R2), R169-176. doi: 10.1093/hmg/ddp326

Chen, H., & Chan, D. C. (2010). Physiological functions of mitochondrial fusion. *Annals of the New York Academy of Sciences, 1201*, 21-25. doi: 10.1111/j.1749-6632.2010.05615.x

Chen, H., Detmer, S. A., Ewald, A. J., Griffin, E. E., Fraser, S. E., & Chan, D. C. (2003). Mitofusins Mfn1 and Mfn2 coordinately regulate mitochondrial fusion and are essential for embryonic development. *The Journal of Cell Biology, 160*(2), 189-200. doi: 10.1083/jcb.200211046

Chen, H. Y., Trumbauer, M. E., Chen, A. S., Weingarth, D. T., Adams, J. R., Frazier, E. G., . . . Qian, S. (2004). Orexigenic action of peripheral ghrelin is mediated by neuropeptide Y and agouti-related protein. *Endocrinology, 145*(6), 2607-2612. doi: 10.1210/en.2003-1596

Chen, L. B. (1988). Mitochondrial membrane potential in living cells. *Annual Review of Cell Biology, 4*, 155-181. doi: 10.1146/annurev.cb.04.110188.001103

Chen, Y., & Sheng, Z. H. (2013). Kinesin-1-syntaphilin coupling mediates activity-dependent regulation of axonal mitochondrial transport. *The Journal of Cell Biology, 202*(2), 351-364. doi: 10.1083/jcb.201302040

Chen, Y. M., Gerwin, C., & Sheng, Z. H. (2009). Dynein light chain LC8 regulates syntaphilin-mediated mitochondrial docking in axons. *Journal of Neuroscience, 29*(30), 9429-9438. doi: 10.1523/jneurosci.1472-09.2009

Choi, W. S., Palmiter, R. D., & Xia, Z. (2011). Loss of mitochondrial complex I activity potentiates dopamine neuron death induced by microtubule dysfunction in a Parkinson's disease model. *Journal of Cell Biology, 192*(5), 873-882. doi: 10.1083/jcb.201009132

Chu, K. M., Chow, K. B., Leung, P. K., Lau, P. N., Chan, C. B., Cheng, C. H., & Wise, H. (2007). Over-expression of the truncated ghrelin receptor polypeptide attenuates the constitutive activation of phosphatidylinositol-specific phospholipase C by ghrelin receptors but has no effect on ghrelin-stimulated extracellular signal-regulated kinase 1/2 activity. *International Journal of Biochemistry & Cell Biology, 39*(4), 752-764. doi: 10.1016/j.biocel.2006.11.007

Chung, C. Y., Seo, H., Sonntag, K. C., Brooks, A., Lin, L., & Isacson, O. (2005). Cell type-specific gene expression of midbrain dopaminergic neurons reveals molecules involved in their vulnerability and protection. *Human Molecular Genetics, 14*(13), 1709-1725. doi: 10.1093/hmg/ddi178

Cicchetti, F., Drouin-Ouellet, J., & Gross, R. E. (2009). Environmental toxins and Parkinson's disease: what have we learned from pesticide-induced animal models? *Trends in Pharmacological Sciences, 30*(9), 475-483. doi: 10.1016/j.tips.2009.06.005

Clark, I. E., Dodson, M. W., Jiang, C., Cao, J. H., Huh, J. R., Seol, J. H., . . . Guo, M. (2006). Drosophila pink1 is required for mitochondrial function and interacts genetically with parkin *Nature* (Vol. 441, pp. 1162-1166). England.

Cleeter, M. W., Cooper, J. M., & Schapira, A. H. (2001). Nitric oxide enhances MPP(+) inhibition of complex I. *FEBS Letters, 504*(1-2), 50-52.

Codrich, M., Bertuzzi, M., Russo, R., Francescatto, M., Espinoza, S., Zentilin, L., . . . Gustincich, S. (2017). Neuronal hemoglobin affects dopaminergic cells' response to stress. *Cell Death and Disease, 8*(1), e2538. doi: 10.1038/cddis.2016.458

Cook, K. L., Soto-Pantoja, D. R., Jin, L., Abu-Asab, M., & Clarke, R. (2014). When is a vesicle not just a vesicle: mitochondrial spheroids and mitochondrial autophagosomes. *Cell & Bioscience, 4*, 66. doi: 10.1186/2045-3701-4-66

Cowley, M. A., Smith, R. G., Diano, S., Tschop, M., Pronchuk, N., Grove, K. L., . . . Horvath, T. L. (2003). The distribution and mechanism of action of ghrelin in

the CNS demonstrates a novel hypothalamic circuit regulating energy homeostasis. *Neuron, 37*(4), 649-661.

Cribbs, J. T., & Strack, S. (2007). Reversible phosphorylation of Drp1 by cyclic AMP-dependent protein kinase and calcineurin regulates mitochondrial fission and cell death. *EMBO Reports, 8*(10), 939-944. doi: 10.1038/sj.embor.7401062

Crute, B. E., Seefeld, K., Gamble, J., Kemp, B. E., & Witters, L. A. (1998). Functional domains of the alpha1 catalytic subunit of the AMP-activated protein kinase. *Journal of Biological Chemistry, 273*(52), 35347-35354.

D'Amelio, M., Ragonese, P., Morgante, L., Reggio, A., Callari, G., Salemi, G., & Savettieri, G. (2006). Long-term survival of Parkinson's disease: a population-based study. *Journal of Neurology, 253*(1), 33-37. doi: 10.1007/s00415-005-0916-7

Dagda, R. K., Cherra, S. J., 3rd, Kulich, S. M., Tandon, A., Park, D., & Chu, C. T. (2009). Loss of PINK1 function promotes mitophagy through effects on oxidative stress and mitochondrial fission. *Journal of Biological Chemistry, 284*(20), 13843-13855. doi: 10.1074/jbc.M808515200

Damier, P., Hirsch, E. C., Agid, Y., & Graybiel, A. M. (1999a). The substantia nigra of the human brain. I. Nigrosomes and the nigral matrix, a compartmental organization based on calbindin D(28K) immunohistochemistry. *Brain, 122 (Pt 8)*, 1421-1436.

Damier, P., Hirsch, E. C., Agid, Y., & Graybiel, A. M. (1999b). The substantia nigra of the human brain. II. Patterns of loss of dopamine-containing neurons in Parkinson's disease. *Brain, 122 (Pt 8)*, 1437-1448.

Date, Y., Kojima, M., Hosoda, H., Sawaguchi, A., Mondal, M. S., Suganuma, T., . . . Nakazato, M. (2000). Ghrelin, a novel growth hormone-releasing acylated peptide, is synthesized in a distinct endocrine cell type in the gastrointestinal tracts of rats and humans. *Endocrinology, 141*(11), 4255-4261. doi: 10.1210/endo.141.11.7757

Dauer, W., & Przedborski, S. (2003). Parkinson's disease: mechanisms and models. *Neuron, 39*(6), 889-909.

Davies, V. J., Hollins, A. J., Piechota, M. J., Yip, W., Davies, J. R., White, K. E., . . . Votruba, M. (2007). Opa1 deficiency in a mouse model of autosomal dominant optic atrophy impairs mitochondrial morphology, optic nerve structure and visual function. *Human Molecular Genetics, 16*(11), 1307-1318. doi: 10.1093/hmg/ddm079

Deas, E., Wood, N. W., & Plun-Favreau, H. (2011). Mitophagy and Parkinson's disease: The PINK1–parkin link *Biochimca et Biophysica Acta* (Vol. 1813, pp. 623-633).

Del Dotto, V., Mishra, P., Vidoni, S., Fogazza, M., Maresca, A., Caporali, L., . . . Zanna, C. (2017). OPA1 Isoforms in the Hierarchical Organization of Mitochondrial Functions. *Cell Reports, 19*(12), 2557-2571. doi: 10.1016/j.celrep.2017.05.073

Delhanty, P. J., van der Eerden, B. C., & van Leeuwen, J. P. (2014). Ghrelin and bone. *Biofactors, 40*(1), 41-48. doi: 10.1002/biof.1120

Deng, H., Dodson, M. W., Huang, H., & Guo, M. (2008). The Parkinson's disease genes pink1 and parkin promote mitochondrial fission and/or inhibit fusion in Drosophila. *Proceedings of the National Academy of Science of the United States of America, 105*(38), 14503-14508. doi: 10.1073/pnas.0803998105

Detmer, S. A., & Chan, D. C. (2007). Functions and dysfunctions of mitochondrial dynamics. *Nature Reviews Molecular Cell Biology, 8*(11), 870-879. doi: 10.1038/nrm2275

Diano, S., Farr, S. A., Benoit, S. C., McNay, E. C., da Silva, I., Horvath, B., . . . Horvath, T. L. (2006). Ghrelin controls hippocampal spine synapse density and memory performance. *Nature Neuroscience, 9*(3), 381-388. doi: 10.1038/nn1656

Dickson, S. L., Leng, G., & Robinson, I. C. (1993). Systemic administration of growth hormone-releasing peptide activates hypothalamic arcuate neurons. *Neuroscience, 53*(2), 303-306.

Ding, H., Gao, J., Zhu, Z., Xiong, Y., & Liu, J. (2008). Mitochondrial dysfunction enhances susceptibility to oxidative stress by down-regulation of thioredoxin in human neuroblastoma cells. *Neurochemical Research, 33*(1), 43-50. doi: 10.1007/s11064-007-9405-y

Ding, W. X., Guo, F., Ni, H. M., Bockus, A., Manley, S., Stolz, D. B., . . . Yin, X. M. (2012). Parkin and Mitofusins Reciprocally Regulate Mitophagy and Mitochondrial Spheroid Formation. *Journal of Biological Chemistry* (Vol. 287, pp. 42379-42388).

Ding, Y. M., Jaumotte, J. D., Signore, A. P., & Zigmond, M. J. (2004). Effects of 6-hydroxydopamine on primary cultures of substantia nigra: specific damage to dopamine neurons and the impact of glial cell line-derived neurotrophic factor. *Journal of Neurochemistry, 89*(3), 776-787. doi: 10.1111/j.1471-4159.2004.02415.x

Dodson, M. W., & Guo, M. (2007). Pink1, Parkin, DJ-1 and mitochondrial dysfunction in Parkinson's disease. *Current Opinions in Neurobiology, 17*(3), 331-337. doi: 10.1016/j.conb.2007.04.010

Doran, E., & Halestrap, A. P. (2000). Cytochrome c release from isolated rat liver mitochondria can occur independently of outer-membrane rupture: possible role of contact sites. *The Biochemical Journal, 348 Pt 2*, 343-350.

Dulovic, M., Jovanovic, M., Xilouri, M., Stefanis, L., Harhaji-Trajkovic, L., Kravic-Stevovic, T., . . . Trajkovic, V. (2014). The protective role of AMP-activated protein kinase in alpha-synuclein neurotoxicity in vitro. *Neurobiology of Disease, 63*, 1-11. doi: 10.1016/j.nbd.2013.11.002

Elmore, S. (2007). Apoptosis: a review of programmed cell death. *Toxicologic Pathology, 35*(4), 495-516. doi: 10.1080/01926230701320337

Engel, J. A., & Jerlhag, E. (2014). Role of appetite-regulating peptides in the pathophysiology of addiction: implications for pharmacotherapy. *CNS Drugs, 28*(10), 875-886. doi: 10.1007/s40263-014-0178-y

Eulitz, D., Pruss, H., Derst, C., & Veh, R. W. (2007). Heterogeneous distribution of kir3 potassium channel proteins within dopaminergic neurons in the mesencephalon of the rat brain. *Cell Mol Neurobiol, 27*(3), 285-302. doi: 10.1007/s10571-006-9118-9

Exner, N., Treske, B., Paquet, D., Holmstrom, K., Schiesling, C., Gispert, S., . . . Haass, C. (2007). Loss-of-function of human PINK1 results in mitochondrial pathology and can be rescued by parkin. *Journal of Neuroscience, 27*(45), 12413-12418. doi: 10.1523/jneurosci.0719-07.2007

Ezquerro, S., Fruhbeck, G., & Rodriguez, A. (2017). Ghrelin and autophagy. *Current Opinion in Clinical Nutrition and Metabolic Care, 20*(5), 402-408. doi: 10.1097/mco.0000000000000390

Fedorow, H., Tribl, F., Halliday, G., Gerlach, M., Riederer, P., & Double, K. L. (2005). Neuromelanin in human dopamine neurons: comparison with peripheral melanins and relevance to Parkinson's disease. *Progress in Neurobiology, 75*(2), 109-124. doi: 10.1016/j.pneurobio.2005.02.001

Ferguson, M., Mockett, R. J., Shen, Y., Orr, W. C., & Sohal, R. S. (2005). Age-associated decline in mitochondrial respiration and electron transport in Drosophila melanogaster. *The Biochemical Journal, 390*(Pt 2), 501-511. doi: 10.1042/bj20042130

Ferreira-Marques, M., Aveleira, C. A., Carmo-Silva, S., Botelho, M., Pereira de Almeida, L., & Cavadas, C. (2016). Caloric restriction stimulates autophagy

in rat cortical neurons through neuropeptide Y and ghrelin receptors activation. *Aging (Albany NY), 8*(7), 1470-1484. doi: 10.18632/aging.100996

Filomeni, G., Graziani, I., De Zio, D., Dini, L., Centonze, D., Rotilio, G., & Ciriolo, M. R. (2012). Neuroprotection of kaempferol by autophagy in models of rotenone-mediated acute toxicity: possible implications for Parkinson's disease. *Neurobiology of Aging, 33*(4), 767-785. doi: 10.1016/j.neurobiolaging.2010.05.021

Friedman, J. R., Lackner, L. L., West, M., DiBenedetto, J. R., Nunnari, J., & Voeltz, G. K. (2011). ER tubules mark sites of mitochondrial division. *Science, 334*(6054), 358-362. doi: 10.1126/science.1207385

Fu, Y., Yuan, Y., Halliday, G., Rusznak, Z., Watson, C., & Paxinos, G. (2012). A cytoarchitectonic and chemoarchitectonic analysis of the dopamine cell groups in the substantia nigra, ventral tegmental area, and retrorubral field in the mouse. *Brain Structure & Function, 217*(2), 591-612. doi: 10.1007/s00429-011-0349-2

Gahete, M. D., Cordoba-Chacon, J., Kineman, R. D., Luque, R. M., & Castano, J. P. (2011). Role of ghrelin system in neuroprotection and cognitive functions: implications in Alzheimer's disease. *Peptides, 32*(11), 2225-2228. doi: 10.1016/j.peptides.2011.09.019

Gahete, M. D., Rincon-Fernandez, D., Villa-Osaba, A., Hormaechea-Agulla, D., Ibanez-Costa, A., Martinez-Fuentes, A. J., . . . Luque, R. M. (2014). Ghrelin gene products, receptors, and GOAT enzyme: biological and pathophysiological insight. *Journal of Endocrinology, 220*(1), R1-24. doi: 10.1530/joe-13-0391

Gandre-Babbe, S., & van der Bliek, A. M. (2008). The novel tail-anchored membrane protein Mff controls mitochondrial and peroxisomal fission in mammalian cells. *Molecular Biology of the Cell, 19*(6), 2402-2412. doi: 10.1091/mbc.E07-12-1287

Gautier, C. A., Kitada, T., & Shen, J. (2008). Loss of PINK1 causes mitochondrial functional defects and increased sensitivity to oxidative stress. *Proceedings of the National Academy of Sciences of the Unites States of America, 105*(32), 11364-11369. doi: 10.1073/pnas.0802076105

German, D. C., & Manaye, K. F. (1993). Midbrain dopaminergic neurons (nuclei A8, A9, and A10): three-dimensional reconstruction in the rat. *Journal of Comparative Neurology, 331*(3), 297-309. doi: 10.1002/cne.903310302

Giráldez-Pérez, R. M., Antolín-Vallespín, M., Muñoz, M. D., & Sánchez-Capelo, A. (2014). Models of α-synuclein aggregation in Parkinson's disease *Acta Neuropathology Community* (Vol. 2).

Gispert, S., Ricciardi, F., Kurz, A., Azizov, M., Hoepken, H. H., Becker, D., . . . Auburger, G. (2009). Parkinson phenotype in aged PINK1-deficient mice is accompanied by progressive mitochondrial dysfunction in absence of neurodegeneration. *PLoS One, 4*(6), e5777. doi: 10.1371/journal.pone.0005777

Glinka, Y., Tipton, K. F., & Youdim, M. B. (1996). Nature of inhibition of mitochondrial respiratory complex I by 6-Hydroxydopamine. *Journal of Neurochemistry, 66*(5), 2004-2010.

Glinka, Y. Y., & Youdim, M. B. (1995). Inhibition of mitochondrial complexes I and IV by 6-hydroxydopamine. *European Journal of Pharmacology, 292*(3-4), 329-332.

Gnanapavan, S., Kola, B., Bustin, S. A., Morris, D. G., McGee, P., Fairclough, P., . . . Korbonits, M. (2002). The tissue distribution of the mRNA of ghrelin and subtypes of its receptor, GHS-R, in humans. *Journal of Clinical Endocrinology and Metababolism, 87*(6), 2988. doi: 10.1210/jcem.87.6.8739

Goldin, M., & Segal, M. (2003). Protein kinase C and ERK involvement in dendritic spine plasticity in cultured rodent hippocampal neurons. *European Journal of Neuroscience, 17*(12), 2529-2539.

Gomez-Lazaro, M., Bonekamp, N. A., Galindo, M. F., Jordan, J., & Schrader, M. (2008). 6-Hydroxydopamine (6-OHDA) induces Drp1-dependent mitochondrial fragmentation in SH-SY5Y cells. *Free Radical Biology and Medicine, 44*(11), 1960-1969. doi: 10.1016/j.freeradbiomed.2008.03.009

Granata, R., Settanni, F., Biancone, L., Trovato, L., Nano, R., Bertuzzi, F., . . . Muccioli, G. (2007). Acylated and unacylated ghrelin promote proliferation and inhibit apoptosis of pancreatic beta-cells and human islets: involvement of 3',5'-cyclic adenosine monophosphate/protein kinase A, extracellular signal-regulated kinase 1/2, and phosphatidyl inositol 3-Kinase/Akt signaling. *Endocrinology, 148*(2), 512-529. doi: 10.1210/en.2006-0266

Grenier, K., McLelland, G. L., & Fon, E. A. (2013). Parkin- and PINK1-Dependent Mitophagy in Neurons: Will the Real Pathway Please Stand Up? *Frontier Neurology, 4* doi: 10.3389/fneur.2013.00100

Guerreiro, P. S., Gerhardt, E., Lopes da Fonseca, T., Bahr, M., Outeiro, T. F., & Eckermann, K. (2016). LRRK2 Promotes Tau Accumulation, Aggregation

and Release. *Molecular Neurobiology, 53*(5), 3124-3135. doi: 10.1007/s12035-015-9209-z

Gundersen, V. (2010). Protein aggregation in Parkinson's disease. *Acta Neurologica Scandinavica. Supplementum.*(190), 82-87. doi: 10.1111/j.1600-0404.2010.01382.x

Guo, C., Sun, L., Chen, X., & Zhang, D. (2013). Oxidative stress, mitochondrial damage and neurodegenerative diseases. *Neural Regeneration Research, 8*(21), 2003-2014. doi: 10.3969/j.issn.1673-5374.2013.21.009

Gutierrez, J. A., Solenberg, P. J., Perkins, D. R., Willency, J. A., Knierman, M. D., Jin, Z., . . . Hale, J. E. (2008). Ghrelin octanoylation mediated by an orphan lipid transferase *Proceedings of the National Academy of Sciences of the United States of America* (Vol. 105, pp. 6320-6325).

Hamdani, N., & van der Velden, J. (2009). Lack of specificity of antibodies directed against human beta-adrenergic receptors. *Naunyn-Schmiedebergs Archives of Pharmacology, 379*(4), 403-407. doi: 10.1007/s00210-009-0392-1

Hang, L., Thundyil, J., & Lim, K. L. (2015). Mitochondrial dysfunction and Parkinson disease: a Parkin-AMPK alliance in neuroprotection. *Annals of the New York Academy of Sciences, 1350*, 37-47. doi: 10.1111/nyas.12820

Hao, X. M., Li, L. D., Duan, C. L., & Li, Y. J. (2017). Neuroprotective effect of alpha-mangostin on mitochondrial dysfunction and alpha-synuclein aggregation in rotenone-induced model of Parkinson's disease in differentiated SH-SY5Y cells. *Journal of Asian Natural Products Reseatch, 19*(8), 833-845. doi: 10.1080/10286020.2017.1339349

Hardy, J. (2010). Genetic analysis of pathways to Parkinson disease. *Neuron, 68*(2), 201-206. doi: 10.1016/j.neuron.2010.10.014

Harkavyi, A., Abuirmeileh, A., Lever, R., Kingsbury, A. E., Biggs, C. S., & Whitton, P. S. (2008). Glucagon-like peptide 1 receptor stimulation reverses key deficits in distinct rodent models of Parkinson's disease. *Journal of Neuroinflammation, 5*, 19. doi: 10.1186/1742-2094-5-19

Hasson, S. A., Kane, L. A., Yamano, K., Huang, C.-H., Sliter, D. A., Buehler, E., . . . Youle, R. J. (2013). High-content genome-wide RNAi screens identify regulators of parkin upstream of mitophagy. *Nature, 504*, 291-295. doi: doi:10.1038/nature12748

Hawley, S. A., Davison, M., Woods, A., Davies, S. P., Beri, R. K., Carling, D., & Hardie, D. G. (1996). Characterization of the AMP-activated protein kinase kinase from rat liver and identification of threonine 172 as the major site at

which it phosphorylates AMP-activated protein kinase. *Journal of Biological Chemistry, 271*(44), 27879-27887.

Heinz, S., Freyberger, A., Lawrenz, B., Schladt, L., Schmuck, G., & Ellinger-Ziegelbauer, H. (2017). Mechanistic Investigations of the Mitochondrial Complex I Inhibitor Rotenone in the Context of Pharmacological and Safety Evaluation. *Science Reports, 7*, 45465. doi: 10.1038/srep45465

Hirsch, E., Graybiel, A. M., & Agid, Y. A. (1988). Melanized dopaminergic neurons are differentially susceptible to degeneration in Parkinson's disease. *Nature, 334*(6180), 345-348. doi: 10.1038/334345a0

Horvath, T. L., Erion, D. M., Elsworth, J. D., Roth, R. H., Shulman, G. I., & Andrews, Z. B. (2011). GPA protects the nigrostriatal dopamine system by enhancing mitochondrial function. *Neurobiology of Disease, 43*(1), 152-162. doi: 10.1016/j.nbd.2011.03.005

Howard, A. D., Feighner, S. D., Cully, D. F., Arena, J. P., Liberator, P. A., Rosenblum, C. I., . . . Van der Ploeg, L. H. (1996). A receptor in pituitary and hypothalamus that functions in growth hormone release. *Science, 273*(5277), 974-977.

Hu, C., Huang, Y., & Li, L. (2017). Drp1-Dependent Mitochondrial Fission Plays Critical Roles in Physiological and Pathological Progresses in Mammals *International Journal of Molecular Sciences* (Vol. 18).

Hutchings, C. J., Koglin, M., & Marshall, F. H. (2010). Therapeutic antibodies directed at G protein-coupled receptors. *MAbs, 2*(6), 594-606. doi: 10.4161/mabs.2.6.13420

Hwang, O. (2013). Role of oxidative stress in Parkinson's disease. *Experimental Neurobiology, 22*(1), 11-17. doi: 10.5607/en.2013.22.1.11

Ichishita, R., Tanaka, K., Sugiura, Y., Sayano, T., Mihara, K., & Oka, T. (2008). An RNAi screen for mitochondrial proteins required to maintain the morphology of the organelle in Caenorhabditis elegans. *Journal of Biochemistry, 143*(4), 449-454. doi: 10.1093/jb/mvm245

Jenner, W. N., & Rose, F. A. (1974). Dopamine 3-O-sulphate, an end product of L-dopa metabolism in Parkinson patients. *Nature, 252*(5480), 237-238.

Jeon, S. M. (2016). Regulation and function of AMPK in physiology and diseases. *Experimental and Molecular Medicine, 48*(7), e245. doi: 10.1038/emm.2016.81

Jiang, H., Li, L. J., Wang, J., & Xie, J. X. (2008). Ghrelin antagonizes MPTP-induced neurotoxicity to the dopaminergic neurons in mouse substantia nigra.

Experimental Neurology, 212(2), 532-537. doi: 10.1016/j.expneurol.2008.05.006

Jiang, P., Gan, M., Ebrahim, A. S., Castanedes-Casey, M., Dickson, D. W., & Yen, S. H. (2013). Adenosine monophosphate-activated protein kinase overactivation leads to accumulation of alpha-synuclein oligomers and decrease of neurites. *Neurobiology of Aging, 34*(5), 1504-1515. doi: 10.1016/j.neurobiolaging.2012.11.001

Jiang, X., & Wang, X. (2004). Cytochrome C-mediated apoptosis. *Annual Review of Biochemistry, 73*, 87-106. doi: 10.1146/annurev.biochem.73.011303.073706

Jin, F., Wu, Q., Lu, Y. F., Gong, Q. H., & Shi, J. S. (2008). Neuroprotective effect of resveratrol on 6-OHDA-induced Parkinson's disease in rats. *European Journal of Pharmacology, 600*(1-3), 78-82. doi: 10.1016/j.ejphar.2008.10.005

Jones, T. R., Carpenter, A. E., Lamprecht, M. R., Moffat, J., Silver, S. J., Grenier, J. K., . . . Sabatini, D. M. (2009). Scoring diverse cellular morphologies in image-based screens with iterative feedback and machine learning. *Proceedings of the National Academy of Sciences of the United States of America, 106*(6), 1826-1831. doi: 10.1073/pnas.0808843106

Jones, T. R. C., A. Golland, P. (2005). Voronoi-Based Segmentation of Cells on Image Manifolds | SpringerLink. *Computer Vision for Biomedical Image Applications*, 535-543. doi: 10.1007/11569541_54

Jorgensen, S. B., Viollet, B., Andreelli, F., Frosig, C., Birk, J. B., Schjerling, P., . . . Wojtaszewski, J. F. (2004). Knockout of the alpha2 but not alpha1 5'-AMP-activated protein kinase isoform abolishes 5-aminoimidazole-4-carboxamide-1-beta-4-ribofuranosidebut not contraction-induced glucose uptake in skeletal muscle. *Journal of Biological Chemistry, 279*(2), 1070-1079. doi: 10.1074/jbc.M306205200

Kamentsky, L., Jones, T. R., Fraser, A., Bray, M. A., Logan, D. J., Madden, K. L., . . . Carpenter, A. E. (2011). Improved structure, function and compatibility for CellProfiler: modular high-throughput image analysis software. *Bioinformatics, 27*(8), 1179-1180. doi: 10.1093/bioinformatics/btr095

Kang, J. S., Tian, J. H., Pan, P. Y., Zald, P., Li, C., Deng, C., & Sheng, Z. H. (2008). Docking of axonal mitochondria by syntaphilin controls their mobility and affects short-term facilitation. *Cell, 132*(1), 137-148. doi: 10.1016/j.cell.2007.11.024

Kang, S. Y., Lee, S. B., Kim, H. J., Kim, H. T., Yang, H. O., & Jang, W. (2017). Autophagic modulation by rosuvastatin prevents rotenone-induced

neurotoxicity in an in vitro model of Parkinson's disease. *Neuroscience Letters, 642*, 20-26. doi: 10.1016/j.neulet.2017.01.063

Kanki, T., Wang, K., Baba, M., Bartholomew, C. R., Lynch-Day, M. A., Du, Z., . . . Klionsky, D. J. (2009). A genomic screen for yeast mutants defective in selective mitochondria autophagy. *Molecular Biology of the Cell, 20*(22), 4730-4738. doi: 10.1091/mbc.E09-03-0225

Karbowski, M., Neutzner, A., & Youle, R. J. (2007). The mitochondrial E3 ubiquitin ligase MARCH5 is required for Drp1 dependent mitochondrial division. *The Journal of Cell Biology, 178*(1), 71-84. doi: 10.1083/jcb.200611064

Karbowski, M., & Youle, R. J. (2011). Regulating mitochondrial outer membrane proteins by ubiquitination and proteasomal degradation. *Current Opinion in Cell Biology, 23*(4), 476-482. doi: 10.1016/j.ceb.2011.05.007

Kim, J., Kundu, M., Viollet, B., & Guan, K. L. (2011). AMPK and mTOR regulate autophagy through direct phosphorylation of Ulk1. *Nature Cell Biology, 13*(2), 132-141. doi: 10.1038/ncb2152

Kim, K. S., Park, D. H., Wessel, T. C., Song, B., Wagner, J. A., & Joh, T. H. (1993). A dual role for the cAMP-dependent protein kinase in tyrosine hydroxylase gene expression. *Proceedings of the National Academy of Sciences of the United States of America, 90*(8), 3471-3475.

Kislin, M., Sword, J., Fomitcheva, I. V., Croom, D., Pryazhnikov, E., Lihavainen, E., . . . Kirov, S. A. (2017). Reversible Disruption of Neuronal Mitochondria by Ischemic and Traumatic Injury Revealed by Quantitative Two-Photon Imaging in the Neocortex of Anesthetized Mice. *The Journal of Neuroscience, 37*(2), 333-348. doi: 10.1523/jneurosci.1510-16.2016

Kitada, T., Pisani, A., Karouani, M., Haburcak, M., Martella, G., Tscherter, A., . . . Shen, J. (2009). Impaired dopamine release and synaptic plasticity in the striatum of parkin-/- mice. *Journal of Neurochemistry, 110*(2), 613-621. doi: 10.1111/j.1471-4159.2009.06152.x

Kitada, T., Pisani, A., Porter, D. R., Yamaguchi, H., Tscherter, A., Martella, G., . . . Shen, J. (2007). Impaired dopamine release and synaptic plasticity in the striatum of PINK1-deficient mice. *Proceedings of the National Academy of Sciences of the United States of America, 104*(27), 11441-11446. doi: 10.1073/pnas.0702717104

Knott, A. B., & Bossy-Wetzel, E. (2008). Impairing the Mitochondrial Fission and Fusion Balance: A New Mechanism of Neurodegeneration. *Annual New York Academy Science, 1147*, 283-292. doi: 10.1196/annals.1427.030

Knott, A. B., Perkins, G., Schwarzenbacher, R., & Bossy-Wetzel, E. (2008). Mitochondrial fragmentation in neurodegeneration. *Nature Reviews Neuroscience, 9*(7), 505-518. doi: 10.1038/nrn2417

Kobayashi, T., & Ikeda, K. (2006). G protein-activated inwardly rectifying potassium channels as potential therapeutic targets. *Current Pharmaceutical Design, 12*(34), 4513-4523.

Koch, A., Yoon, Y., Bonekamp, N. A., McNiven, M. A., & Schrader, M. (2005). A role for Fis1 in both mitochondrial and peroxisomal fission in mammalian cells. *Molecular Biology of the Cell, 16*(11), 5077-5086. doi: 10.1091/mbc.E05-02-0159

Kojima, M., Hamamoto, A., & Sato, T. (2016). Ghrelin O-acyltransferase (GOAT), a specific enzyme that modifies ghrelin with a medium-chain fatty acid. *Journal of Biochemistry, 160*(4), 189-194. doi: 10.1093/jb/mvw046

Kojima, M., Hosoda, H., Date, Y., Nakazato, M., Matsuo, H., & Kangawa, K. (1999). Ghrelin is a growth-hormone-releasing acylated peptide from stomach. *Nature, 402*(6762), 656-660. doi: 10.1038/45230

Korbonits, M., Gueorguiev, M., O'Grady, E., Lecoeur, C., Swan, D. C., Mein, C. A., . . . Froguel, P. (2002). A variation in the ghrelin gene increases weight and decreases insulin secretion in tall, obese children. *Journal of Clinical Endocrinology and Metababolism, 87*(8), 4005-4008. doi: 10.1210/jcem.87.8.8881

Koshiba, T., Detmer, S. A., Kaiser, J. T., Chen, H., McCaffery, J. M., & Chan, D. C. (2004). Structural basis of mitochondrial tethering by mitofusin complexes. *Science, 305*(5685), 858-862. doi: 10.1126/science.1099793

Kumaran, R., & Cookson, M. R. (2015). Pathways to Parkinsonism Redux: convergent pathobiological mechanisms in genetics of Parkinson's disease. *Human Molecular Genetics, 24*(R1), R32-44. doi: 10.1093/hmg/ddv236

Lall, S., Tung, L. Y., Ohlsson, C., Jansson, J. O., & Dickson, S. L. (2001). Growth hormone (GH)-independent stimulation of adiposity by GH secretagogues. *Biochemical and Biophysical Research Communications, 280*(1), 132-138. doi: 10.1006/bbrc.2000.4065

Langston, J. W., Ballard, P., Tetrud, J. W., & Irwin, I. (1983). Chronic Parkinsonism in humans due to a product of meperidine-analog synthesis. *Science, 219*(4587), 979-980.

Lee, J. H., Patel, K., Tae, H. J., Lustig, A., Kim, J. W., Mattson, M. P., & Taub, D. D. (2014). Ghrelin augments murine T-cell proliferation by activation of the phosphatidylinositol-3-kinase, extracellular signal-regulated kinase and

protein kinase C signaling pathways. *FEBS Letters, 588*(24), 4708-4719. doi: 10.1016/j.febslet.2014.10.044

Lee, S., Kim, Y., Li, E., & Park, S. (2012). Ghrelin protects spinal cord motoneurons against chronic glutamate excitotoxicity by inhibiting microglial activation. *Korean Journal of Physiology and Pharmacolology, 16*(1), 43-48. doi: 10.4196/kjpp.2012.16.1.43

Lemasters, J. J., Qian, T., He, L., Kim, J. S., Elmore, S. P., Cascio, W. E., & Brenner, D. A. (2002). Role of mitochondrial inner membrane permeabilization in necrotic cell death, apoptosis, and autophagy. *Antioxidants & Redox Signal, 4*(5), 769-781. doi: 10.1089/152308602760598918

Leung, P. K., Chow, K. B., Lau, P. N., Chu, K. M., Chan, C. B., Cheng, C. H., & Wise, H. (2007). The truncated ghrelin receptor polypeptide (GHS-R1b) acts as a dominant-negative mutant of the ghrelin receptor. *Cell Signalling, 19*(5), 1011-1022. doi: 10.1016/j.cellsig.2006.11.011

Li, B., Zeng, M., Zheng, H., Huang, C., He, W., Lu, G., . . . Xie, R. (2016). Effects of ghrelin on the apoptosis of human neutrophils in vitro *International Journal of Molecular Medicine* (Vol. 38, pp. 794-802).

Li, J., Qi, W., Chen, G., Feng, D., Liu, J., Ma, B., . . . Zhu, Y. (2015). Mitochondrial outer-membrane E3 ligase MUL1 ubiquitinates ULK1 and regulates selenite-induced mitophagy. *Autophagy, 11*(8), 1216-1229. doi: 10.1080/15548627.2015.1017180

Li, J., Uversky, V. N., & Fink, A. L. (2001). Effect of familial Parkinson's disease point mutations A30P and A53T on the structural properties, aggregation, and fibrillation of human alpha-synuclein. *Biochemistry, 40*(38), 11604-11613.

Li, N., Ragheb, K., Lawler, G., Sturgis, J., Rajwa, B., Melendez, J. A., & Robinson, J. P. (2003). Mitochondrial complex I inhibitor rotenone induces apoptosis through enhancing mitochondrial reactive oxygen species production. *Journal of Biological Chemistry, 278*(10), 8516-8525. doi: 10.1074/jbc.M210432200

Liang, C. L., Sinton, C. M., & German, D. C. (1996). Midbrain dopaminergic neurons in the mouse: co-localization with Calbindin-D28K and calretinin. *Neuroscience, 75*(2), 523-533.

Lin, M. T., & Beal, M. F. (2006). Mitochondrial dysfunction and oxidative stress in neurodegenerative diseases. *Nature, 443*(7113), 787-795. doi: 10.1038/nature05292

Liu, L., Xu, H., Jiang, H., Wang, J., Song, N., & Xie, J. (2010). Ghrelin prevents 1-methyl-4-phenylpyridinium ion-induced cytotoxicity through antioxidation and NF-kappaB modulation in MES23.5 cells. *Experimental Neurology, 222*(1), 25-29. doi: 10.1016/j.expneurol.2009.11.009

Liu, S., Sawada, T., Lee, S., Yu, W., Silverio, G., Alapatt, P., . . . Lu, B. (2012). Parkinson's disease-associated kinase PINK1 regulates Miro protein level and axonal transport of mitochondria. *PLoS Genetics, 8*(3), e1002537. doi: 10.1371/journal.pgen.1002537

Liu, X., Kim, C. N., Yang, J., Jemmerson, R., & Wang, X. (1996). Induction of apoptotic program in cell-free extracts: requirement for dATP and cytochrome c. *Cell, 86*(1), 147-157.

Longo, V. D., & Mattson, M. P. (2014). Fasting: molecular mechanisms and clinical applications. *Cell Metabolism, 19*(2), 181-192. doi: 10.1016/j.cmet.2013.12.008

Loson, O. C., Song, Z., Chen, H., & Chan, D. C. (2013). Fis1, Mff, MiD49, and MiD51 mediate Drp1 recruitment in mitochondrial fission. *Molecular Biology of the Cell, 24*(5), 659-667. doi: 10.1091/mbc.E12-10-0721

Lucking, C. B., Durr, A., Bonifati, V., Vaughan, J., De Michele, G., Gasser, T., . . . Brice, A. (2000). Association between early-onset Parkinson's disease and mutations in the parkin gene. *N Engl J Med, 342*(21), 1560-1567. doi: 10.1056/nejm200005253422103

Luscher, C., & Slesinger, P. A. (2010). Emerging roles for G protein-gated inwardly rectifying potassium (GIRK) channels in health and disease. *Nature Reviews Neuroscience, 11*(5), 301-315. doi: 10.1038/nrn2834

Lutter, M., Sakata, I., Osborne-Lawrence, S., Rovinsky, S. A., Anderson, J. G., Jung, S., . . . Zigman, J. M. (2008). The orexigenic hormone ghrelin defends against depressive symptoms of chronic stress. *Nature Neuroscience, 11*(7), 752-753. doi: 10.1038/nn.2139

Manoharan, S., Guillemin, G. J., Abiramasundari, R. S., Essa, M. M., Akbar, M., & Akbar, M. D. (2016). The Role of Reactive Oxygen Species in the Pathogenesis of Alzheimer's Disease, Parkinson's Disease, and Huntington's Disease: A Mini Review. *Oxidative Medicine and Cell Longevity, 2016*, 8590578. doi: 10.1155/2016/8590578

Marcillat, O., Zhang, Y., Lin, S. W., & Davies, K. J. (1988). Mitochondria contain a proteolytic system which can recognize and degrade oxidatively-denatured proteins. *The Biochemical Journal, 254*(3), 677-683.

Maroteaux, L., Campanelli, J. T., & Scheller, R. H. (1988). Synuclein: a neuron-specific protein localized to the nucleus and presynaptic nerve terminal. *Journal of Neuroscience, 8*(8), 2804-2815.

Maroteaux, L., & Scheller, R. H. (1991). The rat brain synucleins; family of proteins transiently associated with neuronal membrane. *Brain Research. Molecular Brain Research, 11*(3-4), 335-343.

McCarthy, S., Somayajulu, M., Sikorska, M., Borowy-Borowski, H., & Pandey, S. (2004). Paraquat induces oxidative stress and neuronal cell death; neuroprotection by water-soluble Coenzyme Q10. *Toxicology and Applied Pharmacology, 201*(1), 21-31. doi: 10.1016/j.taap.2004.04.019

McLelland, G. L., Soubannier, V., Chen, C. X., McBride, H. M., & Fon, E. A. (2014). Parkin and PINK1 function in a vesicular trafficking pathway regulating mitochondrial quality control. *The Embo Journal, 33*(4), 282-295. doi: 10.1002/embj.201385902

McRitchie, D. A., Hardman, C. D., & Halliday, G. M. (1996). Cytoarchitectural distribution of calcium binding proteins in midbrain dopaminergic regions of rats and humans. *The Journal of Comparative Neurology, 364*(1), 121-150. doi: 10.1002/(SICI)1096-9861(19960101)364:1<121::AID-CNE11>3.0.CO;2-1

Meeusen, S., DeVay, R., Block, J., Cassidy-Stone, A., Wayson, S., McCaffery, J. M., & Nunnari, J. (2006). Mitochondrial inner-membrane fusion and crista maintenance requires the dynamin-related GTPase Mgm1. *Cell, 127*(2), 383-395. doi: 10.1016/j.cell.2006.09.021

Meglasson, M. D., Wilson, J. M., Yu, J. H., Robinson, D. D., Wyse, B. M., & de Souza, C. J. (1993). Antihyperglycemic action of guanidinoalkanoic acids: 3-guanidinopropionic acid ameliorates hyperglycemia in diabetic KKAy and C57BL6Job/ob mice and increases glucose disappearance in rhesus monkeys. *Journal of Pharmacol Experimental Therapeutics, 266*(3), 1454-1462.

Mehta, S. L., & Li, P. A. (2009). Neuroprotective role of mitochondrial uncoupling protein 2 in cerebral stroke. *Journal of Cerebral Blood Flow and Metabolism, 29*(6), 1069-1078. doi: 10.1038/jcbfm.2009.4

Mendivil-Perez, M., Velez-Pardo, C., & Jimenez-Del-Rio, M. (2016). Neuroprotective Effect of the LRRK2 Kinase Inhibitor PF-06447475 in Human Nerve-Like Differentiated Cells Exposed to Oxidative Stress Stimuli: Implications for Parkinson's Disease. *Neurochemical Research, 41*(10), 2675-2692. doi: 10.1007/s11064-016-1982-1

Meng, S., Cao, J., He, Q., Xiong, L., Chang, E., Radovick, S., . . . He, L. (2015). Metformin activates AMP-activated protein kinase by promoting formation of the alphabetagamma heterotrimeric complex. *Journal of Biological Chemistry, 290*(6), 3793-3802. doi: 10.1074/jbc.M114.604421

Menzies, J. R., Skibicka, K. P., Leng, G., & Dickson, S. L. (2013). Ghrelin, reward and motivation. *Endocrine Development, 25*, 101-111. doi: 10.1159/000346058

Meredith, G. E., & Rademacher, D. J. (2011). MPTP Mouse Models of Parkinson's Disease: An Update. *Journal Parkinson's Disease, 1*(1), 19-33. doi: 10.3233/jpd-2011-11023

Miklya, I., Goltl, P., Hafenscher, F., & Pencz, N. (2014). [The role of parkin in Parkinson's disease]. *Neuropsychopharmacologia Hungary, 16*(2), 67-76.

Mishra, P., & Chan, D. C. (2014). Mitochondrial dynamics and inheritance during cell division, development and disease. *Nature Reviews Molecular Cell Biology, 15*(10), 634-646. doi: 10.1038/nrm3877

Misko, A., Jiang, S., Wegorzewska, I., Milbrandt, J., & Baloh, R. H. (2010). Mitofusin 2 is necessary for transport of axonal mitochondria and interacts with the Miro/Milton complex. *The Journal of Neuroscience, 30*(12), 4232-4240. doi: 10.1523/jneurosci.6248-09.2010

Mitchell, P. (1961). Coupling of phosphorylation to electron and hydrogen transfer by a chemi-osmotic type of mechanism. *Nature, 191*, 144-148.

Mizushima, N. (2009). Methods for monitoring autophagy using GFP-LC3 transgenic mice. *Methods in Enzymology, 452*, 13-23. doi: 10.1016/s0076-6879(08)03602-1

Moon, M., Kim, H. G., Hwang, L., Seo, J. H., Kim, S., Hwang, S., . . . Park, S. (2009). Neuroprotective effect of ghrelin in the 1-methyl-4-phenyl-1,2,3,6-tetrahydropyridine mouse model of Parkinson's disease by blocking microglial activation. *Neurotoxicity Research, 15*(4), 332-347. doi: 10.1007/s12640-009-9037-x

Moon, Y., Lee, K. H., Park, J. H., Geum, D., & Kim, K. (2005). Mitochondrial membrane depolarization and the selective death of dopaminergic neurons by rotenone: protective effect of coenzyme Q10. *Journal of Neurochemistry, 93*(5), 1199-1208. doi: 10.1111/j.1471-4159.2005.03112.x

Moreira, P. I., Carvalho, C., Zhu, X., Smith, M. A., & Perry, G. (2010). Mitochondrial dysfunction is a trigger of Alzheimer's disease pathophysiology. *Biochimca et Biophysica Acta, 1802*(1), 2-10. doi: 10.1016/j.bbadis.2009.10.006

Moulin, A., Demange, L., Berge, G., Gagne, D., Ryan, J., Mousseaux, D., . . . Martinez, J. (2007). Toward potent ghrelin receptor ligands based on trisubstituted 1,2,4-triazole structure. 2. Synthesis and pharmacological in vitro and in vivo evaluations. *Journal of Medicinal Chemistry, 50*(23), 5790-5806. doi: 10.1021/jm0704550

Muller, T. D., Tschop, M. H., Jarick, I., Ehrlich, S., Scherag, S., Herpertz-Dahlmann, B., . . . Hinney, A. (2011). Genetic variation of the ghrelin activator gene ghrelin O-acyltransferase (GOAT) is associated with anorexia nervosa. *Journal of Psychiatric Research, 45*(5), 706-711. doi: 10.1016/j.jpsychires.2010.10.001

Narayan, S., Liew, Z., Bronstein, J. M., & Ritz, B. (2017). Occupational pesticide use and Parkinson's disease in the Parkinson Environment Gene (PEG) study. *Environ Int, 107*, 266-273. doi: 10.1016/j.envint.2017.04.010

Narendra, D. P., Jin, S. M., Tanaka, A., Suen, D. F., Gautier, C. A., Shen, J., . . . Youle, R. J. (2010). PINK1 is selectively stabilized on impaired mitochondria to activate Parkin. *PLoS Biology, 8*(1), e1000298. doi: 10.1371/journal.pbio.1000298

Nataraj, J., Manivasagam, T., Thenmozhi, J. A., & Essa, M. M. (2017). Neuroprotective effect of asiatic acid on rotenone-induced mitochondrial dysfunction and oxidative stress-mediated apoptosis in differentiated SH-SYS5Y cells. *Nutritional Neuroscience, 20*(6), 351-359. doi: 10.1080/1028415x.2015.1135559

Ng, C. H., Guan, M. S., Koh, C., Ouyang, X., Yu, F., Tan, E. K., . . . Lim, K. L. (2012). AMP kinase activation mitigates dopaminergic dysfunction and mitochondrial abnormalities in Drosophila models of Parkinson's disease. *Journal of Neuroscience, 32*(41), 14311-14317. doi: 10.1523/jneurosci.0499-12.2012

Ni, H. M., Williams, J. A., & Ding, W. X. (2015). Mitochondrial dynamics and mitochondrial quality control. *Redox Biology, 4*, 6-13. doi: 10.1016/j.redox.2014.11.006

Nicholls, D. G. (2004). Mitochondrial membrane potential and aging. *Aging Cell, 3*(1), 35-40.

Niswender, C. M., Johnson, K. A., Luo, Q., Ayala, J. E., Kim, C., Conn, P. J., & Weaver, C. D. (2008). A novel assay of Gi/o-linked G protein-coupled receptor coupling to potassium channels provides new insights into the pharmacology of the group III metabotropic glutamate receptors. *Molecular Pharmacology, 73*(4), 1213-1224. doi: 10.1124/mol.107.041053

O'Neill, H. M., Maarbjerg, S. J., Crane, J. D., Jeppesen, J., Jorgensen, S. B., Schertzer, J. D., . . . Steinberg, G. R. (2011). AMP-activated protein kinase (AMPK) beta1beta2 muscle null mice reveal an essential role for AMPK in maintaining mitochondrial content and glucose uptake during exercise. *Proceedings of the National Academy of Sciences of the United States of America, 108*(38), 16092-16097. doi: 10.1073/pnas.1105062108

Okamoto, K., & Shaw, J. M. (2005). Mitochondrial morphology and dynamics in yeast and multicellular eukaryotes. *Annual Review of Genetics, 39*, 503-536. doi: 10.1146/annurev.genet.38.072902.093019

Olanow, C. W., & Brundin, P. (2013). Parkinson's disease and alpha synuclein: is Parkinson's disease a prion-like disorder? *Movement Disorders, 28*(1), 31-40. doi: 10.1002/mds.25373

Orvedahl, A., Sumpter, R., Jr., Xiao, G., Ng, A., Zou, Z., Tang, Y., . . . Levine, B. (2011). Image-based genome-wide siRNA screen identifies selective autophagy factors. *Nature, 480*(7375), 113-117. doi: 10.1038/nature10546

Otera, H., Wang, C., Cleland, M. M., Setoguchi, K., Yokota, S., Youle, R. J., & Mihara, K. (2010). Mff is an essential factor for mitochondrial recruitment of Drp1 during mitochondrial fission in mammalian cells. *The Journal of Cell Biology, 191*(6), 1141-1158. doi: 10.1083/jcb.201007152

Otsu, N. (1979). *A threshold selection method from gray level histograms.* 9, from http://ieeexplore.ieee.org/stamp/stamp.jsp?arnumber=4310076

Ott, M., Robertson, J. D., Gogvadze, V., Zhivotovsky, B., & Orrenius, S. (2002). Cytochrome c release from mitochondria proceeds by a two-step process. *Proceedings of the National Academy of Sciences of the United States of America, 99*(3), 1259-1263. doi: 10.1073/pnas.241655498

Padmanabhan, K., Eddy, W. F., & Crowley, J. C. (2010). A novel algorithm for optimal image thresholding of biological data. *Journal of Neuroscience Methods, 193*(2), 380-384. doi: 10.1016/j.jneumeth.2010.08.031

Paisan-Ruiz, C., Jain, S., Evans, E. W., Gilks, W. P., Simon, J., van der Brug, M., . . . Singleton, A. B. (2004). Cloning of the gene containing mutations that cause PARK8-linked Parkinson's disease. *Neuron, 44*(4), 595-600. doi: 10.1016/j.neuron.2004.10.023

Palmer, C. S., Osellame, L. D., Laine, D., Koutsopoulos, O. S., Frazier, A. E., & Ryan, M. T. (2011). MiD49 and MiD51, new components of the mitochondrial fission machinery. *EMBO Reports, 12*(6), 565-573. doi: 10.1038/embor.2011.54

Pan, P. K., Qiao, L. Y., & Wen, X. N. (2016). Safranal prevents rotenone-induced oxidative stress and apoptosis in an in vitro model of Parkinson's disease through regulating Keap1/Nrf2 signaling pathway. *Cellular and Molecular Biology (Noisy-le-grand), 62*(14), 11-17. doi: 10.14715/cmb/ 2016.62.14.2

Pankratz, N., Pauciulo, M. W., Elsaesser, V. E., Marek, D. K., Halter, C. A., Wojcieszek, J., . . . Nichols, W. C. (2006). Mutations in DJ-1 are rare in familial Parkinson disease. *Neurosci Lett, 408*(3), 209-213. doi: 10.1016/j.neulet.2006.09.003

Park, J., Lee, S. B., Lee, S., Kim, Y., Song, S., Kim, S., . . . Chung, J. (2006). Mitochondrial dysfunction in Drosophila PINK1 mutants is complemented by parkin *Nature* (Vol. 441, pp. 1157-1161). England.

Passmore, J. B., Pinho, S., Gomez-Lazaro, M., & Schrader, M. (2017). The respiratory chain inhibitor rotenone affects peroxisomal dynamics via its microtubule-destabilising activity *Histochemistry and Cell Biology* (Vol. 148, pp. 331-341).

Pazos, Y., Casanueva, F. F., & Camina, J. P. (2008). Basic aspects of ghrelin action. *Vitamins Hormones, 77*, 89-119. doi: 10.1016/s0083-6729(06)77005-4

Pekkurnaz, G., Trinidad, J. C., Wang, X., Kong, D., & Schwarz, T. L. (2014). Glucose regulates mitochondrial motility via Milton modification by O-GlcNAc transferase. *Cell, 158*(1), 54-68. doi: 10.1016/j.cell.2014.06.007

Perry, S. W., Norman, J. P., Barbieri, J., Brown, E. B., & Gelbard, H. A. (2011). Mitochondrial membrane potential probes and the proton gradient: a practical usage guide. *Biotechniques, 50*(2), 98-115. doi: 10.2144/000113610

Pettersson, I., Muccioli, G., Granata, R., Deghenghi, R., Ghigo, E., Ohlsson, C., & Isgaard, J. (2002). Natural (ghrelin) and synthetic (hexarelin) GH secretagogues stimulate H9c2 cardiomyocyte cell proliferation. *Journal of Endocrinology, 175*(1), 201-209.

Pickrell, A. M., & Youle, R. J. (2015). The roles of PINK1, parkin, and mitochondrial fidelity in Parkinson's disease. *Neuron, 85*(2), 257-273. doi: 10.1016/j.neuron.2014.12.007

Pieczenik, S. R., & Neustadt, J. (2007). Mitochondrial dysfunction and molecular pathways of disease. *Experimental Molecular Pathology, 83*(1), 84-92. doi: 10.1016/j.yexmp.2006.09.008

Pirkevi, C., Lesage, S., Brice, A., & Basak, A. N. (2009). From genes to proteins in mendelian Parkinson's disease: an overview. *Anatomical Record (Hoboken), 292*(12), 1893-1901. doi: 10.1002/ar.20968

Polymeropoulos, M. H., Lavedan, C., Leroy, E., Ide, S. E., Dehejia, A., Dutra, A., . . . Nussbaum, R. L. (1997). Mutation in the alpha-synuclein gene identified in families with Parkinson's disease. *Science, 276*(5321), 2045-2047.

Pradidarcheep, W., Stallen, J., Labruyere, W. T., Dabhoiwala, N. F., Michel, M. C., & Lamers, W. H. (2009). Lack of specificity of commercially available antisera against muscarinergic and adrenergic receptors. *Naunyn-Schmiedebergs Archives of Pharmacology, 379*(4), 397-402. doi: 10.1007/s00210-009-0393-0

Praefcke, G. J., & McMahon, H. T. (2004). The dynamin superfamily: universal membrane tubulation and fission molecules? *Nature Reviews Molecular Cell Biology, 5*(2), 133-147. doi: 10.1038/nrm1313

Price, N. L., Gomes, A. P., Ling, A. J., Duarte, F. V., Martin-Montalvo, A., North, B. J., . . . Sinclair, D. A. (2012). SIRT1 is required for AMPK activation and the beneficial effects of resveratrol on mitochondrial function. *Cell Metabolism, 15*(5), 675-690. doi: 10.1016/j.cmet.2012.04.003

Przedborski, S., Jackson-Lewis, V., Djaldetti, R., Liberatore, G., Vila, M., Vukosavic, S., & Almer, G. (2000). The parkinsonian toxin MPTP: action and mechanism. *Restorative Neurology and Neuroscience, 16*(2), 135-142.

Quintanilla, R. A., & Johnson, G. V. (2009). Role of mitochondrial dysfunction in the pathogenesis of Huntington's disease. *Brain Research Bullitin, 80*(4-5), 242-247. doi: 10.1016/j.brainresbull.2009.07.010

Rajesh, P., & Kelly, E. L. (2007). *Handbook of Parkinson's Disease, Fourth Edition* (4 ed. Vol. 4): Informa.

Ramirez, A., Heimbach, A., Grundemann, J., Stiller, B., Hampshire, D., Cid, L. P., . . . Kubisch, C. (2006). Hereditary parkinsonism with dementia is caused by mutations in ATP13A2, encoding a lysosomal type 5 P-type ATPase. *Nature Genetics, 38*(10), 1184-1191. doi: 10.1038/ng1884

Rana, A., Oliveira, M. P., Khamoui, A. V., Aparicio, R., Rera, M., Rossiter, H. B., & Walker, D. W. (2017). Promoting Drp1-mediated mitochondrial fission in midlife prolongs healthy lifespan of Drosophila melanogaster. *Nature Communications, 8*(1), 448. doi: 10.1038/s41467-017-00525-4

Ravi, S. K., Narasingappa, R. B., Joshi, C. G., Girish, T. K., & Vincent, B. (2017). Neuroprotective effects of Cassia tora against paraquat-induced

neurodegeneration: relevance for Parkinson's disease. *Natural Products Research*, 1-5. doi: 10.1080/14786419.2017.1353504

Reyes, S., Fu, Y., Double, K., Thompson, L., Kirik, D., Paxinos, G., & Halliday, G. M. (2012). GIRK2 expression in dopamine neurons of the substantia nigra and ventral tegmental area. *The Journal of Comparative Neurology, 520*(12), 2591-2607. doi: 10.1002/cne.23051

Reznick, R. M., & Shulman, G. I. (2006). The role of AMP-activated protein kinase in mitochondrial biogenesis. *Journal of Physiology, 574*(Pt 1), 33-39. doi: 10.1113/jphysiol.2006.109512

Rogers, J. H. (1992). Immunohistochemical markers in rat brain: colocalization of calretinin and calbindin-D28k with tyrosine hydroxylase. *Brain Research, 587*(2), 203-210.

Rogers, K. (2017). *G protein-coupled receptor (GPCR)* | *biochemistry.* from https://www.britannica.com/science/G-protein-coupled-receptor

Sakamuru, S., Attene-Ramos, M. S., & Xia, M. (2016). Mitochondrial Membrane Potential Assay. *Methods in Molecular Biology, 1473*, 17-22. doi: 10.1007/978-1-4939-6346-1_2

Samardzic, K., & Rodgers, K. J. (2017). Oxidised protein metabolism: recent insights. *Biol Chem* doi: 10.1515/hsz-2017-0124

Sanchis-Gomar, F., Garcia-Gimenez, J. L., Gomez-Cabrera, M. C., & Pallardo, F. V. (2014). Mitochondrial biogenesis in health and disease. Molecular and therapeutic approaches. *Current Pharmaceutical Design, 20*(35), 5619-5633.

Satou, M., Nishi, Y., Yoh, J., Hattori, Y., & Sugimoto, H. (2010). Identification and characterization of acyl-protein thioesterase 1/lysophospholipase I as a ghrelin deacylation/lysophospholipid hydrolyzing enzyme in fetal bovine serum and conditioned medium. *Endocrinology, 151*(10), 4765-4775. doi: 10.1210/en.2010-0412

Scarpulla, R. C. (2011). Metabolic control of mitochondrial biogenesis through the PGC-1 family regulatory network. *Biochimca et Biophysica Acta, 1813*(7), 1269-1278. doi: 10.1016/j.bbamcr.2010.09.019

Schapira, A. H. (2007). Future directions in the treatment of Parkinson's disease. *Movement Disorders, 22 Suppl 17*, S385-391. doi: 10.1002/mds.21679

Schein, J. C., Hunter, D. D., & Roffler-Tarlov, S. (1998). Girk2 expression in the ventral midbrain, cerebellum, and olfactory bulb and its relationship to the murine mutation weaver. *Developmental Biology, 204*(2), 432-450. doi: 10.1006/dbio.1998.9076

Schwarz, T. L. (2013). Mitochondrial trafficking in neurons. *Cold Spring Harbor Perspectives in Biology, 5*(6) doi: 10.1101/cshperspect.a011304

Seoposengwe, K., van Tonder, J. J., & Steenkamp, V. (2013). In vitro neuroprotective potential of four medicinal plants against rotenone-induced toxicity in SH-SY5Y neuroblastoma cells. *BMC Complementary and Alternative Medicine, 13*, 353. doi: 10.1186/1472-6882-13-353

Sepulveda, B., Mesias, R., Li, X., Yue, Z., & Benson, D. L. (2013). Short- and long-term effects of LRRK2 on axon and dendrite growth. *PLoS One, 8*(4), e61986. doi: 10.1371/journal.pone.0061986

Sezgin, M., & Sankur, B. (2004). Survey over image thresholding techniques and quantitative performance evaluation. *Journal of Electronic Imaging, 13*(1), 146-166. doi: 10.1117/1.1631315

Sha, D., Chin, L. S., & Li, L. (2010). Phosphorylation of parkin by Parkinson disease-linked kinase PINK1 activates parkin E3 ligase function and NF-kappaB signaling. *Human Molecular Genetics, 19*(2), 352-363. doi: 10.1093/hmg/ddp501

Shariff, A., Kangas, J., Coelho, L. P., Quinn, S., & Murphy, R. F. (2010). Automated image analysis for high-content screening and analysis. *Journal of Biomolecular Screening, 15*(7), 726-734. doi: 10.1177/1087057110370894

Sherer, T. B., Kim, J. H., Betarbet, R., & Greenamyre, J. T. (2003). Subcutaneous rotenone exposure causes highly selective dopaminergic degeneration and alpha-synuclein aggregation. *Experimental Neurology, 179*(1), 9-16.

Shi, R. Y., Zhu, S. H., Li, V., Gibson, S. B., Xu, X. S., & Kong, J. M. (2014). BNIP3 interacting with LC3 triggers excessive mitophagy in delayed neuronal death in stroke. *CNS Neuroscience & Therapeutics, 20*(12), 1045-1055. doi: 10.1111/cns.12325

Shimura, H., Hattori, N., Kubo, S., Mizuno, Y., Asakawa, S., Minoshima, S., . . . Suzuki, T. (2000). Familial Parkinson disease gene product, parkin, is a ubiquitin-protein ligase. *Nat Genet, 25*(3), 302-305. doi: 10.1038/77060

Shin, J. H., Ko, H. S., Kang, H., Lee, Y., Lee, Y. I., Pletinkova, O., . . . Dawson, T. M. (2011). PARIS (ZNF746) repression of PGC-1alpha contributes to neurodegeneration in Parkinson's disease. *Cell, 144*(5), 689-702. doi: 10.1016/j.cell.2011.02.010

Simola, N., Morelli, M., & Carta, A. R. (2007). The 6-hydroxydopamine model of Parkinson's disease. *Neurotoxicity Research, 11*(3-4), 151-167.

Slomiany, B. L., & Slomiany, A. (2014). Role of ghrelin-induced phosphatidylinositol 3-kinase activation in modulation of gastric mucosal inflammatory responses

to Helicobacter pylori. *Inflammopharmacology, 22*(3), 169-177. doi: 10.1007/s10787-013-0190-8

Smirnova, E., Griparic, L., Shurland, D. L., & van der Bliek, A. M. (2001). Dynamin-related protein Drp1 is required for mitochondrial division in mammalian cells. *Molecular Biology of the Cell, 12*(8), 2245-2256.

Smith, R. G., Palyha, O. C., Feighner, S. D., Tan, C. P., McKee, K. K., Hreniuk, D. L., . . . Howard, A. D. (1999). Growth hormone releasing substances: types and their receptors. *Hormone Research, 51 Suppl 3*, 1-8. doi: 44375

Son, J. H., Chun, H. S., Joh, T. H., Cho, S., Conti, B., & Lee, J. W. (1999). Neuroprotection and neuronal differentiation studies using substantia nigra dopaminergic cells derived from transgenic mouse embryos. *Journal of Neuroscience, 19*(1), 10-20.

Song, Z., Chen, H., Fiket, M., Alexander, C., & Chan, D. C. (2007). OPA1 processing controls mitochondrial fusion and is regulated by mRNA splicing, membrane potential, and Yme1L. *The Journal of Cell Biology, 178*(5), 749-755. doi: 10.1083/jcb.200704110

Song, Z., Ghochani, M., McCaffery, J. M., Frey, T. G., & Chan, D. C. (2009). Mitofusins and OPA1 mediate sequential steps in mitochondrial membrane fusion. *Molecular Biology of the Cell, 20*(15), 3525-3532. doi: 10.1091/mbc.E09-03-0252

Sonia Angeline, M., Chaterjee, P., Anand, K., Ambasta, R. K., & Kumar, P. (2012). Rotenone-induced parkinsonism elicits behavioral impairments and differential expression of parkin, heat shock proteins and caspases in the rat. *Neuroscience, 220*, 291-301. doi: 10.1016/j.neuroscience.2012.06.021

Soubannier, V., McLelland, G. L., Zunino, R., Braschi, E., Rippstein, P., Fon, E. A., & McBride, H. M. (2012). A vesicular transport pathway shuttles cargo from mitochondria to lysosomes. *Current Biology, 22*(2), 135-141. doi: 10.1016/j.cub.2011.11.057

Stefanis, L. (2012). α-Synuclein in Parkinson's Disease *Cold Spring Harbor Perspectives in Biology* (Vol. 2).

Stocco, A., Lebiere, C., & Anderson, J. R. (2010). Conditional routing of information to the cortex: a model of the basal ganglia's role in cognitive coordination. *Psychological Review, 117*(2), 541-574. doi: 10.1037/a0019077

Storch, A., Kaftan, A., Burkhardt, K., & Schwarz, J. (2000). 6-Hydroxydopamine toxicity towards human SH-SY5Y dopaminergic neuroblastoma cells: independent of mitochondrial energy metabolism. *Journal of Neural Transmission (Vienna), 107*(3), 281-293. doi: 10.1007/s007020050023

Swarnkar, S., Goswami, P., Kamat, P. K., Patro, I. K., Singh, S., & Nath, C. (2013). Rotenone-induced neurotoxicity in rat brain areas: a study on neuronal and neuronal supportive cells. *Neuroscience, 230*, 172-183. doi: 10.1016/j.neuroscience.2012.10.034

Tagaya, M., & Arasaki, K. (2017). Regulation of Mitochondrial Dynamics and Autophagy by the Mitochondria-Associated Membrane. *Advances in Experimental Medicine and Biology, 997*, 33-47. doi: 10.1007/978-981-10-4567-7_3

Taguchi, N., Ishihara, N., Jofuku, A., Oka, T., & Mihara, K. (2007). Mitotic phosphorylation of dynamin-related GTPase Drp1 participates in mitochondrial fission. *The Journal of Biology and Chemistry, 282*(15), 11521-11529. doi: 10.1074/jbc.M607279200

Takahashi, K., Tanabe, K., Ohnuki, M., Narita, M., Ichisaka, T., Tomoda, K., & Yamanaka, S. (2007). Induction of pluripotent stem cells from adult human fibroblasts by defined factors. *Cell, 131*(5), 861-872. doi: 10.1016/j.cell.2007.11.019

Takahashi, K., & Yamanaka, S. (2006). Induction of pluripotent stem cells from mouse embryonic and adult fibroblast cultures by defined factors. *Cell, 126*(4), 663-676. doi: 10.1016/j.cell.2006.07.024

Takayama, S., Xie, Z., & Reed, J. C. (1999). An evolutionarily conserved family of Hsp70/Hsc70 molecular chaperone regulators. *Journal of Biological Chemistry, 274*(2), 781-786.

Tang, Y., & Zucker, R. S. (1997). Mitochondrial involvement in post-tetanic potentiation of synaptic transmission. *Neuron, 18*(3), 483-491.

Tanida, I., Ueno, T., & Kominami, E. (2008). LC3 and Autophagy. *Methods Molecular Biology, 445*, 77-88. doi: 10.1007/978-1-59745-157-4_4

Tanner, C. M., Kamel, F., Ross, G. W., Hoppin, J. A., Goldman, S. M., Korell, M., . . . Langston, J. W. (2011). Rotenone, Paraquat, and Parkinson's Disease *Environmental Health Perspectives* (Vol. 119, pp. 866-872).

Testa, C. M., Sherer, T. B., & Greenamyre, J. T. (2005). Rotenone induces oxidative stress and dopaminergic neuron damage in organotypic substantia nigra cultures. *Brain Research. Molecular Brain Research, 134*(1), 109-118. doi: 10.1016/j.molbrainres.2004.11.007

Thomas, G. M., & Huganir, R. L. (2004). MAPK cascade signalling and synaptic plasticity. *Nature Reviews Neuroscience, 5*(3), 173-183. doi: 10.1038/nrn1346

Thompson, L., Barraud, P., Andersson, E., Kirik, D., & Bjorklund, A. (2005). Identification of dopaminergic neurons of nigral and ventral tegmental area subtypes in grafts of fetal ventral mesencephalon based on cell morphology, protein expression, and efferent projections. *Journal of Neuroscience, 25*(27), 6467-6477. doi: 10.1523/jneurosci.1676-05.2005

Toyama, E. Q., Herzig, S., Courchet, J., Lewis, T. L., Losón, O. C., Hellberg, K., . . . Shaw, R. J. (2016). AMP-activated protein kinase mediates mitochondrial fission in response to energy stress. *Science, 351*(6270), 275-281. doi: 10.1126/science.aab4138

Treberg, J. R., Quinlan, C. L., & Brand, M. D. (2011). Evidence for two sites of superoxide production by mitochondrial NADH-ubiquinone oxidoreductase (complex I). *Journal of Biological Chemistry, 286*(31), 27103-27110. doi: 10.1074/jbc.M111.252502

Tschop, M., Smiley, D. L., & Heiman, M. L. (2000). Ghrelin induces adiposity in rodents. *Nature, 407*(6806), 908-913. doi: 10.1038/35038090

Twig, G., Elorza, A., Molina, A. J., Mohamed, H., Wikstrom, J. D., Walzer, G., . . . Shirihai, O. S. (2008). Fission and selective fusion govern mitochondrial segregation and elimination by autophagy. *Embo j, 27*(2), 433-446. doi: 10.1038/sj.emboj.7601963

Udd, M., Lyytinen, J., Eerola-Rautio, J., Kenttamies, A., Lindstrom, O., Kylanpaa, L., & Pekkonen, E. (2017). Problems related to levodopa-carbidopa intestinal gel treatment in advanced Parkinson's disease. *Brain and Behaviour, 7*(7), e00737. doi: 10.1002/brb3.737

Ueda, K., Fukushima, H., Masliah, E., Xia, Y., Iwai, A., Yoshimoto, M., . . . Saitoh, T. (1993). Molecular cloning of cDNA encoding an unrecognized component of amyloid in Alzheimer disease. *Proceedings of the National Academy of Sciences for the United States of America, 90*(23), 11282-11286.

Valente, E. M., Abou-Sleiman, P. M., Caputo, V., Muqit, M. M., Harvey, K., Gispert, S., . . . Wood, N. W. (2004). Hereditary early-onset Parkinson's disease caused by mutations in PINK1. *Science, 304*(5674), 1158-1160. doi: 10.1126/science.1096284

Valero, T. (2014). Mitochondrial biogenesis: pharmacological approaches. *Current Pharmaceutical Design, 20*(35), 5507-5509.

Van Den Eeden, S. K., Tanner, C. M., Bernstein, A. L., Fross, R. D., Leimpeter, A., Bloch, D. A., & Nelson, L. M. (2003). Incidence of Parkinson's disease: variation by age, gender, and race/ethnicity. *American Journal of Epidemiology, 157*(11), 1015-1022.

Ventorp, F., Bay-Richter, C., Nagendra, A. S., Janelidze, S., Matsson, V. S., Lipton, J., . . . Brundin, L. (2017). Exendin-4 Treatment Improves LPS-Induced Depressive-Like Behavior Without Affecting Pro-Inflammatory Cytokines. *J Parkinsons Dis, 7*(2), 263-273. doi: 10.3233/jpd-171068

Vives-Bauza, C., Zhou, C., Huang, Y., Cui, M., de Vries, R. L., Kim, J., . . . Przedborski, S. (2010). PINK1-dependent recruitment of Parkin to mitochondria in mitophagy. *Proceedings of the National Academy of Sciences of the United States of America, 107*(1), 378-383. doi: 10.1073/pnas.0911187107

Vucicevic, L., Misirkic, M., Janjetovic, K., Vilimanovich, U., Sudar, E., Isenovic, E., . . . Trajkovic, V. (2011). Compound C induces protective autophagy in cancer cells through AMPK inhibition-independent blockade of Akt/mTOR pathway. *Autophagy, 7*(1), 40-50.

Wahlqvist, M. L., Lee, M. S., Hsu, C. C., Chuang, S. Y., Lee, J. T., & Tsai, H. N. (2012). Metformin-inclusive sulfonylurea therapy reduces the risk of Parkinson's disease occurring with Type 2 diabetes in a Taiwanese population cohort. *Parkinsonism Related Disorders, 18*(6), 753-758. doi: 10.1016/j.parkreldis.2012.03.010

Wai, T., & Langer, T. (2016). Mitochondrial Dynamics and Metabolic Regulation. *Trends Endocrinology and Metabolism, 27*(2), 105-117. doi: 10.1016/j.tem.2015.12.001

Wang, H. J., Geller, F., Dempfle, A., Schauble, N., Friedel, S., Lichtner, P., . . . Hinney, A. (2004). Ghrelin receptor gene: identification of several sequence variants in extremely obese children and adolescents, healthy normal-weight and underweight students, and children with short normal stature. *Journal of Clinical Endocrinology and Metababolism, 89*(1), 157-162. doi: 10.1210/jc.2003-031395

Wang, X., Winter, D., Ashrafi, G., Schlehe, J., Wong, Y. L., Selkoe, D., . . . Schwarz, T. L. (2011). PINK1 and Parkin target Miro for phosphorylation and degradation to arrest mitochondrial motility. *Cell, 147*(4), 893-906. doi: 10.1016/j.cell.2011.10.018

Waseem, T., Duxbury, M., Ashley, S. W., & Robinson, M. K. (2014). Ghrelin promotes intestinal epithelial cell proliferation through PI3K/Akt pathway and EGFR trans-activation both converging to ERK 1/2 phosphorylation. *Peptides, 52*, 113-121. doi: 10.1016/j.peptides.2013.11.021

Westermann, B. (2010). Mitochondrial fusion and fission in cell life and death. *Nature Reviews Molecular Cell Biology, 11*(12), 872-884. doi: 10.1038/nrm3013

Winklhofer, K. F., & Haass, C. (2010). Mitochondrial dysfunction in Parkinson's disease. *Biochimica Biophysica Acta, 1802*(1), 29-44. doi: 10.1016/j.bbadis.2009.08.013

Wood-Kaczmar, A., Gandhi, S., Yao, Z., Abramov, A. Y., Miljan, E. A., Keen, G., . . . Wood, N. W. (2008). PINK1 is necessary for long term survival and mitochondrial function in human dopaminergic neurons. *PLoS One, 3*(6), e2455. doi: 10.1371/journal.pone.0002455

Wren, A. M., Small, C. J., Ward, H. L., Murphy, K. G., Dakin, C. L., Taheri, S., . . . Bloom, S. R. (2000). The novel hypothalamic peptide ghrelin stimulates food intake and growth hormone secretion. *Endocrinology, 141*(11), 4325-4328. doi: 10.1210/endo.141.11.7873

Wu, Y., Li, X., Zhu, J. X., Xie, W., Le, W., Fan, Z., . . . Pan, T. (2011). Resveratrol-activated AMPK/SIRT1/autophagy in cellular models of Parkinson's disease. *Neurosignals, 19*(3), 163-174. doi: 10.1159/000328516

Xia, Q., Pang, W., Pan, H., Zheng, Y., Kang, J. S., & Zhu, S. G. (2004). Effects of ghrelin on the proliferation and secretion of splenic T lymphocytes in mice. *Regulatory Peptides, 122*(3), 173-178. doi: 10.1016/j.regpep.2004.06.016

Xia, Y., Saitoh, T., Ueda, K., Tanaka, S., Chen, X., Hashimoto, M., . . . Masliah, E. (2001). Characterization of the human alpha-synuclein gene: Genomic structure, transcription start site, promoter region and polymorphisms. *Journal of Alzheimer's Disease, 3*(5), 485-494.

Xiong, N., Long, X., Xiong, J., Jia, M., Chen, C., Huang, J., . . . Wang, T. (2012). Mitochondrial complex I inhibitor rotenone-induced toxicity and its potential mechanisms in Parkinson's disease models. *Critical Reviews in Toxicology, 42*(7), 613-632. doi: 10.3109/10408444.2012.680431

Xu, Q., Shenoy, S., & Li, C. (2012). Mouse models for LRRK2 Parkinson's disease. *Parkinsonism Related Disorders, 18 Suppl 1*, S186-189. doi: 10.1016/s1353-8020(11)70058-x

Xu, Z., Lin, S., Wu, W., Tan, H., Wang, Z., Cheng, C., . . . Zhang, X. (2008). Ghrelin prevents doxorubicin-induced cardiotoxicity through TNF-alpha/NF-kappaB pathways and mitochondrial protective mechanisms. *Toxicology, 247*(2-3), 133-138. doi: 10.1016/j.tox.2008.02.018

Yamashita, S. I., & Kanki, T. (2017). How autophagy eats large mitochondria: Autophagosome formation coupled with mitochondrial fragmentation. *Autophagy, 13*(5), 980-981. doi: 10.1080/15548627.2017.1291113

Yang, J., Brown, M. S., Liang, G., Grishin, N. V., & Goldstein, J. L. (2008). Identification of the acyltransferase that octanoylates ghrelin, an appetite-stimulating peptide hormone. *Cell, 132*(3), 387-396. doi: 10.1016/j.cell.2008.01.017

Yang, Y., Gehrke, S., Imai, Y., Huang, Z., Ouyang, Y., Wang, J. W., . . . Lu, B. (2006). Mitochondrial pathology and muscle and dopaminergic neuron degeneration caused by inactivation of Drosophila Pink1 is rescued by Parkin. *Proceedings of the National Academy of Sciences of the United States of America, 103*(28), 10793-10798. doi: 10.1073/pnas.0602493103

Yang, Y., Ouyang, Y., Yang, L., Beal, M. F., McQuibban, A., Vogel, H., & Lu, B. (2008). Pink1 regulates mitochondrial dynamics through interaction with the fission/fusion machinery *Proceedings of the National Academy of Sciences of the United States of America* (Vol. 105, pp. 7070-7075).

Yin, Y., Li, Y., & Zhang, W. (2014). The growth hormone secretagogue receptor: its intracellular signaling and regulation. *International Journal of Molecular Sciences, 15*(3), 4837-4855. doi: 10.3390/ijms15034837

Youle, R. J., & van der Bliek, A. M. (2012). Mitochondrial fission, fusion, and stress. *Science, 337*(6098), 1062-1065. doi: 10.1126/science.1219855

Yu, J., Xu, H., Shen, X., & Jiang, H. (2016). Ghrelin protects MES23.5 cells against rotenone via inhibiting mitochondrial dysfunction and apoptosis. *Neuropeptides, 56*, 69-74. doi: 10.1016/j.npep.2015.09.011

Yuan, Y., Zheng, Y., Zhang, X., Chen, Y., Wu, X., Wu, J., . . . Chen, Z. (2017). BNIP3L/NIX-mediated mitophagy protects against ischemic brain injury independent of PARK2. *Autophagy*, 0. doi: 10.1080/15548627.2017.1357792

Zhang, Q., Zhang, J., Jiang, C., Qin, J., Ke, K., & Ding, F. (2014). Involvement of ERK1/2 pathway in neuroprotective effects of pyrroloquinoline quinine against rotenone-induced SH-SY5Y cell injury. *Neuroscience, 270*, 183-191. doi: 10.1016/j.neuroscience.2014.04.022

Zhang, X., Du, L., Zhang, W., Yang, Y., Zhou, Q., & Du, G. (2017). Therapeutic effects of baicalein on rotenone-induced Parkinson's disease through protecting mitochondrial function and biogenesis *Science Reports* (Vol. 7).

Zigman, J. M., Jones, J. E., Lee, C. E., Saper, C. B., & Elmquist, J. K. (2006). Expression of ghrelin receptor mRNA in the rat and the mouse brain. *Journal of Comparative Neurology, 494*(3), 528-548. doi: 10.1002/cne.20823

Zunino, R., Schauss, A., Rippstein, P., Andrade-Navarro, M., & McBride, H. M. (2007). The SUMO protease SENP5 is required to maintain mitochondrial morphology and function. *Journal of Cell Science, 120*(Pt 7), 1178-1188. doi: 10.1242/jcs.03418